Molecular control of actin cortex organisation and dynamics

Amina Yahya Yonis

A thesis submitted to University College London for the degree of

Doctor of Philosophy

London Centre for Nanotechnology

Department of Cell and Developmental Biology UCL

Supervisor: Prof. Guillaume Charras

August 2017

Declaration

I, Amina Yahya Yonis, confirm that the work presented in this thesis is my own. Where information has been derived from other sources, I confirm that this has been indicated in the thesis.

Abstract

The cortex is a ~100nm thick layer of F-actin located under the cell membrane, rich in myosin II and actin-binding proteins. It is essential for cytokinesis, cell locomotion, and tissue morphogenesis. Despite its importance, our knowledge of the cortex is poor. Two actin nucleators, Diaph1 and the Arp2/3 complex, have been shown to generate actin filaments in the cortex. The actin networks generated by these nucleators display clear differences in their organisation and the actin-binding proteins they recruit. Therefore, cells may be able to rapidly control their cortical mechanical properties by regulating the activity of each nucleator.

When I searched for regulators of mDia1 and Arp2/3 in a proteomic analysis of the cortex, I found four candidate nucleation promotion factors (NPFs): IQGAP1, NCKIPSD, Fli-I and the WAVE complex. Interestingly, IQGAP1 and NCKIPSD interact with both Diaph1 and the Arp2/3 complex, suggesting they may participate in crosstalk. I examined the role of each NPF in the generation and maintenance of cortical actin. After examining the localisation of each NPF, I determined their impact on cortical assembly by examining how their depletion affected bleb size. Indeed, reduction in Arp2/3 activity leads to smaller blebs, while large blebs result from a decrease in Diaph1 activity. IQGAP1 and NCKIPSD depletion yielded large bleb phenotypes, WAVE gave a small bleb phenotype consistent with its role in regulating Arp2/3, and Fli-I depletion had no phenotype. Next, I examined changes in F-actin network organisation after NPF depletion with scanning electron microscopy. The density and interconnection of the network were altered, further suggesting the importance of IQGAP1, NCKIPSD and WAVE in controlling the organisation of the actin cortex. I showed that NPF depletion significantly affected successful completion of mitosis in HeLa cells. Finally, in collaboration with other students, I examined how NPFs controlled properties of cell mechanics.

Impact Statement

Formins, such as Diaph1, and the Arp2/3 complex are important for generating actin networks that allow for crucial cellular processes such as cytokinesis, cell locomotion, and tissue morphogenesis.

Both within and outside academia, the work presented in this thesis provides a greater insight into the regulation of actin nucleation at the actin cortex. At present, knowledge regarding the control of Diaph1 and Arp2/3 is poor, thus, the elucidation of interactions discussed in this thesis may help in providing a basis for follow-up work in this field. Cancer-cell invasion into tissues requires the formation of actin-rich structures that are found in invasive cancer cells (podosome/invadopodia). It is known that activation of Arp2/3 is required for podosome formation, thus, although not immediately, the Arp2/3 complex and its regulators could emerge as potential targets for therapeutic intervention. In addition to Arp2/3, formin activity is critical for proper cell division and thus, for the maintenance of genomic integrity during cell division. At present, there have been relatively few studies that directly link formins with disease pathogenesis; future studies are likely to link formins with cancer initiation, given the fundamental role of formins during cytokinesis, as discussed in this thesis. Overall, inappropriate control of formin or Arp2/3 function and expression in humans may be a critical event in cancer development. To understand how NPFs control these nucleators, will prove useful for use in future studies.

In addition, the interdisciplinary nature of the research discussed in this thesis provides a platform for the continuation of collaborative work between biology and physics. The Institute for the Physics of Living Systems (IPLS) at University College London is an example of a cross-faculty institute promoting interdisciplinary approaches combining physics and biology to understand fundamental properties of living systems. This thesis is an example of such collaborations between theory and experimental groups across UCL and internationally. This allows the facilitation of new interactions in which quantitative approaches are combined with theory to provide us with a greater understanding of the fundamental processes governing complex behaviours of living systems, from cells to tissues and organisms.

Acknowledgements

Firstly, I would like to express my gratitude to my supervisor Prof. Guillaume Charras for the continual mentoring, guidance and support granted to me over the past four years throughout my PhD. Many thanks to my secondary supervisor, Prof. Ewa Paluch, for her provision and advice during my studies.

I would like to extend my thanks to my friends, colleagues, and present members of the Charras group: Richard Thorogate; Nargess Khalilgharibi for being the great voice of reason; Anna Bove for teaching me the important life lesson about what real gelato is; Malti Vaghela for making me spend money on clothes, shoes and travel; Jonathan Fouchard for your random inquisitive nature; Alice Wicks for being another bleb person; Ana Lisica for booking the spinning disk all day every day, Manasi Kelkar for splitting my cells when no-one else would; and Daniel Gradeci for the laughs. Thank you all for the happy lunch times in the 'happy place', the chocolate break discussions, the failed attempts of persuading me to drink coffee, the body conditioning sessions at the gym and the salsa lessons. Amongst a multitude of other things, you have provided me with a wealth of knowledge that I will value for the rest of my life. Thank you also to previous members of the Charras group: Majid Malboubi, Thomas Wyatt, Jessica Davies, and Marc de Gennes. A special thanks to the members of the Paluch group: in particular, Priyamvada Chugh, Murielle Serres, and Matthew Smith for their kind assistance.

I would also like to thank all the Human Frontier Science Program (HFSP) collaborators and the members in their group, including Prof. Ewa Paluch, Prof. Philippe Roux in Montréal, Dr. Guillaume Romet-Lemonne in Paris, and Dr. Antoine Jégou also in Paris. In particular, thank you to Prof. Philippe Roux, Dr. Geneviève Lavoie, and Antoine Meant for the support on the BioID project and for looking after me during my three-month project in Montréal. I would also like to acknowledge HFSP for the financial support.

I would further like to acknowledge Dr. Mark Turmaine for supporting use of the Electron Microscopy facility, and Dr. Jemima Burden for the use of the critical point

dryer. Many thanks to the LCN, LMCB and UCL for providing the research facilities that enabled the completion of this research.

Most importantly, I would like to thank my wonderful family for believing in me and supporting me throughout my life and education. Thank you to my father, Yehia Yonis, and my mother, Maria Mohammed Shash, for all that I cannot put into words. Thank you to my siblings Elyas, Hannah, Sumaiya and Maryam for being my best friends and for their famous quote reminding me that 'a PhD is hard, but you make it look so easy'. Thank you to my husband, Mohamed Ahmed, for his support at the most critical time during thesis writing. Lastly, I definitely cannot forget all the massages (and other 'voluntary' acts of kindness) that I've received over the thesis-writing period. I said those would guarantee you a mention in my acknowledgements, so as promised here it is!

Table of Contents

Abbreviations

ABC	Ammonium Bicarbonate
ADP	Adenosine Diphosphate
Arp2/3	Actin-Related Protein 2 And 3
ATP	Adenosine-5'-Triphosphate
BFP	Blue Fluorescent Protein
BirA	BirA-Biotinyl-5'-Adenylate
CDK1	Cyclin-Dependent Kinase 1
cDNA	Complementary DNA
CSB	Cytoskseletal Buffer
C-terminus	Carboxyl-Terminus
DAD	Diaphanous Autoregulatory Domain
DAPI	4'6-Diamidino-2-Phenylindole
Diaph1	Diaphanous Homolog 1
DID	Diaphanous Inhibitory Domain
DMEM	Dulbecco's Modified Eagle's Medium
DMSO	Dimethyl Sulfoxide
DNA	Deoxyribonucleic Acid
ECM	Extracellular Matrix
EDTA	Ethylenediaminetetraacetic Acid
EGTA	Egtazic Acid
ERM	Ezrin, Radixin and Moesin
F-actin	Filamentous Actin
FACS	Fluorescence-Activated Cell Sorting
FBS	Fetal Bovine Serum
FDR	False Discovery Rate
FH1	Formin Homology 1
FH2	Formin Homology 2
G-actin	Globular Actin
G418	Geneticin
GAPDH	Glyceraldehyde 3-Phosphate Sehydrogenase
GAP	GTPase-Activating Proteins
GDI	Guanine Nucleotide Dissociation Inhibitors
GEF	Guanine Nucleotide Exchange Factors
GFP	Green Fluorescent Protein
GTP	Guanosine-5'-Triphosphate
HEK	Human Embryonic Kidney
HeLa	Henrietta Lacks
HEPES	N-2-Hydroxyethylpiperazine-N-2-Ethane Sulfonic Acid
HIV	Human Immunodeficiency Virus
HRP	Horseradish Peroxidase
HS	Horse Serum
IQGAP1	Ras GTPase-Activating-Like Protein IQGAP1
MEM	Minimum Essential Medium
mL	Millilitre
mM	Millimolar

mm	Millimetre
mRNA	messenger RNA
N-terminus	Amino Terminus
NCKIPSD	NCK-Interacting Protein With SH3 Domain
Nap1	Nck-Associated Protein 1
ng	Nanogram
nM	Nanomolar
nm	Nanometre
NPF	Nucleation Promoting Factor
NS	Non-Silencing
PAI	Protein Abundance Index
P_i	Inorganic Phosphate
PBS	Phosphate-Buffered Saline
Pen/strep	Penicillin/Streptomycin
Plk1	Serine/Threonine-Protein Kinase PLK1
PMSF	Phenylmethane Sulfonyl Fluoride
qPCR	Quantitative Polymerase Chain Reaction
RBD	Rho Binding Domain
RhoA	Ras Homolog Gene Family, Member A
RIPA buffer	Radioimmunoprecipitation Assay Buffer
ROCK	Rho-Associated Protein Kinase
rpm	Revolutions Per Minute
RNA	Ribonucleic Acid
RNAi	Ribonucleic Acid Interference
SAINT	Significance Analysis Of INTeractome
SDS	Sodium Dodecyl Sulphate
SEM	Scanning Electron Microscopy
shRNA	Short Hairpin RNA
siRNA	Small Interfering Ribonucleic Acid
Sra1	Specifically Rac1-Associated Protein 1
SV40	Simian Vacuolating Virus 40
VSVG	Vesicular Stomatitis Indiana Virus G Protein
WAVE	WASP-Family Verprolin-Homologous Protein
WASP	Wiskott–Aldrich Syndrome Protein
WH2	WASP-Homology 2
WRC	WAVE Regulatory Complex
WT	Wild Type
µg	Microgram
µL	Microliter
µm	Micrometre
µM	Micromolar

Chapter 1 Introduction

1.1 Actin

First isolated in 1942, actin is the most abundant protein in eukaryotic cells (Straub 1942). One of the earliest recognised functions of actin was its ability to assemble into linear polymers that form the thin filaments of the muscle sarcomeres (Dominguez & Holmes 2011). Actin is essential for many cellular processes, including cell division, intercellular junction formation, migration, chromatin remodelling, transcriptional regulation, vesicle trafficking, and cell shape regulation (Perrin & Ervasti 2010). The ability of this highly conserved protein to regulate such a wide range of cellular processes is due to the existence of many isoforms bearing both overlapping and unique functions. Actin is highly conserved, consisting of six different isoforms encoded by separate genes in mammals. Four isoforms, $\alpha_{cardiac, skeletal, smooth}$, and γ_{smooth}, are expressed in muscle cells; the remaining two, β_{cyto} and γ_{cyto}, are ubiquitously expressed in non-muscle cells (Perrin & Ervasti 2010). All of the isoforms possess very similar amino acid sequences, with no isoform sharing less than 93% identity with any other isoform (Perrin & Ervasti 2010).

Higher-order actin-based networks are important for cell motility, growth and cytokinesis. Actin-filament networks can be categorised into two main types of organisation: parallel unbranched bundles of filament (bristles, microvilli, stereocilia and filopodia), and highly branched filament networks (lamellipodia and the actin cortex). The leading edge protrusions of motile cells consist of sheet-like structures called lamellipodia and rod-like assemblies called filopodia (Chhabra & Higgs 2007). These two leading edge structures differ markedly in their organisation: the lamellipodium is a meshwork of branched actin filaments assembled by the Arp2/3 complex whereas actin filaments in filopodia are parallel and tightly bundled (Faix & Rottner 2006). Yet, filopodia originate from the lamellipodial actin meshwork, indicating that a high degree of plasticity can be achieved locally (Small 2010). The driving force for the generation of both actin structures is the barbed-end elongation of actin filaments polymerising towards the plasma membrane. This process combines contractile forces and adhesion to push the cell edge forward, and is a key step in cell migration. Both filopodia and lamellipodia have clinical relevance in

cancer metastasis. Indeed, cell motility is upregulated during tumour progression and cancer cells crawl across surfaces via the formation of protrusions, invading surrounding tissues (Wang et al. 2005). Although it was long thought that cell movement relied solely on lamellipodia and filopodia, it was recently shown that membrane blebs can drive the plasma membrane forward during movement of some cells (Charras & Paluch 2008; Bergert et al. 2012; Ruprecht et al. 2015).

The three-dimensional structures of actin molecules and actin filaments were determined in 1990 by Holmes and colleagues (Holmes et al. 1990). Individual actin molecules consist of 375 amino acids. Each actin monomer, globular G-actin, has tight binding sites that mediate head-to-tail interactions with other monomers, allowing them to polymerise and form filaments, known as filamentous actin or F-actin (Dominguez & Holmes 2011). All six actin isoforms have two structural domains, large and small, that can be further divided into two subdomains. The small domain comprises subdomain 1 and 2, while the large domain comprises subdomain 3 and 4 (Kabsch et al. 1990). The structure of the actin monomer determined by X-ray crystallography exists as two domains that are bridged by bonds to an adenine nucleotide (ATP/ADP), and a divalent cation (Mg2+/ Ca2+). In particular, the upper cleft is responsible for the interaction with ATP (adenosine triphosphate) or ADP (adenosine diphosphate) and the divalent cation magnesium, whilst the lower cleft binds the majority of known actin binding proteins (Schutt et al. 1993). Each domain is partitioned into two subdomains that allow movement between them (Page et al. 1998).

Crystal studies comparing the structure of actin structure bound to ATP or ADP show that the molecule undergoes at least two conformational changes during the hydrolysis of ATP and the release of Pi (inorganic phosphate) (Blanchoin & Pollard 2002; Nolen et al. 2004; Graceffa & Dominguez 2003). Structures with bound nucleotide (ATP or ADP) are characterised by a closed conformation of the main cleft whereby the large and small domains are in close proximity, whereas nucleotide-free structures are distinguished by an open cleft (Figure 1-1).

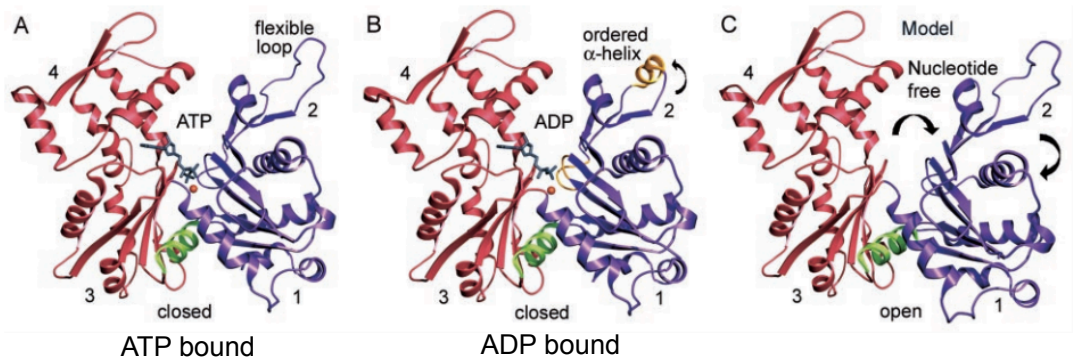

Figure 1-1 Crystal structure of the three conformational states of actin. Domain I (subdomains 1 + 2), and domain II (subdomains 3 + 4) are coloured purple and red, respectively. The domains are connected by a linker α-helix (green). The main changes upon release of Pi occur in the region shown in yellow. Structures A and B represent nucleotide-bound open actin conformations (ATP and ADP respectively), whilst structure C represents the nucleotide-free open conformation (Image from Graceffa & Dominguez 2003).

Actin protomers within a filament are oriented in the same direction; thus, actin filaments have a distinct polarity with biochemically distinguishable ends (plus or barbed end, and minus or pointed end) (Graceffa & Dominguez 2003). This polarity is important for assembly as well as for the directional movement of myosin motor proteins. Using electron microscopy, analyses revealed that actin filaments consist of two strands that twist around one another to form a right-handed helix (Carlier 1991). Under conditions of high protein and salt, G-actin will readily polymerise and assemble into F-actin polymers; this process is known as nucleation-elongation. *In vitro*, actin polymerisation can be studied using viscosity analyses, sedimentation assays, and fluorescence microscopy (T. Kim et al. 2014; Burlacu et al. 1992; Lim & Danuser 2009). The polymerisation of actin can be described as a three-step process consisting of a nucleation, elongation, and steady-state phase (Figure 1-2).

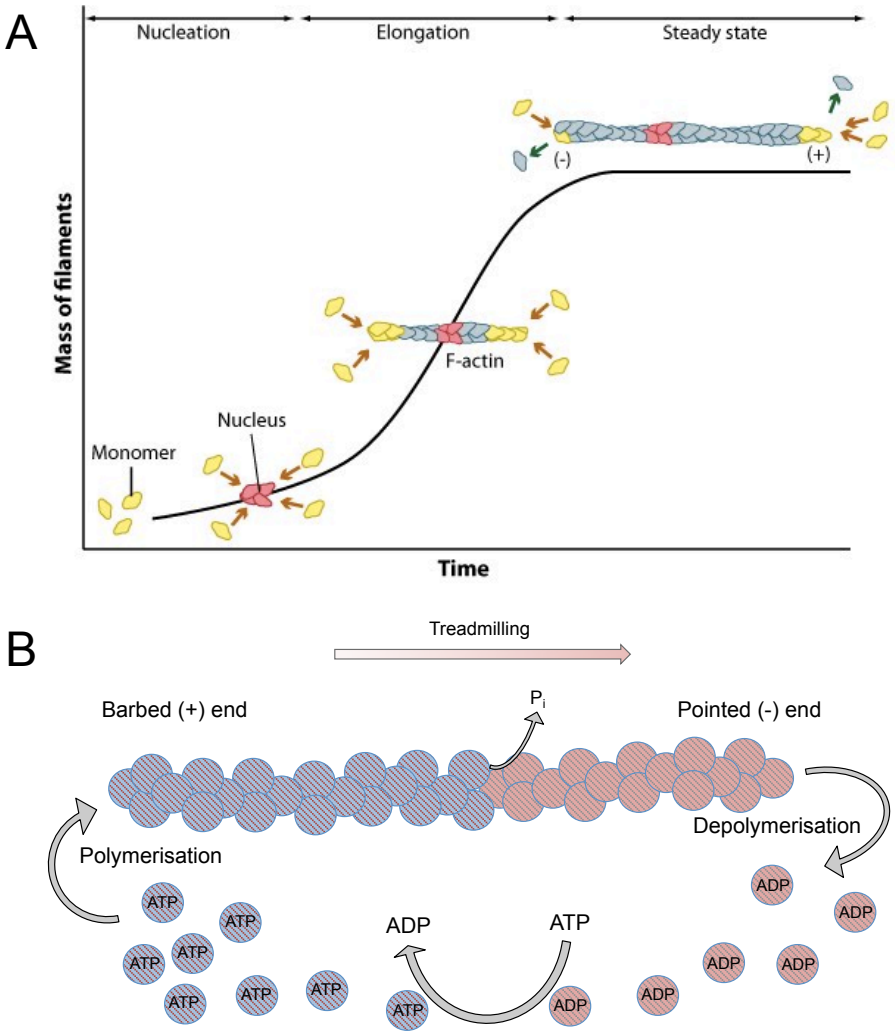

Figure 1-2 Nucleation, elongation and steady state phase of actin filament assembly. A, Diagram showing the three phases of actin filament assembly *in vitro*. During the nucleation phase, three actin monomers form an F-actin nucleus (pink). Once actin nuclei are formed, filament elongation can take place spontaneously and actin monomers are added to both ends of the filament, elongating it. During the steady state, there is no net change in polymer mass and the concentration of free actin monomers at the steady state is known as the critical concentration (C_c). *Permission from MBInfo: www.mechanobio.info; Mechanobiology Institute, National University of Singapore.* **B,** G-actin monomers can spontaneously self-assemble into polarised actin filaments with ATP-actin monomers added to the barbed end and ADP-actin monomers lost from the pointed end. This process known as treadmilling, results in a steady net flow of actin subunits through the filament.

Nucleation involves the formation of a small nucleus consisting of three actin monomers; this event is slow due to kinetic barriers generated by the instability of this aggregate (Figure 1-2**A**, indicated in pink). The generation of actin trimers represents the rate-limiting step of the actin polymerisation process (Nishida & Sakai 1983), but once actin nuclei form, filament elongation can take place spontaneously. A 'lag phase' occurs during the initiation of polymerisation, during which no filaments are observed. During the elongation stage, G-actin is rapidly added at both ends of the growing filament and the rate of elongation is directly proportional to the concentration of free actin in solution (Thomas D. Pollard & Cooper 1986). As the actin filament grows, the system reaches a steady state and the concentration of free actin monomers at this state is known as the critical concentration (C_c) (Cooper et al. 1983). Importantly, the C_c at the two ends of an actin filament is different. The C_c is defined as the concentration level of free ATP-G-actin where the rate of addition is balanced by the rate of loss and no net growth occurs at that end. Actin monomers are added more rapidly at the barbed end than at the pointed end (Pollard & Mooseker 1981). Once the steady state is reached, new ATP bound G-actin subunits are added at the barbed end, whereas old ADP bound G-actin subunits are lost from the pointed end.

Actin monomers are bound to ATP, which is hydrolysed to ADP following their incorporation onto a filament. The ATP hydrolysis occurs in two main steps; first the phosphate bond is cleaved resulting in the generation of actin-ADP. This last step leads to a change in the physical properties of F-actin, which becomes less rigid and more prone to disassembly (Blanchoin & Pollard 2002). Although ATP is not required for polymerisation, ATP-actin monomers polymerise more readily than ADP-bound monomers. At the C_c, the length of a filament is maintained constant, as the newly added actin monomers treadmill along the growing filament from the barbed end to the pointed end, where they dissociate (Figure 1-2**B**).

1.2 Actin binding proteins

The architecture and self-assembly of actomyosin networks is governed by several classes of accessory proteins: nucleators, which initiate filament formation; nucleation promotion factors (NPFs) required for the proper spatial and temporal

control of actin assembly in cells (Duleh & Welch 2010); capping proteins, which bind to filament ends preventing further polymerisation or depolymerisation; depolymerisation factors and severing factors, which disassemble filaments; crosslinkers and stabilising proteins, which organise and stabilise higher-order network structures; and motor proteins, which generate movement and forces between filaments or between a filament and another structure (Figure 1-3). The collective function of these accessory proteins give rise to network properties, such as turnover, and are key in determining and fine-tuning the properties of actomyosin assemblies. In the following sections, I will describe the above proteins and their actions in more detail.

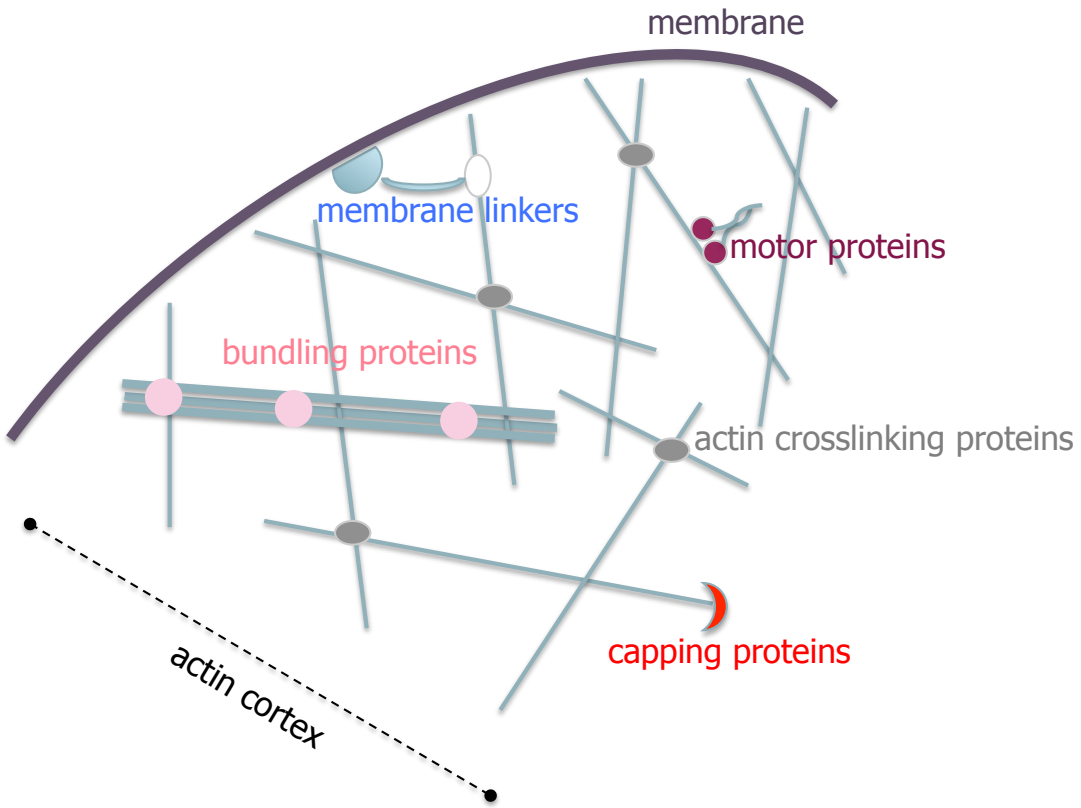

Figure 1-3 The major classes of actin-binding proteins. These structurally diverse proteins direct the location, rate, and timing of actin filament assembly/disassembly, thus modulating the dynamics of the actin cytoskeleton. Treadmilling of actin filaments can be altered by sequestering proteins such as profilin; new filaments are nucleated by nucleators such as the Arp2/3 complex and formins; crosslinking/bundling proteins such as filamin/α-actinin influence the packing and

organisation of actin filaments into secondary structures; capping/severing such as gelsolin/cofilin proteins promote the disassembly of actin filaments. Proteins such as the ERM (ezrin, radixin and moesin) family bind and anchor actin to the membrane or other cytoskeletal networks. There are also a number of proteins that assist in the crosstalk between microtubules and actin, such as tau, which bind to both actin and microtubules simultaneously (Elie et al. 2015).

1.2.1 Actin capping proteins

Capping proteins control access to the free barbed ends of actin filaments and are therefore a major factor affecting actin filament elongation. Capping proteins have a high affinity for barbed ends and are tightly regulated in the cytoplasm resulting in the capping of most barbed ends (Schafer et al. 1996). Capping proteins, such as CapZ or β-actinin, help promote actin assembly by preventing the loss of actin subunits by blocking the exchange of subunits at the fast-growing end of actin filaments (Iwasa & Mullins 2007). CapZ is the most ubiquitous and abundant barbed-end capper, and is required for Arp2/3 complex-mediated assembly of dendritic actin filament networks (Edwards et al. 2014). Capping protein has also been shown to functionally co-regulate filament barbed-end assembly by simultaneously binding barbed ends with Diaph1 formin (Shekhar et al. 2015).

Other capping proteins, such as gelsolin, increase the rate of nucleation by binding G-actin monomers and/or unstable oligomers (Casella et al. 1981). Gelsolin is a multifunctional actin regulatory protein, and the most potent actin filament severing protein identified to date. It initiates severing by binding to the side of an actin filament, resulting in slow severing of the filament regulated by Ca^{2+} (Sun et al. 1999). After severing, gelsolin remains attached to the barbed end as a cap, preventing the reattachment of shorter actin filament and elongation at the barbed end, resulting in the disassembly of the actin network.

1.2.2 Actin filament treadmilling proteins

Many actin monomer-binding proteins maintain the G-actin pool in cells. Important actin monomer binding proteins include profilin, thymosin beta-4 and ADF/cofilin.

Profilin is an essential actin-binding protein that specifically binds G-actin at its barbed end, changing its conformation, stabilising ATP-actin and preventing its association with pointed ends whilst allowing binding to barbed ends (Bugyi & Carlier 2010). It has also been shown that profilin can work simultaneously with formins to facilitate progressive actin filament elongation following nucleation by the formin (Kovar et al. 2006). Profilin-actin binds to formins at the FH1 domain tethering multiple profilin-actin complexes near the growing end of actin filaments (Paul & Pollard 2008). This promotes the progressive addition of actin subunits by generating an artificially high concentration of actin near the barbed end, resulting in rapid elongation (Perelroizen et al. 1996). Profilin uses the energy from ATP hydrolysis generated during actin polymerisation to facilitate actin assembly (Paul & Pollard 2008).

ADF/cofilin proteins remodel the actin cytoskeleton (Bamburg 1999). For example, during cytokinesis, the actin-rich contractile ring shrinks as it contracts through the interaction of ADF/cofilins with both monomeric and filamentous actin (Maciver & Hussey 2002). ADF/cofilin binds monomeric actin in a 1:1 stoichiometry, influencing rapid actin filament turnover. The depolymerising activity is twofold: ADF/cofilins sever actin filaments and also increase the rate at which monomers leave the filament's pointed end (Bamburg 1999). ADF cooperatively binds to F-actin, increasing the treadmilling turnover rate of actin filaments, by depolymerising actin filaments from their pointed ends. Cooperative binding of ADF/cofilin causes the filament to twist and structurally weaken; this causes a modest severing effect that results in pointed end depolymerisation, and a 2-3-fold decrease in the average length (Bamburg 1999).

There are a number of specialised actin-membrane linker proteins that allow F-actin to interface to the cell membrane (T D Pollard & Cooper 1986). Actin-membrane linking is particularly important for actin cortex stability and for enabling shape change to occur in response to cytoskeletal rearrangements in the cortex. There are a number of known actin-membrane linker proteins, including ezrin-radixin-moesin (ERM) proteins, annexins, (Matsui et al. 1998) and filamin.

The ERM proteins play a crucial role in organising membrane domains through their ability to interact with transmembrane proteins and the cytoskeleton. They provide structural links, strengthening the cell cortex and regulating the activities of signal transduction pathways (Fehon et al. 2010). In their inactive form, ERMs exist in a closed conformation with head-to-tail interactions. ERMs are activated through binding to membrane regions rich in phosphatidylinositol, 4,5-bisphosphate (PdIns(4,5)P2), allowing for phosphorylation by kinases such as Rho-associated protein kinase (ROCK) (Matsui et al. 1998). Following phosphorylation, ERMs adopt an open conformation whereby the N-terminal FERM domain binds to the plasma membrane and the C-terminal domain associates with F-actin (Bosk et al. 2011). Studies have shown that ERM may also function upstream to regulate RhoA activity, and interact with proteins that regulate Rho GTPases, including RhoGEF (Rho guanine nucleotide exchange factors) and RhoGDI (Rho GDP-dissociation inhibitor) (D'Angelo et al. 2007). More specifically, phosphorylated ezrin is known to associate with protein Dbl through its NH_2-terminal domain to cause Rho activation (Lee et al. 2004).

The annexins are a family of Ca^{2+}/lipid-binding proteins that have a unique architecture allowing them to dock onto membranes (Rescher 2004). Structurally, annexins are highly α-helical. They mediate regulatory interactions with protein ligands and regulate the annexin-membrane association (Raynal & Pollard 1994).

Filamin family proteins bind to F-actin and a number of scaffolding proteins, including Rho GTPases. Filamin forms a vital scaffolding adaptor and regulatory component that contributes to the mechanical stability of cells by linking the internal F-actin network to membrane receptors and mechanosensitive components, such as those in muscle (Sampson et al. 2003). These include transmembrane proteins such as β-integrins (Sharma et al. 1995), D2 and D3 dopamine receptors (Lin et al. 2001), Kv4.2 potassium channels (Petrecca et al. 2000) and intracellular signalling molecules such as the Rho family of GTPases (Sampson et al. 2003; Ohta et al. 1999). By establishing this critical link, the membrane is stabilised allowing for changes in cell shape associated with cell motility and migration. The blebbing

melanoma cells (M2 cells) used in my work was initially identified as a filamin deficient cell line (Cunningham et al. 1992).

1.2.3 Actin filament bundling and crosslinking proteins

Cells assemble F-actin into structures ranging from networks, where filaments overlap at large angles, to bundles in which parallel filaments are closely packed together (Figure 1-4). A variety in network conformations is important to fulfil differing roles in cells. Networks of cross-linked filaments constitute the cellular cortex, providing mechanical stability and maintaining shape, while F-actin bundles provide support or create membrane protrusions such as lamellipodia (Tseng et al. 2002).

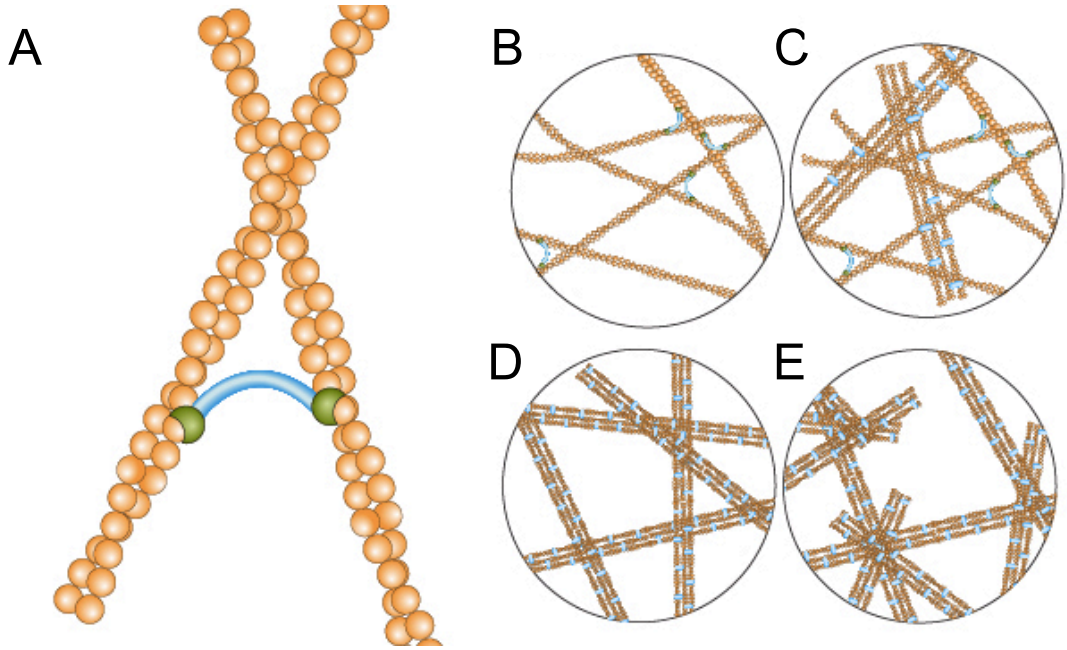

Figure 1-4 Types of actin filament networks produced depend on the concentration of the binding proteins that cross-link filaments together. A, Single protein cross-linking actin filaments. Figures B-D show filament networks produced with increasing protein concentration, respectively: **B,** weakly cross-linked; **C,** composite; **D,** bundles; and **E,** bundle cluster. (Image drawn by Emily Harrington).

F-actin bundling protein fascin and crosslinking protein α-actinin work together to enhance the mechanical properties of F-actin networks (Tseng et al. 2002). α-actinins are a protein family, which generate tight bundles of F-actin. They are a major component of muscle where they bundle actin filaments in the Z-disc of sarcomeres (Sjöblom et al. 2008). α-actinin dimerises in a head to tail manner via rod domains present on both ends. The dimer therefore possesses actin binding regions at each extremity allowing interfacing of adjacent actin filaments (Djinović-Carugo et al. 1999). Fascin, a monomeric protein, is a major actin crosslinking protein found in filopodia. It binds beta-catenin and co-localises with it at the leading edges, and borders of epithelial and endothelial cells (Yamashiro-Matsumura & Matsumura 1985). Fascin forms a "network of bundles" rather than a homogeneous network as seen in α-actinin (Courson & Rock 2010; Kureishy et al. 2002) and undergoes frequent cycles of association and dissociation, independent of the phosphorylation state (Vignjevic et al. 2006). It increases the stiffness of actin networks by reducing the movement of actin filaments through depolymerisation (Meyer & Aebi 1990).

1.2.4 Motor proteins – Myosin II

Motor proteins, such as myosin II, are the driving force behind muscle contraction and are responsible for the active transport of most proteins and vesicles in the cytoplasm (Reymann et al. 2012). Myosin II can move along the surface of a suitable substrate, powered by the hydrolysis of ATP by 'walking' along actin filaments and assembling into mini-filaments, allowing for crosslinking of actin filaments.

Myosin II contains two heavy chains, each about 2000 amino acids in length, which constitute the head and tail domains (Reymann et al. 2012). Each of these heavy chains contains the N-terminal head domain, while the C-terminal tails adopt a coiled-coil morphology, holding the two heavy chains together (Korn 2000). The head of the large protein binds to actin filaments and the tail binds to cargo. In the myosin motor cycle, myosin moves by using the energy provided by ATP hydrolysis in the heads (Wilson et al. 2010). ATP nucleotide binding to the motor domain results in its detachment from F-actin and hydrolysis of ATP to ADP+P_i. This intermediate binds weakly to F-actin. When P_i is released, the motor returns to a nucleotide-free state (Mehta et al. 1999), allowing for the cycle to start again.

Myosin moves along actin filaments towards the plus end, like walking on two legs, by alternately changing the orientation of the head structure (Xiao et al. 2003). Thus, during one cycle, myosin exists in at least three conformational states: a pre-hydrolysis ATP state unbound to actin, an ADP-Pi state bound to actin, and a state after the power stroke is completed (Xiao et al. 2003).

1.2.5 Rho GTPases

Cells receive extracellular stimuli that act to generate changes in the actin cytoskeleton at specific sites, primarily through Rho proteins. Once activated, Rho GTPases bind to a variety of effectors, including protein kinases and some actin-binding proteins, to directly or indirectly affect the cytoskeleton (Symons 1996; Fan & Mellor 2012).

Most Rho GTPases cycle between an active GTP-bound conformation and an inactive GDP-bound conformation, regulated by three types of protein (Rossman et al. 2005). Guanine nucleotide exchange factors (GEFs) catalyse the exchange of GDP for GTP, thereby activating the GTPase, whereas GTPase-activating proteins (GAPs) increase the intrinsic GTP hydrolysis rate of the GTPase, thereby inactivating it (Figure 1-5). Guanine nucleotide dissociation inhibitors (GDIs) sequester the GDP-bound form of some GTPases in the cytosol and prevent them from localising to membranes or being activated by GEFs (Rossman et al. 2005). In the GTP-bound active conformation, Rho GTPases interact with a range of effector proteins, including kinases, actin regulators and adaptor proteins, leading to changes in cell behaviour. The most important members of the Rho GTPase family, RhoA, Rac1, and Cdc42, regulate the formation of essential F-actin structures, such as stress fibers, lamellipodia, and filopodia, respectively (Hall 1998).

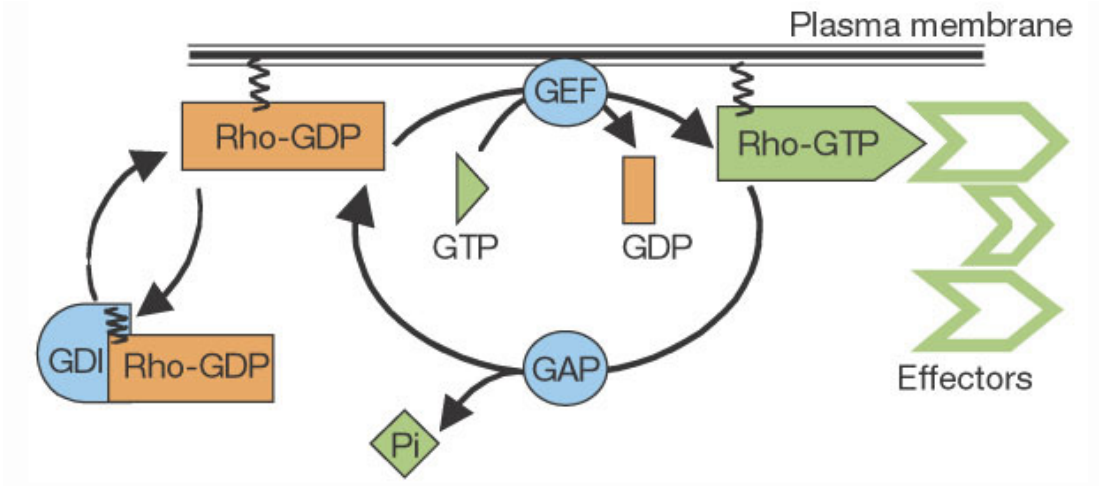

Figure 1-5 The Rho GTPase cycle. Rho GTPases (GDI, GEF and GAP) cycle between an active (GTP-bound) and an inactive (GDP-bound) conformation. This molecular switch controls a wide variety of signal transduction pathways in all eukaryotic cells, in particular regulating the actin cytoskeleton (Image from Etienne-Manneville & Hall 2002).

Formins were first recognised as Rho targets in a two-hybrid screen with yeast (Kohno et al. 1996). As described in more detail later (1.3.2), most formins contain a C-terminal inhibitory autoregulation domain (DAD) and an N-terminal Rho-binding domain (RBD) embedded within the larger inhibitory domain (DID). This DID domain enables auto-inhibition in a head to tail inactive state, and can be relieved by Rho binding (Nezami et al. 2006). The formin Diaph1 is activated only by the Rho family; whereas the related Diaph2 and Diaph3 proteins can be activated by Rac1 and Cdc42 (Lammers et al. 2008). Another well-studied target of Rho is Rho-associated protein kinase (ROCK). ROCK is involved in phosphorylating myosin phosphatase for inactivation and activates myosin light chain, promoting an increase in actomyosin contractility (Kimura et al. 1996). Furthermore, ROCK phosphorylates ERM proteins to promote their activation (Matsui et al. 1998), and is also involved in the inactivation of ADF/cofilin (Maekawa 1999), resulting in the stabilisation of actin filaments. Overall, RhoA has a central role in the cortex with the ability to promote contractility, actin polymerisation and membrane-cortex linking.

1.3 Actin nucleators

Proteins that can stimulate *de novo* actin filament assembly are known as actin nucleators. This is because they facilitate the formation of an actin nucleus (at least a trimer of subunits), which is the rate-limiting step for actin-filament growth (Figure 1-6). The best-characterised actin nucleators are: the Arp2/3 complex, formin proteins, and Spire proteins. Each class has a distinct mechanism of nucleation, suggesting that they participate in the assembly of different actin superstructures within distinct cellular regions or that they generate functionally different actinous structures (Michelot and Drubin, 2011). Despite its importance, our understanding of the regulatory processes involved with actin nucleators in cortical organisation remains poor. In the following section, I will describe the mechanisms of the Arp2/3 and formin protein, Diaph1, as they are most relevant to my project.

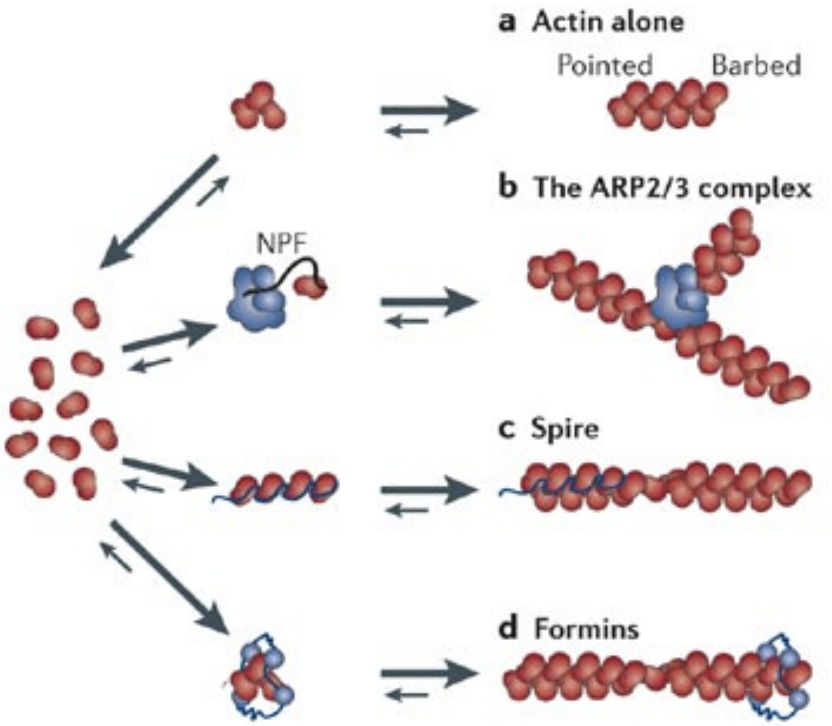

Figure 1-6 Actin filament nucleation mechanisms. Three main classes of protein have been identified that promote rapid initiation of new filament assembly: Arp2/3 complex, spire and formin. The Arp2/3 complex functions as a template for the initiation of a new branched actin filament; the spire proteins form a four tandem G-

actin-binding association to aid polymerisation; and formins promote the nucleation of filaments through stabilising an actin dimer or trimer (Image from Goley & Welch 2006)**.**

1.3.1 The Arp2/3 complex

The actin-related protein-2/3 (Arp2/3) complex was first purified in 1994 from *Acanthamoeba castellanii* based on its affinity for the actin binding protein profilin, and was shown to consist of a stable assembly of seven polypeptides (Machesky et al. 1994). Two of the subunits were actin-related proteins of the ACTR2 (Arp2) and ACTR3 (Arp3) subfamilies, giving the complex its name. The remaining five subunits were named actin-related protein complex, ArpC1-C5, and together formed a relatively stable heptameric complex. Following this identification, the Arp2/3 complex was later identified in other organisms including humans (Winter et al. 1997), and was shown to interact with the side of a pre-existing actin filament (mother filament) inducing the nucleation of a new actin filament (daughter filament) at a regular 70^{o} branch angle resulting in a Y-shaped structure (Mullins et al. 1997).

1.3.1.1 The Arp2/3 complex organisation and actin nucleation ability

Details of the Arp2/3 complex organisation were revealed when a crystal structure of the bovine complex was solved at 2.0-Å resolution (Robinson et al. 2001). The ACTR2 and ACTR3 subunits are structurally similar to actin, as predicted from their sequences, sharing ~47% and ~40% of identity with β-actin, respectively (Kelleher et al. 1995). Of the other five subunits, ArpC2 and ArpC4 form the structural core of the complex, with the remaining subunits organised around them (Gournier et al. 2001). ArpC1 is a seven-bladed β-propeller protein, whereas ArpC3 and ArpC5 are primarily α-helical and are the most peripheral of the subunits (Figure 1-7**A**). The Arp2/3 complex is yet to be captured in its active short-pitch conformation, whereby ActR2 and ActR3 undergo significant conformational changes to mimic the first two subunits of the nascent daughter filament. In the inactive conformation, also known as splayed, the ActR2 and ActR3 subunits are far away from one another and are thus not able to trigger nucleation of a new daughter filament (Gournier et al. 2001).

Upon activation by NPFs, it is thought that ACTR2 moves next to ACTR3 in a short-pitch helix dimer. Subdomains 3 and 4 of ACTR3 and ArpC3 rotate slightly from their positions in the inactive crystal structure (Gournier et al. 2001; Rodnick-Smith et al. 2016). The rest of the subunits (ArpC1, ArpC2, ArpC4 and ArpC5) appear to maintain their positions, fitting into the reconstruction without modification (Rouiller et al. 2008). In the active configuration, the ArpC2-ArpC4 heterodimer provides the main surface for interaction of the complex with the mother filament and anchors ACTR3, the first subunit of the daughter filament (Figure 1-7**B**). ArpC3 and ArpC5 contribute to branching through contact with the mother filament, whilst ArpC1 makes only minor contact with the mother filament (Rouiller et al. 2008).

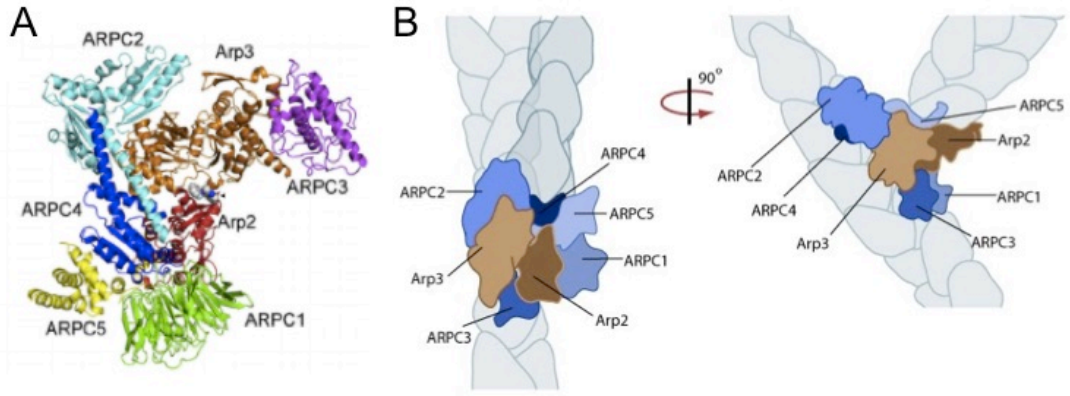

Figure 1-7 Schematic representation of the Arp2/3 complex. A, Ribbon diagram of the crystal structure of the inactive conformation of the Arp2/3 complex. The Arp2/3 complex consists of Arp2 (ACTR2) and Arp3 (ACTR3), and five additional subunits names ArpC1-5 (Baggett et al. 2012). **B,** The Arp2/3 complex initiates a branched filament by binding to the side of a mother filament and recruiting actin monomers. ACTR2 and ACTR3 interact with the pointed end of the daughter filament, and ArpC2 and ArpC3 make substantial contact with the mother filament (*Permission from MBInfo: www.mechanobio.info; Mechanobiology Institute, National University of Singapore).*

1.3.1.2 Regulation of the Arp2/3 complex

Numerous cellular activators and inhibitors modulate the activity of the Arp2/3 complex, providing tight control over its dynamics and the generation of branched actin networks *in vivo*. To date, NPFs known to interact with the Arp2/3 complex fall

into two classes depending on their activity. Class I NPFs bind directly to nucleators and actin monomers, initiating an activating conformational change and recruiting the first actin subunits for the nascent (daughter) filament, whilst class II NPFs lack actin monomer binding regions and instead binds actin filaments (Goley et al. 2004). Thus, class I NPFs activate nucleation, whilst class II NPFs maintain activation (Goley & Welch 2006). In addition to NPFs, ATP is also known to regulate the activity of the Arp2/3 complex.

Class I NPFs

The first class I NPF to be identified was ActA (Welch et al. 1998), a protein required for actin-based bacterial motility. This was then followed by the identification of WASp and WASp-family verprolin-homologous protein (WAVE) (Machesky et al. 1999). Class I NPFs are characterised by their common WCA domain. This domain consists of a WASp-homology-2 (WH2 or W; also called verprolin-homology) domain that binds to G-actin in a manner that enables polymerisation onto the barbed end of a growing filament. This W domain is essential to deliver the first actin monomer to the Arp2/3 subunits (discussed further in 1.3.1) ACTR2 and ACTR3 dimer to form the actin nucleus, which triggers the elongation of the daughter filament. The central (C, also called cofilin-homology or connector) and acidic (A, both regions together are known as CA) regions mediate binding to Arp2/3 (Egile et al. 2005).

Scar, a WASp-related protein, enhances nucleation by the Arp2/3 complex with pre-formed actin filaments, abolishing the spontaneous actin polymerisation lag (Machesky et al. 1999). Machesky et al. discussed the dendritic nucleation hypothesis whereby the association of Arp2/3 with Scar and the side of an actin filament activates nucleation of a new actin filament (Machesky et al. 1999). The association of the Arp2/3 complex with Scar and the side of an actin filament activates nucleation of a new actin filament, which is capped at its pointed end by the Arp2/3 complex and which grows in the barbed direction as a branch of the older filament (Machesky et al. 1999). These results suggested that Scar is likely an endogenous activator or actin polymerisation, different to the inputs of NPFs.

Class II NPFs

Similar to class I NPFs, class II NPFs contain an Arp2/3 binding acidic region, however they lack a G-actin binding region. Instead, they contain an F-actin-binding region that is required to maintain the activation of Arp2/3 (Goley & Welch 2006). Compared to Class I NPFs, Class II NPFs are considered weak Arp2/3 activators (Ammer & Weed 2008; Goley & Welch 2006). It is thought that the mechanism by which class II NPFs activate Arp2/3 might involve a capability to promote the association of Arp2/3 with F-actin. Cortactin, a class II NPF, (Weaver et al. 2001) remains associated with the complex at the branch point (Ammer & Weed 2008), inhibiting branch dissociation (Weaver et al. 2001). Other class II NPFs include F-actin-binding protein 1 (Abp1) and Pan1. Abp1 strongly accumulates at the dynamic leading edge of moving and spreading cells where it colocalises extensively with the Arp2/3 complex (Pinyol et al. 2007). This is dependent on *de novo* actin polymerisation and controlled by signalling cascades, such as activation of Rho-type GTPases (Pinyol et al. 2007).

ATP/ Phosphorylation

ACTR2 and ACTR3 have a nucleotide-binding cleft positioned between subdomain 2 and 4, allowing for binding to ATP. Upon ATP binding, no structural changes take place in ACTR2, whereas subdomain 4 of ACTR3 moves closer to subdomain 2, causing conformational changes that propagate throughout the entire complex (Dayel et al. 2001). The subtle conformational rearrangement of the Arp2/3 complex upon interaction between ATP and ACTR3 is essential to increase the affinity of the complex for the WCA domain by an order of magnitude (Nolen et al. 2004). It is thought that hydrolysis of this ATP could be used to perform work, to provide a signal, or, like the guanine triphosphate (GTP) bound to the α subunit of tubulin heterodimers, may simply stabilise a protein fold. Conventionally, ATP hydrolysis is a timing mechanism that provides a timing mechanism for WASp to release the newly formed branch (Figure 1-8). ATP hydrolysis on the Arp2/3 complex is stimulated by interaction with a single actin monomer and that the interaction is coordinated by the VCA (the Arp2/3-activating region of WASP-family proteins). In this model, the Arp2/3 complex remains associated with the actin filament.

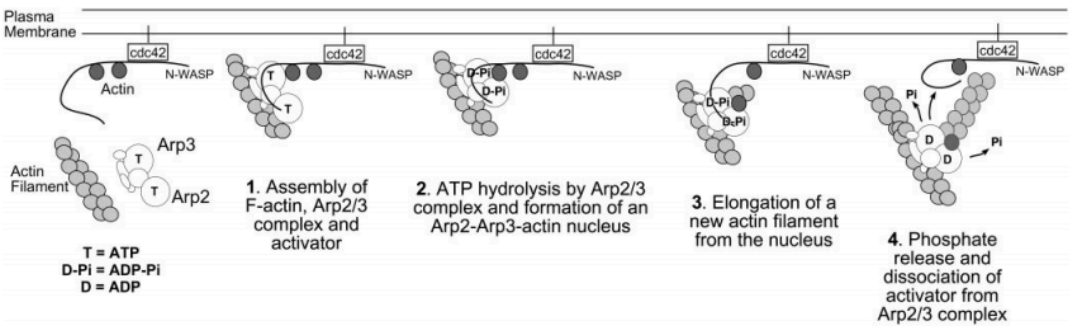

Figure 1-8 Model for the role of the Arp2/3 complex nucleotide binding and hydrolysis in the formation of new actin filaments. 1) The Arp2/3-ATP bound complex binds to the activator, N-WASP, with high affinity. Binding N-WASP brings the actin monomer attached to the WH2 domain of N-WASP in contact with the Arp2/3 complex and this stimulates ATP hydrolysis. 2) ATP hydrolysis to ADP-Pi causes a conformational change on the complex forming a stable nucleus among Arp3, Arp2, and the conventional actin monomer. 3) Elongation of a new actin filament. 4) Phosphate release from the Arp2/3 complex decreases its affinity for N-WASP and allows the Arp2/3 complex to release its membrane-associated activator (Image from Dayel et al. 2001).

While binding of NPFs has long been considered essential to Arp2/3 complex activity, it has also been shown that phosphorylation of the ACTR2 subunit is necessary for Arp2/3 complex activation (Narayanan et al. 2011). Phosphorylation of ACTR2 induces conformational changes permitting activation, and this modification causes reorientation of ACTR2 relative to ACTR3 by destabilising a network of salt-bridge interactions at the interface of the ACTR2, ACTR3, and ArpC4 subunits. Furthermore, recent work has shown that Nck-interacting kinase interacts with the Arp2/3 complex and phosphorylates it to allow activation and increased actin filament assembly (LeClaire et al. 2015). This possibly represents another level of regulation of Arp2/3 complex activity by NPFs. In this framework, Arp2/3 appears to function as a coincidence detector, requiring both NPF binding and phosphorylation of ACTR2 for increased activity (LeClaire et al. 2015).

There are also other regulators of the Arp2/3 complex such as the glial maturation factor (GMF) that was recently reported to bind directly to the Arp2/3 complex to

inhibit nucleation and disassemble branches (Luan & Nolen 2013). Luan and Nolen found that GMF binds the barbed end of ACTR2, overlapping with the proposed binding site of WASp-family proteins.

1.3.1.3 Cellular function of the Arp2/3 complex

The nucleation of branched actin filaments by the Arp2/3 complex plays an important role in many cellular processes including lamellipodial protrusion, phagocytosis, endocytosis, vesicle and organelle motility, and exocytosis (Suraneni et al. 2012).

At the leading edge of the lamella, two types of protrusive structures are observed; ruffling veil-like lamellipodia and thin, spike-like filopodia (Chhabra & Higgs 2007). Ultrastructural data has shown that lamellipodia are composed of orthogonal arrays of actin filaments with branched actin filaments near the leading edge plasma membrane, whereas filopodia contain parallel bundles of actin filaments (Chhabra & Higgs 2007). Elongation at the barbed ends of actin in lamellipodia and filopodia is thought to produce the protrusive force for leading edge advancement (Pollard & Borisy 2003; Bugyi & Carlier 2010). Protein factors regulating actin polymerisation at the leading edge are thus key components of the molecular machinery driving cell motility. The Arp2/3 localises close to the leading edge of lamellipodia (Kelleher et al. 1995) and organises actin into Y-branched networks (Machesky et al. 1999) mediated by the Scar/WAVE complex. Once the Scar/WAVE complex has been recruited at the leading edge, Src-mediated Abl activation results in the phosphorylation of WAVE, which promotes the activation of the Scar/WAVE complex (Sossey-Alaoui et al. 2007). Debranching and bundling of Arp2/3 complex–nucleated actin filaments is thought to be a major pathway for filopodia formation (Svitkina & Borisy 1999).

Arp2/3 complex dysfunction may also be associated with human disease, in particular, cancer metastasis, which relies on the capability of cancer cells to migrate away from primary tumours and invade healthy tissues (Wang et al. 2005; Moulding et al. 2007). Cancer-cell invasion into tissues also requires the formation of actin-rich structures such as podosomes and invadopodia that have adhesive and protrusive

activities and promote the degradation of the extracellular matrix. As the activation of the Arp2/3 complex is required for podosome formation (Linder et al. 1999) as well as lamellipodial formation, the Arp2/3 complex and its regulators have emerged as potential targets for therapeutic intervention.

1.3.2 Formins

Formins are large, 120-220kDa, highly conserved proteins that have essential roles in remodelling the actin and microtubule cytoskeletons to influence eukaryotic cell shape and behaviour (Hetheridge et al. 2012). There are seven known subfamilies of mammalian formins: DAAM, delphilin, Diaphanous related formins (DRFs), FHOD, FMN, FMNL, and INF. The term 'formin' was introduced in 1990 to describe protein products of the *limb deformity* gene in mice that were suggested to play a role in the formation of several organ systems (Maas et al. 1990). Shortly after this, the product of the *Drosophila gene diaphanous*, which was shown to be required for cytokinesis, was found to be homologous to the formin protein (Castrillon & Wasserman 1994). The effect of formins on actin polymerisation was first recognised in the yeast homologue Bni1 (Woychick et al. 1990), and GTPases of the Rho family were identified as activators of formin function (Watanabe et al. 1997). In this literature review, I will focus on the Dia subfamily of formins, in particular Diaph1, due to its prominence in my project.

1.3.2.1 Diaph1 domain architecture and actin nucleation ability

Formin polypeptides have two major functional regions: the 'regulatory' region, and the 'active' region. The C-terminal active region includes the formin homology 1 (FH1) and formin homology 2 (FH2) domains, the defining element of this protein superfamily (Figure 1-9). Many formins (diaphanous-related formins) also have a Dia-autoregulatory domain (DAD).

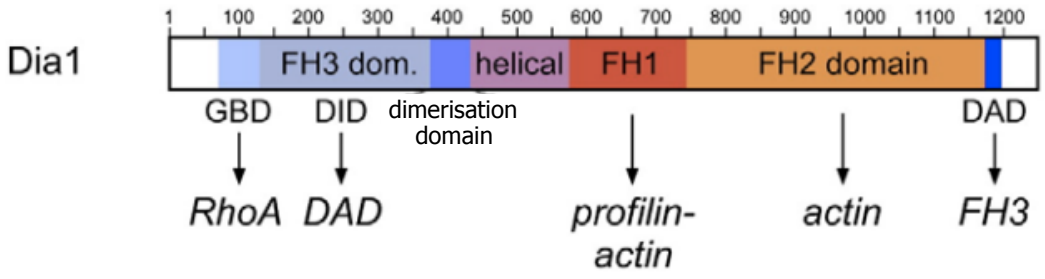

Figure 1-9 Modular domain architecture of human Diaph1. A schematic view on the domain composition as derived from structural analysis and computational prediction. The structural assembly of Diaph1 includes a number of domains: formin homology 1 (FH1), 2 (FH2) and 3 (FH3) domains, the GTPase-binding domain (GBD), the Diaphanous inhibitory domain (DID), a dimerisation domain (DD) followed by a helical region, and the C-terminal Diaphanous autoregulatory domain (DAD). Interaction partners are indicated by arrows below the bar diagram. The intramolecular interaction between the DAD and FH3 domain leads to autoinhibition of the formins (Image from Schönichen & Geyer 2010).

The FH1 domain lacks a secondary structure, and contains binding sites for profilin-actin complexes, acting to increase the local concentration of G-actin around the filament barbed end (Nezami et al. 2006). All formins contain an FH2 domain, a ~400 amino acid long structure located at the C-terminal that binds G- and F-actin directly to nucleate actin filaments (Zigmond 2004). The FH2 domain forms a doughnut-shaped dimer that encircles the F-actin barbed end and is only functional in a dimeric state (Romero et al. 2004). Profilin influences both FH2 mediated nucleation of new filaments and elongation at the barbed end. It is thought that the FH1 domain could provide profilin–actin complexes in a pre-oriented conformation, which would increase the elongation rate (Schönichen & Geyer 2010). The FH2 domain remains bound to the barbed end of the nascent actin filament leading to linear actin filaments through stabilising polymerisation (Zigmond et al. 2003). Once a filament is nucleated, the dimeric FH2 domain moves progressively with the growing barded end (Shekhar et al. 2015), whilst permitting new monomer addition (Pruyne et al. 2002). Overall, formins govern both nucleation and elongation phases.

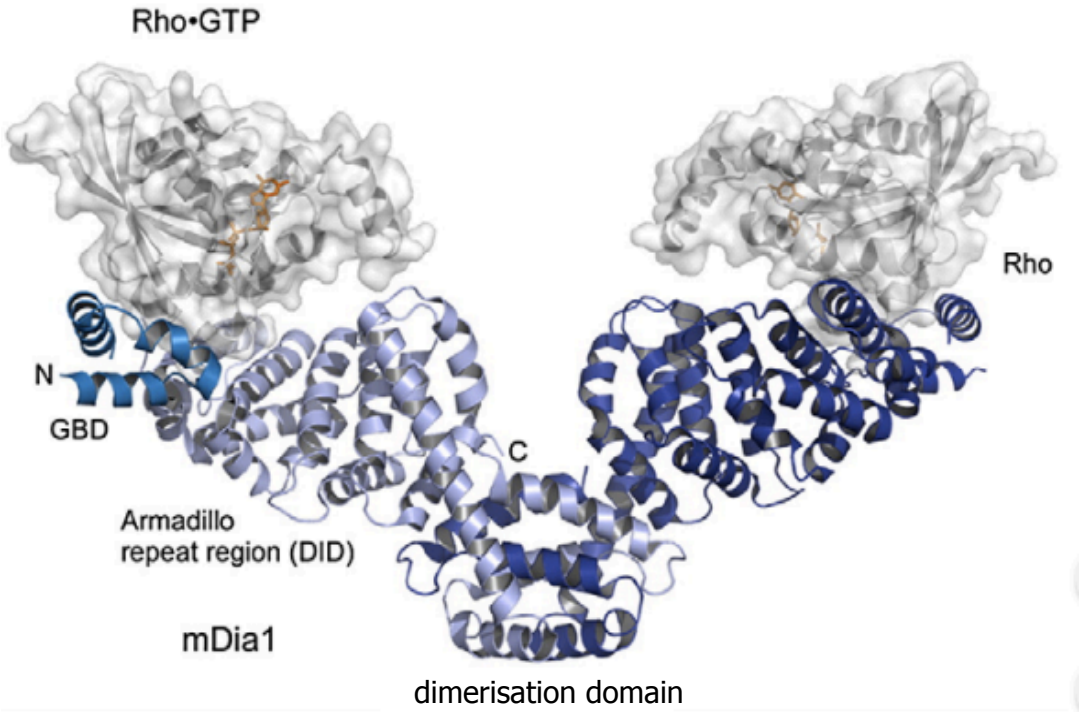

Figure 1-10 Structure of the N-terminal regulation domains of Diaph1 (mDia1) in the dimer conformation. At the N-terminus, the GTPase-binding domain (GBD) is linked to the FH3 domain, while the C-terminus (consisting the DID armadillo repeat region) leads into a dimerisation subdomain in Diaph1. This dimerisation domain is formed by three α-helices, two of which from each monomer form a tightly intertwined four helical bundle. Adapted from (Image from Schönichen & Geyer 2010).

Located at the N-terminal, the FH3 domain is the least conserved module of mammalian formins and is involved in formin regulation. First described by Petersen et al. the FH3 domain is described as the DAD recognition domain. Typically, the DAD-DID interaction mediates autoinhibition, strongly inhibiting actin assembly by the FH1 and FH2 domains (Nezami et al. 2006). Diaph1 exhibits an all-helical armadillo repeat fold consisting of five repeats, with the concave site of the armadillo repeat structure forming the recognition surface for the C-terminal DAD motif (Figure 1-10) (Schönichen & Geyer 2010). The C-terminal DAD domain is composed of two signal sequences that are recognised by the FH3 domain, leading to an autoinhibition of the formin. The GTPase-binding domain (GBD) precedes the FH3 domain at the N-terminus, with a role in interacting with GTPases of the Rho

family (Watanabe et al. 1999) such as Rho, Rac and Cdc42. The central part in between the FH3 and FH1 domain appears helical, however its function and detailed structure is still unknown (Schönichen & Geyer 2010). In terms of actin nucleation, it has been reported that Diaph-mediated assembly of cortical actin is substantially faster than average, whilst Arp2/3-mediated assembly is substantially slower (Kovar et al. 2006; Romero et al. 2004).

1.3.2.2 Regulation of Diaph1

Formin activity is regulated through a succession of stages. The inactive 'resting' state is maintained through the DAD-DID autoinhibition (Chesarone et al. 2010). Release from this inhibitory state occurs through activation by Rho GTPases. Although Rho proteins help disrupt DAD-DID interactions and promote actin assembly, they likely do not stay associated with formins throughout their active period as this would require unrealistically high concentrations of Rho proteins compared to their measured concentrations (Seth et al. 2006). This suggests that RhoGTPase interaction with formins is transient and that other factors are involved in activating formins or maintaining them active. It has been reported that post-translational modifications (such as phosphorylation), interactions with nucleation promoting factors such as Flightless-I (Higashi et al. 2010), IQGAP1 (Brandt et al. 2007), and/or recruitment by the Abelson interactor 142 (Abl1, a component of the WAVE complex) may work together with Rho to activate Diaph1 and maintain it active by stabilising its relieved open conformation (Figure 1-11). On the other hand, NCKIPSD has been reported as a negative regulator of formins (Eisenmann et al. 2007). Detailed interactions with NPFs will be discussed in 1.4.

The opening of the DAD-DID domain leaves the DID domain bound to the plasma membrane, allowing the FH2 domain and adjacent DAD to initiate actin assembly. The conformational change induced by the DAD release is thought to provide the flexibility in the FH2 dimer assembly that allows actin binding and the stair-stepping actin polymerisation mechanism (Schönichen & Geyer 2010). The FH2 dimer creates an environment that favours actin monomer addition to generate actin filaments. It remains bound to the barbed end of the nascent actin filament whilst new actin subunits are rapidly added. This elongation step is further accelerated by

the involvement of the FH1 domain, which recruits and delivers profilin-actin complexes to the growing barded end. Finally, the formin and attached actin filament dissociate from the membrane allowing the actin filament to become incorporated into an actin network (Chesarone et al. 2010).

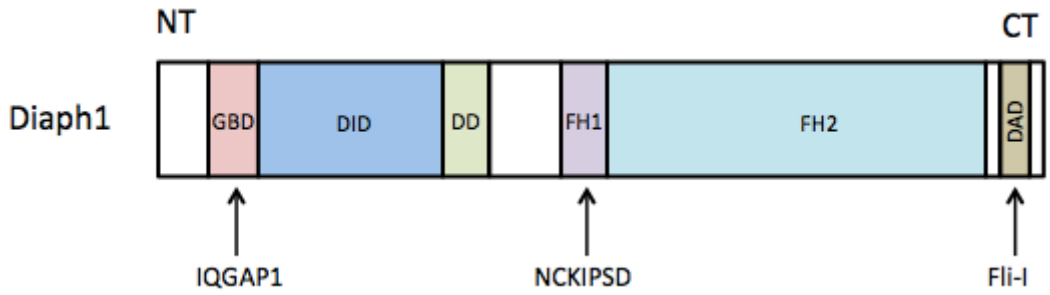

Figure 1-11 Proposed mechanisms of Diaph1 interaction with NPFs. The structure of Diaph1 includes a GBD, DID and DD (dimerisation domain) domain at the N-terminal; an FH1, FH2 and DAD domain at the C-terminal. Interaction of Diaph1 with **FliI** involves the binding of FliI to the C-terminal region of Diaph1 to support the relief of inhibition by RhoA and enable actin filament nucleation. Interaction of Diaph1 with **IQGAP1** involves the binding of IQGAP1 to the N-terminus GBD domain of Diaph1. The interaction of Diaph1 and **NCKIPSD** is not well studied, however it is believed that NCKIPSD binds to the FH1 region of Dia-related formins and acts to negatively regulate them.

1.3.2.3 Cellular functions of formins

Formin family proteins are well known regulators of actin cytoskeletal dynamics during cell division and migration, and are reported to play important roles in immunity and development.

During cell division, changes in cell morphology, chromosome segregation, and vesicular trafficking are all fundamental events that are governed by dynamic cytoskeletal remodelling, with formins playing a central role in generating actin networks (DeWard et al. 2010). The process of cytokinesis requires the formation of an actin-rich contractile ring that constricts to induce plasma membrane invagination. Here, formins, nucleate and elongate F-actin for the cytokinetic ring (Bohnert et al. 2013). Completion of cytokinesis is marked by abscission of the daughter cells. In

particular, Diaph1 has been shown to localise to the spindle and midbody (Tominaga et al. 2000) in dividing HeLa cells. It has been shown that depletion of Diaph1 results in cytokinetic failure due to the perturbation of actin cortex stability during mitosis (Bovellan et al. 2014). Furthermore, the generation of Diaph1-depleted cells is thought to contribute to cancer initiation and progression (Ganem et al. 2007). Formins control adherent cancer cell migration and invasion by assembling actin-rich protrusive structures and stabilising microtubules (Bartolini et al. 2008). Formins perform similar functions in immune cells, with studies from Diaph1 knockout mice showing that they also play a role in immune cell proliferation (Sakata et al. 2007). In prostate cancer cells, the formin Diaph3 was shown to control microvesicle formation, which could lead to oncogenic signal transmission to nearby cells (Di Vizio et al. 2009).

Diaph1 has also been implicated in promoting the formation of actin-rich lamellipod protrusions by building F-actin filaments and directing signalling networks at the leading edge of migrating cells (Sarmiento et al. 2008). In the context of N-WASp-depleted adenocarcinoma cells, Diaph1 drives actin-enriched cellular protrusions and stress fiber formation in a RhoA-dependent manner (Sarmiento et al. 2008). It was shown that Diaph1 knockdown inhibited formation of focal contacts, decreased lamellipodial thickness and impeded leading edge dynamics in migrating cells (Zaoui et al. 2008). Furthermore, studies have shown processive actin polymerisation of formins in response to physical stress applied to the cell surface (Higashida et al. 2013).

1.4 Nucleation promoting factors

NPFs play a key role in controlling the assembly of actin networks nucleated by the Arp2/3 complex and Diaph1 (Campellone & Welch 2010). I have focused my literature review on four NPFs that are relevant to my project: Flightless-I, IQGAP1, NCKIPSD and the WAVE complex.

1.4.1 Flightless-I

The flightless I (Fli-I) protein is a member of the gelsolin family (Campbell et al. 1993). In addition to the gelsolin domain, an actin binding domain, Fli-I contains leucine-rich repeats (LRR) at its N-terminus, involved in protein interactions. Fli-I has been associated with linking the actin cytoskeleton to signal transduction pathways (Claudianos & Campbell 1995). In particular, Higashi *et al*. demonstrated that Fli-I positively regulates linear actin assembly mediated by Diaph1 via two mechanisms (Higashi et al. 2010). Firstly, Fli-I binds directly to Diaph1 and enhances its intrinsic actin polymerisation activity by recruiting actin monomers to the Diaph1 FH1-FH2 domains (Figure 1-11), elevating the F-actin assembly activity (Figure 1-12). Secondly, Fli-I assists RhoA in disrupting the DID-DAD interaction. This dual function was demonstrated for both Diaph1 and dishevelled associated activator of morphogenesis 1 (Daam1), both diaphanous-related formins. It is currently unknown how this interaction is biologically relevant.

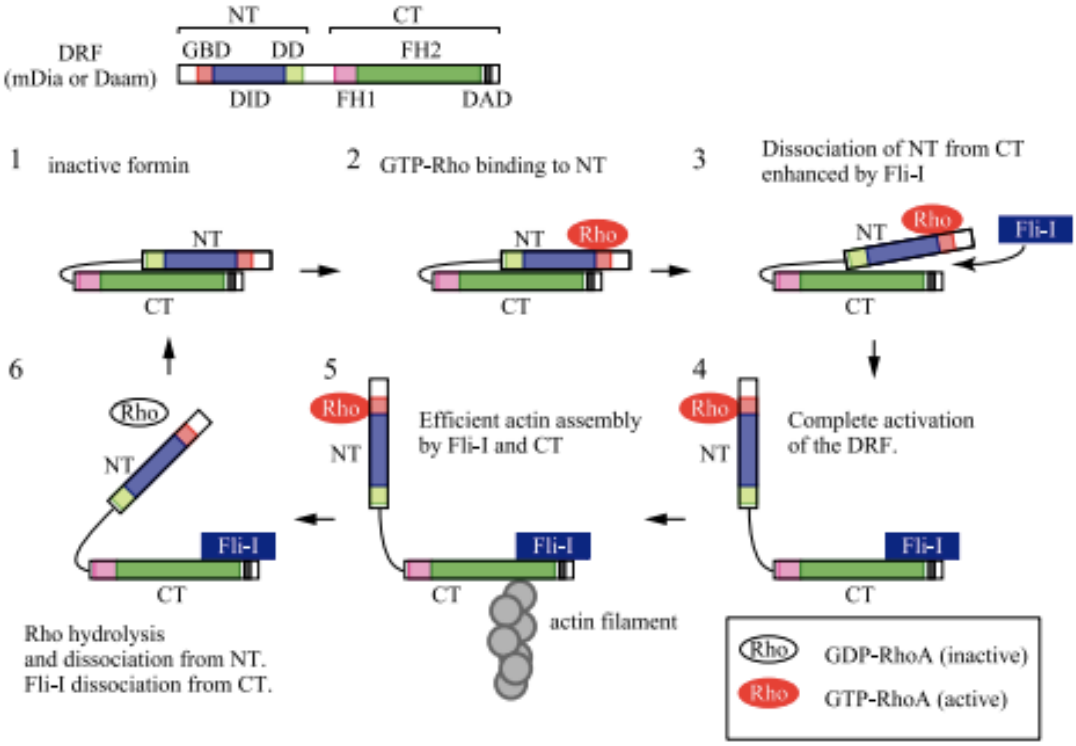

Figure 1-12 Model for the regulation of Diaphanous-related formin (DRF)-mediated assembly by Rho and Fli-I. 1) Without GTP-Rho, DRF is kept inactive through the autoinhibitory DID-DAD interaction. 2) Upon GTP-Rho binding, the

DID-DAD interaction becomes partially perturbed. 3) Subsequent Fli-I binding to the DAD segment competitively accelerates the dissociation of the DID domain from the DAD segment. 4) The disruption of DID-DAD interaction results in the exposure of the FH1-FH2 domains. 5) The FH1- FH2 domains assemble the actin filaments in cooperation with Fli-I bound to the DAD segment. 6) Inactivation of Rho by GTP hydrolysis results in the dissociation of GDP-Rho from the GBD domain, and Fli-I is released from the DAD segment, leading to inactivation of DRF by re-association of the DID domain and the DAD segment (Image from Higashi et al. 2010).

1.4.2 IQGAP1

IQGAPs are actin-binding proteins that scaffold a plethora of molecules to modulate many cellular functions such as cell-cell adhesion, transcription, cytoskeletal architecture, and selected signalling pathways (Roy et al. 2005). IQGAP1, first described in 1994 (Weissbach et al. 1994), is ubiquitously expressed and is the best characterised isoform of the three expressed in mammals (IQGAP1, IQGAP2 and IQGAP3). Structurally, IQGAP1 contains isoleucine-glutamine (IQ) repeats, a GTPase activating protein (GAP) homology domain, a calponin homology (CH) domain, a coiled-coil (CC) domain, a WW domain, and a Ras GAP C-terminus (RGCT) domain (**Figure 1-14**). It is thought that the CH domain directly regulates actin polymerisation; the CC domain and IQ repeats facilitates the binding of IQGAP1 to ERM proteins, connecting components of the plasma membrane to the actin cytoskeleton (Liu et al. 2014; Nammalwar et al. 2014); and the GAP domain interacts, recruits and stabilises some Rho family GTPases (Casteel et al. 2012). Thus, IQGAP1 scaffolding allows regulators of actin organisation such as Cdc42 and Rac1 to be placed in close proximity to where actin filaments dock at the plasma membrane enabling tight spatial control of actin dynamics directly at the plasma membrane (Nammalwar et al. 2014; Jacquemet & Humphries 2013). This link to the Rho family proteins and the membrane supports the role of IQGAP1 as a cortical protein (Ramalingam et al. 2015).

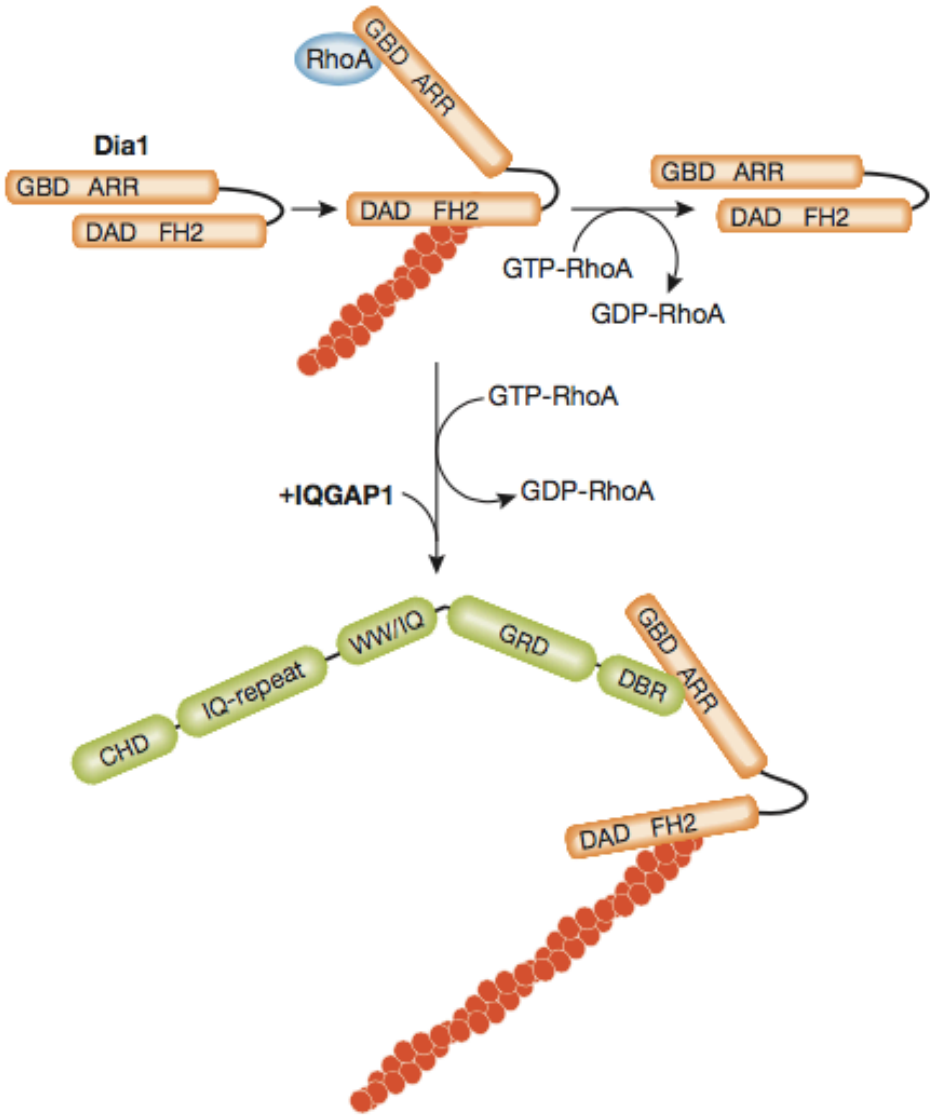

Figure 1-13 Model of IQGAP1-dependent regulation of Diaphanous 1. GTP-bound RhoA relieves autoinhibition of Dia1 (orange) between the diaphanous autoregulatory domain (DAD) and the armadillo repeat region (ARR). RhoA- GTP is rapidly hydrolysed. In the presence of IQGAP1 (green), the ARR of Dia1 binds to the diaphanous binding region (DBR) of IQGAP1 and stabilises Dia1 in its active conformation. CHD, calponin homology domain; FH2, formin homology 2; Dia1, Diaphanous 1; GBD, GTPase-binding domain; GRD, Gap related domain; IQGAPs, proteins containing calmodulin-binding IQ motifs and with homology to GTPase activating proteins (GAPs); WW, domain with two conserved Trp (W) residues (Image from Brandt et al. 2007).

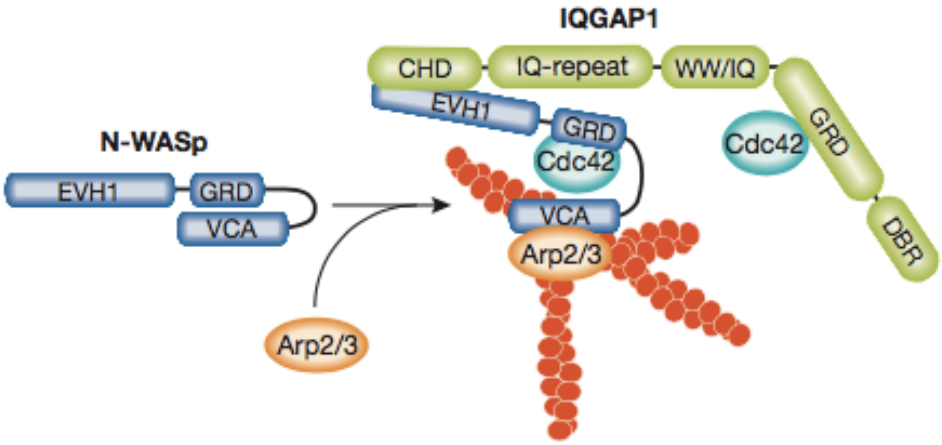

Figure 1-14 Model of IQGAP1-dependent regulation of N-WASp and Arp2/3. N-WASp (dark blue) is shown in its autoinhibited conformation. IQGAP1 (green) and GTP-Cdc42 bind to N-WASp to relieve autoinhibition. The open conformation of N-WASp stimulates the Arp2/3 complex and promotes branched actin filament polymerisation. In addition, IQGAP1 might also support the open conformation of N-WASp through stabilisation of active Cdc42. Arp2/3, actin related protein 2/3; CHD, calponin homology domain; DBR, diaphanous binding region (154 amino acids); EVH1, Ena/VASP-homology 1; GRD, Gap related domain (408 amino acids); IQGAPs, proteins containing calmodulin-binding IQ motifs and with homology to GTPase activating proteins (GAPs); N-WASp, neural-Wiskott–Aldrich syndrome protein; VCA, verprolin-connecting-acidic domain; WW, domain with two conserved Trp (W) residues (220 amino acids) (Image from Brandt et al. 2007).

Regulation of the cytoskeleton was one of the earliest recognised functions of IQGAP1. Numerous studies have suggested a role for IQGAP1 in actin dynamics, cell adhesion, remodelling of the actin network, and organisation of the microtubule network, although its specific role is not completely understood. Once activated, possibly through phosphorylation (Grohmanova et al. 2004), IQGAP1 acts as a master regulator for localised F-actin assembly through two scenarios: the N-WASp-Arp2/3 pathway and the Diaph1 pathway (**Figure 1-14**). In the first case, it is believed that IQGAP1 and Cdc42 bind in synergy to N-WASp to relieve its autoinhibition (**Figure 1-16**A) (Le Clainche et al. 2007). The open conformation of N-WASp simulates the Arp2/3 complex and promotes branched actin filament polymerisation. In the second mechanism, IQGAP1 directly binds Diaph1 to stabilise

the RhoA-mediated release of autoinhibition and allow linear actin assembly (Brandt et al. 2007). It is currently an open question as to why IQGAP1 appears to have direct control of the two most potent actin nucleators that generate structurally different actin filament networks. Furthermore, IQGAP1 has been shown as necessary for Diaph1 leading edge localisation (Brandt et al. 2007), which has been implicated in stabilising microtubules at the cell front (Wen et al. 2004). Thus, IQGAP1 may also act as a facilitator of communication between the filamentous actin and the microtubule networks.

It has also been shown that IQGAP1 regulates actin assembly by capping its barbed ends (Pelikan-Conchaudron et al. 2011). IQGAP1 can also bind directly to actin to promote cross-linking of actin filaments through its CHD domain, in a fashion similar to other actin-cross-linking proteins such as filamin and α-actinin (Kimura et al. 1996).

IQGAP1 is also critical for the formation and contraction of the actomyosin ring in dividing yeast cells by localising to the bud neck in anaphase (Shannon & Li 1999). Adachi et al. reported a cytokinetic block with the knockdown of IQGAP1 (Adachi et al. 2014). IQGAP1 has also been shown to localise to the basolateral membrane of epithelial cells to correctly orient the mitotic spindle (Bañón-Rodríguez et al. 2014). Overall, it appears that IQGAP1 has a large inventory of binding partners and hence, its involvement in cellular processes is manifold.

1.4.3 NCKIPSD

NCK-interacting protein with SH3 domain (NCKIPSD), also known as SPIN90, WISH, and Dia-interacting protein (DIP), is a poorly understood actin regulator that is composed of a Src homology 3 (SH3) domain, proline-rich motifs, and a serine/threonine- rich region (LRR). Similarly to IQGAP1, NCKIPSD has been shown to regulate actin filament assembly through Arp2/3 (Dae et al. 2006) and formins (Eisenmann et al. 2007).

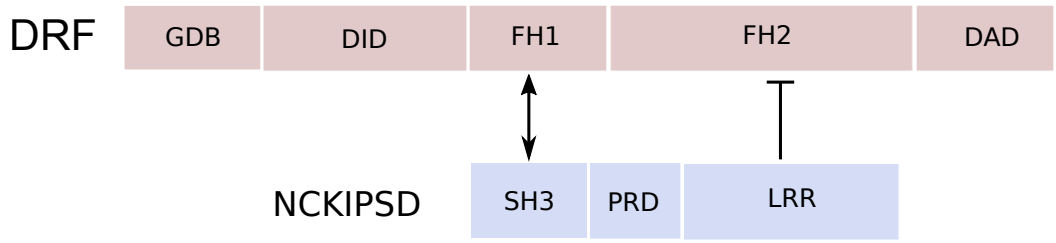

Figure 1-15 NCKIPSD domain architecture. NCKIPSD interacts with the FH1 domain of Diaphanous related formins (DRFs) via the SH3 domain (54 amino acids), and is also thought to interact with and inhibit Diaph3-mediated filament assembly via LRR domain mediated inhibition of the FH2 domain. GDB, GTPase-binding domain; DID, Diaphanous-inhibitory domain; FH1, formin homology 1; FH2, formin homology 2; DAD, Dia-autoregulatory domain; PRD, proline-rich domain (76 amino acids); LRR, leucine-rich domain (123 amino acids).

Wagner *et al*. demonstrated that NCKIPSD directly activates the Arp2/3 complex without the requirement for binding to mother filaments (Wagner et al. 2013). Once bound, NCKIPSD stimulates steric changes to allow ACTR2 and ACTR3 to come into close proximity and activate filament nucleation, stimulating formation of the short-pitch conformation. Wagner *et al*. demonstrated that this distinct NCKIPSD-activated Arp2/3 complex produced many short, linear filaments that did not branch, instead of the characteristic branched networks normally nucleated by the Arp2/3 complex when it is activated by WASp or WAVE (Wagner et al. 2013). Thus, NCKIPSD-mediated activation of the Arp2/3 complex may not require mother filaments, acting as a mechanism to provide seed filaments for network assembly (Figure 1-16**B**) (Wagner et al. 2013). Intriguingly, NCKIPSD has also been shown to bind to N-WASp and activate Arp2/3 independently of Cdc42 (Fukuoka et al. 2001). In this study, NCKIPSD instead of Cdc42 also activates actin polymerisation to the level induced by Cdc42, through binding of WASP via its SH3 domain. This contradicts the direct binding to Arp2/3 as discussed above, however the interaction of NCKIPSD to activate nucleators isn't well understood, and provides another possible interaction pathway.

The other known NCKIPSD binding partner involves the interaction with Diaph1 (Eisenmann et al. 2007). Eisenmann *et al*. revealed the two following interactions:

Diaph1-FH1 domain binding to NCKIPSD-SH3 domain, and Diaph1-FH2 domain binding to NCKIPSD-LRR domain (Eisenmann et al. 2007). In this study, although NICKIPSD interacted with both Diaph1 and Diaph3, the FH2-LRR interaction was shown to inhibit only Diaph3-dependent filament assembly. This negative regulation suggested a novel role for the control of actin dynamics by NCKIPSD. The authors also studying blebbing as the actin architecture plays a fundamental role in the control of the blebbing and bleb initiation involves local changes in the contractility of the actinomyosin cytoskeleton (Eisenmann et al. 2007). They showed that NCKIPSD-induced blebbing is independent of Diaph1 and Arp2/3, however Diaph3 function is required. Dynamic blebbing is indicative of the integrity of the cell cortex, and is an effective readout of cortical tension, further suggesting the importance of NCKIPSD-mediated actin cortex assembly and polymerisation. Interestingly, this study demonstrated a role for NCKIPSD in the control of both non-branched and branched actin-filament assembly that is mediated by Diaph-related formins and activators of the Arp2/3 complex, respectively (Eisenmann et al. 2007).

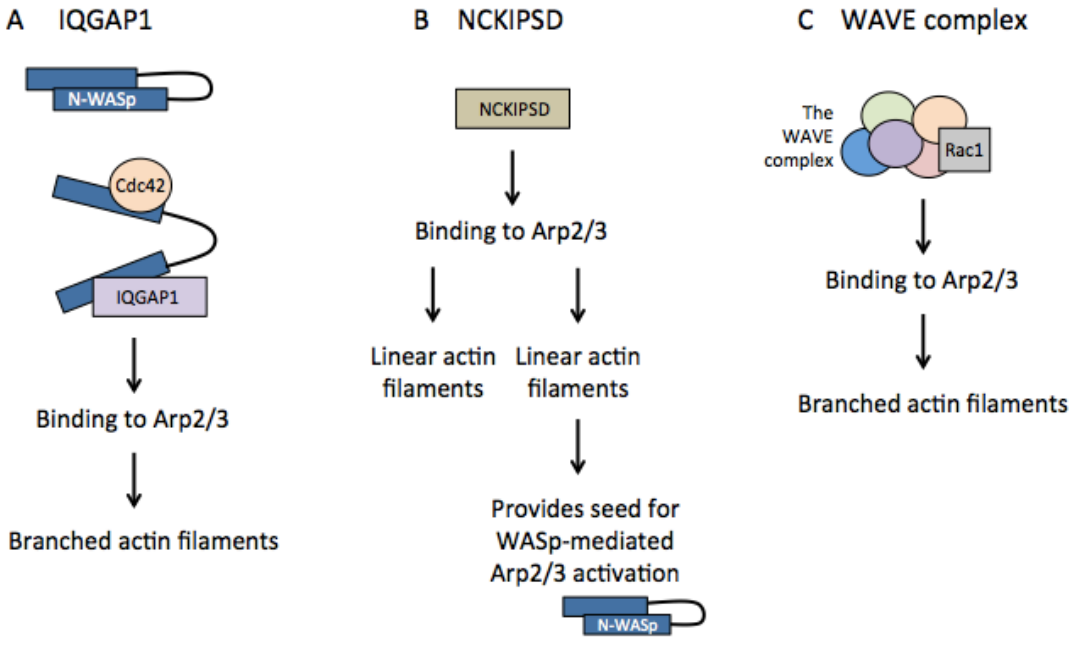

Figure 1-16 Proposed mechanisms of Arp2/3 activation by NPFs. A, Activation of Arp2/3 by IQGAP1 requires the dual binding of cdc42 and IQGAP1 to N-WASp in order to relieve its autoinhibition; N-WASP then activates the Arp2/3 to nucleate

branched actin filaments. **B,** Activation of Arp2/3 by NCKIPSD involves the binding of NCKIPSD to Arp2/3, stimulating the generation of unbranched filaments. This provides seeds for N-WASp-mediated Arp2/3 complex activation. These two processes are independent. **C,** Activation of Arp2/3 by the WAVE complex involves the initial binding of Rac1 to the WAVE regulatory complex (WRC) for activation; the WAVE complex is then recruited to the membrane where it activates Arp2/3 and promotes the nucleation of branched actin filaments.

1.4.4 The WAVE complex

The WAVE complex (also called SCAR) is central to the control of cellular actin dynamics (Chen et al. 2010). The WAVE complex consists of five proteins: Nap1, Abi, Sra1, Wave1 and HSPC300 (Brick1). The WAVE complex is defined by a conserved C-terminal VCA motif that lies on the surface of the Sra1 subunit. It comprises of one or two WASP homology 2 (WH2) domains, which binds to monomeric actin, followed by a short central (C) region and an acidic (A) domain, which interacts with the Arp2/3 complex (Chen et al. 2010). WAVE typically exists in its inhibited state whereby a conserved surface of Sra1 and residues of Wave1 bind the VCA and GTPase binding domain (GBD), to form a 'meander region'. Rac1, a Rho GTPase family member, plays an important role in activating the WAVE complex (Figure 1-16**C**), without disrupting the integrity of the complex, through the binding of the VCA. Another mode of WAVE complex activation is via phosphorylation of the Wave protein subunit by the Abl kinase (Lebensohn & Kirschner 2009). Together, Rac1 activation and phosphorylation are thought to destabilise the meander region and its interactions with Sra1, leading to the release of the VCA domain of Wave1 from its interaction with Sra1 and Nap1 and subsequent activation of the WRC (Chen et al. 2010). Once activated, the WAVE complex is able to activate the Arp2/3 complex through steric conformational changes (Goley et al. 2004). The C-region (VCA domain) of the WAVE1 subunit subsequently orients the actin monomer for proper interaction with Arp2/3, leading to the nucleation of branched actin filaments (Kelly et al. 2006).

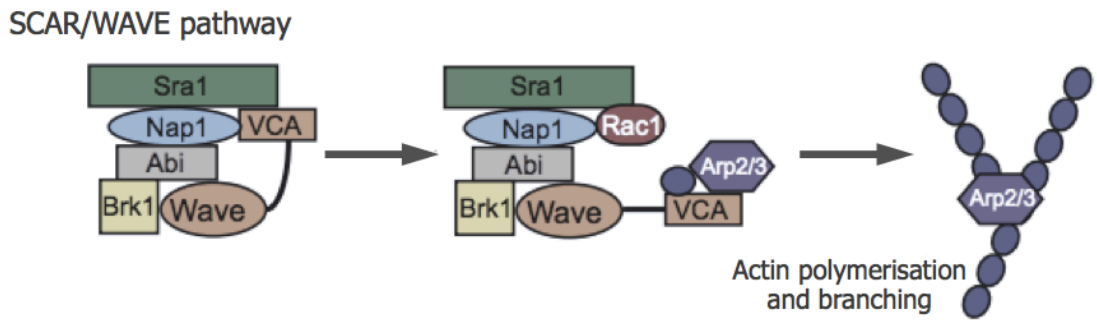

Figure 1-17 The mechanism of SCAR/WAVE mediated Arp2/3 activation. Activation occurs upon binding of the complex to the small GTPase Rac1, releasing the VCA domain of Wave1 to bind to, and activate, the Arp2/3 complex. It has been reported that activated Rac1 alters the conformation of the Scar/Wave complex but does not physically disrupt it. Once active, the Arp2/3 complex is able to initiate actin nucleation and generate dendritic filament networks (Adapted from Abmayr & Pavlath 2012).

The interaction of the WAVE complex with Arp2/3 has been studied extensively. However, a less understood interaction of the Abi subunit with Diaphanous has been suggested as a link for the formation and stability of cell-cell junctions through actin polymerisation (Ryu et al. 2009); these intercellular junctions are important for tissue morphogenesis and signalling. In this research, Abi proteins were shown to colocalise with Diaphanous at cell junctions and interact in the absence of a fully assembled WAVE complex, highlighting their importance in regulating intercellular junctions.

It is well established that GTP-loaded Rac1 induces lamellipodia and membrane ruffles by activating the Arp2/3 complex via WAVE proteins (Ridley 2001; Miki et al. 1998). In accordance, WAVE proteins have been found to accumulate at the tips of these projections (Hahne et al. 2001) where actin polymerisation is thought to be initiated and maintained, providing the propulsive force for membrane extension. WAVE2 has been shown to be essential for formation of lamellipodial structures at the cell periphery stimulated by growth factors (Yamazaki et al. 2005). WAVE has also been implicated in driving myosin-independent cytokinesis, through stabilising the furrow and allowing symmetrical division (King et al. 2010).

1.5 The actin cytoskeleton

First discussed in the 1980s (Small 1988; Bray & White 1988), the actin cortex is a dynamic layer of actin filaments, myosin motors, and actin-binding proteins situated below the plasma membrane (Salbreux et al. 2012). Although an important structure in the cell, far less is known about the cell cortex than about lamellipodia or filopodia. There remains much to investigate about the structure and composition of the cortex, how it assembles actin filaments to allow for the various structural requirements, and how this assembly is regulated. Over the past decade, an increasing number of biological and biophysical investigations have focused on the actin cortex, including my work presented in this thesis.

1.5.1 Functions of the actin cortex

The actin cortex plays a central role in cell motility. Assembly dynamics and contractility of this layer are thought to generate cortical tension, drive cytokinesis, and play a central role in cell locomotion and tissue morphogenesis (Bray & White 1988). On a microstructural level, contractile forces that are coordinated and generated from the actomyosin cortex, powered by the motor protein myosin II (Charras et al. 2006), push the cell edge forward to enable cell migration. Two main modes of force generation are incorporated; polymerisation and branching of actin networks, or pulling forces via the collective actin of myosin motors drawing actin filaments together.

In 2D, cells often migrate by forming lamellipodia at their front. In response to guidance cues in the extracellular matrix (ECM), cells form lamellipodia are a classic example that incorporates both modes of force generation. At the leading edge in the direction of movement, lamellipodium protrusions are generated at the front to extend, and pushes the membrane forward (Tang & Gerlach 2017). As the lamellipodium protrudes, a contractile lamellum, situated immediately behind the lamellipodium is needed for translocation of the cell body and formation of new adhesions to the substrate (Ridley 2011). After this, the rear of the cell detaches from the substrate through contractions of the actomyosin cortex. In this process, the actin cytoskeleton, the intermediate filament network, and microtubules are involved in

the regulation of cell motility. It has also been suggested that crosslinking and bundling of cytoskeletal filaments may generate contractile forces within the cortex, independent of myosin activity (Sun et al. 2010). In 3D matrices, lamellipodial migration is rare and the cells often use either mesenchymal, amoeboid, or blebbing modes of migration (Friedl & Bröcker 2000). Polarised cells moving by blebbing are dependent on cortex formation at the leading edge of the cell (Pinner & Sahai 2008). Finally, it has been shown that, in extracellular matrix gels, cortical contractions help to push the cell nucleus through small constrictions (Lämmermann et al. 2008).

The actin cortex is also a key determinant of cell morphology due to its dynamic plasticity, resulting from the continual turnover and rearrangement of its protein constituents and network (Salbreux et al. 2012). It has been shown that the actomyosin meshwork must dynamically contract, but remain attached to adherens junctions for cell shape change and to propagate forces across the epithelium (Jodoin et al. 2015). F-actin turnover is upregulated and F-actin levels are downregulated in ventral cells that undergo apical constriction in order to promote force balance and apical constriction (Jodoin et al. 2015). Changes in cell shape are necessary for processes such as cell migration, tissue homeostasis and cellular differentiation (Chalut & Paluch 2016) and shape change requires changes in the mechanical properties of the cortex. Mechanical properties such as stiffness and tension of a cell are main determinants that dictate shape change. Following a short deformation, both the plasma membrane and the underlying cortical actin network have been shown to recover their shape (Haase & Pelling 2013b); this resistance to deformation was found to be largely dependent upon the cytoskeleton (Haase & Pelling 2013a). Spatially non-uniform contractile properties in the mother cell have been shown to generate different-sized daughter cells following neuroblast division (Ou et al. 2010), emphasising the importance of the actin cortex in cellular processes.

1.5.2 Actin cortex organisation, assembly and regulation

The actin cortex appears as a dense meshwork of actin filaments when examined by scanning electron microscopy (Figure 1-18) (Charras et al. 2006). Actin filaments exist as bundles, and become part of a network of filaments protruding into the cell interior. This structural organisation provides a framework that supports the plasma

membrane and, therefore, determines a cell's shape (Charras et al. 2006). In bundles, the actin filaments are closely packed in parallel arrays, whereas in a network the actin filaments crisscross, and are loosely packed. In addition to actin, the cortex consists of other accessory proteins, including, nucleators, nucleation promotion factors, actin crosslinking proteins, bundling proteins, cappers, depolymerisers and motor proteins (dos Remedios et al. 2003). Actin is usually attached to the plasma membrane indirectly via ERM proteins. They have a crucial role in organising membrane domains through their ability to interact with transmembrane proteins and the cytoskeleton (Ponuwei 2016). In doing so, they can provide structural links to strengthen the cell cortex and regulate the activities of signal transduction pathways (Fehon et al. 2010).

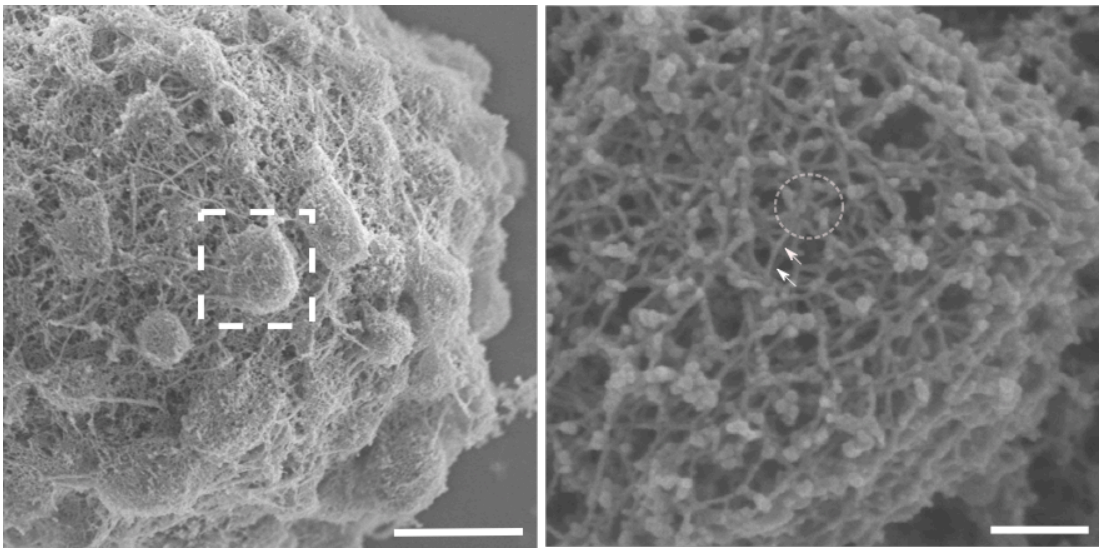

Figure 1-18 Electron micrograph of the actin cytoskeleton of a blebbing M2 cell. Right: enlargement of boxed area on the left hand side. The cortex is formed by a meshwork of actin forming a network, regions of crosslinking and bundling are apparent (circled knot). Filaments can be identified (arrows). Scale: left – 2µm, right – 200nm.

Bovellan *et al*. revealed that two proteins generated the majority of cortical actin: the formin Diaph1, and the Arp2/3 complex (Bovellan et al. 2014). In this study, the authors began by identifying proteins that were highly abundant in the cortex through proteomic analysis on isolated cortices. A subsequent protein knockdown screen revealed that Diaph1 and Arp2/3 contributed a similar amount of F-actin to the

cortex, but had different accumulation kinetics. Further work revealed that filaments with different lengths are present throughout the cortex and these are generated through distinct mechanisms: short-lengths for Arp2/3-nucleated filaments and long-lengths for formin-nucleated filaments (Fritzsche et al. 2016; Bovellan et al. 2014).

It is thought that the small GTPase, RhoA, regulates the cortex (Etienne-Manneville & Hall 2002). This molecular switch is the most studied cortical regulator, and has been reported to orchestrate the behaviour of cells through its interaction with proteins involved in actin polymerisation and myosin II recruitment (Charras et al. 2006). RhoA activity has been linked to the regulation of morphogenesis, migration, cell division, adhesion and microtubule dynamics (Jaffe & Hall 2005). In addition to this, recent data has shown that RhoD, a GTPase, antagonises the function of RhoC, also a GTPase, which represents an example of crosstalk, whereby the action of one GTPase regulates the activity of another to regulate the cortex (Durkin et al. 2017).

It has also been demonstrated that epidermal growth factor receptor kinase substrate 8 (Eps8) and ezrin are important regulators of rapid actin reassembly for the initiation and retraction of protruded blebs (Aoki et al. 2016). In the expansion phase of membrane blebbing, Rnd3 and p190B–Rho–GAP inhibit the activation of RhoA. As the protruded membrane areas become enlarged, the relative concentration of Rnd3 decreases. Sporadic activation of RhoA leads to ROCK phosphorylation of Rnd3 and removal of p190B–Rho–GAP from the membrane. Thus, RhoA activation is amplified and sustained by the positive-feedback loop. ROCK also phosphorylates ezrin and activated ezrin recruits, which leads to reassembly of the actin cortex (Aoki et al. 2016). Here, it was found that a RhoA–ROCK–Rnd3 feedback loop determined the local reassembly sites of the actin cortex during membrane blebbing.

1.5.3 The actin cortex in blebbing

The lifecycle of a bleb can be subdivided into three steps: nucleation, expansion, and retraction. Bleb nucleation is initiated by an actomyosin-driven increase in intracellular pressure causing the formation of a membrane protrusion (Charras et al. 2005). Two mechanisms have been put forward to explain bleb formation; delamination of the cell membrane from the actin cortex (Charras et al. 2005), or a

rupture of the cellular actin cortex (Paluch et al. 2005). In the case of delamination, it is thought that the initial separation of membrane and cortex is dependent upon the strength and/or quantity of adhesions between the membrane and the cortex via actin-membrane linker proteins i.e. ERM proteins, and their regulators (Charras 2008). ERM proteins are of particular importance in the contractile cortex as they localise to the cell membrane and link the actin cortex to the plasma membrane (Charras et al. 2006).

Once nucleated, the bleb undergoes expansion whereby the surface area and volume of the bleb increases rapidly. This increase in surface area may occur through a number of scenarios: unfolding of membrane folds, inflow of lipids through bleb neck, and tearing of the membrane from the cell cortex (Charras 2008). However, currently the exact mechanism underlying increase in surface area remains unclear. Blebs are devoid of an actin cortex at the beginning of expansion (Charras et al. 2005). Once actin cortex regrowth begins, the ezrin is the first protein to be recruited to blebs. This is followed by the sequential recruitment of actin, actin-bundling proteins, and contractile proteins such as tropomyosin and myosin. Actin accumulation experiments show that it is likely that the formation of a sufficiently strong actin cortex halts bleb growth (Bovellan et al. 2014). The final stage, retraction, is powered by myosin II contraction (Charras et al. 2006). Myosins are actin-dependent motor proteins that produce movement and force through ATP hydrolysis. They use actin as a track along which to move, usually from the pointed- to barbed-end. During retraction, the bleb membrane and the newly formed actin cortex crumples and the membrane returns to its retracted position.

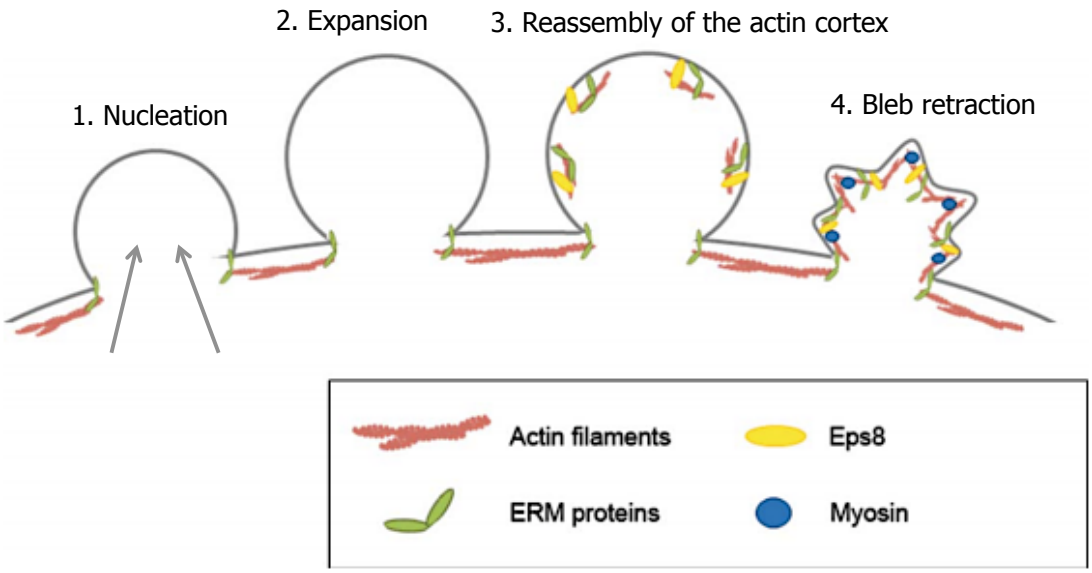

Figure 1-19 The lifecycle of a bleb. Membrane blebs are formed when the plasma membrane is detached from the actin cortex (1) by an increase in intracellular pressure or by a local rupture in the actin cortex. After expansion of membrane protrusion (2), ERM family proteins and Eps8 are recruited to the protruded bleb membrane to link the actin cytoskeleton to the membrane. Then, reassembly of actin filaments occurs rapidly by de novo polymerisation mediated by the Arp2/3 complex and Diaph1 (3) and covers the protruded membrane. Finally, myosin is recruited to actin cortex and its motor activity powers retraction (4) (Image from Ikenouchi & Aoki 2016)**.**

1.5.4 The actin cortex in cytokinesis

Cell division in eukaryotic cells is highly complex, involving the coordination of multiple cellular processes and drastic remodelling of the actin cytoskeleton. Before a dividing cell enters mitosis, it undergoes a period of growth called interphase (Bertoli et al. 2013). Around 90 percent of a cell's time in the normal cellular cycle may be spent in interphase. Mitosis consists of four basic phases: prophase, metaphase, anaphase, and telophase. Cell rounding upon entry into mitosis is accompanied by a reduction in the focal contacts and an increase in cortical rigidity (Chugh et al. 2017). After cytokinesis, cells reattach to their substratum and reorganise their cytoskeletal networks for interphase. The concerted changes in cell

shape and adhesion as cells prepare to enter mitosis suggest intense cross-signalling events between focal contacts and cell cycle signalling (Heng & Koh 2010).

Interphase cells enter mitosis, whereby the extensive actin cytoskeleton network is rapidly disassembled and reorganised (prophase to metaphase), resulting in characteristically round cells due to the retraction of cellular protrusions (Heng & Koh 2010). For cells to abandon their spread interphase morphology they must first decrease adhesion to their substrate through the disassembly of focal adhesion complexes (Dao et al. 2009); this occurs in parallel to changes in intracellular osmotic pressure (Stewart et al. 2011). Complete reorganisation of the actin cytoskeleton is also required for mitotic cell rounding. Here, interphase structures, such as stress fibres, are disassembled upon entry to mitosis and actin filaments are recruited to the cortex, directly underlying the plasma membrane (Maddox & Burridge 2003; Kunda et al. 2008). Mitotic spindle formation requires a defined geometric space allowing the cell to become spherical ensuring that all chromosomes are captured quickly at mitosis by bringing them together with spindle microtubules in a small enough space (Cadart et al. 2014). This geometric requirement is a key process necessary for the requirements of division (Luxenburg et al. 2011). This is also accompanied by a reduction in the focal contacts and an increase in cortical rigidity. The actin network is also required in the separation of centrosomes, dependent upon the cortical flow of actin and the myosin network (Rosenblatt et al. 2004; Uzbekov et al. 2002).

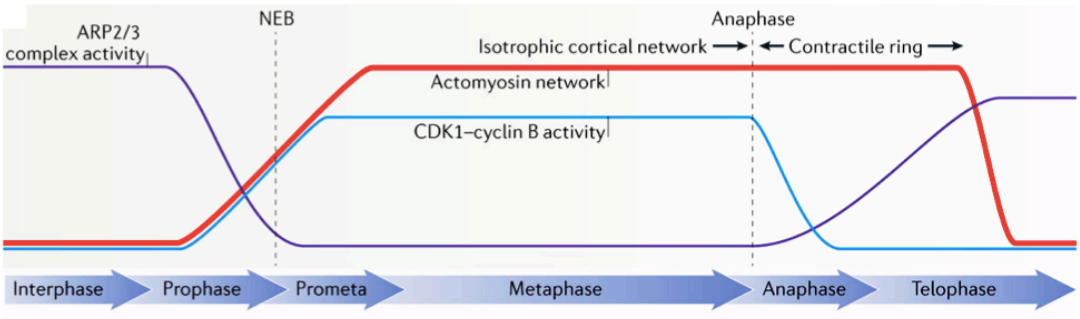

Figure 1-20 Cell shape changes during mitosis. As the levels of CDK1–cyclin B activity rise (blue line), the cell begins the assembly of its cortical actomyosin network (red line); both of these events are accelerated by loss of the nuclear–

cytoplasmic compartment boundary. The cortical actomyosin network that is assembled upon entry into mitosis is largely independent of the activity of the actin nucleator ARP2/3 complex (purple line), which is inhibited at the onset of prophase. At anaphase, this mitotic actomyosin network is remodelled to generate a contractile actomyosin ring at the cell centre. The ARP2/3 complex is then reactivated as cells re-enter interphase. (Image from Ramkumar & Baum 2016)**.**

At the onset of anaphase, the cells elongate, round and rapidly pinch into two by the formation of an equatorial furrow, producing two independent daughter cells (Zhang & Robinson 2005). Actin rearranges and localised to the cleavage furrow, forming part of the contractile ring (Figure 1-21) central to the overall process of cell division, known as cytokinesis. Animal cell cytokinesis is initiated during anaphase, when the decline of cyclin-dependent kinase 1 (CDK1) activity leads to a stabilisation of microtubules and reorganisation of the mitotic spindle (Figure 1-20) (Fededa & Gerlich 2012). Another essential factor in central spindle assembly, Aurora B, ensures tight temporal coordination between chromosome segregation and cytokinesis and is kept active by unsegregated chromatin at the division plane to inhibit abscission until the division plane is cleared of chromatin (Steigemann et al. 2009). It is known that F-actin and the microtubule cytoskeleton coordinate and remodel throughout cell division to allow for changes in cell shape, orientation and positioning (Lancaster & Baum 2014; Evangelista et al. 2002). These successive cell shape modifications require myosin II contraction and exocytosis (Lecuit & Wieschaus 2000).

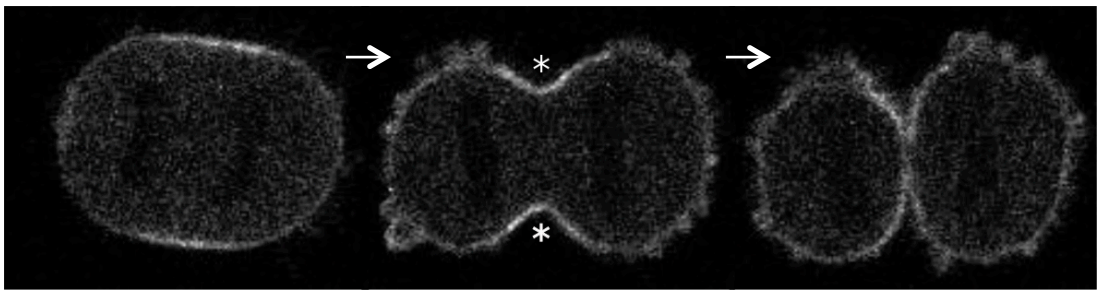

Figure 1-21 Mouse fibroblast cell expressing LifeAct-GFP (F-actin marker) in the process of cell division; images showing anaphase, telophase, and cytokinesis. During anaphase, there is an enrichment of actin prior to furrow formation. At telophase, actin is strongly localised at the cortex forming a contractile

ring (asterisk) at the cleavage furrow. Lastly, in cytokinesis, actin undergoes dynamic rearrangement in all regions of the dividing cell and is strongly localised at the boundary of daughter cell division where actomyosin contraction occurs (Image courtesy of Dr. Priyamvada Chugh and Prof. Ewa Paluch).

During mitosis, the rearrangement of actin is crucial and reliant upon the activity of nucleators and actin-binding proteins. There is a shift in the dominance of different cortical actin nucleators at the onset of mitosis, from the Arp2/3 complex to formins (Bovellan et al. 2014). This is apparent in cells entering mitosis in culture through the loss of Arp2/3-generated actin-based membrane protrusions, lamellipodia (Ibarra et al. 2005). This loss of lamellipodial actin is accompanied by the activation of the formin-based actin nucleator Diaphanous (Rosa et al. 2015), and drives the assembly of a cortical network of actin filaments. Importantly, once activated, through physical association with Rho-family GTPases, Diaphanous generates non-branched actin filaments, suitable for the generation of cortical tension by myosin II minifilaments (Skau et al. 2009).

An intact actin cytoskeleton is important during cell cycle progression. The importance of the cortex in the cell cycle has been extensively studied through the use of drugs that interfere with actin filament turnover in cells. Depolymerisation of actin filaments by toxins such as cytochalasin D and latrunculin B has been reported to delay progression of mitosis in primary cells and fission yeast, suggesting that an intact actin cytoskeleton is required for the efficient onset of mitosis (Lee & Song 2007). In addition, the actin cytoskeleton has been shown to be required for correct biogenesis of the mitotic spindle, a role traditionally reserved for the microtubules. Indeed, studies have shown that spindle assembly is disrupted when actin is depolymerised (Uzbekov et al. 2002) and myosin II is inhibited (Rosenblatt et al. 2004). Some recent observations have suggested that actin and microtubule structures may act synergistically in the assembly and positioning of the mitotic apparatus (Woolner et al. 2008).

The small GTPases belonging to the Rho family are well-known players involved in the regulation and remodelling of the actin cytoskeleton and are crucial for cell motility and morphogenesis (Etienne-Manneville & Hall 2002). Rho GTPases have

been found to regulate cell cycle progression acting at many stages, with two main sites of action: one at the G1/S transition and the other during cytokinesis. RhoA organises the assembly of the contractile ring and induces the actomyosin-driven constriction of the cleavage furrow (Barr & Gruneberg 2007). The activities of RhoA effectors have also been implicated in spindle formation during early mitosis and completion of cytokinesis, participating in the abscission process where daughter cells completely separate (Schmidt et al. 2007). There are a number of other proteins, CDK1, Plk1 and Aurora kinases, which are also actin cytoskeleton regulators, providing further insight into how cell cycle progression can regulate the actin cytoskeleton, and vice versa.

Overall, it appears that the regulation of the actin cytoskeleton and cell cycle are functionally connected. The nature of this functional integration is not well understood, in particular, whether proteins known to regulate the actin cytoskeleton are implicated in cell cycle control.

1.6 Aims

The cortex is a 0.1 to 1 μm thick layer of actin and associated proteins that underlies the cell membrane and determines the shape of animal cells. Whereas the biology of some actin structures (lamellipodia, filopodia) is well understood, the events leading to the formation and subsequent regulation of a submembranous actin cortex are not due to the lack of a good model system. It is essential for cytokinesis, cell locomotion, and tissue morphogenesis, making it an important physical component of the cell.

Prior work in the laboratory has shown that two actin nucleators, Diaph1 and the Arp2/3 complex, generate actin filaments in the cortex. To study actin assembly in the cortex, I aim to use blebs as a model system. I aim to search for regulators, nucleator promoting factors (NPFs), of Diaph1 and Arp2/3 through depletion studies in M2 and HeLa cells. I will examine the role of each NPF identified through localisation studies and impact of depletion upon various markers. The first marker will be bleb size, a reporter of cortical actin assembly. Following this, I will examine changes in F-actin network organisation using scanning electron microscopy (SEM).

SEM will allow for the identification of alterations of the interconnection and density of the network, further suggesting an important role of the particular NPF.

It has also been previously shown that Arp2/3 and Diaph1 depletion has a serious impact upon progression through mitosis and on cell survival. Thus, I will deplete HeLa cells of selected NPFs and study the impact of depletion upon the cell cycle. As an addition, in collaboration with other students, I will also examine how NPFs control properties of cell mechanics.

Chapter 2 Materials & Methods

2.1 Cell Culture

For the initial screen to determine the role of proteins on cortical actin nucleation, I imaged the impact of protein depletion on blebbing. I reasoned that changes in cortical actin nucleation and actin accumulation rate due to nucleator and NPF depletion should be most obvious in blebs because they are initially devoid of F-actin. For this, I used M2 melanoma cells that bleb continuously and have a well-defined cortex. Thus, they are a good model system to study cortex composition and assembly. HeLa cells were subsequently used to investigate the role of regulators of actin nucleator activity during the cell cycle.

2.1.1 M2 cells

M2 cells are derived from a primary human melanoma, lacking in the actin crosslinker filamin A (Cunningham et al. 1992). They were cultured in Minimal Essential Medium growth medium with Earle's salts (MEM, Gibco), supplemented with penicillin/streptomycin antibiotics (Gibco), and 10% of a mix of fetal bovine serum (FBS) (Sigma) and newborn calf serum (Sigma) (20:80). For subculture, cells were washed with phosphate-buffered saline (PBS, Invitrogen), detached from the flask surface using 0.05% trypsin-EDTA (Gibco), centrifuged at 1500rpm for 3min and resuspended into fresh growth medium, split in a 1:5 ratio. Optimal growth conditions were maintained with cells cultivated in a humidified 5% CO_2 incubator at 37^{o}C.

M2 cell lines

A previously established M2 LifeAct-Ruby cell line was used to study the effect of various protein knockdowns and F-actin dynamics (previously established by Dr. Miia Bovellan). LifeAct is a small 17 amino acid peptide that binds exclusively to F-actin, allowing the visualisation and imaging of actin dynamics in cells. It was originally extracted from the Abp140 protein in yeast (Riedl et al. 2008). The M2 LifeAct-Ruby cell line was grown in the presence of 500µg/mL G418 (Calbiochem).

For this project, a number of derivatives of the M2 LifeAct-Ruby cell lines were generated. These stably expressed GFP or BFP and an shRNA targeting ACTR2, ARPC2, Diaph1, Flightless-I, IQGAP1, NCKIPSD, Sra1 and Nap1. For generation of stable knockdown lines, shRNA plasmids were linearised with Ssp1 restriction enzyme (New England Biolabs) and transfected into M2 LifeAct-Ruby cells with Lipofectamine 2000 (see 2.2.1). Transfected cells were selected with 1µg/mL puromycin (Calbiochem) for several weeks while maintaining selection with 500µg/mL G418.

2.1.2 HeLa cells

HeLa cells are immortal human cells derived from a tissue sample taken in 1951 from Henrietta Lacks, a patient with cervical cancer (Syverton & Scherer 1952). HeLa cells were cultured in DMEM (Gibco) supplemented with penicillin/streptomycin and 10% FBS. Cells were subcultured at a ratio of 1:5 and cultivated similarly to M2 cells.

HeLa cell lines

For this project, a number of derivatives of the HeLa cell lines were generated. These stably expressed GFP or BFP and an shRNA targeting ACTR2, ARPC2, IQGAP1, NCKIPSD, Sra1, Nap1, BAIAP2, VANGL1 and MARK2. For generation of stable knockdown lines, shRNA plasmids were linearised with Ssp1 restriction enzyme (New England Biolabs) and transfected into HeLa cells with Lipofectamine 2000 (see 2.2.1). Transfected cells were selected with 1µg/mL puromycin (Calbiochem) for several weeks.

2.1.3 HEK293T cells

Human embryonic kidney cells 293 (HEK293) are a cell line originally derived from the kidney cells of a human embryo (Graham et al. 1977). For my project, HEK293T cells were used for generation of lentiviruses encoding shRNA constructs. HEK293T cells are particularly useful for generation of adenoviruses, retroviruses, and lentiviruses as they are quick and easy to reproduce and maintain, have a high

efficiency of transfection and protein production, and can faithfully translate and process proteins (Stepanenko & Dmitrenko 2015).

HEK293T cells are derived from HEK293 cells but stably express the SV40 large T antigen, which can bind to SV40 enhancers of expression vectors to increase protein production (Yao-Cheng et al. 2014). HEK293T cells were cultured in DMEM (Gibco) supplemented with penicillin/streptomycin and 10% FBS. Cells were subcultured at a ratio of 1:5 and cultivated similar to HeLa cells.

2.1.4 Freezing cells for long-term storage

For long-term storage, cells were frozen and kept in liquid nitrogen. To do this, 75-90% confluent cells were washed once in PBS and trypsinised. Once detached, cells were centrifuged as described above, the supernatant was aspirated and the pellet was resuspended in 'freezing media' (DMEM/MEM + 10% DMSO + 20% FBS). Resuspended cells were aliquoted into 1.5mL cryogenic vials, put into a cell freezer, and stored at -80^{o}C for 24 hours before transferring into liquid nitrogen.

Frozen cells were recovered by thawing at room temperature, diluting in 10mL of fresh medium in a falcon tube before centrifuging for 5 minutes at 1500rpm to remove DMSO. Cells were then resuspended in fresh culture medium and transferred to a flask.

2.2 Transfection

2.2.1 Lipofectamine 2000 (shRNA studies)

Transfections were performed using a liposome-mediated method. Lipid-mediated gene delivery uses lipids to allow a cell to absorb exogenous DNA. Transfer of genetic material into the cell takes place via liposomes, vesicles that can fuse with the cell membrane.

The day before transfection, cells were plated on 6-well plates (35mm well diameter, Corning) and incubated in growth medium. For transfection, two preparatory mixtures were made; (1) cDNA from a miniprep was diluted in 100µL Opti-MEM

(Gibco) and (2) 3µl Lipofectamine 2000 (Invitrogen) was diluted in 100µL Opti-MEM. Miniprep cDNA purification was done according to manufacturer's instructions using QIAprep miniprep kit (Qiagen). Mixtures 1 and 2 were combined and incubated at room temperature for 20-30 minutes. Growth medium was removed from each well and the cells were washed with PBS. Wells were then replenished with 800µl Opti-MEM supplemented with the Lipofectamine-cDNA mixture. Cells were incubated for four hours, after which the transfection mixture was aspirated and replaced with normal culture medium.

To generate cell lines with stable gene knock down, pGIPZ shRNA (Open Biosystems, Table 2-1) constructs expressing the shRNA together with BFP/GFP fluorophores were used. Fluorescent protein expression allowed identification of transfected cells. To obtain viable cell lines with a high level of protein depletion, both 250ng and 500ng of purified and linearised shRNA were initially transfected into cells. The shRNA vector encoded a puromycin resistance gene therefore cells were selected with 1µg/mL puromycin.

Table 2-1 pGIPZ shRNA constructs (Human). The columns of the table contain the name of the construct, accession number of the targeted gene, manufacturer's oligo ID, and the mature sense sequence of each construct used in the shRNA.

Construct	Accession	Oligo ID	Sequence
Non-silencing	-	RHS4346	-
Diaph1_22	NM_001079812	V3LHS_392378	CAGATAGTTCTGCACAAGA
ACTR2/Arp2_63	NM_005722	V3LHS_341063	TTCTTGGTACTCTTGTCGG
ACTR3/Arp3_82	NP_005712.1	V3LHS_382341	TCGCTTCAACATGCCAGCT
ArpC2_25	NM_005731	V2LHS_199425	ATTTCAAAGAAATACTGAC
IQGAP1_07	NM_003870	V3LHS_334306	AGGTTGACTTCACAGAAGA
NCKIPSD_95	NM_016453	V3LHS_341595	TTCTCTTGCACATTTTCTT
NCKIPSD_98	NM_184231	V3LHS_341598	TCAGGAGCAACAACAGCTT
Flightless-I_22	NM_002018	V3LHS_386022	ACTGTGGAAGACACACACT
CYFP1/Sra1_63	NM_001324125	V2THS_258463	TTAATAATCTCATCTTTGC

NCKAP1/Nap1_66	NM_205842	V3LHS_347966	TATAGAGAAGCATAACTCA
Wave2_14	NM_006990	V2LHS_95114	TATCCTTGGTGTCCTGCAG

2.2.2 Lipofectamine RNAi max (siRNA studies)

The Lipofectamine RNAi max reagent (Invitrogen) was used to transfect cells with siRNA (Table 2-2). siRNA stocks were made by resuspending siRNA in RNase-free buffer at a final concentration of 20µM. Stocks were aliquoted into smaller volumes to limit freeze-thaw cycles, and stored at -20^{o}C.

The day prior to siRNA transfection, cells were plated onto a 6-well plate. To transfect siRNA, a reaction mix was prepared. Tube 1 contained 200µl Opti-MEM and 2µl of siRNA (20µM), whilst tube 2 contained 200µl Opti-MEM and 4µl Lipofectamine RNAi max. Tube 1 and 2 were then combined and incubated at room temperature for 20 minutes. Plated cells were washed with PBS, and the medium was replaced with 1.6mL of growth medium without FBS. Finally, the transfection mix was added to cells and incubated at 37^{o}C. After 24 hours, the transfection medium was replaced with fresh growth medium. Cells were generally used for experiments 72 hours after transfection. To test siRNA efficiency, a western blot and/or qPCR was run.

Note: Diaph1 siRNA and Nap1 siRNA were used at half concentration (10µM) due to the strength of their phenotype. Protein depletion was verified using Western blotting.

Table 2-2 siRNA ON-TARGETplus pool sequences (Human, GE Dharmacon), Diaph1 Stealth siRNA (Human, Thermo Fisher). The name of the construct, the four target sequences contained in the pool, and manufacturer's oligo ID for each siRNA pool.

Construct	Target sequence	Oligo ID
Non-silencing	UGGUUUACAUGUCGACUAA UGGUUUACAUGUUGUGUGA	D-001810-10-05

	UGGUUUACAUGUUUUCUGA UGGUUUACAUGUUUUCCUA	
ACTR2/ARP2	GAAAGAGCAUUUAUCGUUU GAACAUGGAUCUUAGAGUC AGAAUGGAAUGGACUCUUA UGGUGUGACUGUUCGAUAA	L-012076-02-0005
Diaph1	GGCUUCAAUAUCAGCUUCCUCUGUA	HSS102771
IQGAP1	GAACGUGGCUUAUGAGUAC GCAGGUGGAUUACUAUAAA CGAACCAUCUUACUGAAUA CAAUUGAGCAGUUCAGUUA	L-004694-00-0005
NCKIPSD	GAGAAACGAGUUCGAGUCU GCACGCCUUUCGCCCAGUU CCGAGAAGCUGUUGUUGCU CGAGAGAUGUGCAAGGAAU	L-021376-00-0005
Flightless-I	UUAACAAGAAUGAGCGGAA ACGAAGACCUAGACGGCAU CCGGGAAGGUGAAACGCGA CAACCAGGGCAUCGUGUAU	L-017506-01-0005
Nap1/NCKAP1	CAUCCUAUCUUAUCGACAA GCAGACGACUUUAUAGAUA GGAGAAUGUUGAUGUGUUA GGUCGUAGCUCUUUCUUCA	L-010640-00-0005
Sra1/CYFIP1	GCACAAUCCUGCAGUACGU GGAGAGAAUUCGCAAGUUC GAUAAACGGUUACGAUCAG GAGUACGGCUCUCCUGGUA	L-014185-00-0005

2.2.3 Transient Transfections for localisation studies

For the study of protein localisation, 1µg of purified cDNA of the GFP tagged protein of interest was transfected into cells plated onto 25mm coverslips. Lipofectamine 2000 was used as the transfection agent (see 2.2.1). Cells were imaged after overnight incubation and discarded after use.

2.2.4 Fluorescence Activated Cell Sorting (FACS)

The Flow Cytometry Core Facility at UCL Great Ormond Street Institute of Child Health carried out FACS using a FACSAria III. All sorting experiments were run alongside Stephanie Canning and Dr Ayad Eddaoudi.

Flow cytometer was used to generate a population of cells that expressed a homogenous level of GFP/BFP-tagged construct of interest. Cells to be FACSed were grown to full confluence in a T75 dish (10 million cells). Negative wild-type control cells, without GFP/BFP expression were also grown in a T75 dish prior to sorting. On the day of sorting, cells were trypsinised and centrifuged at 1500rpm for 3 minutes. Cells were resuspended with 5mL FACS medium (for 100mL: 5mL EGTA K/Na (final concentration, 1mM), 2mL HEPES (Thermo Fisher, final concentration, 25mM), 93mL Gey's Balanced Salt Solution (Sigma-Aldrich) and 1g BSA (Sigma-Aldrich, 1%)) then filtered through a cell strainer (100μm pore size, Fisher Scientific) to remove clumps. The high pressure during sorting can cause the sort buffer to become basic. Thus, the added HEPES buffer maintains the pH at 7.0 - 8.0. The use of EGTA prevents the formation of aggregates. Gey's Balanced Salt Solution contains phosphate bicarbonate buffered cell suspension and washing solution. During FACS, the positive cells (top 5% of those expressing the desired fluorophore) were collected in a 15 mL falcon tube containing fresh Gey's medium. After sorting, sorted cells were centrifuged for 5 min at 1500rpm and plated into on well of a 6/12-well plate, and amplified.

2.3 Transduction

2.3.1 Viral Transfection (shRNA studies)

In addition to the liposome-mediated method described above, some stable lines were generated using the following lentiviral method learnt from Dr. Geneviève Lavoie during a 3-month internship in the laboratory of Prof. Philippe Roux at the University of Montréal, Institute of Immunology and Cancer (IRIC).

Lentiviral vectors are advantageous as they can stably and rapidly integrate a transgene or shRNA into the genome of most cell types (Sakuma et al. 2012). For

this project, lentiviral vectors derived from the human immunodeficiency virus (HIV-I) were used. Essential lentiviral (HIV-1) genes must be expressed in these cells to allow the generation of lentiviral particles. These genes are usually expressed by several plasmids: (i) a lentiviral expression plasmid, such as pLV-Green, containing the psi (Ψ) packaging sequence and the transgene gene of interest inserted between the lentiviral LTRs allow target cell integration, (ii) a packaging plasmid, such as pLV-HELP, encoding the *pol, gag, rev* and *tat* viral genes and containing the *rev*-response element (RRE); and (iii) a pseudotyping plasmid, such as pLV-iVSV-G, encoding the G protein of the Vesicular Stomatitis Virus (VSV-G) envelope gene.

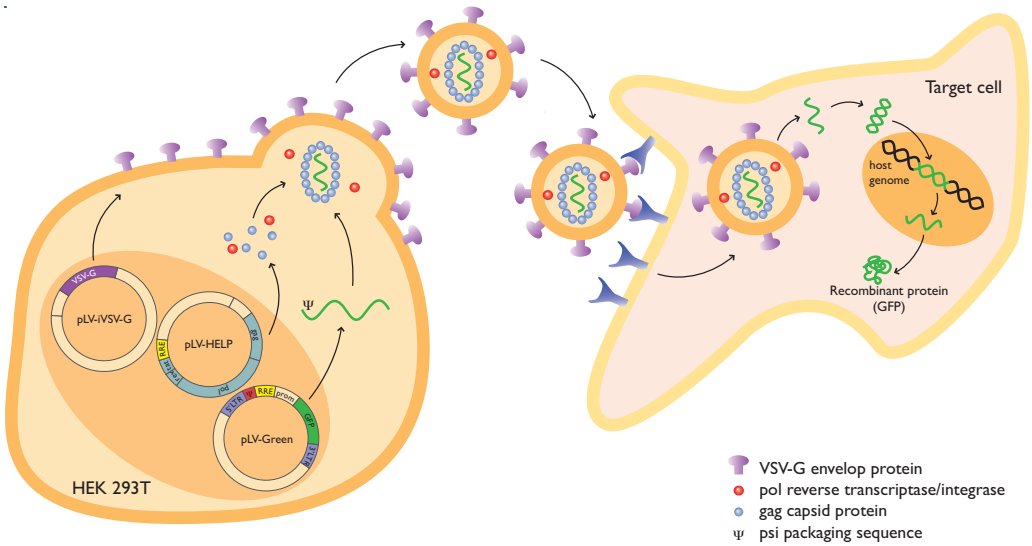

Figure 2-1 Lentiviral vector production in HEK293T cells and target cell transduction. Essential lentiviral (HIV-1) genes must be expressed in HEK293 cells to allow the generation of lentiviral particles. HIV-1 genes are expressed by several plasmids: (i) a lentiviral expression plasmid, such as pLV-Green, containing the psi (Y) packaging sequence and the transgene gene inserted between the lentiviral LTRs allow target cell integration, (ii) a packaging plasmid, such as pLV-HELP, encoding the pol, gag, rev and tat viral genes and containing the rev-response element (RRE); and (iii) a pseudotyping plasmid, such as pLV-iVSV-G, encoding the G protein of the Vesicular Stomatitis Virus (VSV-G) envelope gene. Cells are transfected, and the supernatant is used to transduce the target cells. Once in the target cells, the viral RNA is reverse-transcribed, imported into the nucleus and stably integrated into the

host genome (Figure from InvivoGen Insight, Innovation within reach – Spring 2010).

To transfect HEK293T cells with the necessary cassette of plasmids, the calcium phosphate transfection method was used. In the morning of the transfection day, 2 million HEK293T cells were seeded in a 75cm^2 flask. 4 hours later, the transfection mix was prepared. Tube 1 contained HBS (NaCl (280mM), Na_2HPO_4 (1.5mM) and HEPES (50mM) in water at pH 7). Tube 2 contained water, $CaCl_2$ (2M), viral plasmids (1.5µg pMDLg/pREE, 1.5µg pRSV-Rev and 3µg pMD2-VSVG) and 6µg of the shRNA plasmid (Table 2-3).

Medium was removed from the HEK293T flask and fresh medium was added to the flask. The contents of tube 2 was added to tube1 drop by drop, and mixed gently. This transfection mix was then added to cells and incubated. From then on, biosafety level 2 precautions were taken when handling. This transfection method generates a precipitate that is dispersed onto the cultured HEK293T cells. Cells take up the precipitate via endocytosis or phagocytosis.

The day after transfection, culture medium was replaced with warm growth medium. Cells that were to be infected were seeded at 0.25 million (HeLa cells) and 0.5 million (M2 cells) in 10 cm dishes. On the third day, the virus supernatant was collected from the HEK293T flasks and filtered through 0.45µm filters to remove all cell debris. Hexametrine dibromide (Sigma) was added to a final concentration of 5µg/mL to aid viral entry. The filtered virus supernatant was added onto the host cells, and the transduction process began. Host cells were left to grow for 3 days after infection and HEK293T cells were discarded safely. Three days after infection, cells were washed at least twice with PBS and fresh medium containing puromycin (1µg/mL) was added to begin selection. Over the next couple of days, cells were split at least once or twice to ensure all virus particles have been removed from the medium. To confirm mRNA transcript and protein depletion, I used western blotting and/or qPCR.

Table 2-3 PLKO shRNA constructs (Human). The columns of the table contain the name of the construct, accession number of the targeted gene, manufacturer's oligo ID, and the mature sense sequence of each construct used in the shRNA.

Construct	Accession	Oligo ID	Sequence
PLKO (Empty)	-	SHC001	-
Flightless-I_63	NM_002018	TRCN0000152063	CCGGCCATTTCAAGAGGAAGTTCATCTCGAGATGAACTTCCTCTTGAAATGGTTTTTG
Flightless-I_51	NM_002018	TRCN0000157051	CCGGGCTGCCACAGATCAACTACAACTCGAGTTGTAGTTGATCTGTGGCAGCTTTTTG
IQGAP1_85	NM_003870	TRCN0000047485	CCGGCCAGTAATCTACATTTCCATTCTCGAGAATGGAAATGTAGATTACTGGTTTTTG
IQGAP1_87	NM_003870	TRCN0000047487	CCGGGCATCCACTTACCAGGATATACTCGAGTATATCCTGGTAAGTGGATGCTTTTTG
Nap1/NCKAP1_41	NM_013436	TRCN0000151941	CCGGCCTCTCAATCAAGATACTCAACTCGAGTTGAGTATCTTGATTGAGAGGTTTTTTG
NCKIPSD_43	NM_016453	TRCN0000278443	CCGGCTAGAGGAGCTGCTGCATATTCTCGAGAATATGCAGCAGCTCCTCTAGTTTTTG
NCKIPSD_72	NM_016453	TRCN0000141072	CCGGCTAGAGGAGCTGCTGCATATTCTCGAGAATATGCAGCAGCTCCTCTAGTTTTTTG
BAIAP2_48	NM_006340	TRCN0000060948	CCGGGCGCTGAAGAAATACCAGACTCTCGAGAGTCTGGTATTTCTTCAGCGCTTTTTG
VANGL1_91	NM_138959	TRCN0000062091	CCGGCTACAAAGATTTCACCATCTACTCGAGTAGATGGTGAAATCTTTGTAGTTTTTG
MARK2_84	NM_004954	TRCN0000001584	CCGGAGATGATGAACTAAAGCCTTACTCGAGTAAGGC TTTAGTTCATCATCTTTTTT
Kirrel3_79	NM_032531	TRCN0000005579	CCGGCCGTTCCCAGAGAAATCTCAACTCGAGTTGAGATTTCTCTGGGAACGGTTTTT

2.4 Imaging

2.4.1 Confocal Microscopy (Spinning Disk)

Live-cell imaging and immunofluorescence experiments were performed on an inverted confocal microscope (IX81, Olympus) with a spinning disk head (Yokogawa, CSU22). Cells plated on 25mm glass coverslips were mounted in a

sample holder, and imaged in Leibovitz L-15 (Gibco) medium supplemented with 10% FBS. L-15 lacks phenol red and is CO_2 independent, allowing experimentation without environmental control. Images were acquired with an Andor iXon camera using 100x oil-immersion objective and analysed using Image J (http://rsbweb.nih.gov/ij/) and Microsoft Excel software. Images were acquired using 488nm excitation light and collecting emission at 525nm for GFP-tagged constructs, 561nm excitation light and collecting emission at 617nm for Lifeact Ruby, and 405nm excitation light and collecting emission at 447nm for BFP-tagged constructs.

To evaluate bleb size in live M2 cells, cells needed to be detached and replated on the day of the experiment to obtain a high proportion (>90%) of blebbing cells, as the cells spread and stop blebbing 24-48 hours after plating. Time-lapse movies of the cells were then acquired at 20s intervals for 5 minutes.

2.4.2 Permeabilisation-fixation

In some cases when examining protein localisation to the cortex, we used permeabilisation-fixation to decrease cytoplasmic background. Prior to the permeabilisation-fixation, cells were imaged as described above (see 2.4.1). At a chosen time point, L-15 imaging media was quickly replaced with a permeabilisation-fixation solution composed of 0.5% Triton-X (Thermo Scientific) and 0.25% glutaraldehyde (Sigma) diluted into cytoskeleton buffer (CSB). The 10x stock of CSB consists of 500mM Imidazole, 500mM KCL, 5mM $MgCl_2$, 1mM K-EDTA, 10mM K-EGTA. The Triton-X detergent removed the membrane and membrane-bound proteins, allowing the escape of unbound cytoplasmic proteins. This allowed for clear visualisation of proteins bound to the cytoskeleton.

2.4.3 Long term Time-Lapse Microscopy

Multi-position long-term time-lapse microscopy was performed on a Zeiss Axiovert 200M time-lapse microscope at the LMCB – MRC Laboratory for Molecular Cell Biology UCL. Training and support for this light microscope facility was provided by Dr Andrew Vaughan.

To assess the impact of protein depletion on cell morphogenesis during the cell cycle, HeLa cells were examined using long-term time-lapse imaging. To increase the proportion of mitotic cells, cells were arrested in S-phase with a single thymidine block by treatment with 2mM thymidine (Sigma-Aldrich) for 16-24 hours. The block was released by replacing thymidine containing medium with normal DMEM medium ~7-8 hours before the start of imaging.

During imaging, cells were maintained at 37 °C and supplied with 5% CO_2 on the microscope stage. Multi-position long-term time-lapse microscopy was performed using a 20X air objective. All experiments were repeated at least 3 times with at least 10-15 positions imaged per well. Experiments examining cell lines with stable shRNA depletion were plated the day before imaging. Experiments examining single and combination transient siRNA knockdowns were imaged beginning 48 hours after transfection. Time-lapse data was analysed with FIJI using the Bio-Importer plugin and progression outcomes were tabulated (Table 2-4).

Table 2-4 Classification of progression through the cell cycle or failure for HeLa cells during long term time-lapse imaging experiments.

		Position 1	Position 2	Position 3
Normal				
Death in interphase				
Death after interphase with rounding	Prophase			
	Metaphase			
	Anaphase			
	Telophase			
Death after interphase without rounding				
Oscillation and fail				
Oscillation and divide				
Death after dividing (couldn't spread)				
Divide and regress				
Bleb size				

2.4.4 Scanning Electron Microscopy

To examine the molecular scale organisation of the actin cortex, I performed Scanning Electron microscopy using a JEOL7401 Field Emission Scanning Electron Microscope (JEOL, Tokyo, Japan) at the Anatomy Building, UCL. Training, support and coating of coverslips was provided by Dr Mark Turmaine. Critical point drying of the samples was carried out at the LMCB – MRC Laboratory for Molecular Cell Biology UCL, and all training was provided by Dr Jemima Burden. The protocol for scanning electron microscopy of the actin cortex was adapted from that of Tatyana Svitkina for examining the lamellipodium (Svitkina 2009).

Cells were plated onto 13mm glass coverslips and allowed to attach (three hours for M2 cells, overnight for HeLa cells). After an initial wash with L-15, the membrane was quickly removed using CSB containing 0.5% Triton-X and 0.25% glutaraldehyde. This was followed by a second extraction with 2% Triton-X and 1% CHAPS in CSB. Cells went through a second fix with 2% glutaraldehyde in a 0.1M cacodylate buffer at pH 7.4. A final tannic acid (LabGuard) and 2% uranyl acetate fix were carried out before dehydration of cells with a series of ethanol dilutions (starting at 10% and proceeding stepwise to 100%). Cells were dried using a critical point dryer (Leica EM, CPD 300) and coverslips were mounted onto 12mm cylinder stubs (Agar Scientific) using 12mm carbon adhesive discs (Agar Scientific). Finally, coverslips were coated with platinum-palladium.

Cells were imaged using the JEOL7401 Field Emission Scanning Electron Microscope (JEOL, Tokyo, Japan). For consistency, images of each M2 bleb were taken at 30kx, 50kx, 70kx, and 90kx magnifications. The results presented are representative of imaging of 8-10 cells, and at least two blebs per cell. Similarly, HeLa cells were imaged at two distinct positions: above the nucleus, and around the cell's periphery.

2.4.5 Drug Treatments

Latrunculin B (Merck Biosciences), an actin-sequestering drug (Coué et al. 1987), was used at a concentration of 750nM to depolymerise F-actin in HeLa cells. CK666

(Tocris), a small molecule inhibitor against the Arp2/3 complex (Nolen et al. 2009) was used to study the role of the Arp2/3 complex in the cortex.

Cells were first imaged for 10 time points at 10s intervals to provide baseline behaviour for comparison, then 100μM CK666 was added and the cells were incubated for 3min at room temperature. During this time, the microscope was refocused choosing a plane that cut through the centre of the nucleus. This was necessary because CK666 caused increased rounding of the cells. After a 3-minute incubation, cells were imaged for an additional 20 time points. For all drugs, an amount of DMSO corresponding to the volume that the drug was diluted in was used as a vehicle control.

2.4.6 Immunofluorescence sample preparation

For immunofluorescence, cells were fixed for 10 minutes with 2% formaldehyde, 0.1% glutaraldehyde and 0.2% Triton X (Sigma) in CSB. After fixing, 1% Triton X was added for 5 minutes and then cells were washed three times with PBS and finally, they were blocked with PBS containing 10% horse serum (HS) for 3x5 minutes at room temperature. During the last wash, Hoechst 33342 was added for 5 minutes to allow nuclear staining. To allow examination of the F-actin cytoskeleton, cells were incubated with phalloidin-567 (1:200 in PBS/HS, Life Technologies) in a moist, dark chamber for 60 minutes at room temperature. The cells were then washed three times with PBS/HS and mounted with FluorSave reagent (Calbiochem).

2.5 Molecular biology

2.5.1 RNA extraction

qPCR analysis was carried out by Prof. Phillippe Roux and Dr. Geneviève Lavoie at the University of Montréal, Institute of Immunology and Cancer (IRIC).

Confirmation of knockdown efficiency by shRNA or siRNA was verified by qPCR. mRNA was extracted from cells harvested from a T25/T75 flask using the RNAeasy mini-kit (Qiagen). Before mRNA isolation, cells were resuspended, lysed and homogenised with the provided lysis buffer (RLT supplemented with β-

mercaptoethanol). Resuspended cells were further disrupted by quickly passing through a small gauge needle twice. Cells were transferred to a QIA spin column and centrifuged at 14,000 RPM for 2 minutes at room temperature. The spin column was subsequently washed with 70% ethanol before RNA elution with 30µl of nuclease-free water. RNA was stored at -80^{o}C before being sent on dry ice to Montréal for qPCR analysis.

2.5.2 Western blotting

Western blotting was performed with an SDS-PAGE electrophoresis system (XCell SureLock Mini-Cell, Invitrogen) to assess the level of protein expression in control and knockdown cells.

Cells were cultured in T25 flasks prior to whole cell lysate production. Cells were trypsinised and gently washed with PBS to remove all residual growth medium. The pellet was resuspended with RIPA lysis buffer supplemented with sodium orthovanadate, PMSF in DMSO and a protease inhibitor cocktail (Santa Cruz Biotechnology). After resuspension, the lysate was centrifuged at 4C for 4 minutes. The supernatant was transferred to a clean 1.5mL eppendorf tube and an equal volume of LaemmLi SDS-Sample Buffer (2x, Sigma) was added. The sample was then denatured at 95C for 5 minutes. The lysate was stored at -80C for long-term storage. For use, the lysate was thawed at room temperature and re-boiled for 5 minutes before loading (10-15µl) onto the gel.

For running the gel, 4-12% gradient precast gels (Invitrogen) were used and run at 200V and 50mA for 45-60 minutes at room temperature. 5µl of prestained protein ladder plus (10-250 kDa, Sigma Aldrich) was loaded to monitor protein separation. Once running was complete, samples were transferred to a polyvinylidene difluoride (PVDF) membrane (Immobilion P-transfer membrane, Millipore) for 2 hours at 200V and 220mA at 4C. Prior to antibody probing, the membrane was blocked with 5% milk with continuous agitation for 1 hour at room temperature. The membrane was cut as appropriate and probed with appropriate primary antibodies overnight (see **Error! Reference source not found.**) at 4C with continuous shaking. GAPDH Novus Biological) was used as a protein loading control for all protein runs.

Table 2-5 List of primary antibodies used in Western blotting. Suppliers, dilution, and host species are also indicated.

Protein	Product No & Vendor	Dilution	Species
GAPDH (control)	NB300-221, Novus Biological	1:10,000	Mouse
Diaph1	ab96784, Sigma/AbCAM	1:200	Rabbit
Arp2	sc-10125, Santa Cruz	1:100	Goat
Arp3	#4738, Cell Signalling	1:200	Rabbit
IQGAP1	WH0008826M1, Sigma-Aldrich	1:200	Mouse
NCKIPSD	ab88467, AbCAM	1:500	Mouse
Nap1/NCKAP1	ab96715, AbCAM	1:500	Rabbit
Sra1/CYFP1	ab156016, AbCAM	1:1000	Rabbit
Flightless-I	ab108594, AbCAM	1:1000	Rabbit

The following day, the membrane was washed 5 times and stained with horseradish peroxidase-conjugated secondary antibody (anti-mouse IgG, GE healthcare; anti-rabbit IgG, GE healthcare; anti-goat IgG, abCAM) diluted at 1:100,000 in 5% milk for 1 hour at room temperature. The membrane was washed again, and an enhanced chemiluminescence (ECL, GE Healthcare) mixture was pipetted onto the membrane.

Protein levels were detected with the CCD-based imaging ImageQuant LAS 4000 system. An image was taken in continuous intervals of 1 minute. A single image of the ladder was also taken as a reference. Images were analysed with Image J to determine relative protein concentration.

2.5.3 Transformation and plasmid replication

DNA transformation was performed to amplify plasmids and generate stocks of bacteria expressing the plasmids of interest. The plasmid was introduced into chemically competent *Escherichia coli* DH5α bacterial cells (Life Technologies). For transformation, 2µl of miniprep DNA was added to 50µl of thawed bacteria. The cells were tapped gently to ensure mixing of DNA, and then incubated on ice for 30 minutes. Each transformation tube was heat-shocked by placing into a 42C water

bath for 30 seconds, after which the tube was placed on ice for 2 minutes. Lastly, 250µl of warm Luria-Bertani broth (LB, Life Technologies) was added to the bacteria and they were incubated with shaking at 37C for 1 hour.

After incubation, 100µl of bacteria was plated onto LB-agar plates (25g/l of bactoagar in LB media) containing kanamycin or ampicillin at the appropriate concentrations for selection. Bacteria were evenly distributed on the plate using an L-shaped glass pasteur pipette (Fisher Scientific). Plates were incubated at 37C overnight. After incubation, a well-grown isolated colony was selected and inoculated into a tube containing 3mL LB-medium and the appropriate antibiotic. The bacteria were cultured with vigorous shaking at 37C overnight. Approximately 18 hours later, the bacteria were collected by centrifugation (1min, 14,000 RPM) and plasmid DNA was isolated using QIAprep Miniprep Kit (Qiagen) and eluted in 30µl of milli-Q water.

To make a bacterial stock, a mix of 750µl bacteria and 250µl glycerol was transferred to a cryogenic vial and kept at -80^{o}C.

2.6 Image processing and analysis

2.6.1 M2 blebbing phenotype quantification

In order to identify the phenotype generated as a result of knockdown by shRNA, M2 cells were imaged with optical microscopy (see 2.4.1) and bleb size was evaluated. Cells containing the shRNA construct were identified based upon appropriate FP expression. In order to quantify different phenotypes, cells were categorised by their bleb size: no blebs, small blebs, normal blebs or large blebs. Bleb size distribution for each cell was assessed from videos, and not the stills shown in this thesis. Statistical comparisons between non-silencing control cells and shRNA-targeted cells were carried out using chi-squared tests. Results were deemed significant for $p<0.01$.

2.6.2 Estimation of cortical mesh size from Scanning Electron Microscopy images

The JAVA programme used to recognise, segment and calculate the size of the cortical mesh was developed with Dr Matthew Smith (Prof. Ewa Paluch group, MRC-UCL). Matthew provided continuous support and guidance for this quantification.

To quantitatively assess changes in mesh size induced by protein depletion, I collaborated with Matthew Smith to develop a quantitative method. Images of the actin cortex at 70k magnification were selected because single filaments could easily be identified and because they possessed a relatively large field of view. Using FIJI, a plugin (Trainable WEKA segmentation), was 'trained' to recognise and differentiate between filaments and gaps in the cortical mesh visible in SEM images (Figure 2-2), thus identifying and highlighting the upper most cortical mesh level. The areas of these gaps were tabulated and converted to nm^2 through the use of a Matlab programme.

Data was collected and analysed by arranging into frequency tables using different bin sizes (nm) for analysis of small holes and large holes, and cumulative graphs were drawn. For each condition, I analysed 2-3 blebs on 6-7 representative cells and the data presented represents the common trend.

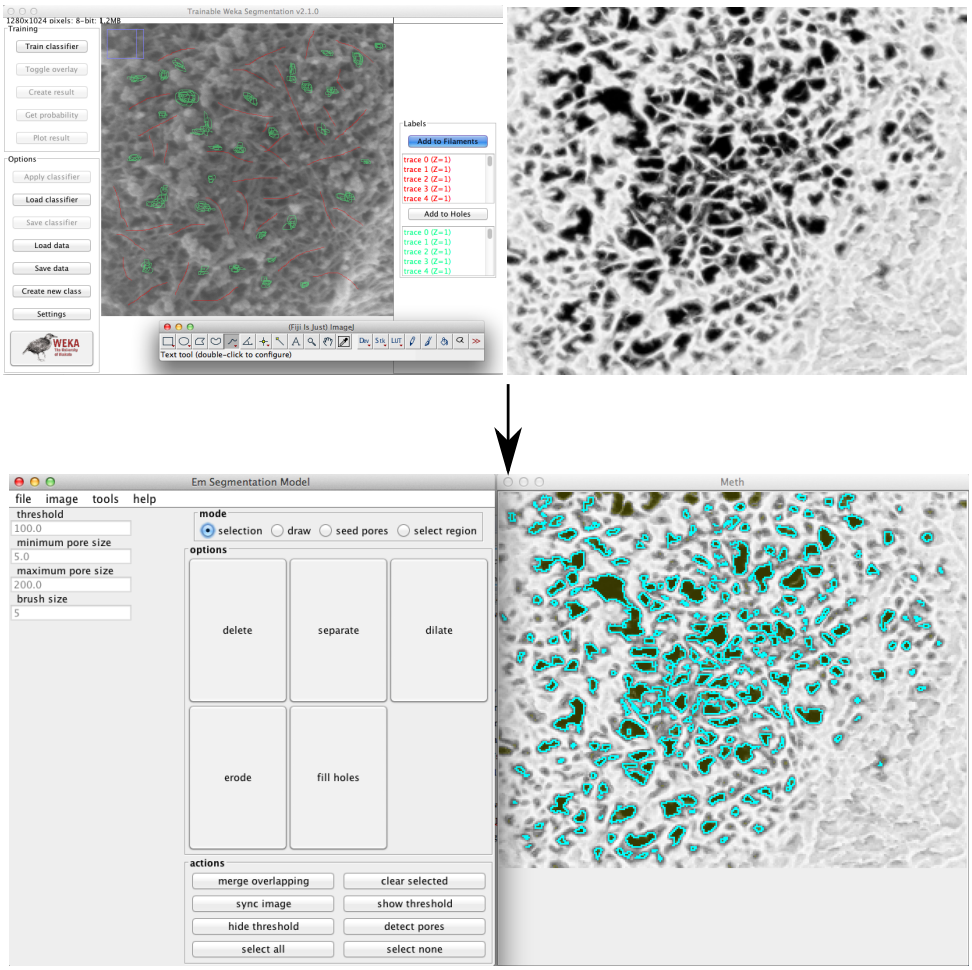

Figure 2-2 Estimation of cortical mesh size from SEM images. The WEKA segmentation plugin is trained to segment filaments (red) and mesh 'gaps' (green) from acquired electron micrographs. Following this, each gap is highlighted individually (lower right panel), and its area is measured for analysis. All micrographs used are at 70x magnification.

2.7 BioID

In July 2015, I was awarded a three-month Bogue Fellowship by the Department of Cell and Developmental Biology, funding a visit to the laboratory of Prof. Phillippe Roux at the IRIC of the University of Montréal. During my time in Montréal, biotin identification (BioID), a new and powerful proximity-dependent labelling approach was used to map novel interactions. Dr. Geneviève Lavoie carried out cloning of all BirA constructs. Antoine Meant generated all stable cell HeLa lines prior to the start of the project, and analysed the mass spectrometry data with SAINTexpress as detailed below.

2.7.1 BioID stable cell lines

The first step in the BioID approach is constructing an expression plasmid in which the gene of interest is fused with BirA* (see appendix 11.1 for full sequence). The fusion constructs also included an epitope tag (i.e. myc, FLAG) that allows both optical and biochemical detection of the fusion protein. BirA* is a 33.5 kDa protein, and the BirA*-fusion is usually made at either the N or C terminus of the target protein. This fusion is thought not to impair localisation, stability, or function of the target protein. The biotinylation activity of the BirA*-fusion protein, which is essential to the success of the method, was assessed by blotting cell lysates with streptavidin-HRP.

The following HeLa cell lines were used for the BioID experiments: FLAG (no BirA*) control, BirA* control, BirA*-GFP control, Diaph1-BirA*, Diaph1ΔDAD-BirA*, Arp3-BirA* and ArpC4-BirA*. Lines were constructed by viral transduction and cultured in 15cm dishes, in HeLa growth medium (DMEM, FBS and penicillin/streptomycin) supplemented with 200µg/mL hygromycin (Sigma) for selection.

2.7.2 Cell line characterisation

First, we verified expression of the BioID constructs and searched for the optimal duration for biotin treatment. This consists of two steps requiring optimisation: firstly to check protein induction with tetracycline to ensure sufficient BirA protein expression, and secondly to establish the time of biotinylation incubation for a sufficient signal.

To characterise the most effective tetracycline induction time, 100,000 cells were plated onto 6-well plates in growth media without hygromycin antibiotic. The day after plating, cells were induced by adding 1µg/mL tetracycline (Sigma) for the following durations: 24 hours, 12 hours, 8 hours, 4 hours and 0 hour (control). Cells were then washed with cold PBS, scraped with the addition of 150µl of Laemmli SDS-sample buffer, and collected into an Eppendorf. This whole-cell lysate was stored at -20^{o}C.

To characterise the best duration for biotinylation, cells were plated as above and induced for 24 hours. Biotin (50µM, BioBasic) was added for the following durations: 24 hours (added at the same time as tetracycline), 12 hours, 8 hours, 4 hours, 2 hours, and 0 hour (control). Cells were then washed with cold PBS, scraped with the addition of 150µl of Laemmli SDS-sample buffer, and collected into an Eppendorf. This whole cell lysate was stored at -20°C. Characterisation of biotinylation durations reduced non-specific binding between biotin and other non-proximal proteins.

2.7.3 Western blotting

Probing induced proteins

Prepared lysate samples were separated by SDS-PAGE (60V, overnight) and transferred to a PVDF membrane (see 2.5.2). The membrane was probed with FLAG primary antibodies overnight at 4°C with continuous shaking. Tubulin (Novus Biological) was used as a protein loading control for all protein runs. Protein levels were detected by developing blots on x-ray films with 15 seconds exposure.

Table 2-6 List of primary antibodies used to probe induction and biotinylation.

Protein	Product No & Vendor	Dilution	Species
Tubulin (control)	ab6046, abCAM	1:5000	rabbit
FLAG	F1804, Sigma-Aldrich	1:2000	mouse
HRP-Streptavadin	RPN123IV, GE Healthcare	1:5000	-

Probing biotinylated proteins

Prepared lysate samples were separated by SDS-PAGE (200V, 2 hours) and transferred to a PVDF membrane (see 2.5.2). Prior to antibody probing, the membrane was blocked with 5% BSA for 1 hour at room temperature, followed by a 1 hour incubation with HRP-conjugated streptavidin. The membrane was washed three times, and developed on x-ray films for 10 minutes.

2.7.4 Affinity capture of biotinylated proteins

On the first day, BirA* stable cell lines were grown on two 15 cm plates (5 million cells per plate). The next day, cells were treated with 1µg/mL tetracycline and medium supplemented with 50µM biotin for 24 hours (Figure 2-3). Cells were collected on the third day by scraping with 2mL cold PBS into falcon tubes. At this stage, the two plates for each cell line were pooled. Cells were pelleted at 500g for 5 minutes at 4°C, and stored at -80°C until ready for cell lysis and affinity purification.

The collected cell pellet was resuspended in 1.5mL cold RIPA lysis buffer, before adding 1µl (250 units) of Benzonase (Sigma-Aldrich) to degrade DNA/RNA. Lysates were sonicated on ice at 20% amplitude (3 x 10 second bursts with 2 seconds rest intervals). Sonicated samples were then centrifuged for 20 minutes at 13,000rpm at 4°C and the supernatant were collected in a clean Eppendorf. Prior to affinity capture, streptavidin-sepharose beads (GE Healthcare) were washed 3 times with 1mL RIPA buffer. Beads were spun for 2 minutes at 3000rpm, and the supernatant was discarded between each wash. The lysate was added to the washed beads and incubated at 4°C for 3 hours.

After incubation, the beads were spun for 2 minutes at 3000rpm and the supernatant was discarded. 1mL of RIPA lysis buffer was added to the beads and spun for 2 minutes at 3000rpm. This wash-spin was repeated three times. Beads were then washed with 1mL of 50mM Ammonium Bicarbonate (ABC, pH 8.5) and the supernatant was discarded. This wash was repeated three times. Lastly, beads were resuspended in 100µl of 50mM ABC and supplemented with 10µl (1µg) of trypsin. Beads were incubated overnight at 37^{o}C with continuous rotation.

The next day, another 1µg of trypsin was added to beads and incubated for a further 4 hours. Beads were then pelleted at 3000rpm for 2 minutes. The supernatant (containing the peptides) were transferred to a new Eppendorf. The remaining beads were rinsed twice in 100µl of chromatography-grade water (Sigma-Aldrich) and pooled with the collected supernatant, to ensure the complete collection of bound peptides. Between each wash, beads were vortexed and spun for 2 minutes at 3000rpm.

Formic acid was added (final concentration of 2%) to the collected peptides to end digestion, and the sample was spun for 10 minutes at 10,000 rpm. The supernatant was transferred to a new tube (ensuring not to collect any beads) and the sample was dried using SpeedVac (Thermo Scientific). Before sending for mass spectrometry, dry peptides were resuspended in 13µl of a 5% formic acid aqueous solution.

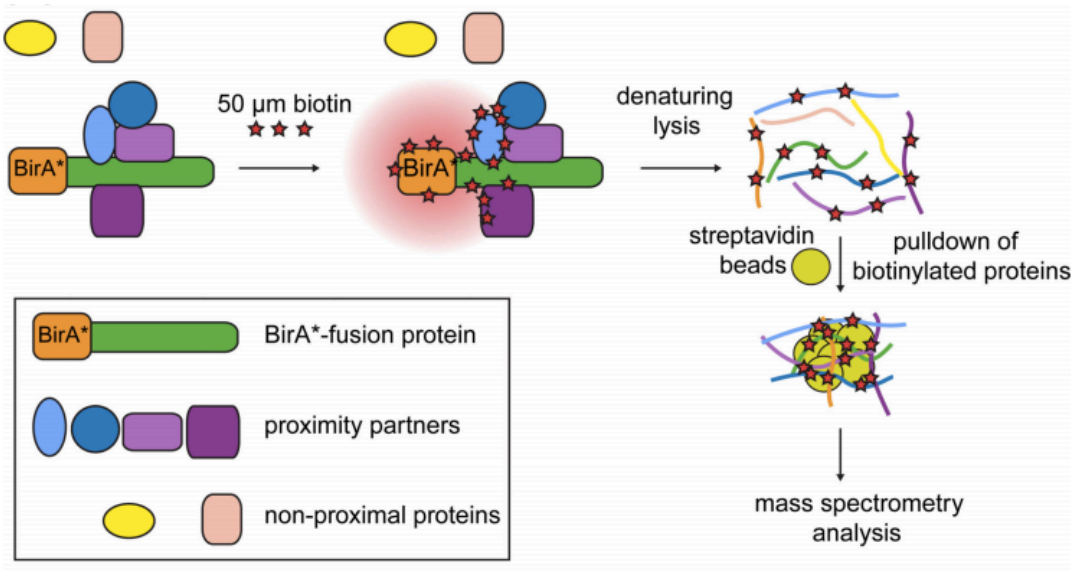

Figure 2-3 The protein of interest is tagged with a mutant form of E. coli biotin ligase BirA (R118G), denoted as BirA*. Following incubation of cells with biotin, BirA* biotinylates proteins that are in the proximity of the BirA*-fusion protein and these are referred to as "proximity interactors." The labelling radius of BirA* is estimated to be around 10 nm; proteins outside this radius are denoted as "nonproximal proteins". Following biotinylation, proteins are solubilised and biotinylated proteins are precipitated by streptavidin beads for mass spectrometry analysis (Adapted from Firat-Karalar & Stearnsx 2015)**.**

2.7.5 Mass spectrometry and data analysis

Affinity captured peptides were sent to the proteomics core facility at the IRIC to be identified by mass spectrometry.

For each prey the results consists of 4 biological replicates giving the total numbers of spectral counts identified and the total number of spectral counts obtained for the 12 biological control replicates. For example, for the protein BSG, using

Diaph1DAD as a bait, we identified 5,6,3,6 peptides in the replicates and 0 in the controls. To determine if the number of spectral counts identified with the bait differs significantly from those identified in a non-specific interaction, we use the SAINTexpress software (specific analysis of interactome, http://saint-apms.sourceforge.net/Main.html), which allows us to compare and determine the potential for a real interaction between bait and a specific prey. This potential will depend on: 1) the reproducibility of the spectral counts identified for a prey among bait biological replicates, 2) the abundance of spectral counts for this same prey identified for control baits: FLAG (no BirA*) control, BirA* control, BirA*-GFP control).

For each prey, the two biological replicates of the bait with the highest scores are involved in the computation of the scores by SAINTexpress analysis (e.g. 5|6|3|6 -> 6 and 6 for BSG). After that, the software compared the two replicates to four hypothetical controls. For each prey, the 12 biological control replicates are compressed in four new controls. The compression of the biological replicates is done randomly to give this hypothetical new control. Using this method allows to obtain a more stringent and robust analysis of the results.

Finally, the software presents a range of scores but two used as determinants: the Avg(P) also called SAINT score and the Bayesian false discovery rate (FDR). The aim of SAINT is to convert the label-free quantification (spectral count) for a prey protein identified in a purification of the bait into the probability of a true interaction between the two proteins (Choi et al. 2011). The FDR represents the ordering of interactions in decreasing order of probability, Avg(P), allowing the selection of a threshold that considers the average of the complement probabilities as the Bayesian FDR. Preys with an Avg(P) >0.85 are conserved and considered as good potential interactors. Prey with a BFDR<0.05 are also kept to give at least 95% chance of identifying something real. The other prey is discarded, as they are likely the result of non-specific interactions.

Chapter 3 The actin cortex contains several NPFs

The foundation of my PhD, which I have developed to produce this thesis, is a study by Dr. Miia Bovellan and colleagues, led by my supervisor, Dr. Guillaume Charras (Bovellan et al. 2014). This chapter summarises the published research by Dr. Miia Bovellan and introduces some data that I produced during the first few months of my PhD. Section 3.1 details the previous work completed by Dr. Miia Bovellan; section 3.2 details the repeat experiments carried out by myself of the work in 3.1; section 3.3 details new follow-on experiments that I carried out; and section 3.4 details previous work that formed the basis of my project.

3.1 Previous research contributions

The contractile actin cortex is recognised as the main determinant of cell shape and is crucial for many important physiological processes. However, little was known about the proteins that participate in nucleating the cortex and the regulation of cortex assembly. Using proteomics based on isolated blebs, consisting mostly of actin cortex and membrane, Bovellan *et al*. detected the presence of the formin Diaph1 and all seven subunits of the Arp2/3 complex in the cortex (Bovellan et al. 2014). Imaging studies revealed their localisation at the cell periphery, consistent with the reasoning that a nucleator with a role in nucleating the cortex would be found in the cortex or the membrane. Overall, Bovellan *et al.* introduced the concept of a differential contribution of the Arp2/3 complex and Diaph1 in nucleating and assembling the cell cortex (Bovellan et al. 2014).

When I joined the laboratory, Bovellan *et al.* had initially used a chemical inhibitor, CK666, to reduce the activity of the Arp2/3 complex. CK666 is a small-molecule inhibitor that exerts its inhibitory function by stabilising the inactive state of the Arp2/3 complex through the steric block of the movement of ACTR2 and ACTR3 subunits into their activated conformation (Gournier et al. 2001; Nolen et al. 2004). Although its use is widespread, there is some evidence to suggest that results are not consistent with gene-silencing techniques. Thus, my initial aim was to deplete Arp2/3 subunits using shRNA interference to validate the results obtained with the use of CK666.

3.2 The Arp2/3 complex and Diaph1 generate the majority of cortical actin

One limitation of CK666 is that the inactive Arp2/3 complex is still present, allowing it to interact with binding partners or assemble into a complex, albeit lacking activity. To achieve a high degree of confidence and validate the results obtained from chemical inhibition, I depleted subunits of the Arp2/3 complex using an shRNA-silencing interference-mediated approach. In this approach, target mRNA is destabilised by the expression of a short hairpin RNA; this is processed into siRNA and binds to target mRNA leading to target-specific stable mRNA depletion. I established stable cell lines of blebbing M2-Lifeact cells with knockdowns for ACTR2 and ACTR3 subunits, and Diaph1. Non-silencing shRNA constructs were used to control for non-specific effects of silencing via the shRNA vector. Gene knockdown efficiency by the targeting shRNA was assessed with quantitative real-time PCR (qPCR) and western blotting (Figure 3-1).

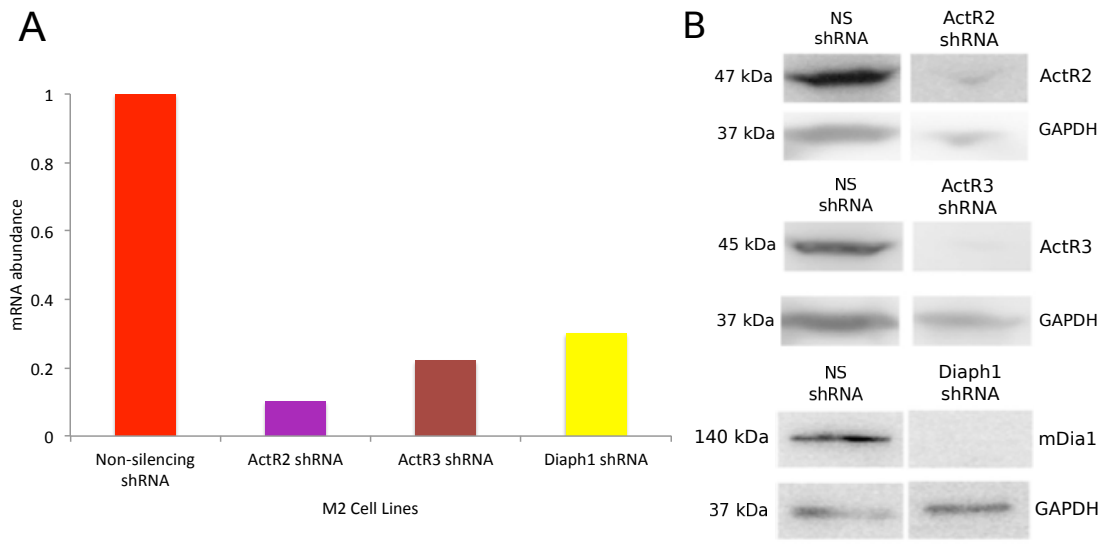

Figure 3-1 Validation of nucleator depletion in M2 cells. A, mRNA transcript abundance of ACTR2 (Arp2), ACTR3 (Arp3), and Diaph1 using qPCR; this revealed high knockdown in ACTR2 (90% knockdown), ACTR3 (78% knockdown) and Diaph1 (70% knockdown) in stable knockdown M2 cell lines. **B,** Western blot showing protein levels in stable knockdown M2 cells expressing NS, ACTR2, ACTR3, and Diaph1 shRNA, probed with anti-ACTR2, anti-ACTR3, anti-mDia1 and anti-GAPDH.

Both protein and RNA analysis confirmed significant depletion of ACTR2, ACTR3 and Diaph1 in the M2 lines generated. Following this, stably depleted cells were imaged by confocal microscopy to investigate the effect of nucleator depletion on bleb size. Changes in bleb size reflect changes in the rate of actin regrowth under the bleb membrane, with increases in growth rate associated with small blebs and decreases associated with large blebs. Bovellan *et al.* found that the rate of *de novo* actin assembly in Diaph1-depleted cells was 2-fold slower than in controls. In contrast, perturbation of Arp2/3 activity by CK666 or ArpC2 shRNA both led to an approximately 2-fold increase in actin assembly rate (Bovellan et al. 2014). Regrowth rate could affect bleb size because of percolation effects. Percolation theory describes the behaviour and formation of a connected network. For example, during the cortical actin network under the bleb membrane, the expansion of a bleb would continue until a few continuous chains of actin filaments span the whole perimeter of the bleb. To explain the change in regrowth rate observed upon nucleator depletion, it was reasoned that if a slower-than-average nucleator is depleted, assembly speed would increase. Conversely, if a faster-than-average nucleator is depleted, assembly speed will decrease. Depleting Diaph1, a fast actin nucleator (Romero et al. 2004), would result in slower actin regrowth, explaining the formation of a larger bleb. This is the opposite for depleting Arp2/3, a slower actin nucleator.

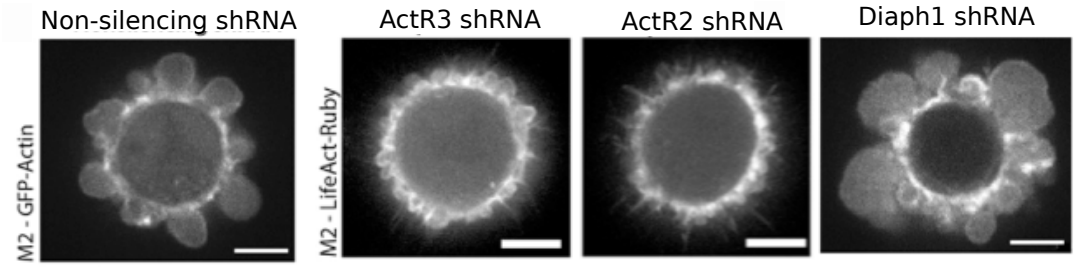

Figure 3-2 shRNA depletion of the Arp2/3 complex or Diaph1 leads to changes in bleb size. Live confocal microscopy image of M2 melanoma cells stably expressing GFP-actin and stably transfected with non-silencing shRNA, cells stably expressing Lifeact-Ruby and stably transfected with ACTR2, ACTR3 or Diaph1 shRNA. Depletion of Arp2/3 subunits results in small blebs, and depletion of Diaph1 results in large blebs, (scale bars: 5μm). Still images taken from live movies.

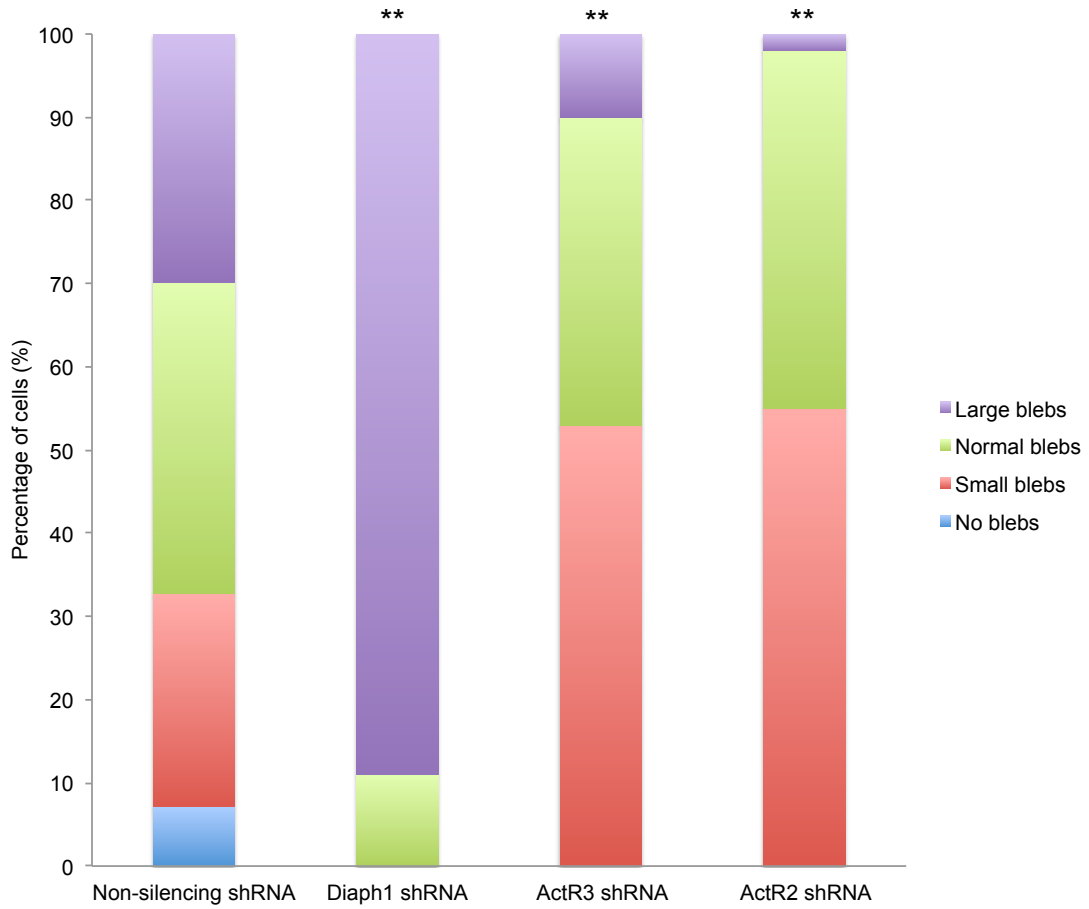

Figure 3-3 Distribution of blebbing phenotypes in M2 cells. M2 cells were depleted of Diaph1, ACTR3 or ACTR2 by shRNA interference. Cells depleted of Diaph1 produced a high proportion of large blebs, whilst Arp2/3 depleted cells generated mostly small blebs. When compared to cells stably expressing non-silencing shRNA, cells expressing Diaph1 shRNA, ACTR3 shRNA and ACTR2 shRNA all showed significantly altered bleb distributions (**$p<0.01$, chi-squared test). (Non-silencing shRNA n=211 cells, Diaph1 shRNA n=155 cells, ACTR3 shRNA n=101 cells and ACTR2 shRNA n=120 cells). Experiments were repeated four times.

Using cells with Lifeact-Ruby expression, we can image the regrowth of cortex and measure bleb size in M2 cells. Stable depletion of Arp2/3 complex subunits (ACTR3 and ACTR2) led to significant decreases in bleb size (Figure 3-2). On the other hand, stable depletion of Diaph1 resulted in 88% of cells producing large blebs (Figure 3-3). Although explainable through actin regrowth speed differences as described above, it is also possible that other factors participate in controlling bleb size. For

example, depletion of an important actin nucleator, such as Diaph1, could weaken the cortex due to lower F-actin polymerisation, resulting in larger expansion of the bleb. The influence of contractility cannot be ruled out in this instance, as contractility generates the pressure that drives bleb growth. The actin cortex is a network composed predominantly of actin and myosin. These two proteins work together to regulate mechanics, dynamics and the organisation of the actin cortex. Thus, the reduction or loss of actin will have an impact upon actomyosin organisation, potentially resulting in a change of bleb size.

The actin cytoskeleton plays a key role by providing a scaffold contributing to the definition of cell shape, force for driving cell motility and cytokinesis, amongst other processes. A thorough understanding of these processes requires insight into the spatial and temporal organisation of actin filaments into diverse higher-order structures, such as networks, parallel bundles, and contractile arrays. To further examine the impact of nucleator depletion on cortex organisation, scanning electron microscopy (SEM) was used to provide such high-resolution images of the actin filaments constituting the actin cortex. It was reasoned that the effect of depletion should be most apparent in blebs because generation of their cortex necessitates *de novo* cortical actin polymerisation.

In the control conditions, the actin cortex mesh appears homogenous, with the appearance of single filaments (Figure 3-4**A/B**, arrow). Depletion of Arp2/3 complex subunits (ACTR2 and ACTR3) led to visibly longer actin filaments (Figure 3-4C/D, arrows). This was consistent with results obtained by inhibition of Arp2/3 complex activity using CK6666. Depletion of Diaph1 led to an increase in areas devoid of actin filaments and the overall organisation was potently affected (Figure 3-4**E/F**). Furthermore, a combined depletion of Diaph1 with CK666 resulted in an overall loss of actin density and further disorganisation of the actin cortex (Figure 3-4**G/H**). This data demonstrates that in M2 cells, Arp2/3 and Diaph1 have an important role in controlling bleb size and filament organisation, supporting their involvement in actin cortex nucleation.

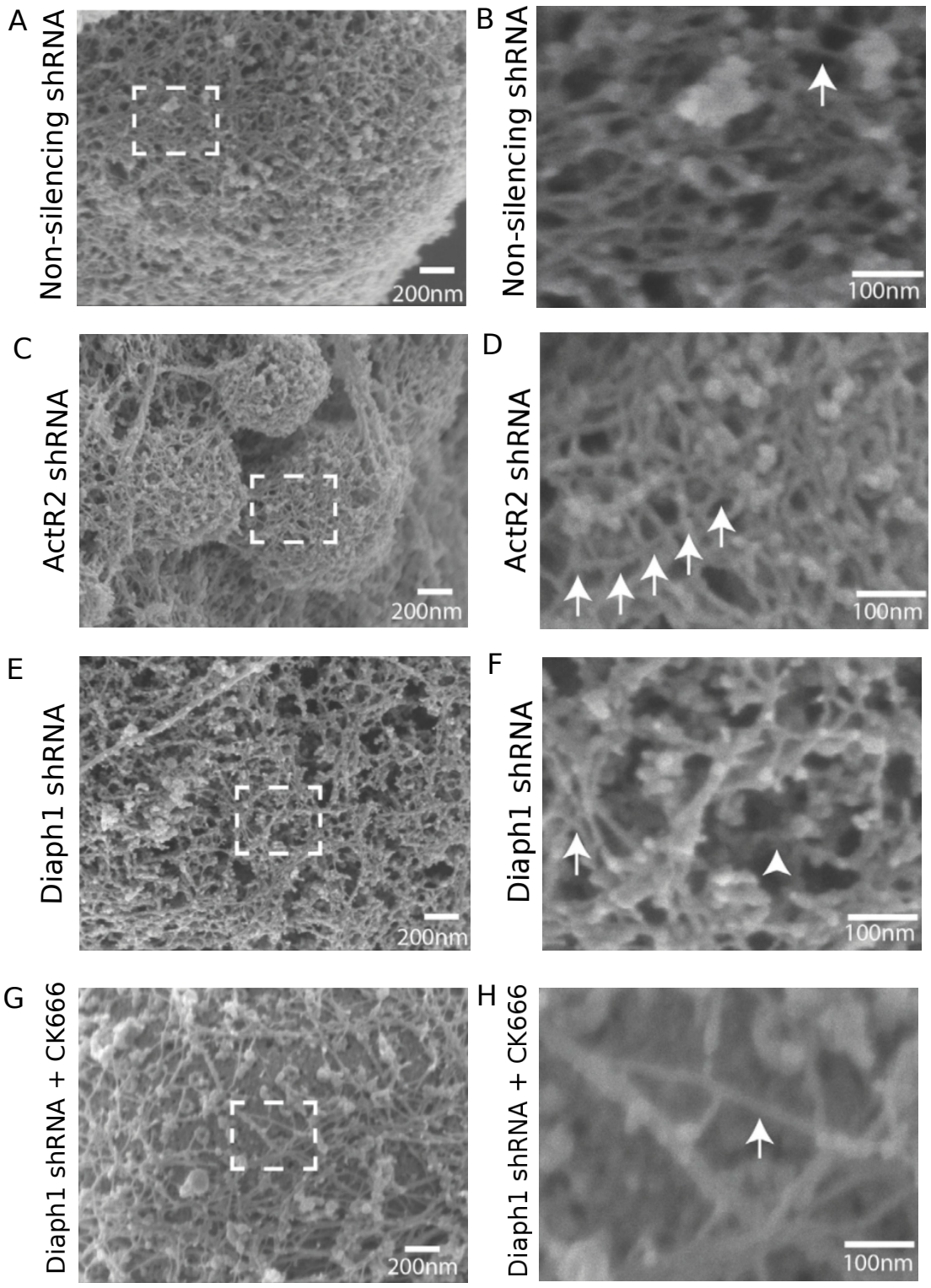

Figure 3-4 shRNA depletion of the actin nucleators leads to cortex architecture changes. Representative scanning electron micrographs of the actin cortex at the surface of a bleb in detergent-extracted M2 cell stably expressing non-silencing shRNA **(A/B)**, ACTR2 shRNA **(C/D)**, Diaph1 shRNA **(E/F)**, or stably expressing Diaph1 shRNA cells and treated with the Arp2/3 complex inhibitor CK666 **(G/H)**. B,

D, F and H are magnifications of the boxed zones in A, C and E respectively. **A/B,** The cortex is composed of a dense mesh of overlapping filaments primarily oriented tangential to the bleb surface. The actin filament density within the mesh appears approximately uniform. Individual filaments can clearly be distinguished (white arrow). **C/D,** The cortex appears less uniform than in control cells with areas of high filament density (white arrow) alternating with large gaps devoid of filaments (arrowhead). **E/F,** Filaments appear generally longer than in control cells and can be traced over several hundred nanometers (white arrows). **G/H,** The actin cortex is visibly less dense than in control cells. Only few actin filaments (white arrow) subsist with gaps of several hundred nanometers in between.

3.3 Diaph1 and Arp2/3 depletion significantly increased cell cycle failure

Eukaryotic cell division, in particular, requires a contractile ring of actin and myosin that cleaves the cell in two. This ring remains dynamic with F-actin continually turning over. Thus, actin polymerisation driven by nucleator activity is a central process in cytokinesis, and an important process that warrants further understanding. To this aim, I generated individual stable HeLa cells depleted for ACTR2 and ArpC2 by shRNA (Figure 3-5). The stable depletion of Diaph1 led to an unviable cell population, so instead I used siRNA to allow for temporary silencing.

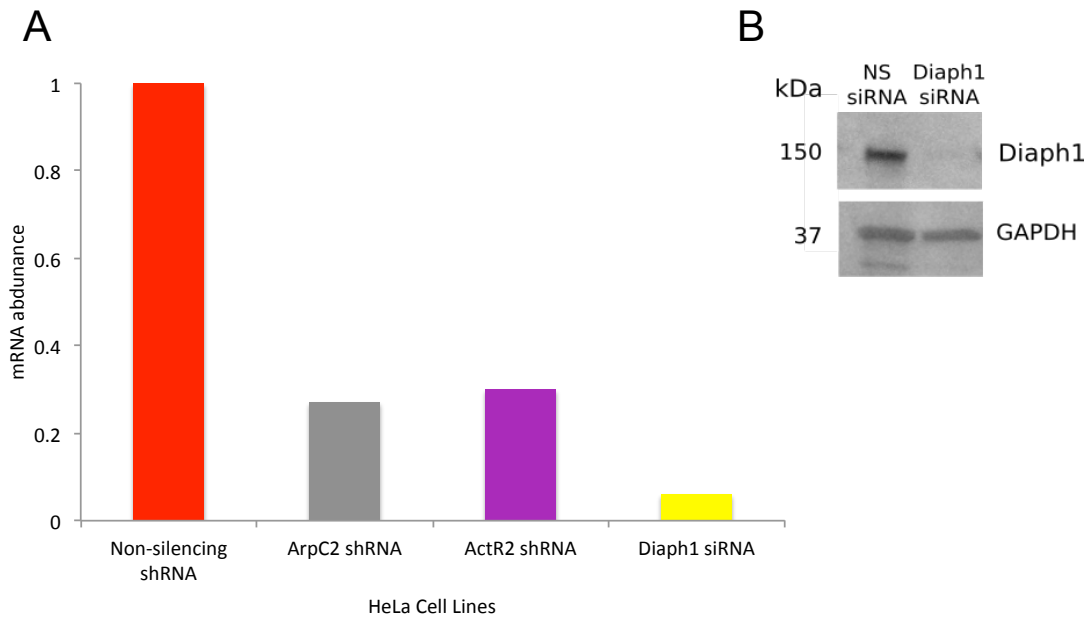

Figure 3-5 **Validation of protein depletion in HeLa cells. A,** mRNA transcript abundance of ArpC2, ACTR2 (Arp2), and Diaph1 using qPCR; this revealed high

knockdown in ArpC2 (73% knockdown) and ACTR2 (70% knockdown) in stable knockdown HeLa cell lines, and Diaph1 (94% knockdown) using siRNA depletion. **B,** Western blot showing protein levels in stable knockdown HeLa cells expressing NS and Diaph1 siRNA, probed with anti-mDia1 and anti-GAPDH as a loading control.

To reflect the succession of morphological changes leading up to, and following the division of cells, I categorised each cell as either 'normal' or having 'failed to progress' normally through the cell cycle. The 'failure to progress' group had numerous subdivisions, including those that died at the various stages in mitosis, and those that presented an abnormal event during the division, such as oscillations. This fine categorisation allowed for the pinpointing of the stage of cell division that was disrupted by the knockdown, reflecting the importance of the regulator at that particular stage of the cell cycle. The results observed are graphically represented as displayed in Figure 3-6.

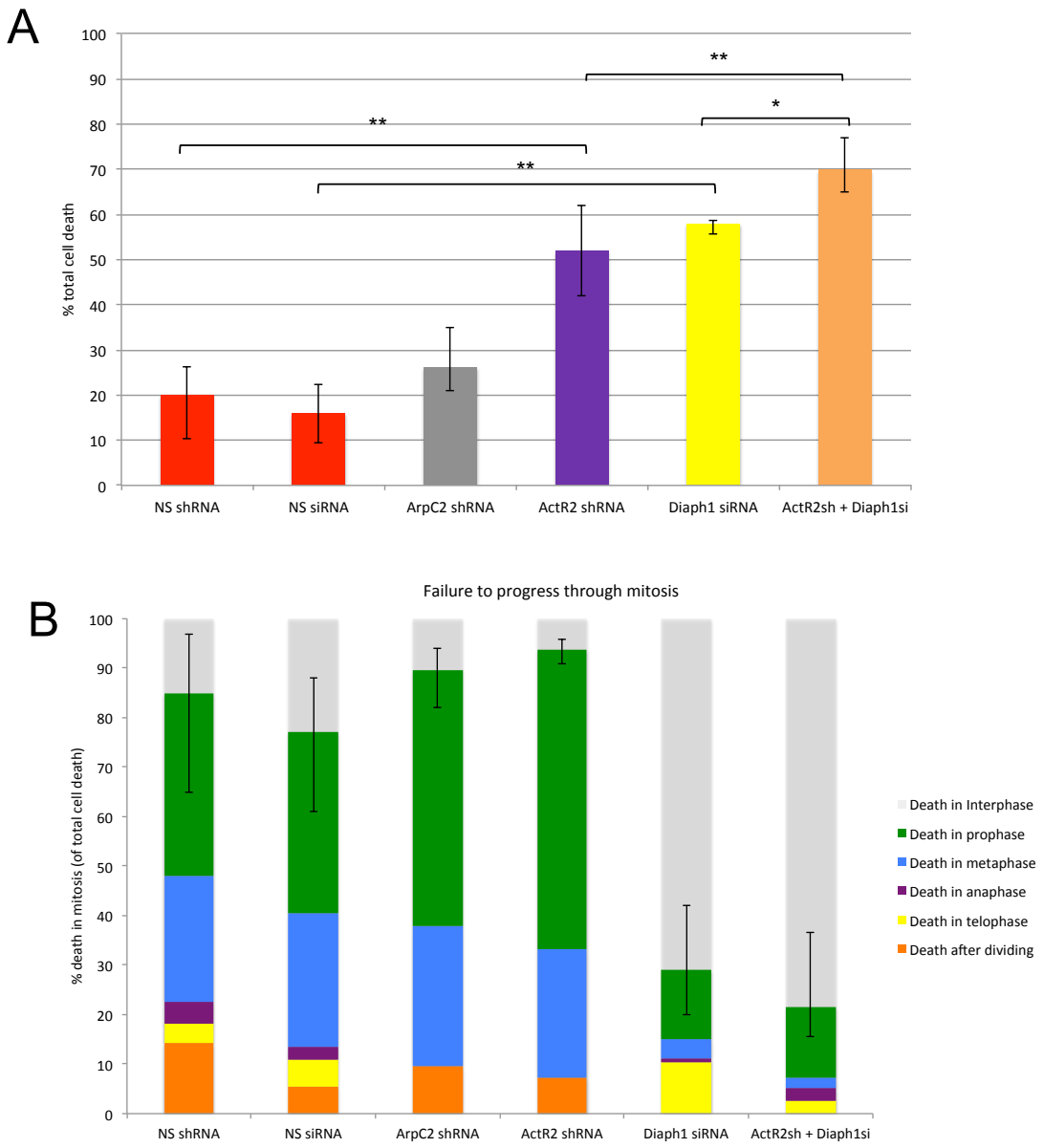

Figure 3-6 Nucleator depletion affects progression through the cell cycle and interrupts it at different stages. HeLa cells were imaged for 19 hours (overnight) in temperature-controlled conditions, data was analysed and presented graphically. A, When compared to cells transfected with non-silencing shRNA/siRNA, cells depleted in ACTR2 and Diaph1 showed significantly reduced rates of successful cell cycle progression (**p<0.01). When compared to single transfections of ACTR2 (**p<0.01) and Diaph (*p<0.05), cells depleted of both ACTR2 and Diaph1 showed a significant increase in total cell death. In contrast, cells depleted for ArpC2 did not display a significant difference (p=0.42). Results were gathered from 4 independent experiments examining: Non-silencing shRNA

(n=936 cells), non-silencing siRNA (n=178 cells), ArpC2 shRNA (n=423 cells), ACTR2 shRNA (n=611 cells), Diaph1 siRNA (n=200 cells), ACTR2 shRNA + Diaph1 siRNA (n=219 cells). Data was analysed with a Chi-squared statistical test. **B,** Distribution of cell deaths as a function of cell cycle stage. Cells that died during interphase are represented in grey, cells that died in prophase in green, metaphase in blue, anaphase in purple, telophase in yellow and after dividing in orange, are shown. Cells that died after dividing includes those that divide and regress, those that divide and could not spread, and cells that oscillated. All knockdown lines show a high proportion of cell death occurring in mitosis, however, cells depleted of Diaph1 typically die during interphase.

Depletion of ArpC2 did not significantly affect progression through cytokinesis, consistent with previous results obtained from siRNA depletion (Bovellan et al. 2014). However, ArpC2 depletion gave rise to increased cell blebbing in interphase, also consistent with a previous study (Derivery et al. 2008). Here, it was surprising to see that ACTR2 and ACTR3 had different impacts on successful progression through the cell cycle. Interestingly, depletion of ACTR2 displayed a significant effect on the progression of division past mitosis (Figure 3-6**A**).

Bovellan *et al.* demonstrated the perturbation of actin cortex stability during mitosis as a result of Diaph1 siRNA depletion (Bovellan et al. 2014). This was confirmed by my results (Figure 3-6**A**) where total cell death exceeded 50%, a figure much higher than the controls. Although the death rate is similar to ACTR2 depletion, I did notice a difference in the specific cell cycle stage at which death occurred. Cells depleted of Diaph1 predominately tended to fail in interphase (Figure 3-6**B,** Figure 3-7**D**). On the contrary, cells depleted of ACTR2 instead failed during early mitosis (Figure 3-7**B**). This suggests a differing role for both actin nucleators in reorganising the actin cortex during the cell cycle. Failure during interphase may indicate failure to remodel the cytoskeleton prior to mitosis, where the cells abandon the spread morphology characteristic of interphase and adopt a round shape. Conditions that disturb mitotic cell rounding have been observed to be detrimental to spindle morphogenesis (Kunda et al. 2008) and orientation (Théry et al. 2007), suggesting interdependence between mitotic cell rounding and other aspects of mitosis. Moreover, it has been shown that a uniform Diaph1-dependent F-actin cortex coincides with initial rounding during mitosis (Ramanathan et al. 2015).

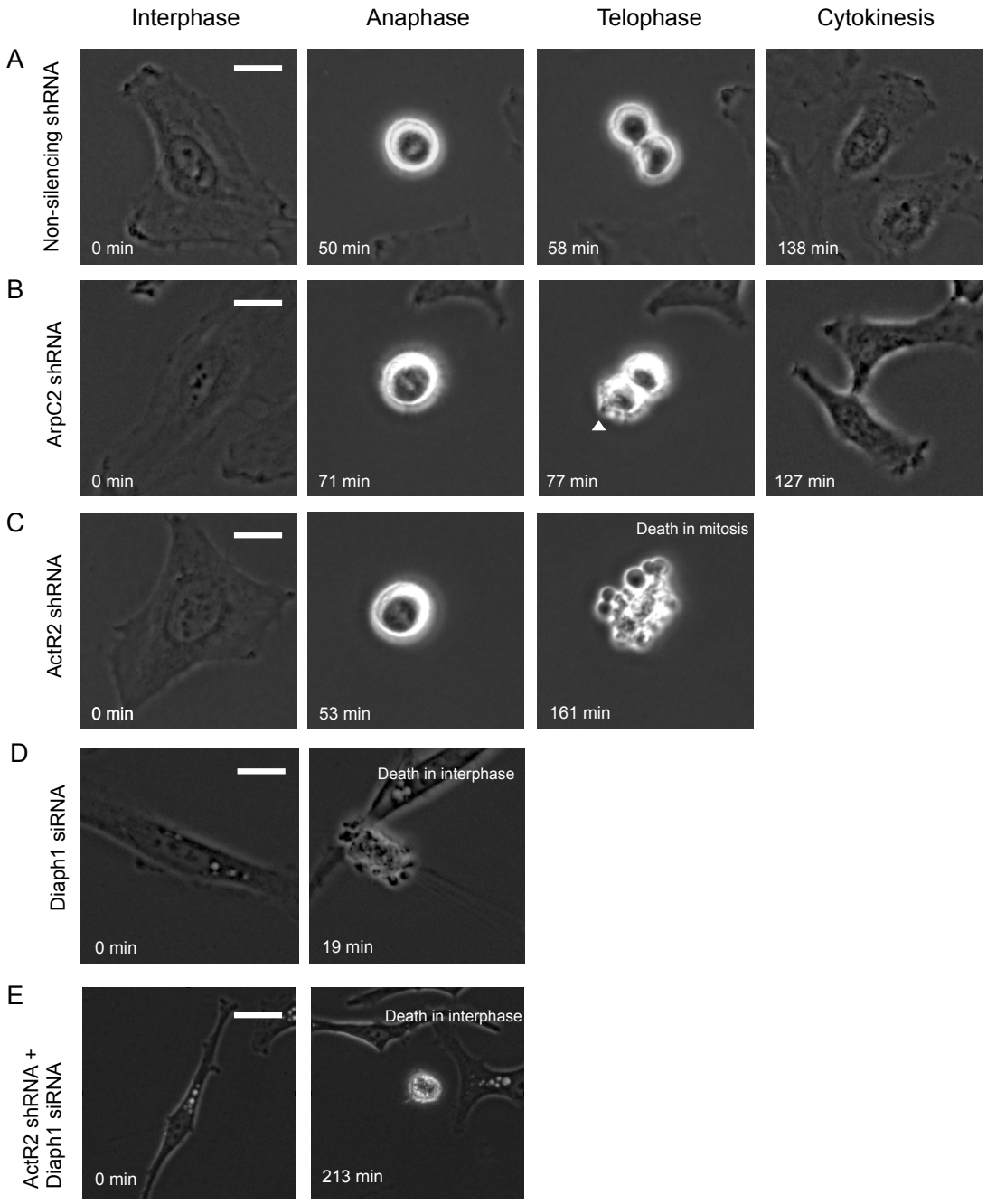

Figure 3-7 Live cell imaging of shRNA silenced HeLa cells using phase contrast microscopy. HeLa cells were imaged for 19 hours (overnight) in temperature-controlled conditions, and stills were taken from the live movies. A, Control cells progress through mitosis abandoning the flat morphology of interphase, then advance through the stages of mitosis before cell cleavage and abscission where the daughter cells separate. **B,** ArpC2 shRNA cells appear normal with the presentation of small blebs during mitosis (arrowhead). **C,** ACTR2 shRNA cells were very blebby during mitosis, with many cells dying at this stage. **D,** Diaph1 siRNA cells appear more

elongated in interphase and frequently die during interphase. **E,** Combined depletion of ActR2 (with shRNA) and Diaph1 (with siRNA) resulted in a decrease in cell survival, with the majority of cells dying in interphase. Scale: 20μm.

Finally, the double depletion of Diaph1 and ACTR2 led to a substantial increase in overall cell death in HeLa cells (Figure 3-6**A,** Figure 3-7**E**) when compared to single depletion, adding up to a total of 70% failure. This further supports the importance of both Diaph1 and the Arp2/3 complex as major contributors to nucleation of the actin cortex.

3.4 Cortical nucleation promoting factors identified through proteomics

The identification of the Arp2/3 complex and Diaph1 as major contributors to the nucleation of the actin cortex led to an important follow up question: *how is the activity of actin nucleators regulated in the cell cortex following activation by RhoGTPases?* In addition to the detection of the Arp2/3 complex and Diaph1, proteomic analysis of the cortical fraction identified a number of actin-regulating proteins (Table 3-1). These proteins are thought to interact with Arp2/3 and/or Diaph1 to regulate actin polymerisation via distinct mechanisms and are called nucleation-promoting factors (NPFs). NPFs maintain nucleator activity or directly activate nucleators downstream of RhoGTPases.

The motivation for this investigation is that understanding how NPFs control actin assembly is critical to determine how cells control their mechanical properties through changing the organisation of cortical actomyosin. Thus, for a holistic appreciation of F-actin nucleation by Arp2/3 and Diaph1, it becomes important to focus upon the upstream signalling mechanisms that maintain or relay activation downstream of RhoGTPases.

Table 3-1 Nucleation-promoting factors detected by proteomics in the detergent-insoluble fraction of separated blebs. Analysis of three independent biological replicates revealed ~170 actin-binding proteins, actin regulatory proteins, and proteins known to interact with actin binding proteins. Detected peptide numbers were averaged over three experiments. The following proteins: Flightless-I, NCKIPSD, IQGAP1 and three subunits of the WAVE complex were detected at a high degree of confidence and reproducibility (more than 3 peptides detected in at least two separate experiments). Protein abundance index (PAI) was calculated based on spectral counts. Prof. Philippe Roux carried out proteomic analysis.

	Protein	kDa	Average no. of peptides	PAI
	Flightless	144.8	24	16.67
	NCKIPSD	78.9	5.6	7.10
	IQGAP1	189.3	80.6	42.65
WAVE complex	WAVE2	54.3	2.8	5.12
WAVE complex	SRA1	14.5	19.2	132.35
WAVE complex	NAP1	12.9	12.4	95.98

PAI – Protein Abundance Index

Examination of the proteomic results revealed the presence of several NPFs in the actin cortex of blebs: WAVE complex subunits (Sra1/Nap1) (Bovellan et al. 2014), IQGAP1 (Biro et al. 2013), Flightless-I, and NCKIPSD (also known as DIP/WISH/Spin90). All of these proteins have additionally been identified as substrates modulated by phosphorylation during the cell cycle in HeLa cells (Olson & Nordheim 2010; Dephoure et al. 2008). The WAVE complex is activated by Rac and activates nucleation via the Arp2/3 complex (Steffen et al. 2004). NCKIPSD has been shown to interact with both Diaph1 (Eisenmann et al. 2007) and Arp2/3 (Dae et al. 2006). Flightless-I is a RhoA effector that binds to the DAD domain of formins to prevent autoinhibition (Higashi et al. 2010), suggesting it also acts as a class II NPF. IQGAP1 is a large scaffolding protein activated by Cdc42 and Rac1, and shown to interact with WAVE, WASp and Diaph1 through its different domains (Brandt et al. 2007; Foroutannejad et al. 2014; Gorman et al. 2012). In both cases, it prevents

inactivation of its interactor, suggesting it acts as a class II NPF. Thus, these NPFs appear promising candidates for controlling the length and organisation of actin filament networks, as well as coordinating the activity of cortical nucleators.

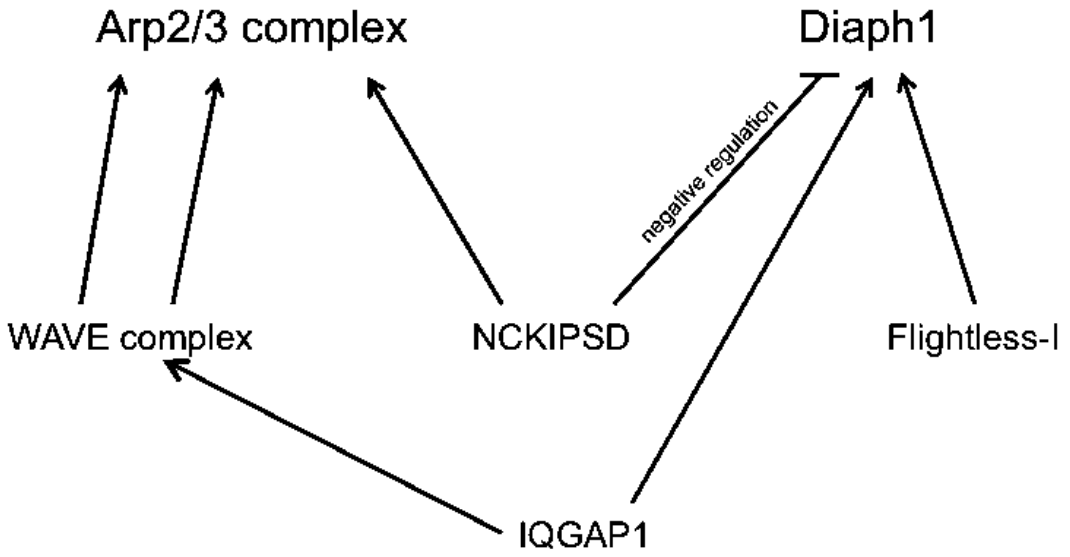

Figure 3-8 Schematic of potential interactions between NPFs and cortical nucleators. Based on the literature, the following interactions are grouped into those that activate nucleation via the Arp2/3 complex, and those that activate nucleation via Diaph1. There is evidence for NCKIPSD and IQGAP1 interacting with both Arp2/3 and Diaph1, although the interaction between NCKIPSD and Diaph1 is thought to be inhibitory.

3.5 Conclusion

Overall, my initial data confirms the concept of a differential contribution of the Arp2/3 complex and Diaph1 in nucleating and assembling the cell cortex introduced in Bovellan *et al*. The perturbation of both Arp2/3 and Diaph1 led to profound changes in actin cortex organisation, indicating that they play a crucial role in generating cortical actin in the submembraneous F-actin cortex in M2 and HeLa cells. Recent work has shown that formin-nucleated filaments are, on average, ten times longer than Arp2/3-nucleated filaments, however formin-generated filaments represent less than 10% of all actin filaments (Fritzsche et al. 2016). Kinetically, both nucleators appear to have distinct roles in cortical actin nucleation, suggesting

differential contribution towards F-actin assembly, dependent upon the physiological needs.

Furthermore, NPFs that modulate nucleator activity were identified and subdivided into two categories based on their proposed role in literature: those that interact with the Arp2/3 complex and those that interact with Diaph1. Many actinous structures require formins and the Arp2/3 complex for their formation. It is possible that both nucleators cooperate to generate the actin network (Bovellan et al. 2014). Alternatively, it has been proposed that the difference in structure induced by each nucleator could dictate specific filament function (Michelot & Drubin 2011). Both cases underline the importance of coordinating the activity of each nucleator for the generation of actinous structure and for dictating its mechanical properties. As a consequence, the control of crosstalk between nucleators is a subject of great interest. Here, I investigate the role of the identified proteins: IQGAP1, NCKIPSD, Flightless-I and the WAVE complex, as potential NPFs interacting with Diaph1 or Arp2/3. I also investigate their role in supporting and maintaining activation through stabilisation of active nucleator conformations, and interacting with other small molecules.

Chapter 4 Candidate NPFs localise to the actin cortex

Cortex reassembly was investigated in two cell lines; M2 cells, because they display a visible cortex throughout the cell cycle, bleb, and thus need to reassemble cortex continuously, and HeLa cells, because they have a well-defined cortex during metaphase. I performed an imaging screen to check for cortical localisation of candidate NPFs, reasoning that NPFs that localised to the cortex were good candidates for regulating cortical actin nucleators.

4.1 Localisation in M2 cells

To determine nucleator localisation, I transfected GFP tagged full length IQGAP1, NCKIPSD, Flightless-I and the WAVE complex subunits Sra1 and Nap1 in M2 cells stably expressing the F-actin reporter LifeAct-Ruby. As shown in Figure 4.1, IQGAP1 displayed a clear cortical localisation and formed a well-defined rim under bleb membranes. When I imaged the bleb life cycle, I found that blebs were initially devoid of IQGAP1 and that IQGAP1 was recruited after bleb growth had ceased. The other proteins I examined displayed a strong cytoplasmic signal, perhaps because of a high bound/unbound ratio. Indeed, if most of the proteins of interest are not bound to the actin cytoskeleton, this will result in high cytoplasmic fluorescence, obscuring the lower amount of cortical bound protein and making it difficult to distinguish above background. Another potential issue is that the GFP tag might interfere with protein function.

To overcome issues due to high cytoplasmic background, I decided to attempt permeabilisation-fixation experiments after initial baseline imaging. In this approach, the unbound fraction is removed by permeabilisation, allowing the bound fraction to be visualised through stabilisation by fixation. I observed that Flightless-I localised strongly to the cortex but was less apparent in blebs (**Figure 4-1**, arrow). This could suggest that it may not be important for recruitment and reassembly of the actin cortex but rather gets recruited once a mature cortex has been re-established. Both NCKIPSD and IQGAP1 clearly localised to the cortex (**Figure 4-1**, arrow), and were also visible underneath the membrane of blebs (**Figure 4-1**, asterisk). Sra1 and Nap1 did not display strong cortical localisation and remained predominantly cytoplasmic

after permeabilisation. Similar results were obtained with other subunits of the WAVE complex. However, as the WAVE complex is a well-established Arp2/3 interactor and it was identified with high certainty in the cortex we decided not to rule it out for further study. Interestingly, cells transfected with Sra1 and Nap1 had markedly less blebs than untransfected cells, perhaps signifying that overexpression of WAVE complex subunits leads to changes in cytoskeletal organisation. This issue made it difficult to analyse the patterns of expression during blebbing. Similar localisation were also obtained by Dr Guillaume Charras using immunostaining in M2 cells, except for the WAVE complex that showed a clear enrichment in blebs. Together these results support Flightless-I, IQGAP1 and NCKIPSD as good candidates for regulating cortical actin nucleation.

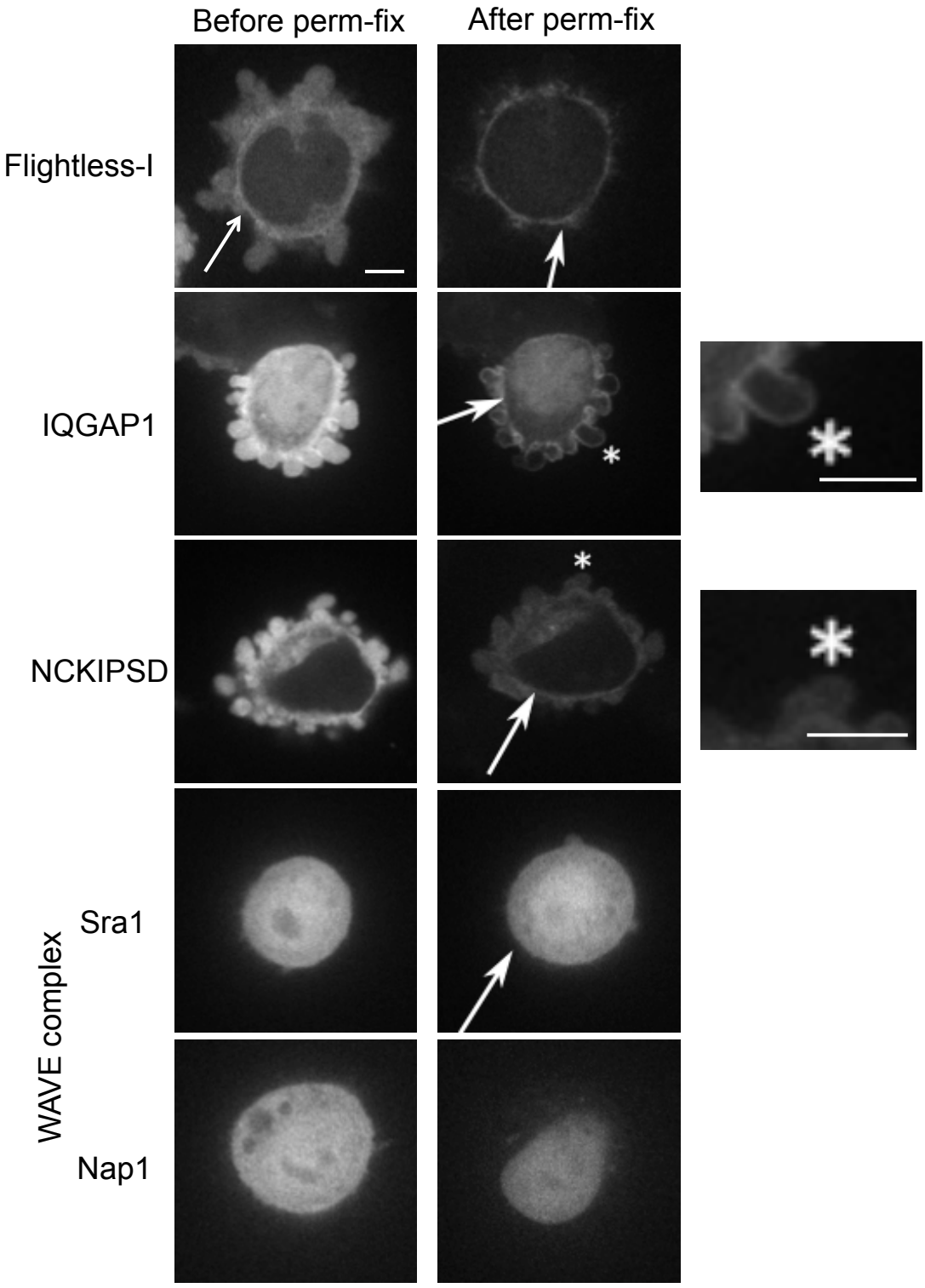

Figure 4-1 Localisation of candidate NPFs in M2 cells. Full-length proteins with GFP tags were transfected into cells. Transfected cells were imaged for a few frames to provide a baseline, after which the imaging medium was replaced by medium containing detergent and fixative. During this time, I continued imaging, allowing for

the cortical localisation to be visualised. Arrows point to regions of localisation at the cortex; asterisks point to regions of localisation at the cell blebs. Scale bar: 5μm.

4.2 Localisation in HeLa cells

I then proceeded to examine localisation in HeLa cells in interphase using the same permeabilisation fixation strategy. For all proteins, localisation appeared more cytoplasmic before permeabilisation (**Figure 4-2**). Similar to localisation in M2 cells, IQGAP1 had the strongest cortical expression at the actin cortex, supporting a possible role in regulating actin nucleation at the cortex. Flightless appeared to show a weak cortical expression at the actin cortex, also supporting its potential role in regulating actin nucleation at the cortex. Localisation of NCKIPSD was not as apparent as Flightless and IQGAP1, even with removal of the membrane. WAVE2, a WAVE subunit detected in the earlier proteomics, displayed some cortical localisation, albeit not uniform across the cell.

As overexpression may lead to mislocalisation of proteins, we also carried out immunostaining experiments to confirm localisation of endogenous proteins in interphase and metaphase. In mitotic cells, IQGAP1 revealed a clear cortical localisation (**Figure 4-3**), however immunostainings for other proteins showed higher cytoplasmic background (Flightless-I, NCKIPSD, WAVE2 and Sra1). Despite this, Flightless-I. Wave2 and NCKIPSD did show some enrichment at the cortex (arrows). These data could either reflect a low proportion of active protein bound to the cortex or be due to poor quality antibodies.

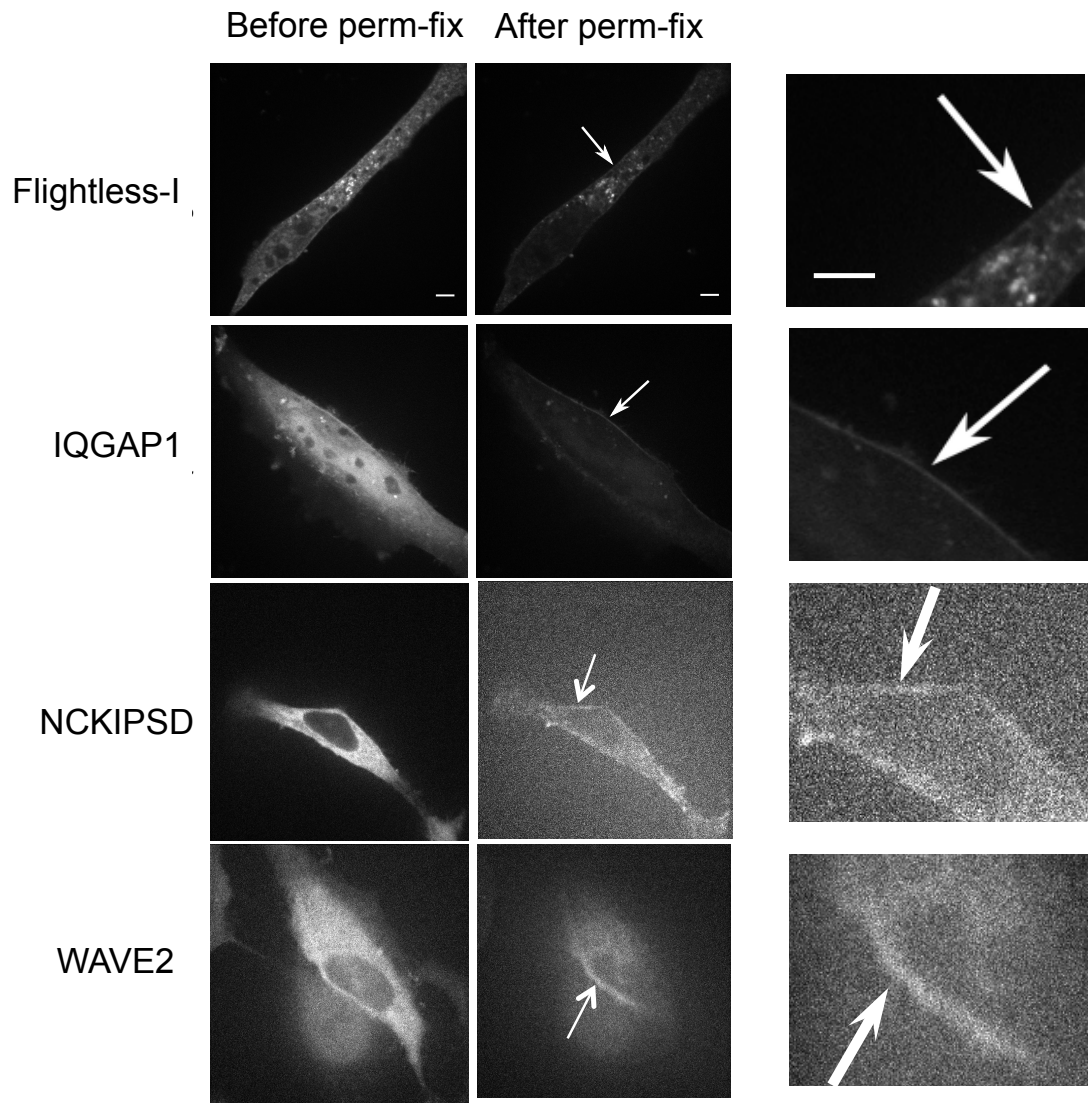

Figure 4-2 Localisation of candidate NPFs in interphase HeLa cells. Full-length proteins with GFP tags were transfected into cells. Transfected cells were imaged for a few frames to provide a baseline, after which the imaging medium was replaced by medium containing detergent and fixative. During this time, I continued imaging, allowing for the cortical localisation to be visualised. Arrows point to regions of localisation at the cortex; asterisks point to regions of localisation at the cell blebs. Scale bar: 5μm.

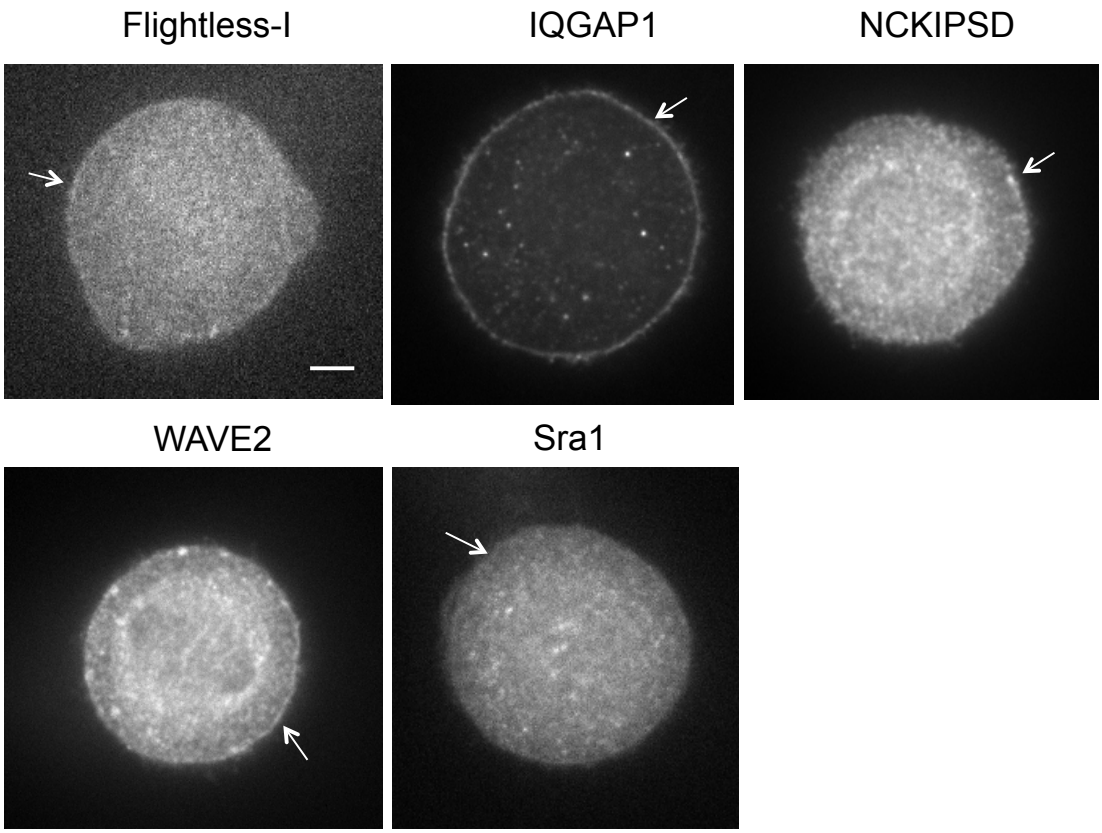

Figure 4-3 Immunostaining localisation of NPFs in mitotic HeLa cells. Arrows point to regions of localisation at the cortex. Scale bar: 5μm. Images taken by Dr Guillaume Charras.

4.3 Conclusion

Overall, IQGAP1, NCKIPSD and Fli-I appear to localise to the cortex, with IQGAP1 most strongly localised. This makes these NPFs good candidates for regulation of cortical actin nucleators. Localisation of the WAVE complex subunits was more challenging to obtain, however as previously mentioned, the WAVE complex is a well-established Arp2/3 interactor and has been identified with high certainty in the cortex. Never the less, it is important to note that WAVE2 and Sra1 were not seen at the cortex, possibly due to the GFP tag affecting its localisation or incorporation into the complex.

Chapter 5 NPF depletion affects bleb size

To investigate the role of NPFs in modulating nucleator activity, I examined how their depletion affected bleb size. There are many candidate actin-binding proteins that have been identified in the literature, however little is known about their mechanism of action and relative contribution to the assembly of actin, especially within the actin cortex. Bleb size is a good reporter of the effect of perturbing an important actin nucleator, or in this case NPF, because generation of their cortex necessitates *de novo* cortical actin polymerisation. Based on previous work, depletion of Arp2/3 or Diaph1 yields a small or large blebbing phenotype, respectively (Bovellan et al. 2014). I hypothesised that the depletion of an NPF important for regulation of a nucleator would result in phenocopying of the bleb size. I directed my initial focus towards the proteins detected by mass spectrometry of the cortex in isolated blebs: Flightless-I, IQGAP1, NCKIPSD and the WAVE complex (Table 3-1).

To this aim, I generated stable M2 cell lines depleted for each of the NPFs identified. These cells also stably expressed Lifeact-Ruby to allow for imaging of F-actin. Depletions were verified with qPCR to quantify mRNA transcript levels (Figure 5-1**A**), and western blotting to quantify protein levels (Figure 5-1**B**).

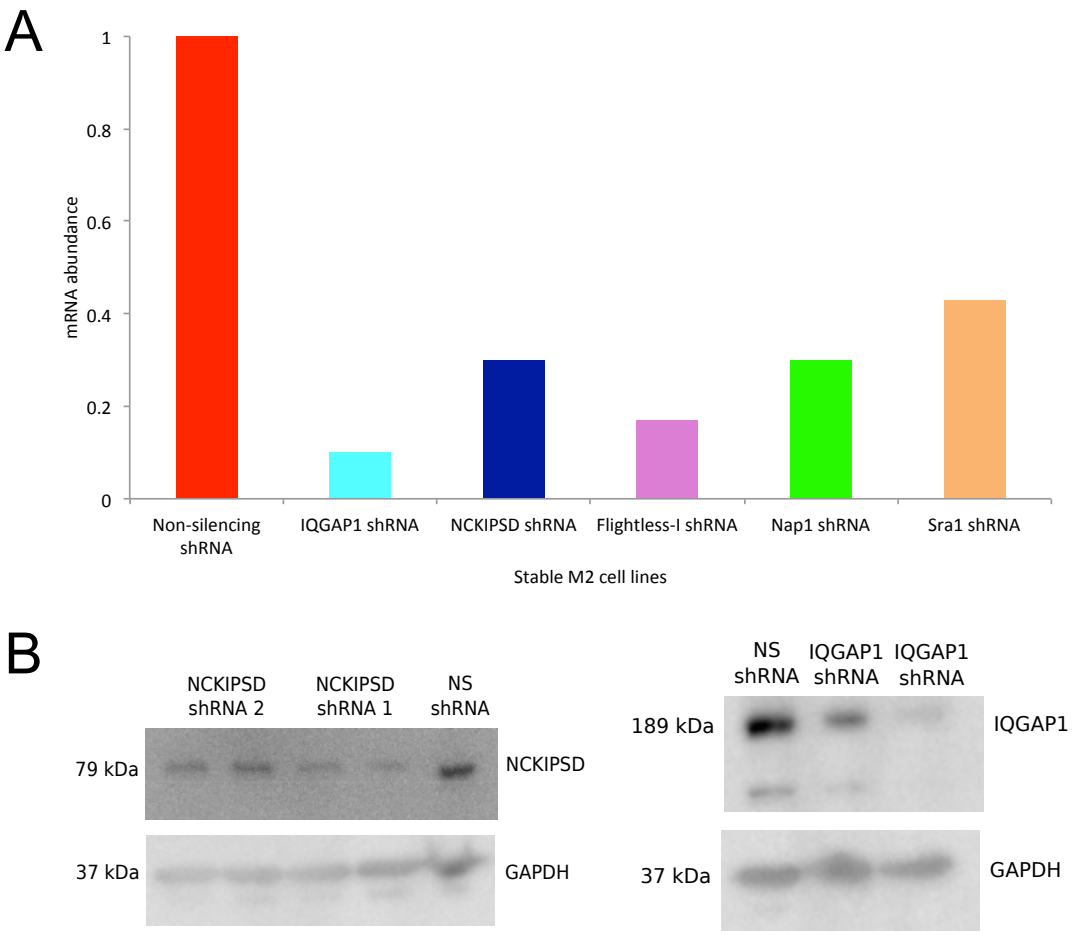

Figure 5-1 Validation of protein depletion in M2 cells. A, mRNA transcript abundance of IQGAP1, NCKIPSD, Flightless-I, Nap1 and Sra1 using qPCR; this revealed high knockdown in IQGAP1 (90% knockdown), NCKIPSD (70% knockdown), Flightless-I (83% knockdown), Nap1 (70% knockdown) and Sra1 (67% knockdown) in stable knockdown M2 cell lines using shRNA depletion. **B,** Western blot showing protein levels in stable knockdown M2 cells expressing NS, NCKIPSD (shRNA1, 72% protein depletion; shRNA2, 63% protein depletion) and IQGAP1 shRNA (85% protein depletion), probed with anti-NCKIPSD, anti-IQGAP1 and anti-GAPDH as a loading control.

5.1 Depletion of Flightless-I has no effect on bleb size in M2 cells

The first actin-binding protein that I studied was Flightless-I (FliI). I reasoned that if FliI was needed for Diaph1 activation as suggested in the literature (Higashi et al.

2010), its depletion would lead to the observation of large blebs, comparable to what is observed for Diaph1 depletion (Bovellan et al. 2014).

To confirm FliI knockdown, I performed qPCR to quantify mRNA. Results obtained from qPCR experiments revealed a knockdown of 83% (Figure 5-1). I observed no significant phenotype accompanying FliI depletion in M2 cells (Figure 5-2), with the majority of blebs categorised as 'normal' sized (Table 5-1, Figure 5-6).

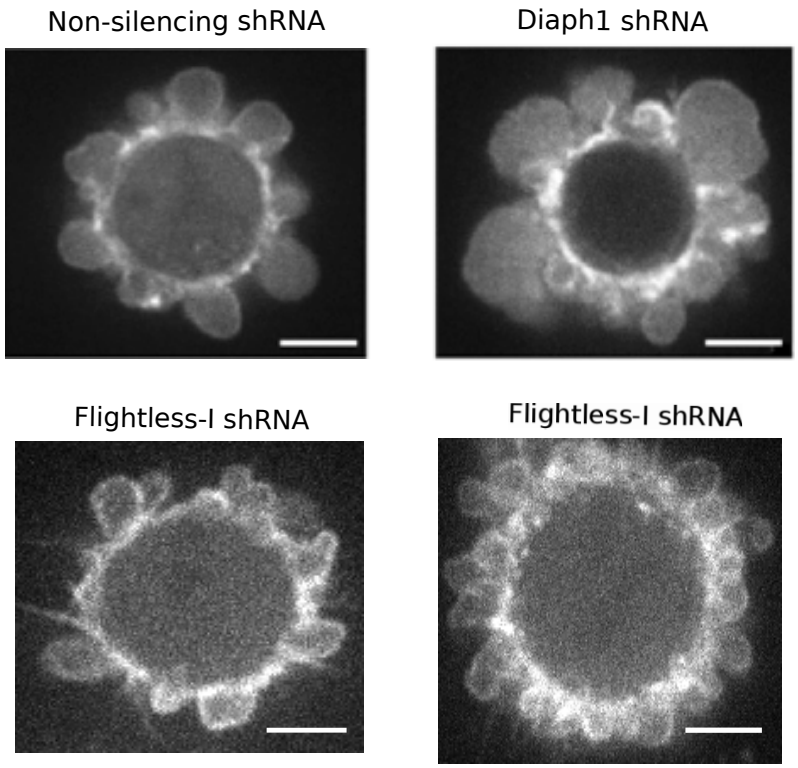

Figure 5-2 Representative images of M2 cells expressing Lifeact-Ruby and different shRNA constructs, scale - 5µm. FliI shRNA bleb size was not significantly different compared to non-silencing shRNA cells.

Overall, FliI revealed no significant phenotype in M2 cells, suggesting that it may not play an important role in the control of actin regrowth in blebs. Actin nucleation by Diaph1 is important for the normal progression of the cell cycle; thus, it is possible that the depletion of FliI may produce more profound effects when examining progression through the cell cycle. Therefore, I did not rule out a role for FliI and continued to study it in further experiments in HeLa cells.

5.2 IQGAP1 depletion phenocopies Diaph1 knockdown

I next investigated IQGAP1 as a potential NPF. As previously mentioned, it is thought that IQGAP1 has a dual role in regulating Diaph1-mediated nucleation and the activity of the Arp2/3 complex; thus, the expected depletion phenotype could not be readily hypothesised. To detect and validate IGQAP1 knockdown, I performed qPCR and western blotting to quantify mRNA and protein levels, respectively. Results obtained from qPCR experiments revealed a 90% knock down in mRNA transcripts and high protein depletion (85% protein depletion) (Figure 5-1).

A clear and significant phenotype of large blebs was observed with the depletion of IQGAP1 in M2 cells, with almost 60% of cells displaying large blebs compared to 25% of large blebs in the control cells (Table 5-1, Figure 5-6). This is similar to the large bleb phenotype observed with the knockdown of Diaph1, but not consistent with the small bleb phenotype observed upon Arp2/3 complex subunit depletion (Figure 5-3). The observed phenotype suggests that the removal of IQGAP1 affects Diaph1 activity. Although the phenotypic analysis suggests that IQGAP1 controls actin nucleation via regulation of Diaph1, the results do not exclude the existence of other Diaph1 activators.

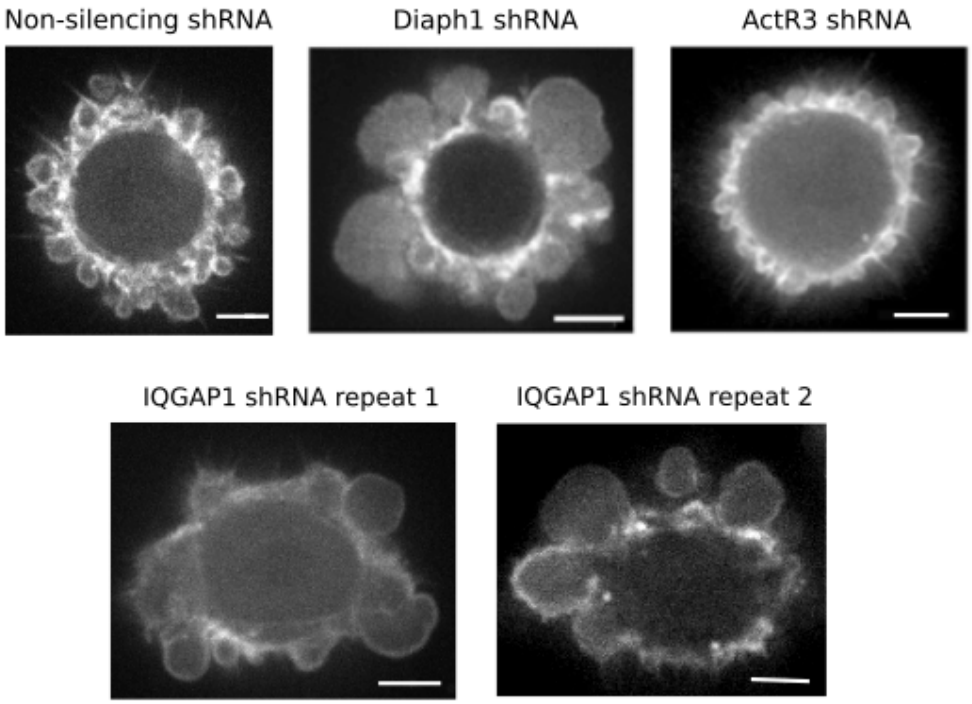

Figure 5-3 Representative images of M2 cells expressing Lifeact-Ruby and different shRNA constructs, scale - 5μm. IQGAP1 shRNA bleb size was significantly larger compared to non-silencing shRNA cells.

5.3 NCKIPSD depletion phenocopies Diaph1 knockdown

Similar to IQGAP1, NCKIPSD appears to be an important protein, which may act to coordinate the activity of both cortical nucleators. To evaluate the effect on bleb size, a stable cell line with NCKIPSD depletion was generated in M2 cells. Results obtained from qPCR experiments revealed a 70% knockdown, and western blotting revealed a protein knockdown of shRNA 1 and 2 of 72% and 63% protein depletion, respectively. It has been reported that NCKIPSD negatively regulates Diaph3 and interacts with Diaph1 (Eisenmann et al. 2007); and for this reason I decided to examine if Diaph1 may also be negatively regulated. If this were the case, I would expect to see smaller blebs, as the removal of an inhibitor would allow increased Diaph1 activity. Furthermore, if NCKIPSD was important for regulation of Arp2/3, I would expect to also see small blebs, similar to the Arp2/3 depleted small bleb phenotype previously reported. Contrary to both predictions, the NCKIPSD depletion had a phenotype associated with large blebs (Figure 5-4). 45% of cells depleted of NCKIPSD displayed large blebs, significantly more than displayed in

control cells (Figure 5-6, Table 5-1). This suggests that NCKIPSD is acting through the Diaph1 nucleation pathway as an activator. This is contrary to its perceived role as a negative regulator of Diaph1 or as a positive regulator of Arp2/3 due to the lack of a phenocopy in bleb size. Here, it is important to remember that NCKIPSD has been reported to nucleate small linear filaments via Arp2/3, and these may have a different function to the usual dendritic arrays present when WASp or the WAVE complex activates Arp2/3.

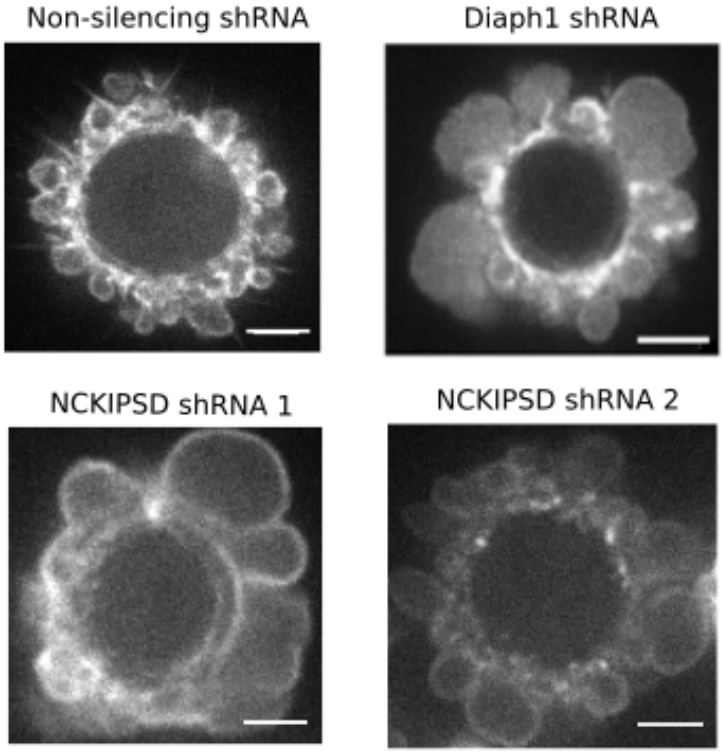

Figure 5-4 Representative images of M2 cells expressing Lifeact-Ruby and different shRNA constructs, scale - 5µm. NCKIPSD shRNA bleb size was significantly larger compared to non-silencing shRNA cells.

5.3.1 WAVE complex depletion phenocopies Arp2/3 complex depletion

The WAVE complex is a well-studied and well-characterised NPF, known to control actin cytoskeletal dynamics through activity of the Arp2/3 complex (Semba et al. 2006). I began my investigation by generating stable M2 cell lines depleted for the three detected subunits: Nap1, Sra1 and WAVE2. After qPCR analysis, I decided not to continue investigating WAVE2 due to weak mRNA depletion. On the other hand,

shRNA depletion of Sra1 and Nap1 resulted in a 57% and 70% knockdown of mRNA, respectively (Figure 5-1). In M2 cells, Cells with Sra1 and Nap1 knockdown displayed a very strong phenotype of small blebs similar to that seen with a depletion of the Arp2/3 complex (Figure 5-5). Nap1 depleted cells presented an overwhelming small bleb phenotype, with 90% of cells displaying either small blebs or no blebs. Similarly, 80% Sra1 depleted cells displayed either small blebs or no blebs. This is a significant shift in phenotype compared to only 30% of cells in the control group that display small or no blebs (Figure 5-6, Table 3-1). This result is consistent with the role of the WAVE complex as a potent Arp2/3 activator, and in particular, Sra1 and Nap1 being the binding interface for activation of the Arp2/3 complex (Chen et al. 2010).

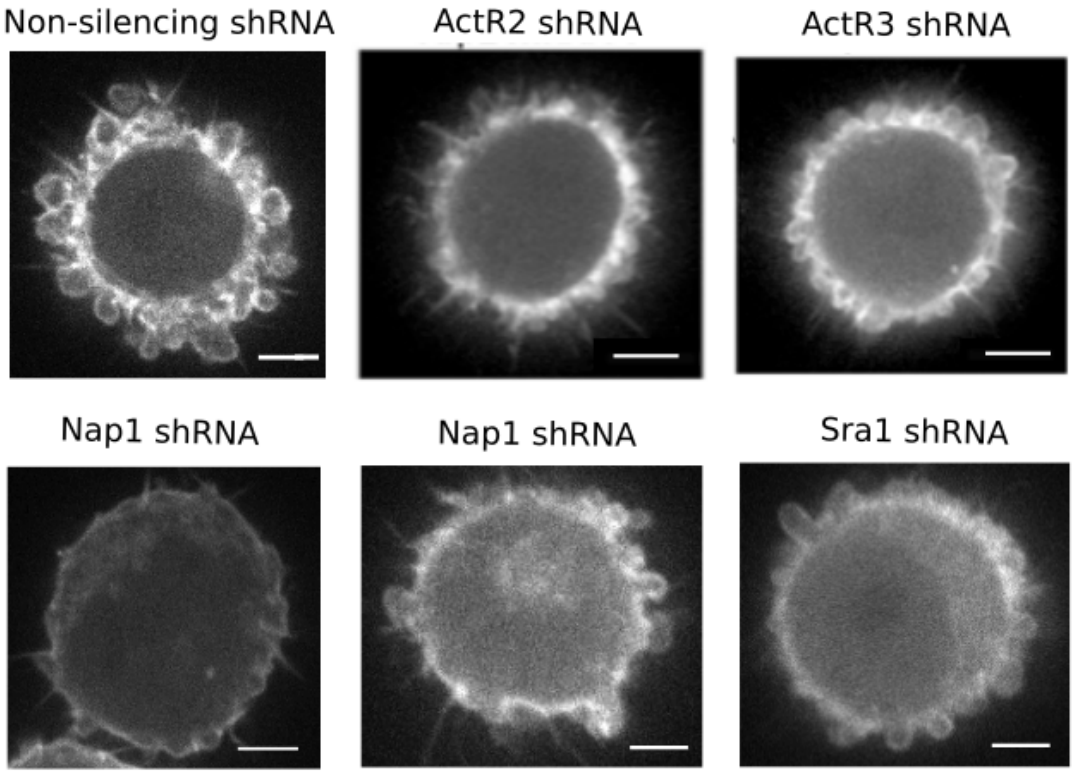

Figure 5-5 Live confocal imaging of M2 cells stably expressing LifeAct-Ruby. Cells depleted for Nap1 or Sra1 presented very small blebs, similar to Arp2/3 knockdown. A large number of cells also presented no blebs at all, scale - 5µm.

Table 5-1 ***Raw data and statistical analysis of the phenotypes observed in the shRNA screen with M2 blebbing cells.*** Cells were counted and categorised into groups according to bleb size: no blebs, small blebs, normal blebs, and large blebs. For each shRNA construct, observed distributions were compared to expected numbers based on the categorisation observed in non-silencing shRNA control using a chi-squared test. Differences were considered significant for **p<0.01.

	Phenotype	Observed number of cells in each category	Expected number of cells in each category based on control	P-Value (CHITEST)
CONTROL (non-silencing shRNA)	No blebs	15		
	Small blebs	54		
	Normal blebs	79		
	Large blebs	63		
Flightless-I shRNA	No blebs	12	13	<0.01
	Small blebs	22	48	
	Normal blebs	114	70	
	Large blebs	39	56	
IQGAP1 shRNA	No blebs	20	13	<0.01
	Small blebs	15	48	
	Normal blebs	45	71	
	Large blebs	109	56	
NCKIPSD shRNA	No blebs	7	9	<0.01
	Small blebs	17	32	
	Normal blebs	45	47	
	Large blebs	56	37	
Sra1 shRNA	No blebs	8	2	<0.01
	Small blebs	24	10	
	Normal blebs	7	15	
	Large blebs	0	12	
Nap1 shRNA	No blebs	15	3	<0.01
	Small blebs	22	10	
	Normal blebs	3	15	
	Large blebs	0	12	

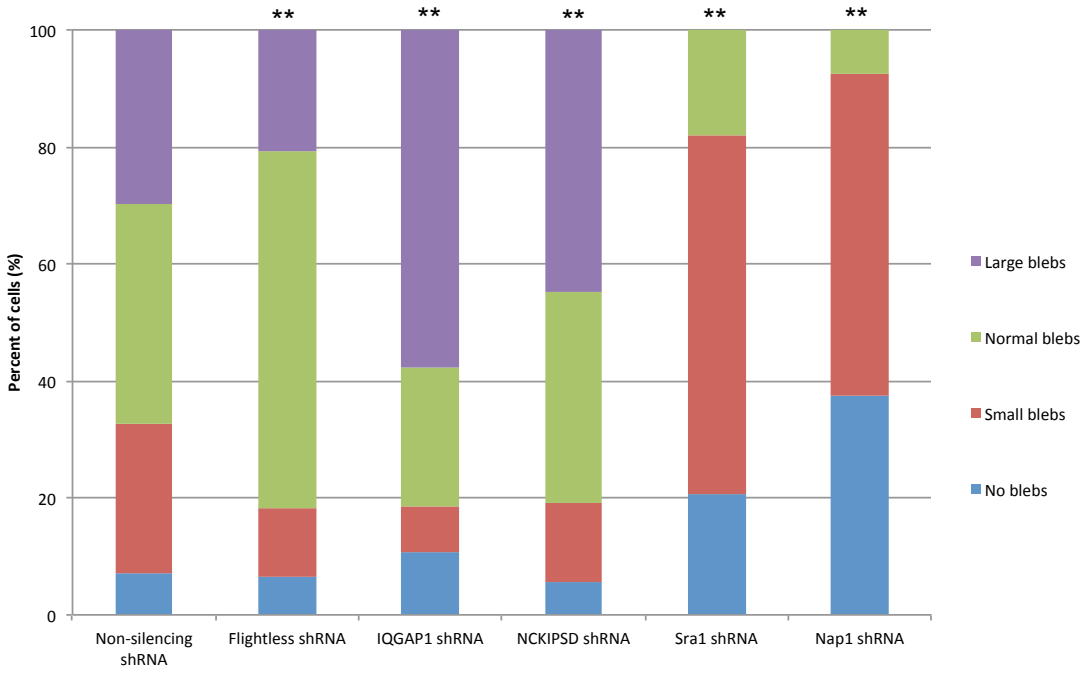

Figure 5-6 Distribution of blebbing phenotypes observed in M2 knockdown cells. IQGAP1 and NCKIPSD shRNA depleted cells mostly displayed large blebs. Sra1 and Nap1 shRNA depleted cells displayed a prominent small bleb phenotype, with no large blebs observed. FliI depleted cells displayed mostly normal sized blebs. When compared to cells stably expressing non-silencing shRNA, cells expressing Flightless-I shRNA, IQGAP1 shRNA, NCKIPSD shRNA, Sra1 shRNA and Nap1 shRNA showed significantly different bleb distributions (**, $p<0.01$). Five independent experiments per cell line examining: 211 cells for non-silencing, 187 for Flightless-I, 189 for IQGAP1, 125 for NCKIPSD, 39 for Sra1 and 40 for Nap1.

5.4 Potentiation of the WAVE small bleb phenotype with drug treatments

To further assess the impact of drug treatments on bleb size and to determine which pathway each NPF regulates, I attempted to potentiate the M2 Nap1 shRNA small bleb phenotype with drugs. For this, I combined Nap1 stable cell line depletion with treatment of CK666 (an Arp2/3 inhibitor), or with SMIFH2 (a formin inhibitor). I reasoned that if there was no noticeable change in bleb size with treatment, this suggests that the drug is acting in the same pathway as the inhibitor. Whereas, if there was a clear change in phenotype, this may suggest that the drug is acting in a distinct complementary pathway. As Nap1 is likely to activate Arp2/3, I reasoned that the addition of CK666 to Nap1 depleted cells should not exhibit a change in the

proportion of the small bleb phenotype. I reasoned that the addition of SMIFH2 would possibly result in the weakening of the small bleb phenotype due to the inhibition of formins, thus balancing out the remaining nucleator.

To compare Nap1 potentiation under the different conditions, counts for the small bleb phenotype were collected; these included those cells categorised as having 'no blebs' or 'small blebs'. M2 cells treated with CK666 presented an overall majority of small blebs, whilst those treated with SMIFH2 presented a minority of cells with the small bleb phenotype (Figure 5-7). This is consistent with results of blebbing phenotypes observed in Arp2/3 and Diaph1 shRNA depleted cells (Bovellan et al. 2014). For use, the chemical inhibitors CK666 and SMIFH2 are dissolved in DMSO, and as a control Nap1 shRNA and DMSO were also combined. The addition of DMSO did not have a significant effect on bleb size compared to Nap1 depleted cells alone ($p=0.83$). The potentiation of Nap1 with CK666 resulted in no significant change of the small bleb with the addition of CK666 ($p=0.91$) (Figure 5-7), providing further evidence supporting the Nap1 and Arp2/3 interacting pathway.

When treating to control cells, SMIFH2, a general formin inhibitor, resulted in cells with the large bleb phenotype, consistent with Diaph1 depletion results. SMIFH2 treatment to Nap1 depleted cells did not change the overwhelming small phenotype of Nap1 depleted cells, however there was a significant decrease in the percent of cells classified as presenting small blebs (**$p<0.01$). I expected to see a change of overall bleb size towards the more normal sized phenotype due to the balancing out of remaining nucleators. SMIFH2 is known to have a short longevity of activity, meaning that after a few weeks, it no longer inhibits formins. This may have had an impact on the results observed. Furthermore, this combination was only experimented once, and requires repeating to validate these results.

It would be interesting to carry out similar potentiation experiments with the other NPFs, IQGAP1 and NCKIPSD to further study their interactive pathways. In fact, with regards in particular to NCKIPSD, potentiation with chemical inhibitors may give a better understanding of the interplay and dual role of interacting with both Diaph1 and the Arp2/3 complex. This approach, similar to that carried out with Nap1 depletion, will reveal any differences in phenotype, reflected by the degree of

nucleator inhibition. This will also reveal which of its effects on Arp2/3 or Diaph1 dominates the phenotype observed in live cell imaging experiments.

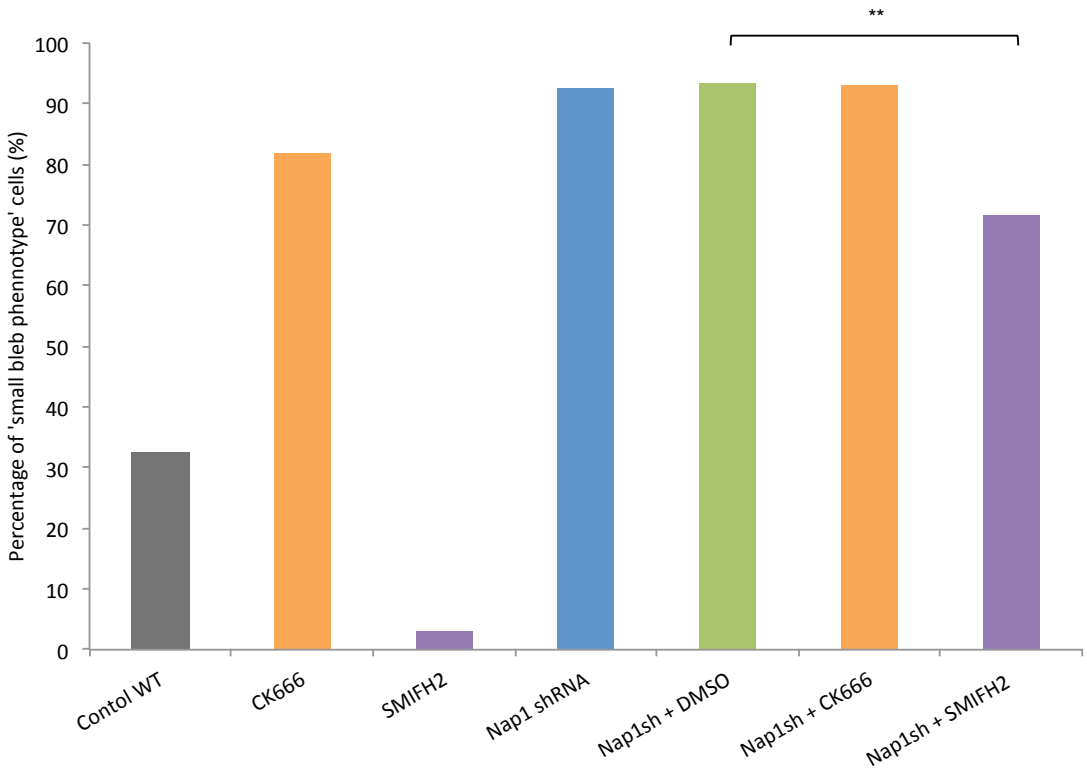

Figure 5-7 Potentiation of M2 Nap1 shRNA phenotype with CK666 and SMIFH2. CK666 100µM treated cells mostly displayed small blebs, and SMIFH2 10µM treated cells displayed mostly larger blebs. Similar to CK666 treatment, Nap1 knockdown cells displayed a prominent small bleb phenotype. The comparison between controls Nap1 shRNA and Nap1 shRNA + DMSO did not show significant deviations in the quantity of small bleb phenotype ($p=0.83$). The comparison between Nap1 shRNA + DMSO and Nap1 shRNA + CK666 did not show significant deviations in the quantity of small bleb phenotype ($p=0.91$). The comparison between Nap1 shRNA + DMSO and Nap1 shRNA + SMIFH2 did show significant deviations in the quantity of small bleb phenotype (**$p<0.01$, chi-squared test). One independent experiment per condition examining: 211 cells for non-silencing, 22 for CK666, 69 for SMIFH2, 40 for Nap1 shRNA, 168 for Nap1 shRNA + DMSO, 72 for Nap1 shRNA + CK666, and 67 for Nap1 shRNA + SMIFH2.

5.5 Conclusion

The main goal is to understand how NPFs function in modifying the cortex organisation, thickness, dynamics and mechanical properties. As a first step, I began by investigating the effect that depletion of candidate NPFs had upon bleb size. This initial screen served to provide an assessment of the involvement of each NPF in generation of cortical actin, determined by the impact on bleb size.

In these experiments, I found that IQGAP1 depletion and NCKIPSD depletion both had phenotypes associated with large blebs, suggesting that they primarily affect Diaph1 activity. Depletion of the WAVE regulatory complex subunits Nap1 and Sra1 both gave rise to a small bleb phenotype, consistent with their known role in regulating Arp2/3 complex activity and suggesting that the WAVE complex controls Arp2/3 activity in blebs. Flightless-I depletion had no consistent effect on bleb size, suggesting that it may not play an important role in the control of cortical actin regrowth in blebs (Table 5-2). Together, these experiments suggest that IQGAP1, NCKIPSD and the WAVE complex play a role in controlling cortex regrowth under the membrane of blebs.

Table 5-2 Summary of blebbing phenotypes observed in M2 cells with depletion of nucleator or NPF. Diaph1 and Arp2/3 depletion results in large and small blebs, respectively. Depletion of Flightless-I had no effect on bleb size. IQGAP1 and NCKIPSD depletion resulted in large blebs. Sra1 and Nap1 depletion resulted in small blebs.

Normal size blebs	Large bleb phenotype	Small bleb phenotype
Non-silencing control	Diaph1 depletion	Arp2/3 depletion
Flightless-I depletion	IQGAP1 depletion	Sra1 depletion
	NCKIPSD depletion	Nap1 depletion

As a complement to shRNA depletion, it would be interesting to carry out some rescue experiments. RNAi rescue experiments are performed to confirm target RNAi specificity because the exogenously expressed protein should rescue the loss-of-function phenotype. Here, constructs are designed to reintroduce the knocked down recombinant protein. To rescue the blebbing phenotype, I would reintroduce the full-length protein from a species that is not targeted by the shRNA. Other experiments could also attempt to rescue the phenotype with specific domains of the protein to determine which mediate its function. For example, for IQGAP1, I would rescue with the full-length protein but also with the Diaph1-binding region (DBR), which I would expect to rescue my protein given my experiments.

There is also the possibility of rescuing with an agonist of Diaph1-related formins, IMM01. This chemical inhibitor disrupts the autoinhibitory interaction between diaphanous inhibitory domain (DID) and diaphanous autoregulatory domain (DAD) interaction. With this, it would be possible to treat lines depleted for activators of Diaph1.

Chapter 6 Cortex molecular organisation is regulated by NPFs

To link cellular scale observations to molecular level mechanism, I examined how NPFs controlled cortical organisation using scanning electron microscopy (SEM). Electron microscopy allows for a higher-level understanding of the cortical organisation, and allows for the link between physical structure and mechanical function to be considered. Mesh size is an important determinant of cortical mechanics because the organisation of the actin cortex controls the rigidity and mechanical stability of the cell surface and drives shape changes by acting as a scaffold for myosin motor contractility. The organisational features of the actin cortex, such as bundling, cross-linking, density and filament length, contribute to the physical and mechanical properties of the actin cortex. Here, the effect of depleting a protein important for the promotion of actin assembly should be most apparent in blebs that necessitate *de novo* actin nucleation for cortex formation. As in previous work (Bovellan et al. 2014), we found that depletion of Diaph1 led to large gaps within the cortex, while Arp2/3 depletion led to the appearance of longer filaments but no clear change in actin density.

6.1 IQGAP1 depletion phenocopies Diaph1 depletion

I have shown that IQGAP1 depletion phenocopies Diaph1 depletion in the bleb size assay. Therefore, I studied the effect that loss of IQGAP1 has on the cortical organisation, and compared this to what has been observed in Diaph1 depleted cells. As previously described, depletion of Diaph1 led to extensive changes in cortical actin organisation, with large gaps in the cortex devoid of actin filaments (Figure 6-1**B**, asterisk). This is very different from the homogeneous mesh observed in control conditions, with a gap size of approximately 30 nm (Figure 6-1**A**). Consistent with a role in controlling Diaph1, IQGAP1 depletion led to cortices with large gaps. There were also areas of high filament density (Figure 6-1**C**, circled). The cortex appears less dense, particularly in areas devoid of actin filaments. Mechanistically, RhoA binds to the autoinhibited conformation of Diaph1, to open and activate it, allowing subsequent actin nucleation. It has been shown that RhoA only partially (15%) activates Diaph1 (Li & Higgs 2003; Li & Higgs 2005; Maiti et al. 2012). This suggests that further binding partners, such as IQGAP1, are required to amplify the

effect of RhoA to efficiently activate Diaph1 *in vivo*. With this in mind, and comparing with my data, it is possible that Diaph1 retains some nucleating activity without the requirement of further stabilising activity by IQGAP1.

The comparison of cortical organisation between Diaph1 and IQGAP1 knockdown cells further supports a role for IQGAP1 as an important player controlling Diaph1-mediated actin nucleation. Although a significant organisational disruption is evident in IQGAP1 depleted cells, there remain regions of uniform filaments and the phenotype is less pronounced than in Diaph1 depleted cells. This is consistent with the phenotypic observation of blebs discussed above; it can be seen that the blebs are not as large and uniform around the cell as with Diaph1 depletion (Figure 5-3).

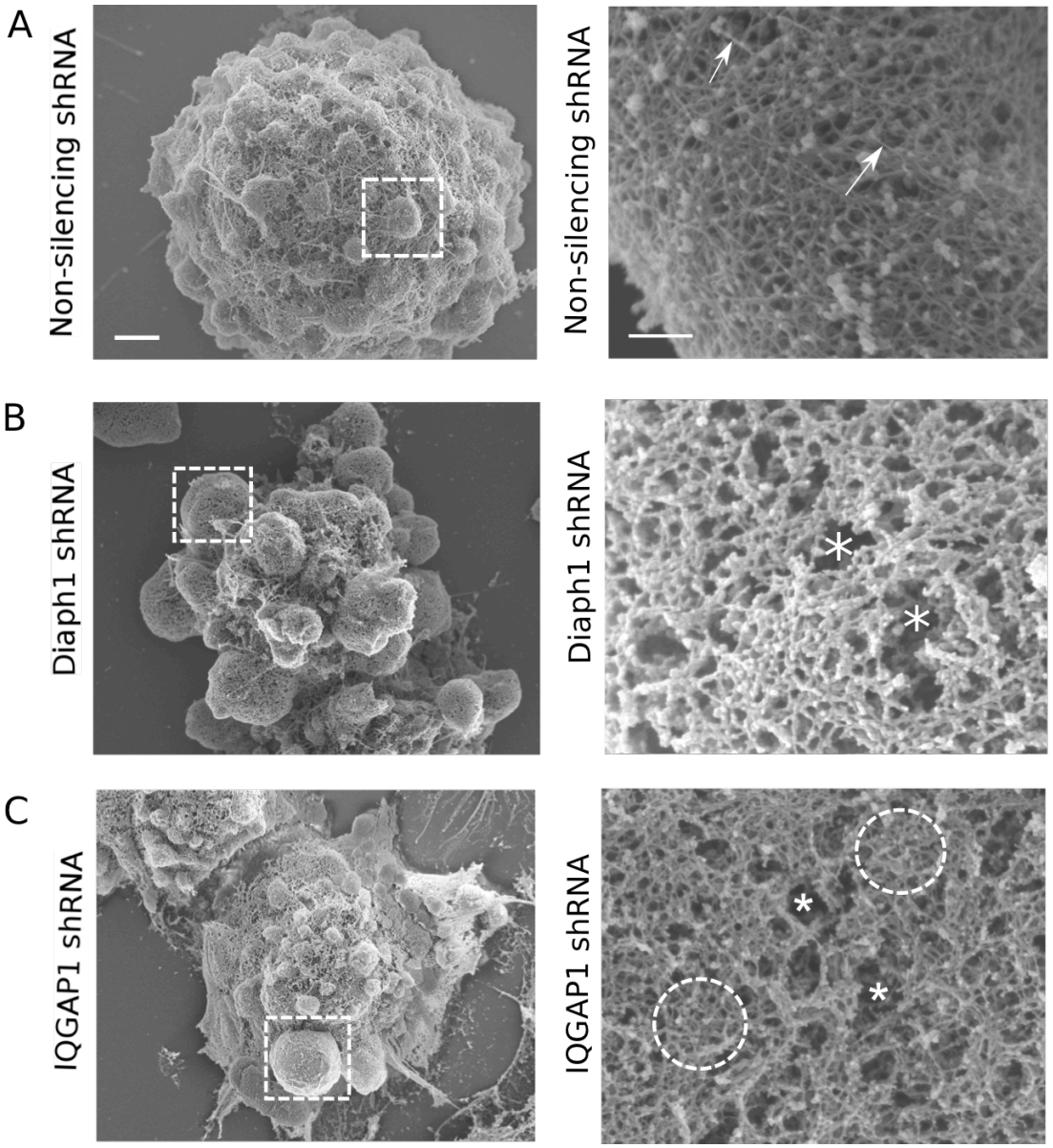

Figure 6-1 Scanning electron micrographs of membrane extracted M2 cells. Right hand side panels are magnifications of boxed areas from left hand side panels. **A,** Non-silencing shRNA M2 cells display a homogenous mesh with single filaments visible (arrows). **B,** Diaph1 shRNA knockdown cells have large blebs with regions devoid of actin filaments (asterisk). The mesh appears generally disorganised. **C,** IQGAP1 shRNA depleted cells present some disorder and areas devoid of actin filaments (asterisk) are visible. Some areas of cortex homogeneity are visible (circled) Scale; left panels 2µm, right panels 100nm.

6.2 NCKIPSD depletion leads to denser cortical actin

In the case of NCKIPSD knockdown, electron microscopy was deemed especially advantageous to visualise the overall structure of cortical actin filaments, as the blebbing phenotype was unexpected. One hypothesis was that a reduction in the number of unbranched actin filaments nucleated by NCKIPSD activation of Arp2/3 would result in increased formation of branched filaments, changing the overall architecture of the cortex. In this case, I would expect filaments with more interconnections, and regions devoid of filaments as a result of the inhibition of NCKIPSD. On the contrary, the depletion of NCKIPSD caused a tightening of the overall actin cortex mesh (Figure 6-2). This cortical organisation is different from that seen in Diaph1 depleted cells, and also very different from that of Arp2/3 depleted cells.

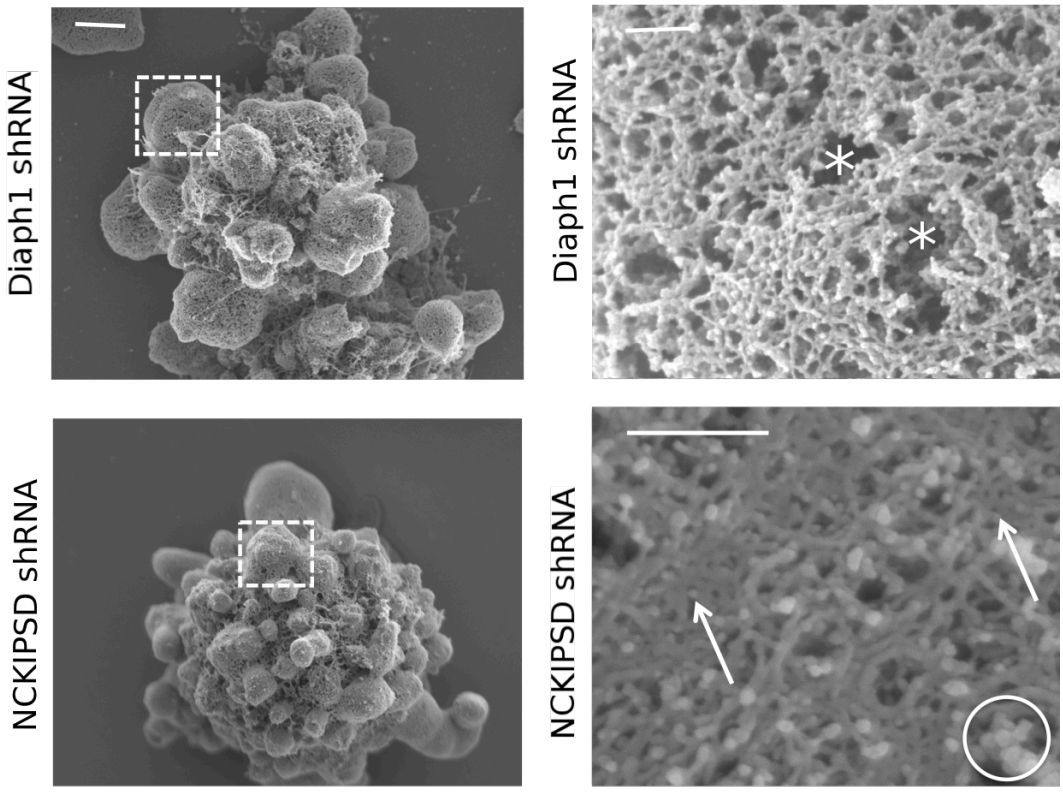

Figure 6-2 Scanning electron micrographs of membrane extracted M2 cells. The actin cortex of NCKIPSD shRNA depleted cells features a very tight mesh with regions where single actin filaments appear stumpy, highly bundled and indistinguishable (circle). There was also an increase in unknown aggregates at the

surface, possibly a feature of the sample preparation. Scale; left panels 2μm, right panels 100nm.

The increase in filament density may stem from generation of unbranched actin networks via WAVE activation of Arp2/3 in the absence of NCKIPSD, which generates unbranched filaments with Arp2/3. Thus, WAVE and NCKIPSD may compete for Arp2/3. Furthermore, NCKIPSD has been shown to bind to Diaph1 but not inhibit its elongation activity. Therefore, NCKIPSD may serve as a scaffolding protein in addition to being an NPF. In this hypothesis, NCKIPSD would generate an actin seed via Arp2/3 nucleation and bring a Diaph1 dimer into contact with the newly created barbed end. In this hypothesis, we should find that co-depletion of NCKIPSD and WAVE leads to large blebs with low actin density. Another hypothesis is that the high density comes from release of Diaph1 inhibition due to depletion of NCKIPSD. In this case, we should see that co-depletion of Diaph1 and NCKIPSD should lead to large blebs with low actin density.

To visually represent the relative production of linear vs. branched actin filaments by Diaph1 and Arp2/3, I have drawn a schematic as shown below. Diaph1 always generates linear filaments, and Arp2/3 generates branched filaments except when activated through NCKIPSD (Figure 6-3**A**). When NCKIPSD is depleted (Figure 6-3**B**), there are a greater proportion of branched filaments being nucleated, which could explain the increase in cortical density. It has recently been shown that formin-nucleated filaments make up only 10% of the total number of cortical filaments, and are, on average, 10 times longer than Arp2/3-nucleated filaments (Fritzsche et al. 2016). The proportion of Arp2/3 nucleated filaments has been heavily skewed towards branched filament topologies, explaining the apparent increase in density. It should be noted, however, that this explanation does not take into account other activators of Diaph1 or Arp2/3, and only considers the contributions by IQGAP1, NCKIPSD and WAVE.

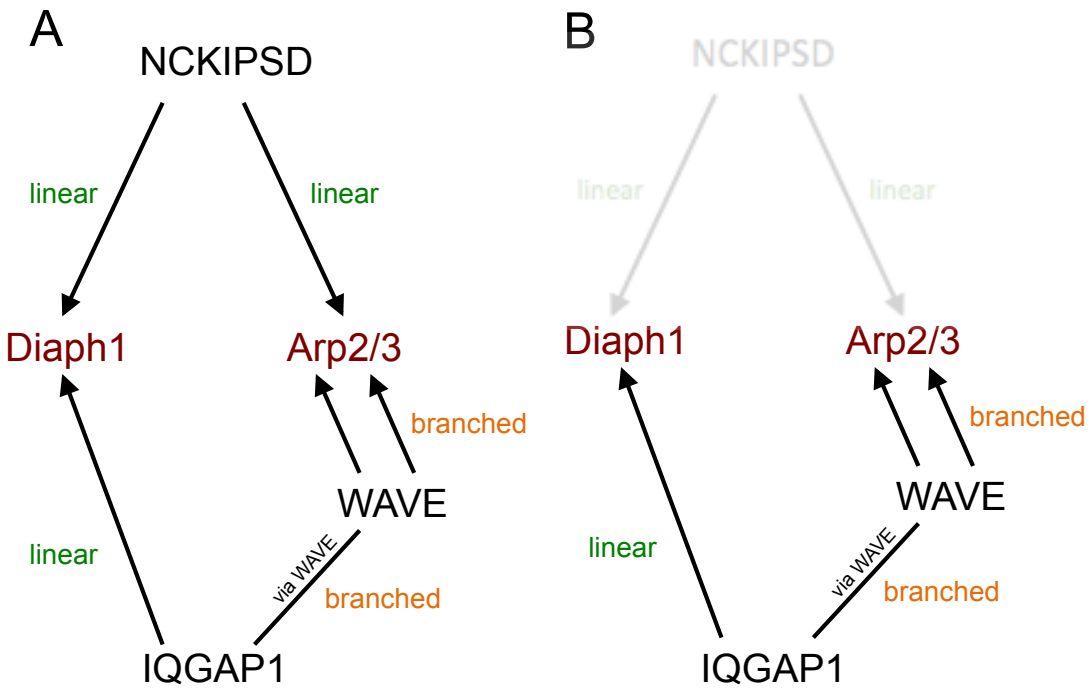

Figure 6-3 Generation of linear vs. branched actin filaments may be modulated by the identity of NPFs interacting with the Arp2/3 complex and Diaph1. A, Diaph1 exclusively generates linear actin filaments, whilst the Arp2/3 complex generates branched actin filaments except when activated through NCKIPSD. **B,** Depletion of NCKIPSD results in the removal of pathways resulting in linear actin filament nucleation via Diaph1 and Arp2/3.

6.3 WAVE subunit depletion leads to a cortex with longer filaments

Depletion of the WAVE regulatory complex subunits Nap1 and Sra1 both gave rise to a small bleb phenotype, consistent with their known role in regulating Arp2/3 complex activity. I further expected to see a similar cortical organisation in WAVE depletion as in Arp2/3 depleted cells. Previous work showed that Arp2/3 depletion led to longer filaments that could be traced over several hundred nanometres (Figure 6-4**A**). Depletion of the Arp2/3 complex would reduce the generation of branched filaments. Using electron microscopy, I observed long actin filaments in the actin cortex of cells depleted for Nap1 and Sra1 (Figure 6-4**B/C**) WAVE complex subunits. The small size of blebs made imaging a single bleb difficult, as even the most expanded bleb was sometimes very small. This further supports the role of the WAVE complex acting as an NPF for the Arp2/3 complex in the cortex.

It has also been demonstrated that the WAVE complex can drive myosin-independent cytokinesis through a spindle-directed signalling pathway (King et al. 2010). Thus, it would also be interesting to observe the effect that depletion of WAVE has upon the progression through the cell cycle in HeLa cells. Because of this, I would expect the depletion of WAVE subunits to have a significant impact on cell division.

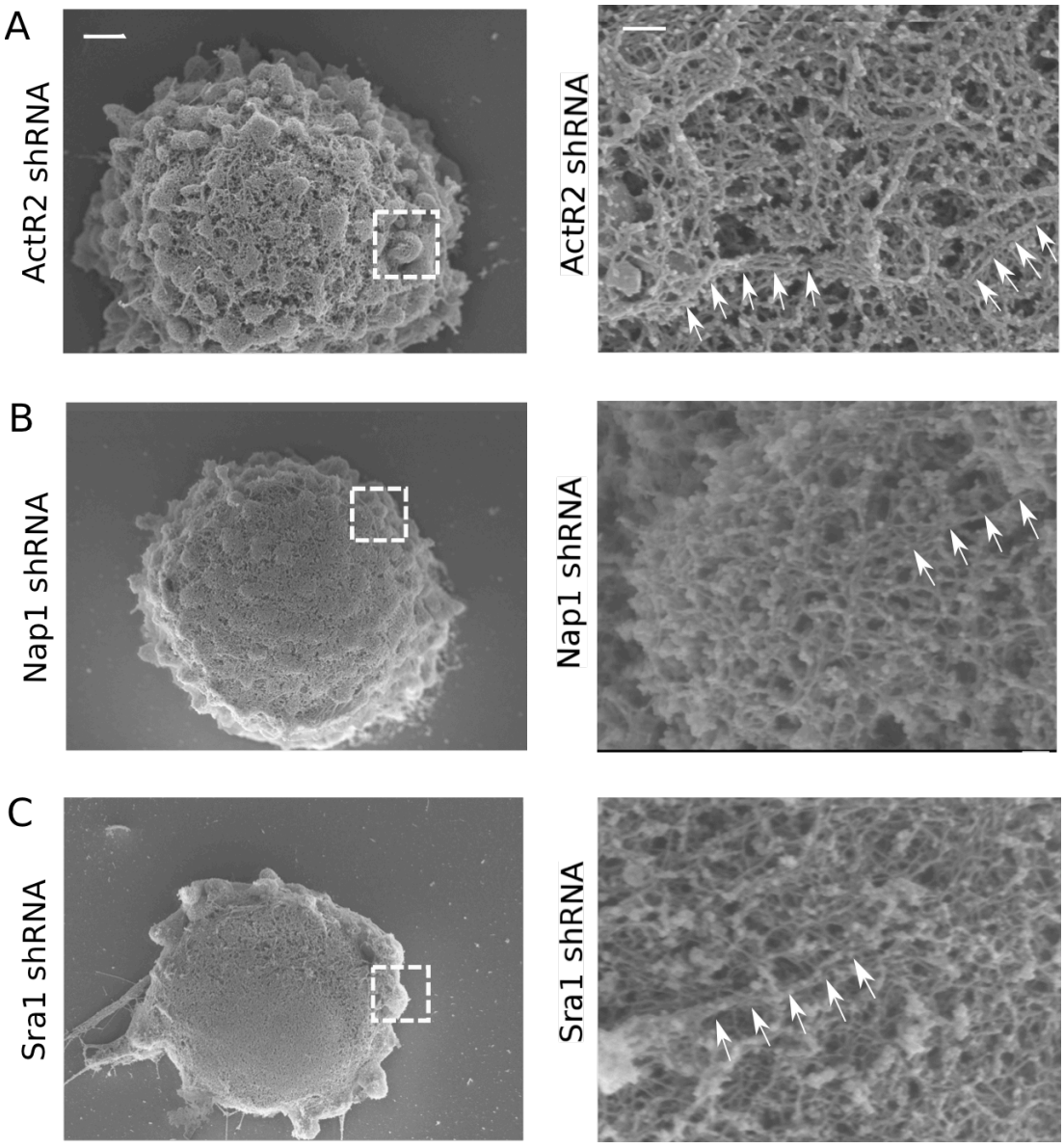

Figure 6-4 Scanning electron micrographs of membrane extracted M2 cells. A, The actin cortex of ACTR2 shRNA depleted cells features long actin filaments traced up to several hundred nanometres (arrows). **B/C,** Nap1 and Sra1 shRNA (WAVE complex subunits) actin cortex features similar long actin filaments. These

filaments also appear bundled at times. The arrows follow the length along a single filament. Scale; left panels 2μm, right panels 100nm.

6.4 Quantitative analysis of changes in actin cortex mesh induced by NPF and nucleator depletion

To quantify the actin cortex mesh, a method for segmenting and recognising the 'gaps' of the cortex was developed in collaboration with Dr. Matt Smith, LMCB. Initially, SEM micrographs were input into a trainable FIJI plugin (WEKA segmentation) to differentiate between the actin filaments and gaps in the cortex. For this, a few actin filaments were manually selected and a few gaps were manually identified. The plugin was then able to use this limited information to automatically distinguish between the two categories: filaments and gaps for the whole image. The plugin then output the location and area of all of the identified gaps. Using the data collected, I was able to determine the mesh sizes from cells depleted of the different NPFs.

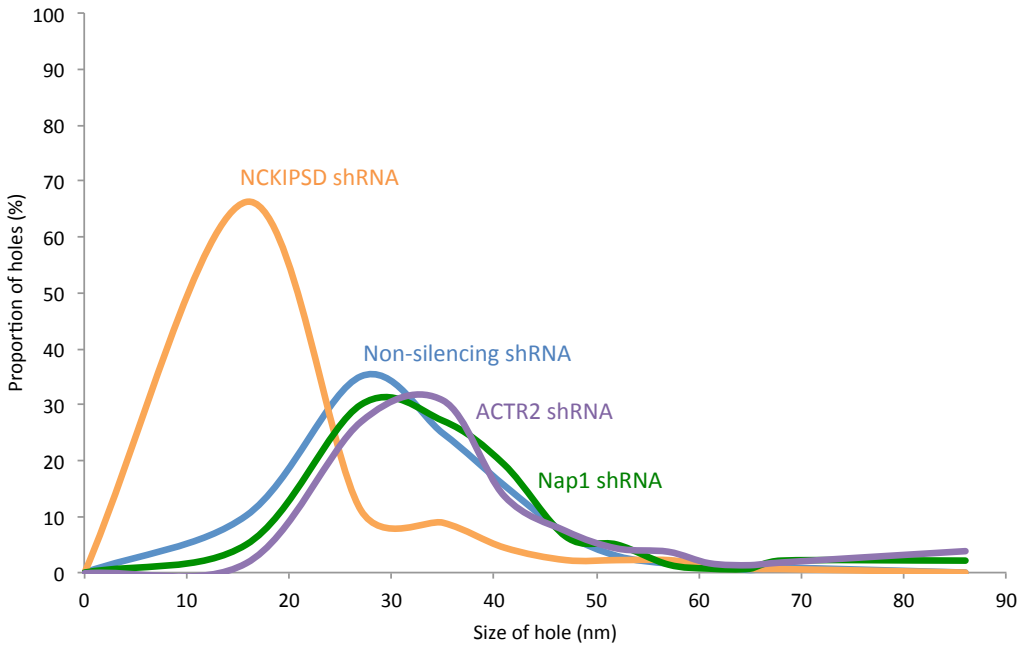

Figure 6-5 Quantitative segmentation analysis of SEM micrographs. The actin mesh of membrane extracted M2 cells was analysed to determine the proportion of holes that are a certain size (indicated by their size in nm). As qualitatively determined previously, the non-silencing control, ACTR2 shRNA and Nap1 shRNA mesh size did not differ much (average size is around 30nm). The mesh size of

NCKIPSD shRNA cells appears tight, with the holes also revealed as smaller than the controls (mostly less than 25nm), in agreement with the image data.

Each condition represents seven micrograph images that were analysed individually, before pooling. To generate the quantitative segmentation analysis of SEM micrographs as shown in the graphs, data was binned into bins of 5 nm for Figure 6-5 and binned into 20 nm for Figure 6-6. This allowed for proper representation of the different sized holes that are reflected by the depletion of Diaph1 and its proposed NPFs, or Arp2/3 and its proposed NPFs.

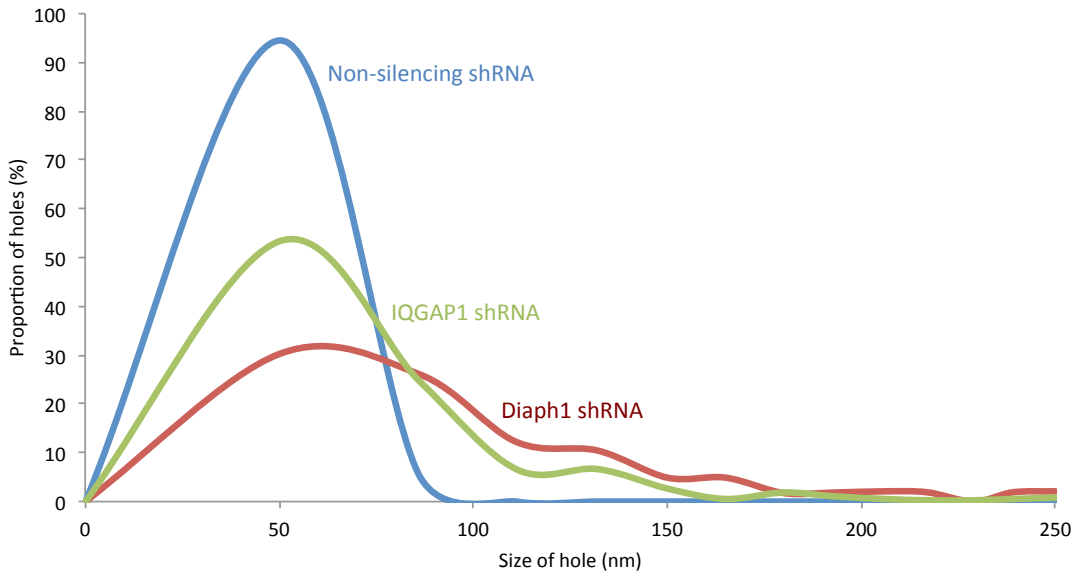

Figure 6-6 Quantitative segmentation analysis of SEM micrographs. The actin mesh of membrane extracted M2 cells was analysed to determine the proportion of holes that are a certain size (indicated by their size in nm). IQGAP1 and Diaph1 depleted cells displayed the largest holes (size of up to 250nm).

Previous work has reported a 30 nm mesh size in the cortex of M2 cells (Bovellan et al. 2014), corresponding well to the expected size of actin-dependent membrane protein confinement zones (Kusumi et al. 2011). In agreement with this, the mesh in the non-silencing control cells displayed a peak at 28nm with 100% of the actin cortex mesh gaps falling between 20 and 60nm (Figure 6-5, blue). ACTR2 and Nap1 depleted cells also featured a similar mesh size range, with 2-3% of holes above 75 nm (Figure 6-5, purple/green). As expected, Diaph1 depleted cells had a greater spread of mesh sizes, with 75% of holes greater than 75 nm (Figure 6-6, red).

IQGAP1 depleted cells replicated this mesh size pattern, however, there was a greater proportion of holes falling below the 75 nm range (Figure 6-6, green). Interestingly, NCKIPSD depleted cells had a very narrow range of mesh size, with almost all the holes at less than 25 nm (Figure 6-5, orange). It is important to comment on the variation in the non-silencing shRNA trace, suggesting that the numbers may not be repeatable.

This quantification strongly supported the judgements made from visually analysing the electron micrographs. In terms of mesh size, Arp2/3 and Nap1 can be grouped; Diaph1 and IQGAP1 appear to yield similar results; and NCKIPSD may be involved in a role different to that observed with other NPFs. We know that depleting both Arp2/3 and Diaph1 leads to substantial detriment in actin cortex organisation, affecting actin localisation and cortex stability. It would have been interesting to measure the size of the cortex in M2 cells with a dual depletion for both Arp2/3 and Diaph1 to further confirm potentiation as seen in other experiments. It should be noted, however, that measurements on fixed cells may suffer from artefacts such as cell shrinkage and altered architecture of the plasma membrane and actin networks. Therefore, the determination of actin cortex density and membrane-cortex distance measurements might best be performed on living cells.

6.5 Conclusion

Consistent with a role in controlling Diaph1 suggested by the blebbing phenotype, IQGAP1 depletion led to cortices with large gaps although the effect was less pronounced than Diaph1 shRNA. WAVE subunit depletion led to a cortex with longer filaments, consistent with its role in controlling Arp2/3 activity and the small bleb phenotype obtained upon depletion. NCKIPSD depletion led to a clear increase in cortical density, which was surprising given the large bleb phenotype that observed in live imaging that is consistent with a reduction in Diaph1 activity.

Based on these results, it appeared that depletion of NCKIPSD disrupted Diaph1 activity but increased density. NCKIPSD has been shown to contribute to the nucleation of unbranched actin filaments via Arp2/3 (Wagner et al. 2013). This unbranched organisation is more advantageous for myosin-mediated contractions

than the branched topologies obtained through WAVE-mediated Arp2/3 activation. A reduction in Diaph1 actin polymerisation and cortex weakening could explain the large bleb phenotype observed with NCKIPSD depletion. NCKIPSD depletion would also limit the formation of unbranched actin filaments; thus, I would expect this to be demonstrated through an observed modification of cortical contractility. Cortical contractility is especially crucial in the formation of the furrow during cell division. With this in mind, I predicted that there would be a perturbation of cell division observed with the depletion of NCKIPSD.

Chapter 7 NPF depletion perturbs the cell cycle

The actin filament network is crucial for dictating cell shape, and participates in the dynamic regulation of cellular functions. In HeLa cells, cells adhere to the substratum during interphase and spread to assume their characteristic shape supported by the actin cytoskeleton. This actin cytoskeleton is reorganised during mitosis to form rounded cells with increased cortical rigidity. The most dramatic changes in eukaryotic cytoskeletal organisation and dynamics occur during passage through mitosis. Here, the actin cytoskeleton is reorganised after mitosis, allowing cells to regain their spread shape and attachment to the substratum. The modulation of such drastic changes in cell shape in coordination with cell cycle progression suggests a tight regulatory interaction between cytoskeleton signalling, cell-cell/cell-matrix adhesions and mitotic events.

Given the importance of the actin cortex in numerous stages of the cell cycle and that NPFs appeared to control the activity of actin nucleators, I reasoned that depletion of NPFs may perturb normal progression through the cell cycle. For example, IQGAP1 depletion phenocopies Diaph1 depletion, suggesting that it activates and works via Diaph1. Thus, I would expect a similar outcome while following progression cells depleted of IQGAP1 through the cell cycle.

7.1 Generation of NPF depleted stable lines in HeLa cells

To this aim, I generated stable HeLa cell lines depleted for each of the NPFs identified using shRNA. Protein depletions were verified with qPCR to quantify mRNA (Figure 7-1**A**) and western blotting to quantify protein levels (Figure 7-1**B**). Certain shRNA knockdowns (Diaph1, Nap1, Sra1) were lethal and for those, stable cell lines were not made but instead siRNA was used. siRNA depletion was also verified by qPCR and western blotting. All shRNA knockdown lines had a strong depletion; similarly, siRNA depletions were also high.

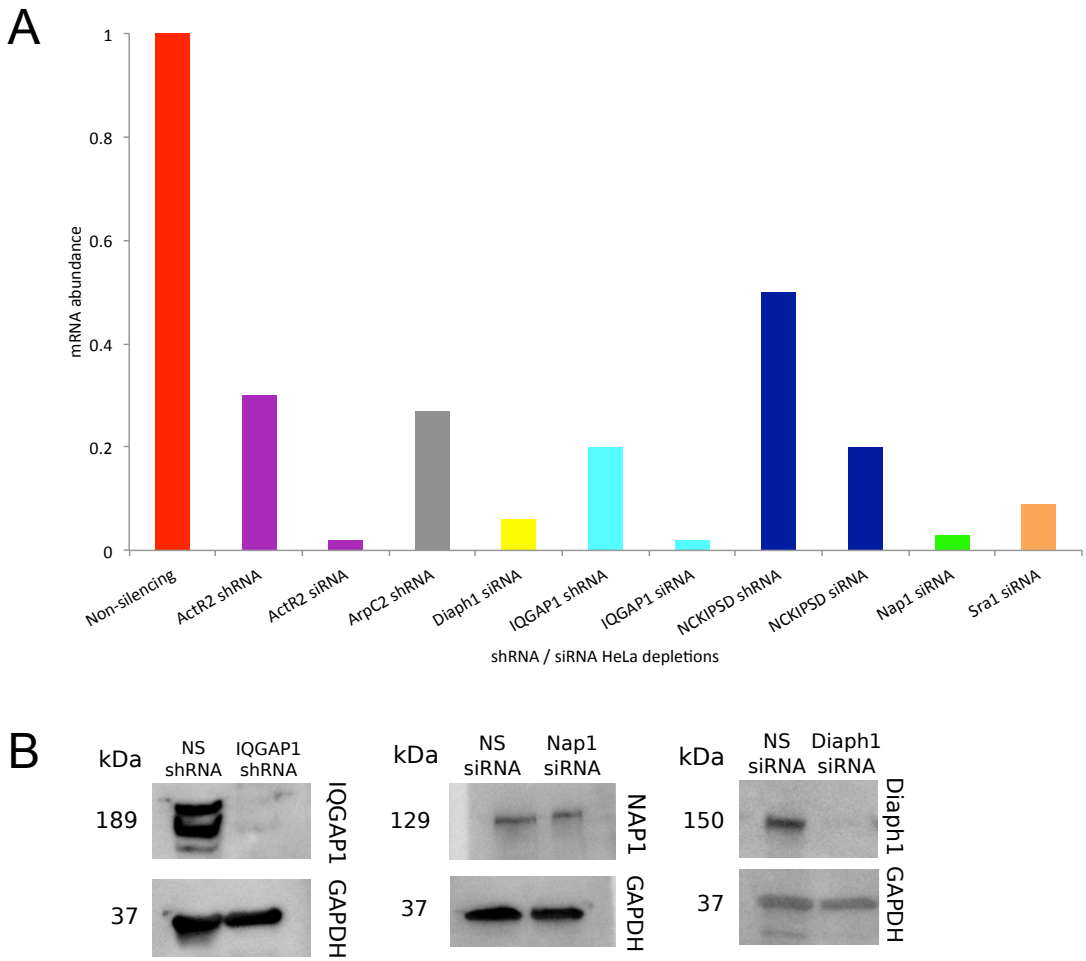

Figure 7-1 A, mRNA transcript abundance of ACTR2 (Arp2) shRNA, ACTR2 (Arp2) siRNA, ArpC2 shRNA, Diaph1 siRNA, IQGAP1 shRNA, IQGAP1 siRNA, NCKIPSD shRNA, NCKIPSD siRNA, Nap1 siRNA and Sra1 siRNA using qPCR; this revealed high knockdown in ACTR2 (Arp2) shRNA (70% knockdown), ArpC2 shRNA (73% knockdown), IQGAP1 shRNA (80% knockdown), and NCKIPSD shRNA (50% knockdown) in stable knockdown HeLa cell lines. qPCR revealed high knockdown in ACTR2 siRNA (98% knockdown), Diaph1 siRNA (94% knockdown), IQGAP1 siRNA (98% knockdown), NCKIPSD siRNA (80% knockdown), Nap1 siRNA (97% knockdown) and Sra1 siRNA (91% knockdown). **B,** Western blot showing protein levels in stable knockdown HeLa cells expressing NS and IQGAP1 shRNA, probed with anti-IQGAP1 and anti-GAPDH as a loading control. Western blot showing protein levels in knockdown HeLa cells expressing NS, Nap1, and Diaph1 siRNA, probed with anti-Nap1 and anti-Diaph1 as a loading control.

7.2 NPF depletion has an impact on normal cell cycle progression

To assess the impact on cell cycle progression upon depletion, NPF knockdown lines were imaged and classified into the following categories: those that progressed normally through the cell cycle (Table 7-1**A**), those that died in interphase (Table 7-1**B**) and those that died in mitosis (Table 7-1**C**). A further categorisation of those that died in mitosis was made into groups that died during prophase, metaphase, anaphase, telophase or other. Cells in the 'other' group included cells that oscillated before death, cells that divided and regressed, and cells that divided but failed to spread.

Table 7-1 Categories of HeLa cell cycle progression A, Cells that progressed through the cell cycle normally **B,** Cells that died in interphase **C,** Cells that died during the various stages of mitosis – prophase, metaphase, anaphase, telophase, and other.

A	Normal progression	
B	Death in interphase	
C	Death in mitosis	Prophase, Metaphase, Anaphase, Telophase
	Oscillation & fail	
	Oscillation & divide	
	Death after dividing	
	Divide and regress	

In the live imaging of non-silencing shRNA HeLa cells, most cells progressed through the cell cycle normally. They were able to round, divide and spread robustly (Figure 7-2, see Vid1, USB). Even in control conditions, a small number of cells die, mostly due to failures in mitosis. In the NPF depleted lines, shown later, some knockdowns result in a higher number of cells dividing into three, or even four, daughter cells. In the control condition, cells that progress normally through the cell cycle complete cytokinesis in an average of just over two hours (130 minutes, 60 control cells analysed). This timing is taken from the moment rounding is first

detected, until the daughter cells have divided. Certain malfunctions can result in a delay during mitotic cell rounding or during abscission where the daughter cells separate after cytokinesis.

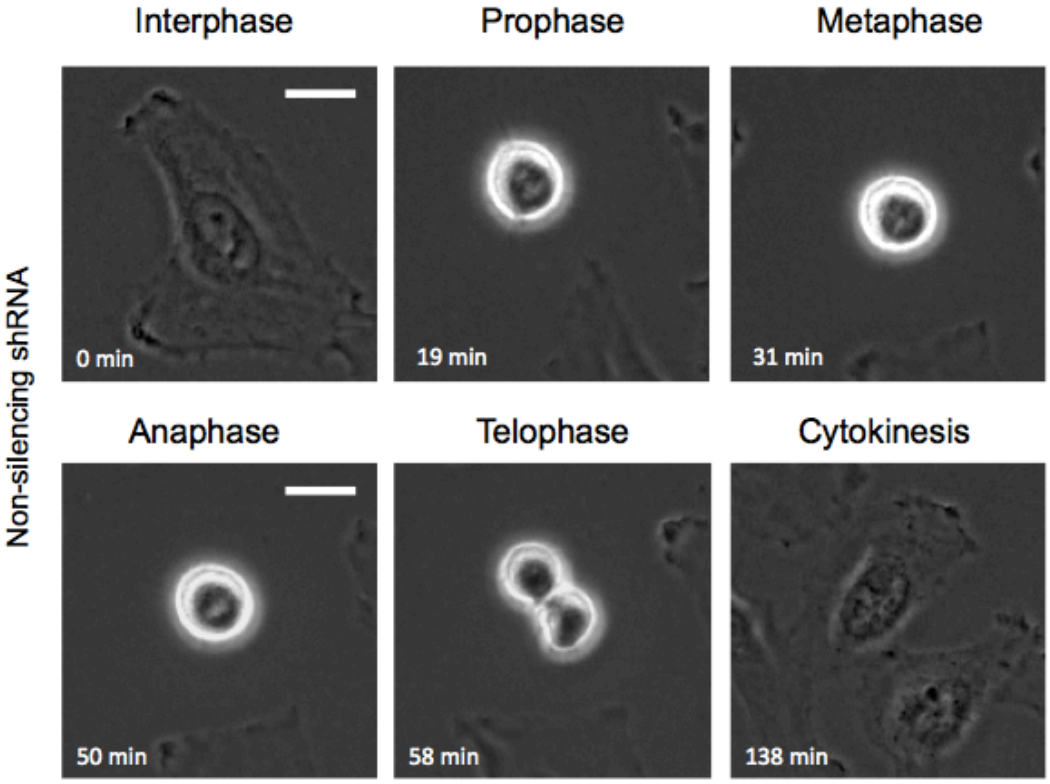

Figure 7-2 Live cell phase imaging of non-silencing shRNA HeLa cells. Control cells progress through the cell cycle in an average of 130 min (time from the beginning of mitotic rounding until daughter cells have divided). Here, cells round up abandoning the flat morphology of interphase, then advance through the stages of mitosis before cell cleavage and abscission where the daughter cells separate. Scale bar: 20µm (see Vid1, USB).

Firstly, the overall impact on cell progression was studied in cells depleted of a single NPF. I looked for similarities between depletion of NPF and depletion of nucleator. In previous work, Diaph1 depletion led to a significant increase in cell death during the cell cycle (Bovellan et al. 2014). The situation is more complex with the Arp2/3 complex as ArpC2 depletion does not affect progression through the cell cycle but ACTR2 depletion does. Diaph1 depletion was further accompanied by an increase in the incidence and size of blebs during anaphase and cytokinesis (Bovellan

et al. 2014). Thus, I examined how depletion of each NPF in turn affected cell cycle progression and actin cortex morphology.

In the previous bleb size studies, Flightless-I had no phenotype when depleted and I hypothesised that it might play a role in cell cycle progression. However, depletion of Fli-I showed no increase in cell death in HeLa cells, and surprisingly, significantly decreased the incidence of cell death (Figure 7-3). This indicates a function of Fli-I separate from a cortical NPF function in the cell cycle. As discussed before, Fli-I may have a role in other actin related processes in the cortex.

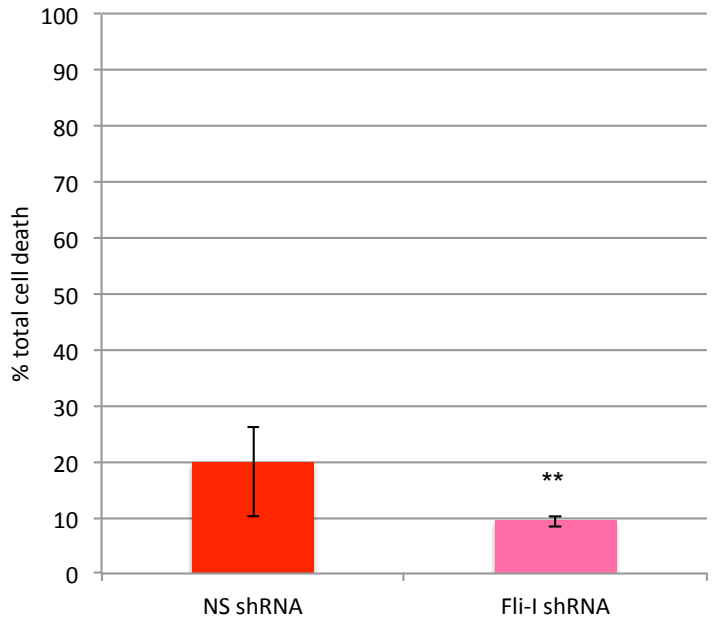

Figure 7-3 Flightless-I depletion affects cell survival. When compared to cells transfected with non-silencing shRNA, cells depleted in Fli-I showed significantly different rates of successful cell cycle progression (**$p<0.01$). Results were gathered from 3 independent experiments examining: non-silencing shRNA (n=399 cells), Fli-I shRNA (n=178 cells). Data was analysed with a chi-squared test.

Next, I investigated the effect on cell cycle progression of depleting IQGAP1 or NCKIPSD. Both IQGAP1 and NCKIPSD depletion led to cells with a significantly higher total cell death compared to the non-silencing controls (Figure 7-4). 50% of cells with a Diaph1 knockdown do not progress through the cell cycle as normal, but

this value is significantly lower for both IQGAP1 and NCKIPSD knockdown, albeit staying significantly higher than for controls.

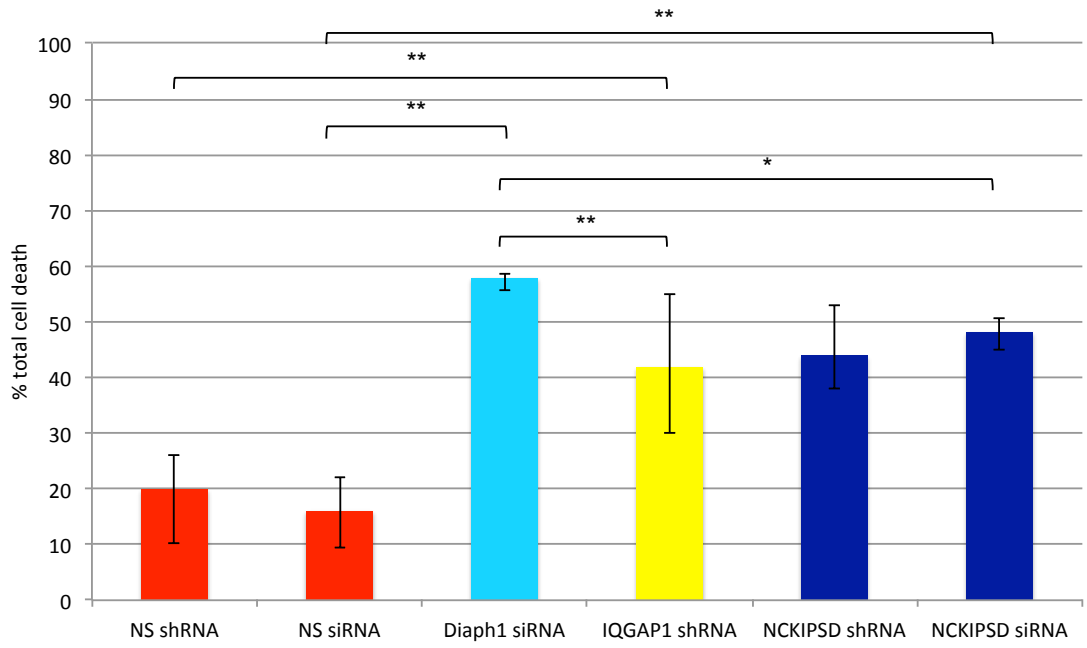

Figure 7-4 Progression through mitosis categorised by total cell death when depleted with NPFs thought to modulate Diaph1 activity. When compared to cells transfected with non-silencing shRNA, cells depleted in IQGAP1 displayed significantly increased rates of total cell death (**p<0.01). There is no significant difference between NCKIPSD shRNA/siRNA depletion (p=0.19). Compared to Diaph1 depletion, both IQGAP1 (**p<0.01) and NCKIPSD (*p<0.05) depletion resulted in a significantly lower percent of total death. Results were gathered from 3 independent experiments examining: non-silencing shRNA (n=399 cells), non-silencing siRNA (n=178 cells), Diaph1 siRNA (n=185 cells), IQGAP1 shRNA (n=528 cells), NCKIPSD shRNA (n=462 cells), NCKIPSD siRNA (n=515 cells). Data was analysed with a chi-squared test.

The data shows that IQGAP1 and NCKIPSD play an important role in allowing normal cell cycle progression. Similar to previous experiments, the phenotype seen in IQGAP1 knockdown is not as intense as with Diaph1 knockdown, supporting the existence of other Diaph1 activators. Morphologically, Diaph1 cells are characteristically quite thin and elongated in interphase (see Vid2, USB) with most abruptly dying in interphase (Figure 7-5**B**). IQGAP1 depleted cells were extremely

blebby throughout mitosis (see Vid3, USB), with very large blebs seen especially at the poles, suggesting cortical instability. These cells typically divide asymmetrically, and take an increased time during all stages of the cell cycle (Figure 7-5**C**). The delay in IQGAP1 depleted cells appears to be most pronounced from the start of rounding to anaphase. IQGAP1 knockdown cells that progress past interphase take 114 minutes on average, compared to 50 minutes in control cells. As Figure 7-5**C** shows, after cytokinesis, there is a delay in abscission of the daughter cells, with a visible connection of the intercellular bridge connecting the two daughter cells. This delay in severing will be discussed in 7.3. Similarly, cells depleted of NCKIPSD were also very blebby during mitosis (see Vid4, USB), with a high number failing to progress past mitosis. NCKIPSD knockdown cells were less spread in interphase compared to the controls, and those cells that did survive went through multiple rounding attempts before the final rounding allowing the cell to enter mitosis. In addition, cells often underwent several cycles of rounding and spreading before finally rounding for mitosis. Alteration in cell shape poses difficulties in critical mitotic processes such as spindle assembly, signalling, and targeting processes during check point regulation and may be responsible for the increase in abnormal mitosis behaviour (Lancaster & Baum 2014).

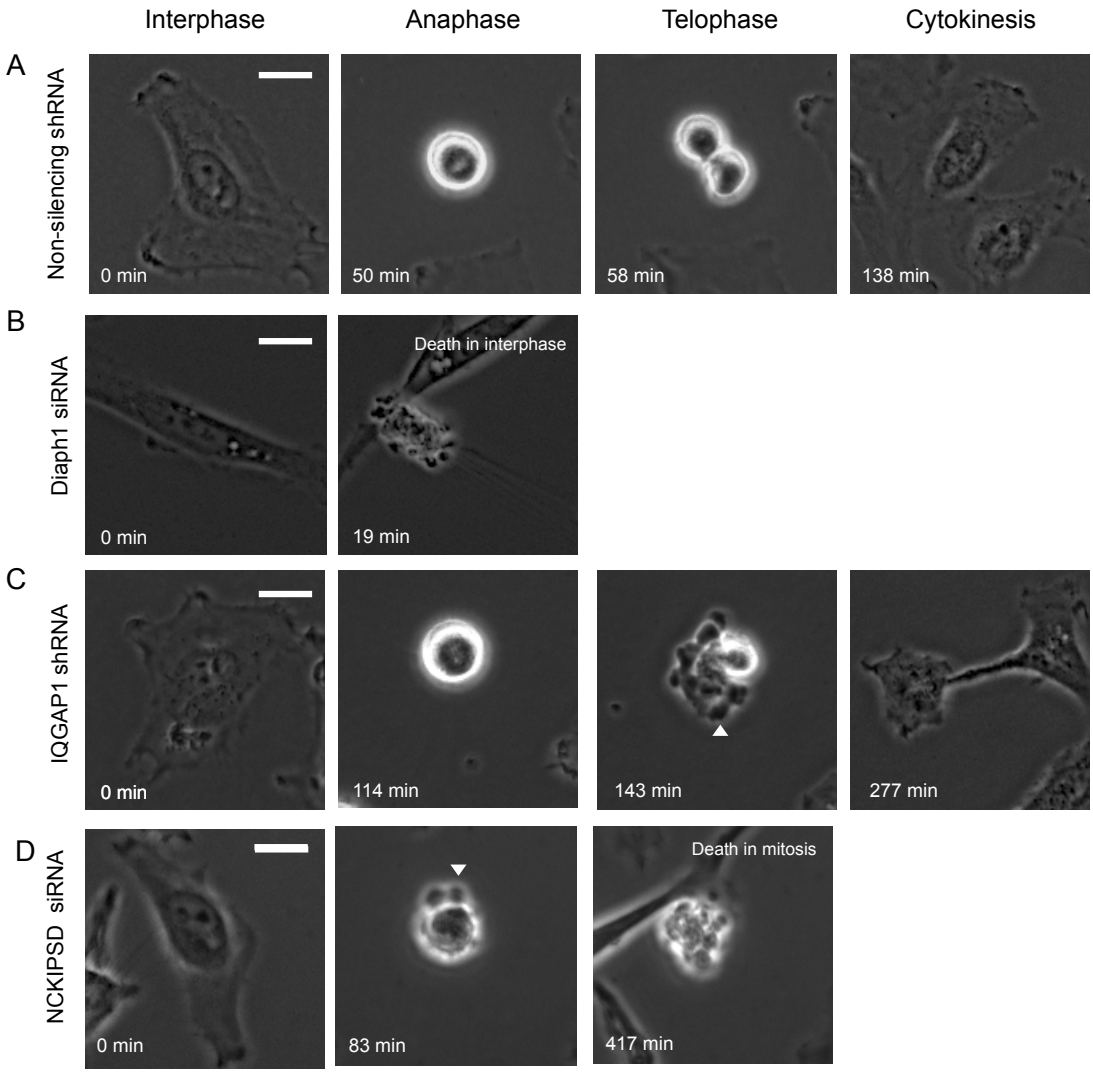

Figure 7-5 Live cell imaging of shRNA silenced HeLa cells using phase contrast microscopy. A, Control cells progress through the cell cycle abandoning the flat morphology of interphase, then advance through the stages of mitosis before cell cleavage and abscission where the daughter cells separate. **B,** Diaph1 siRNA cells appear more elongated in interphase and frequently die during interphase. **C,** IQGAP1 shRNA cells are very blebby during mitosis (arrowhead), and those that survived were unable to sever the intracellular connection between the daughter cells. **D,** NCKIPSD siRNA cells were less spread in interphase, very blebby during mitosis (arrowhead) and many depleted cells failed to progress through mitosis. Scale: 20μm.

Depletion of subunits of the WAVE regulatory complex, Nap1 and Sra1, has consistently been shown to phenocopy Arp2/3 knockdown in our assays. Thus, I

expected to see a large impact on total cell death, similar to that I see with ACTR2 depletion. Surprisingly, Sra1 and Nap1 depletion had no significant effect on total cell death (Figure 7-6), similar to ArpC2 depletion. This is also consistent with observations using the Arp2/3 inhibitor CK666 (Bovellan et al. 2014).

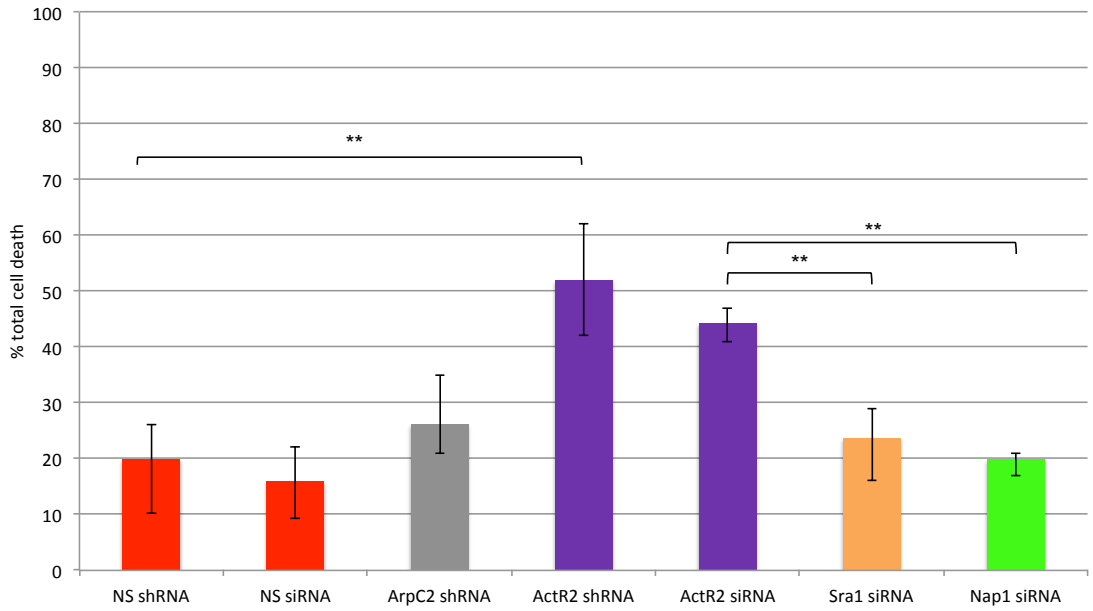

Figure 7-6 Progression through mitosis categorised by total cell death when depleted with NPFs thought to modulate Arp2/3 activity. When compared to cells transfected with non-silencing shRNA, cells depleted in ACTR2 shRNA/siRNA displayed significantly increased rates of total cell death. There is no significant difference between ACTR2 shRNA/siRNA depletion (p=0.07). ArpC2 depletion does not significantly increase cell death (p=0.42). Depletion of both WAVE complex subunits, Nap1 (p=0.44) and Sra1 (p=0.29), did not significantly affect cell death. Results were gathered from 3 independent experiments examining: non-silencing shRNA (n=399 cells), non-silencing siRNA (n=178 cells), ArpC2 shRNA (n=443 cells), ACTR2 shRNA (n=382 cells), ACTR2 siRNA (n=594 cells), Sra1 siRNA (n=629 cells), Nap1 siRNA (n=542 cells). Data was analysed with a chi-squared test.

In addition to the cell death phenotypes induced by siRNA, I also generated cell lines depleted in Sra1 and Nap1 with shRNA. Depletion of Sra1 and Nap1 with shRNA led to extensive changes in the morphology of the cell. Knockdown cells were generally very rounded and grew in clumps, failing to spread as expected (see Vid8

and Vid10, USB). There appeared to be a loss of attachment between the cell and the substrate, making them less adherent and extremely easy to detach. This is consistent with previous work that highlighted the Arp2/3 complex's importance for cell spreading. Arp2/3 complex inhibition has been shown to greatly alter the structural organisation of actin in spreading cells (Henson et al. 2015). In my experiments, this characteristic made it very difficult to count the cells and analyse the acquired data, as it sometimes appeared like the cell survived even though it may have died (Figure 7-7**F**). Thus, instead of using shRNA-depleted cells, I used siRNA-depleted cells that did not exhibit clumping to such extent (see Vid7 and Vid9, USB). Both Nap1 and Sra1 siRNA depleted cells were less spread than controls and all cells displayed small sized blebs during mitosis (Figure 7-7**D, E**). Cells depleted for WAVE complex subunits were able to go through cytokinesis, albeit at a much slower rate. Similar to NCKIPSD depleted cells, WAVE knockdown cells often underwent several cycles of rounding and spreading before finally rounding for mitosis.

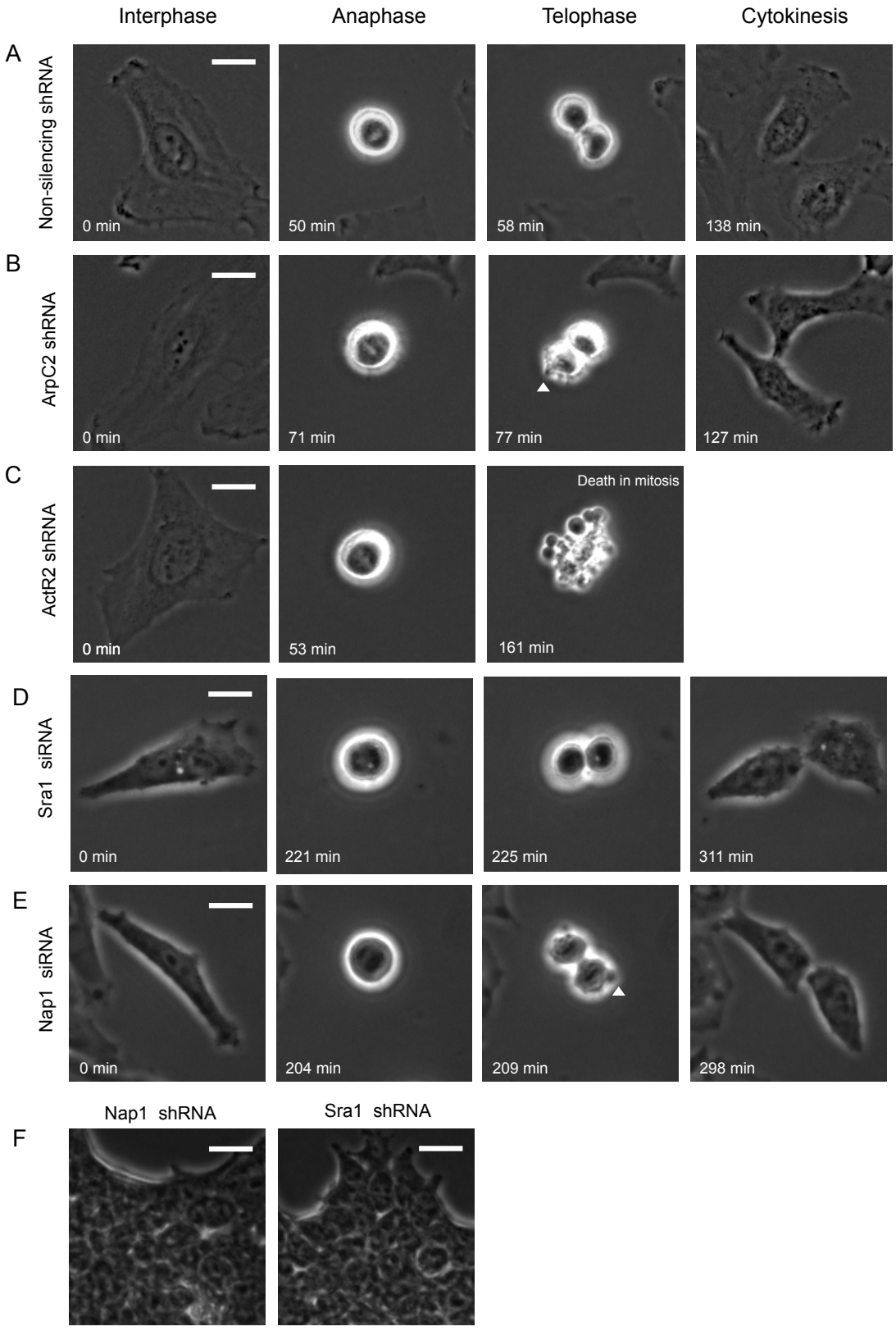

Figure 7-7 Live cell imaging of silenced HeLa cells using phase contrast microscopy. A, Control cells progress through the cell cycle as normal, abandoning the flat morphology of interphase, then advance through the stages of mitosis before

cell cleavage and abscission where the daughter cells separate. **B,** ArpC2 shRNA cells appear normal with the presentation of small blebs during mitosis (arrowhead). **C,** ACTR2 shRNA cells were very blebby during mitosis, with many cells dying at this stage. **D,** Sra1 siRNA cells were less spread in interphase and progressed through mitosis significantly more slowly. **E,** Nap1 siRNA cells were less spread in interphase with the presentation of small blebs during mitosis (arrowhead). **F,** Nap1 and Sra1 shRNA cells have a very strong phenotype, promoting growth in colonies making it difficult to analyse or study. These shRNA cells were not used further in this investigation. Scale: 20μM.

7.3 NPF depletion induces changes in the duration of mitotic stages

When analysing long-term movies of cells depleted in NPFs, I noticed that some depletions appeared to perturb the duration of various mitotic stages. To this aim, I analysed the captured videos to determine the duration of each mitotic stage in NPF depleted cells and compared these to control cells.

I quantified two events: rounding timing and abscission timing (Figure 7-8). Rounding timing represents the time from the first sign of rounding to a completely rounded cell. In terms of the cell cycle, rounding is concurrent with nuclear envelope breakdown at the onset of mitosis and is completed before anaphase. The abscission timing represents the time required to progress from anaphase to the end of cytokinesis. Cytokinesis, initiated at anaphase onset, cleaves the cytoplasm until only a small bridge termed the midbody remains between the two daughter cells. With time, the midbody is severed in a process called abscission, resulting in complete separation of the two daughter cells. During analysis, I noticed that pinpointing the exact timing of abscission timing is challenging because it is difficult to tell if the daughter cells have completely separated. Thus, for ease of analysis in this section and for consistency, I measured the time when the daughter cells have completely cleaved but not completely separated.

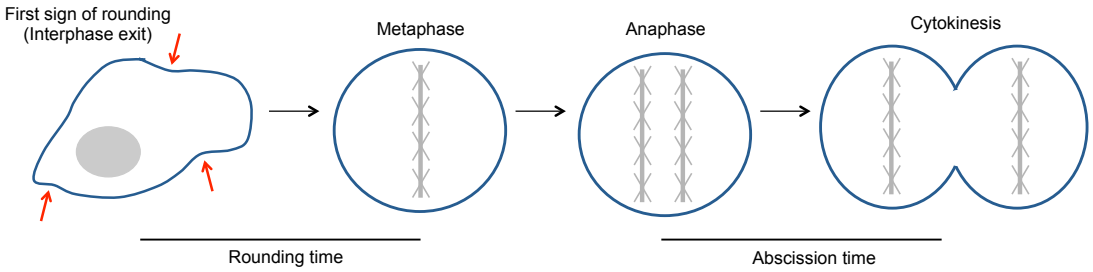

Figure 7-8 Quantification of rounding time and abscission time in HeLa cells. Rounding timing represents the time from the first sign of rounding (interphase exit) to a completely rounded cell in metaphase. Abscission time represents the duration between anaphase to the end of cytokinesis where the daughter cells are held together only by a small bridge.

7.3.1 NPFs significantly perturb rounding duration

Mitotic cell rounding is likely important for chromosome segregation and the positioning of the cytokinetic furrow, making it an important process to study and to understand the role of the actin cortex during this stage (Maddox & Burridge 2003). It has been shown that F-actin is required for coordinated retraction of the cell margin at the onset of mitosis, demonstrating that the actin cytoskeleton plays an active role in mitotic cell rounding (Cramer & Mitchison 1997). Conditions that disturb mitotic cell rounding have been observed to be detrimental to spindle morphogenesis and orientation (Kunda et al. 2008), suggesting that mitotic cell rounding is a key stage for successful completion of mitosis. Many studies have observed a role for actin and associated proteins in cortical retraction and rigidity (Maddox & Burridge 2003). It is known that cortical stiffness increases at mitotic entry (Kunda et al. 2008; Maddox & Burridge 2003) participating to the immobilisation of specific proteins in the actin network (Théry & Bornens 2008). At mitotic onset, the assembly of a linear uniform Diaph1-dependent F-actin cortex coincides with initial rounding, promoting cortical rigidity (Ramanathan et al. 2015).

In cells transfected with NS shRNA, I measured a mean rounding duration of 19 (±6) minutes, consistent with previous work (Sivakumar et al. 2014). Mitotic rounding time was calculated by determining the duration between when the cell began rounding and when rounding was complete. Diaph1 and IQGAP1 depleted cells had

a significantly quicker rounding time with a mean of 6 (±6) minutes and 9 (±6) minutes, respectively, half the time of control cells (Figure 7-9). The similarity in effect of IQGAP1 and Diaph1 rounding is consistent with our other observations that suggest IQGAP1 plays a role in maintaining Diaph1 activity.

ACTR2 and NCKIPSD depletion had an effect opposite to Diaph1 and IQGAP1 depletion. ACTR2 and NCKIPSD depleted cells appeared take significantly longer in rounding when compared to the controls, with a mean of 30 (±20) minutes and 29 (±12) minutes, respectively. Sra1 and Nap1 depleted cells displayed quicker rounding time, with a mean of 8 (±5) minutes and 13 (±20) minutes, respectively. This was unexpected because in most of my experiments, Sra1 and Nap1 depletion phenocopies ACTR2 depletion. Examination of the videos of Sra1 and Nap1 depleted cells showed that these cells spread very little. Therefore, the limited spreading of Nap1 and Sra1 depleted cells may contribute to shortening their rounding time.

It has been shown that formin-nucleated bundled F-actin networks tend to a better substrate for myosin II contractility than networks nucleated by Arp2/3 (Ramanathan et al. 2015). Stewart *et al.* showed that mitotic rounding depends both on the actomyosin cytoskeleton and the cells' ability to regulate osmotic swelling (Stewart et al. 2011). The cortex resists the swelling forces coming from osmotic effects. Thus, if a cell is less contractile, it can round faster. Depletion of IQGAP1 or Diaph1 would make less contractile filaments, and hence increase rounding speed, as the cell is able to resist the osmotic forces better. This could be one explanation for the fast rounding times recorded with IQGAP1 and Diaph1 depletion. It is also possible that there may also be a weakening of cell–substrate adhesion that leads to the rapid detachment and subsequent rounding. Depletion of the WAVE subunits also resulted in a quicker rounding time, contrary to expectation based on slower Arp2/3 depletion rounding time. As mentioned above, these cells were already much more morphologically round compared to the controls. This could mean that the time recorded in this case may not be accurate to represent the total rounding time from the spread morphology. On the other hand, ACTR2 and NCKIPSD depletions led to significantly slower rounding times. It has been shown that depletion of the Arp2/3

complex has no effect on either cortical tension or cortical F-actin enrichment (Ramanathan et al. 2015), however other studies have shown that Arp2/3 does have a role in potentiating actin cortex stability (Watanabe et al. 1997). In this case, it is possible that depletion of Arp2/3 perturbs the turnover of actin at the cortex needed for proper cell rounding, meaning that the cell takes longer to acquire its round morphology. Such as in the case of NCKIPSD, multiple rounding attempts are seen, which could show that the depletion of these nucleators affects the signalling pathways required for the initiation and completion of rounding.

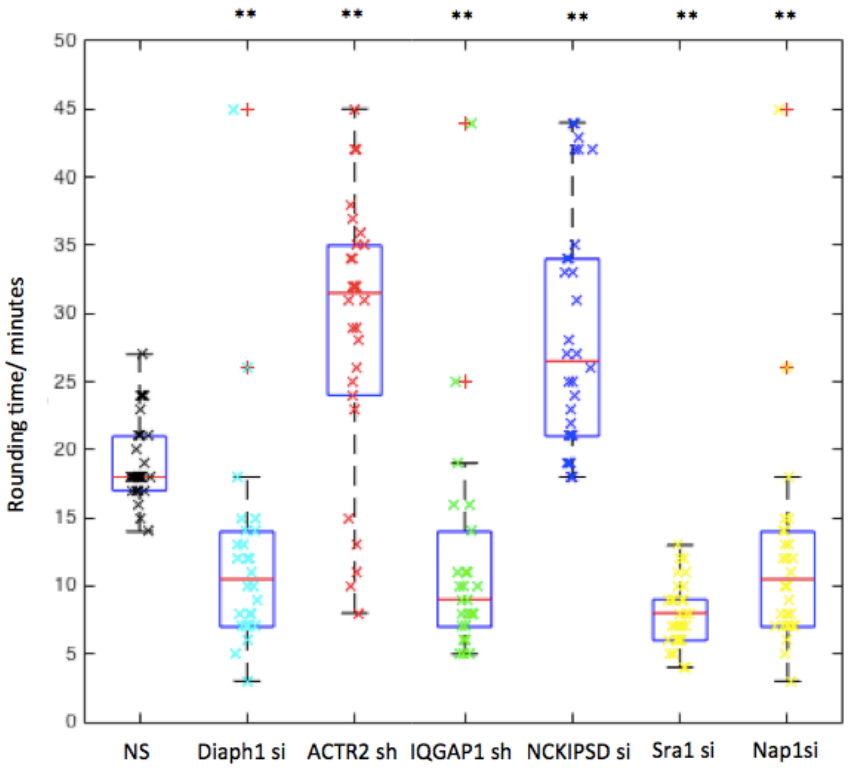

Figure 7-9 Duration of mitotic cell rounding is perturbed by nucleator and NPF silencing. The duration of mitotic rounding was plotted for each nucleator and NPF knockdown. ACTR2 shRNA and NCKIPSD siRNA depletion significantly slowed rounding, whilst Diaph1 siRNA, IQGAP1 shRNA, Sra1 siRNA and Nap1 siRNA depletion significantly decreased rounding time (**$p<0.01$). Whiskers indicate minimum and maximum actin rounding times. 30 cells were analysed for each siRNA/shRNA HeLa depletion. Data was analysed with a Mann-Whitney U-Test.

7.3.2 Abscission time durations

In my experiments, abscission time is measured from anaphase to the end of cytokinesis, where the daughter cells are held together only by a small bridge (Figure 7-8). In the final step of cytokinesis, the mother cell cleaves into two until the daughter cells are connected only by the midbody (Weiss 2012). This sequence of events makes it interesting to study in more detail. The contractile actin cortex, in particular, is crucial for the cleavage of the furrow, allowing the consequential separation of the daughter cells. Separation of mother and daughter cells involves coordinated actomyosin ring contraction (Kunda et al. 2008; Carreno et al. 2008; Kunda et al. 2012) and septum synthesis, followed by septum destruction. Diaph1 has been reported as localised to the mitotic spindle from anaphase to telophase, suggesting a role of Diaph1 in the spindle-cleavage furrow interaction during cell division (Kato et al. 2001). These events occur in precise and rapid sequence once chromosomes are segregated and are linked with spindle organisation and mitotic progress by intricate cell cycle control machinery (Weiss 2012). This mitotic exit is important to allow daughter cells to re-enter G1 to allow for the next division, and this tight regulation ensures that both daughter cells are viable upon separation.

Depletion of Diaph1, NCKIPSD and ACTR2 caused a significantly longer time for abscission, whilst IQGAP1 also significantly increased abscission time, albeit to a lower significance ($p=0.01$). Interestingly, Nap1 and Sra1 depletion did not result in significant changes to abscission timing (Figure 7-10), again not an expected result based on the comparison with Arp2/3 subunit depletion. The greatest change I noticed was in NCKIPSD depleted cells, where most cells took double the amount of time for abscission compared to the controls (Figure 7-10). Between anaphase and cytokinesis, the actin cortex undergoes a series of shape changes; elongating the cell, relaxation of the cortical actomyosin network at cell poles, and the concentration of actomyosin at the cell centre to form a contractile ring (Ramkumar & Baum 2016). Depletion of an important actin nucleator, such as Diaph1 or Arp2/3, would likely have an impact on the progression through these actin cortex dependent processes (Evangelista et al. 2002).

It was challenging to calculate the time of total separation of daughter cells due to the ambiguity of when the cells truly separate, and during times of asymmetric division it is difficult to select the point at which the daughter cells cleave. These results confirm that nucleators and NPFs are important for active polymerisation (and depolymerisation) of actin filaments, to contribute towards the assembly, maintenance and closure of the contractile ring. As a follow-up, it would be interesting to look at F-actin during these stages, and to further interrogate nuclear localisation. It would be informative to study the role of microtubules in the cleavage of cells at cytokinesis, and to study the septum, given their role in abscission.

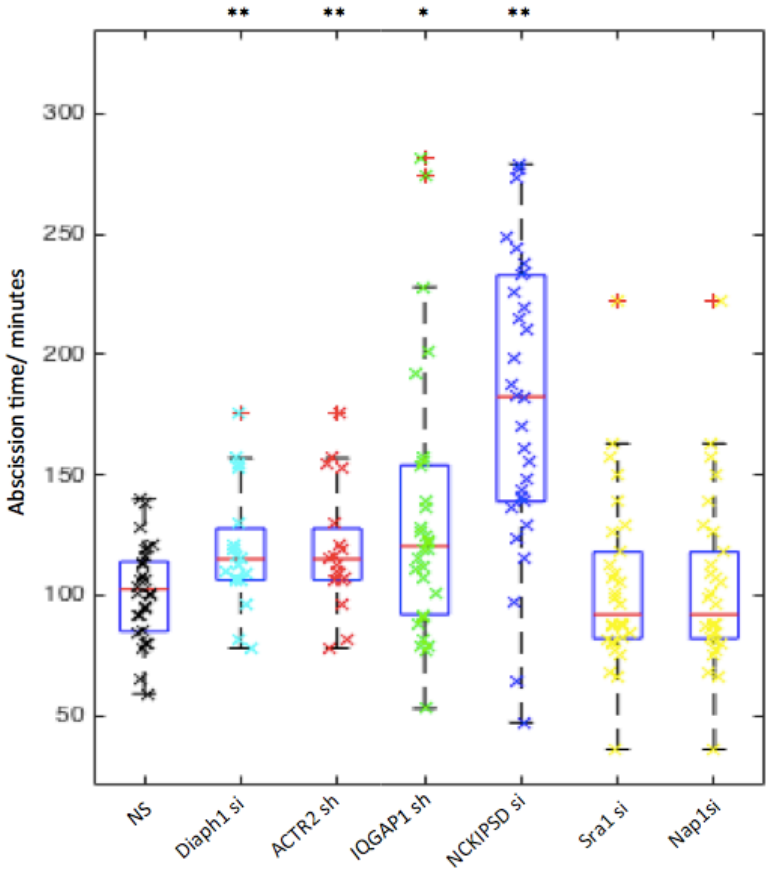

Figure 7-10 Duration of abscission time is perturbed by nucleator and NPF silencing. The duration of abscission time was plotted for each nucleator and every NPF knockdown. The start of anaphase was identified for each cell and the end of cytokinesis was identified. Abscission timing was determined by calculating the difference between these two events. Diaph1 siRNA, ACTR2 shRNA, NCKIPSD siRNA and IQGAP1 depletion significantly slowed abscission time (**p<0.01,

*p<0.05), whilst Sra1 siRNA (p=0.74) and Nap1 siRNA (p=0.46) depletion did not significantly change abscission time. Whiskers indicate minimum and maximum abscission times. 30 cells were analysed for each siRNA/shRNA HeLa depletion. Data was analysed with a Mann-Whitney U-Test.

7.4 Specific stage of cell cycle failure differs between NPFs

To further understand the impact that NPF depletion has upon the cell cycle and to identify similarities between NPF and nucleator, I identified the exact stage at which death occurred. Determining the exact stage of mitotic failure can allow for a greater insight into the differential roles that the nucleators and NPFs play within each stage.

As I have shown previously, Diaph1 knockdown cells predominantly die during interphase (71% of death in interphase of total cell death), apparently because they are unable to round into mitosis. Those cells that make it through to mitosis appear to die in early mitosis during prophase, or late mitosis during telophase (Figure 7-11). This observation is not mimicked by depletion of IQGAP1 (15% of death in interphase of total cell death), or NCKIPSD (40% of death in interphase of total cell death). Cells with an IQGAP1 knockdown predominantly died in mitosis, particularly in the first two stages, prophase (45% of death in prophase of total cell death) and metaphase (28% of death in metaphase of total cell death). I observed cells round up quicker than expected (Figure 7-9), but then begin blebbing profusely once they entered into mitosis, often resulting in cell death. Around 10% of cells died after furrowing, due to being unable to spread; this is categorised as ‘death after dividing’. Interestingly, IQGAP1 depleted cells do not copy Diaph1 depleted cells in the pattern and stage of cell death, suggesting that it may have other roles in the cell cycle or because of a weaker impact on Diaph1 activity.

NCKIPSD depleted cells showed similar patterns of cell death with siRNA and shRNA gene silencing (Figure 7-11). Of the cells that die, there is an equal proportion that die in interphase and in mitosis. Surprisingly, some cells progress through most of mitosis, divide and then regress, a process where the daughter cells combine post-cytokinesis. These cells likely die due to abscission failure, and do not represent a healthy cell population. Cells that regress are unable to spread, and may

suggest issues with previous chromosome segregation meaning that they require recombination of daughter cells to possibly regain chromosome stability. Again, the pattern of death seen in NCKIPSD depleted cells is not similar to that seen in Diaph1 knockdown cells, adding another layer of uncertainty to the potential NCKIPSD interaction. This observation could be because of more extensive perturbation to Diaph1 activity or because the nucleators participate in a particular stage of mitosis. The role of NCKIPSD in the cell cycle has not been studied in the literature, however both the Arp2/3 complex and Diaph1 have been identified as being important for regulating actin cortex stability during mitosis (Bovellan et al. 2014). Thus, NCKIPSD could be playing a role in regulating both Arp2/3 and Diaph1 at different stages of the cell cycle. Further investigations are required to understand its role.

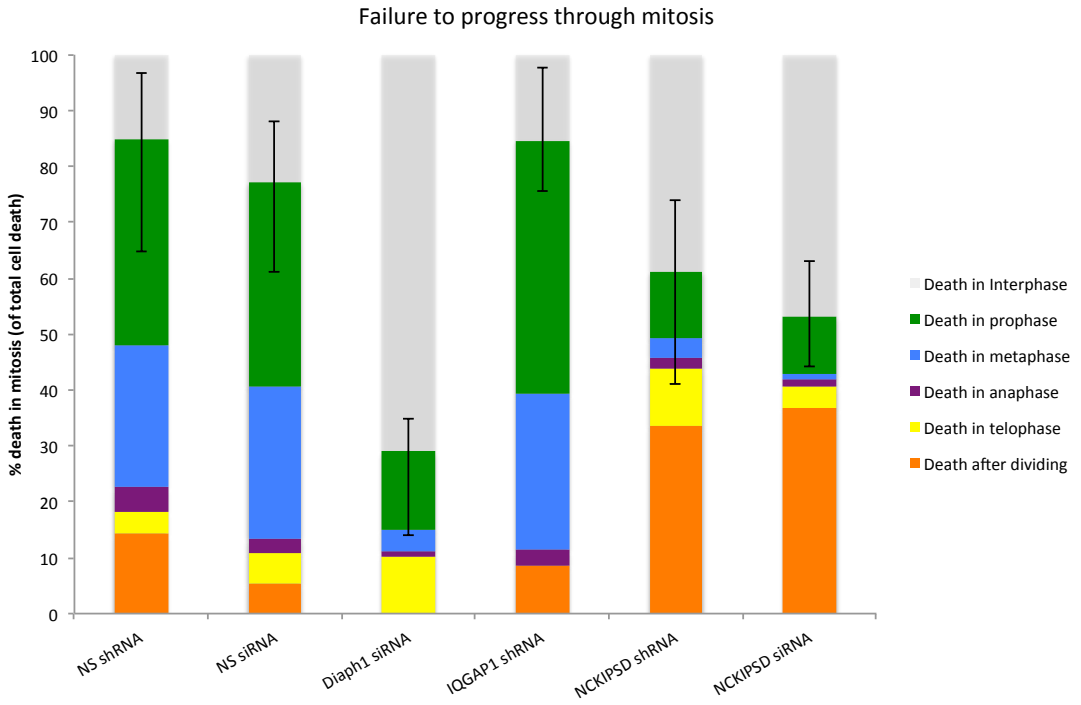

Figure 7-11 Nucleator depletion affects progression through mitosis and interrupts it at different stages. Distribution of cell deaths as a function of cell cycle stage. Cells that died during interphase are represented in grey, cells that died in prophase in green, metaphase in blue, anaphase in purple, telophase in yellow and after dividing in orange, are shown. Cells that died after dividing includes those that divide and regress, those that divide and could not spread, and cells that oscillated. All knockdown lines show a high proportion of cell death occurring in mitosis,

however, cells depleted of Diaph1 typically die during interphase. Results were gathered from 4 independent experiments examining: non-silencing shRNA (n=936 cells), non-silencing siRNA (n=178 cells), Diaph1 siRNA (n=200 cells), IQGAP1 shRNA (n=528), NCKIPSD shRNA (n=462), and NCKIPSD siRNA (n=515).

As I have shown previously, Arp2/3-subunit depleted cells predominantly die during mitosis, an observation opposite of that seen with Diaph1 depleted cells. More specifically, of those cells that died, ArpC2 and ACTR2 knockdown cells die in early mitosis, namely prophase (55% of death in prophase of total cell death) and metaphase (27% of death in metaphase of total cell death) (Figure 7-12). It is also important to note that ACTR2 depletion with siRNA yields a different pattern of death, despite resulting in the same amount of total death. The results suggest that cells were able to successfully round but were unable to organise the chromosomes as necessary to allow for continuation of the cell cycle cytokinesis. During these stages we know that the Arp2/3 complex and formins are important for generating newly polymerised actin filaments and pre-existing actin cables to contribute to initial assembly of the contractile ring. This ring remains a dynamic structure in which actin and other ring components continuously assemble and disassemble from the ring every minute. The rate of actin polymerisation can influence the rate of cleavage. Thus, actin polymerisation driven by the Arp2/3 complex and formins is a central process in cytokinesis, and could explain the interruption during the cell cycle with the depletion of the various nucleators/NPFs. Knockdown of the WAVE complex subunits, Sra1 and Nap1, also resulted in an interesting pattern of death, with most cells dying during anaphase (44% of death in anaphase of total cell death) and during prophase (26% of death in prophase of total cell death), respectively.

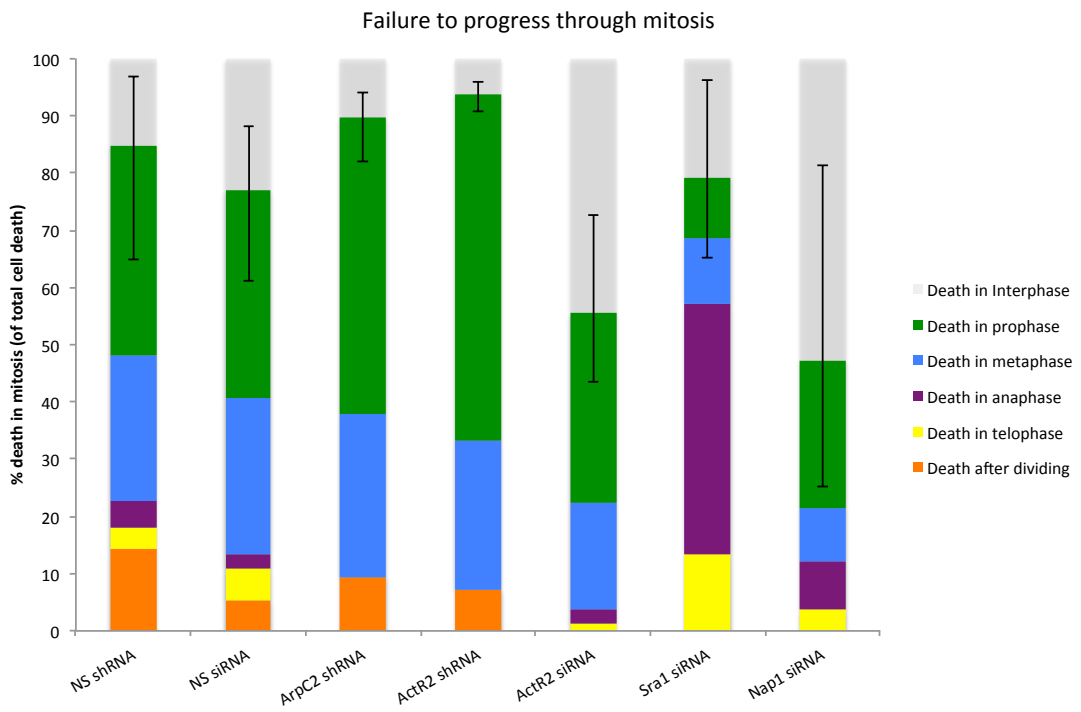

Figure 7-12 Nucleator depletion affects progression through mitosis and interrupts it at different stages. Distribution of cell deaths as a function of cell cycle stage. Cells that died during interphase are represented in grey, cells that died in prophase in green, metaphase in blue, anaphase in purple, telophase in yellow and after dividing in orange, are shown. Cells that died after dividing includes those that divide and regress, those that divide and could not spread, and cells that oscillated. All knockdown lines show a high proportion of cell death occurring in mitosis. Results were gathered from 4 independent experiments examining: non-silencing shRNA (n=936 cells), non-silencing siRNA (n=178 cells), ArpC2 shRNA (n=423 cells), ACTR2 shRNA (n=611 cells), Sra1 siRNA (n=629 cells), and Nap1 siRNA (n=542 cells).

From the results, it appears that Diaph1 has a crucial importance during interphase, whilst the other actin-binding proteins, ACTR2, NCKIPSD and IQGAP1, seem to be more critical during mitosis. Mitosis is the most sensitive part of the cell cycle, requiring a multitude of signalling pathways and shape changes supported by actin cortex rearrangements, most likely dictated by the nucleators explored in this thesis. The patterns of cell death comparing death in mitosis and interphase reported in the graphs above do not follow a specific pattern based on the phenotypes groups

(Diaph1-interacting and Arp2/3-interacting) that have been observed in the other experiments. To be able to entirely understand the results, further investigations are required whereby depleted cells with particular markers (i.e. actin, myosin, tubulin) are followed during the cell cycle. This may give an advanced insight into the particular aberrations that are occurring to result in death at the stages identified.

7.5 Combined silencing of NPF and nucleators to determine the signalling pathway

Next, I attempted to determine which nucleator each NPF mainly interacted with by combining NPF and nucleator knockdown. My hypothesis is that if I deplete a nucleator and an NPF that controls its activity, then the proportion of cells successfully making it through the cell cycle will not change compare to nucleator depletion alone. Conversely, if the NPF controls the other nucleator, then I should see an increase in cell death because I would be affecting two independent pathways. Indeed, when Bovellan et al perturbed the activity of both nucleators, they found a significant increase in failure to progress through the cell cycle.

For all experiments, I combined an shRNA stable cell line with siRNA to achieve a double knockdown. As a control, I used the nucleator shRNA stable line and transfected this with a non-silencing siRNA. All experiments were analysed between the controls and the single knockdown, and considered statistically significant if $**p<0.01$/$*p<0.05$.

7.5.1 Total cell death in NPF and nucleator knockdown in HeLa cells

I first began with combining Diaph1 knockdown with NPFs IQGAP1 and NCKIPSD. As I did not manage to generate a viable Diaph1 knockdown line with shRNA, I combined Diaph1 siRNA with stable lines showing IQGAP1 and NCKIPSD knockdown. Given my other experimental results, I expected to see no change in cell death when combining IQGAP1 depletion with Diaph1 knockdown, and an increase in death when combining IQGAP1 depletion with Arp2/3 knock down. Depletion of NCKIPSD has shown to phenocopy Diaph1 in the initial bleb size studies, however in many other experiments, NCKIPSD copied neither Diaph1

nor Arp2/3. Hence, for the combined depletion of NCKIPSD and Diaph1, I was unsure of what to expect.

In fact, depletion of Diaph1 and IQGAP1 significantly increased the amount of death when compared to Diaph1 siRNA alone (Figure 7-13). It could be that depleting IQGAP1 completely shuts down all Diaph1 nucleated actin, resulting in the increase in death seen. However, qPCR analysis and Western blot analysis revealed that Diaph siRNA gave ~94% knockdown in Diaph1 transcript and 95% knockdown in protein (Figure 7.1). Therefore, this hypothesis is unlikely. This therefore suggests that IQGAP1 may also play a role in regulation of Arp2/3 complex activity or in other important process in cell division.

If NCKIPSD played a role as a Diaph1 inhibitor as reported in the literature (Eisenmann et al. 2007), then I would expect depletion of NCKIPSD should rescue Diaph1 depleted lines by relieving inhibition on the remaining Diaph1. Interestingly, the combination of NCKIPSD and Diaph1 did not significantly change in the total cell death when compared to Diaph1 alone ($p=0.25$). This further supported the role of NCKIPSD as a Diaph1 activator rather than an inhibitor. I did not co-deplete WAVE and Diaph1, because WAVE is well-known Arp2/3 activator and has not been reported to interact with Diaph1.

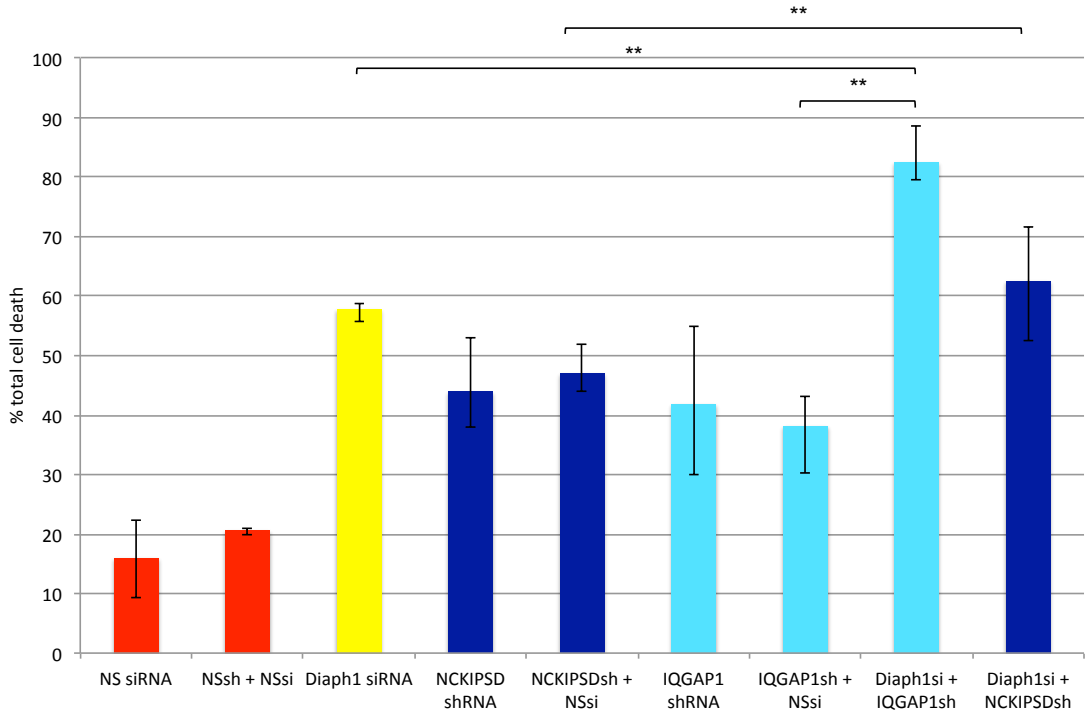

Figure 7-13 Diaph1 and NPF combined depletion affects progression through mitosis. When compared to cells transfected with IQGAP1 shRNA + NS siRNA, cells depleted in IQGAP1 and Diaph1 showed significantly increased rates of total cell death (**p<0.01). When compared to cells transfected with Diaph1 siRNA, cells depleted in IQGAP1 and Diaph1 showed significantly increased rates of total cell death (**p<0.01). When compared to cells transfected with NCKIPSD shRNA + NS siRNA, cells depleted in NCKIPSD and Diaph1 showed significantly increased rates of total cell death (**p<0.01). When compared to cells transfected with Diaph1 siRNA, cells depleted in NCKIPSD and Diaph1 showed no significant difference in total cell death (p=0.25). Results were gathered from 3 independent experiments examining: non-silencing shRNA (n=399 cells), non-silencing shRNA + siRNA (n=256 cells), Diaph1 siRNA (n=185 cells), NCKIPSD shRNA (n=462), NCKIPSDsh + NSsi (n=402), IQGAP1 shRNA (n=528), IQGAP1sh + NSsi (n=385), Diaph1si + IQGAP1sh (n=200 cells), Diaph1si + NCKIPSDsh (n=742 cells).

I then carried out double depletions with the Arp2/3 complex and NPFs. WAVE is a well-known Arp2/3 activator, thus I expected to see no change when combining ACTR2 and WAVE knockdowns. Co-depletion of ACTR2 and Nap1 showed no significant change in total cell death (Figure 7-14) when compared to ACTR2

depletion alone (p=0.33). This result confirms WAVE as a major interactor and activator of the Arp2/3 complex, and further adds to the data supporting this interaction in controlling Arp2/3 activity in the cortex.

The double depletion of ACTR2 + NCKIPSD significantly increases total cell death when compared to the ACTR2 depletion alone (Figure 7-1). This is consistent with a role an activator of the Arp2/3 complex, and supports data from the other experiments suggesting that NCKIPSD acts via a different pathway. ACTR2 + NCKIPSD depletion is comparable to NCKIPSD alone; the additional depletion of ACTR2 does not potentiate the NCKIPSD phenotype. This again, supports the role of NCKIPSD acting via a pathway different to Arp2/3. The double depletion of IQGAP1 + ACTR2 appeared to significantly decrease overall cell death when compared to ACTR2 alone and IQGAP1 alone (*$p<0.05$). This suggests that a rescuing effect on the depletion of ACTR2. This does not support a role of IQGAP1 in Arp2/3 activation, as its depletion has resulted in a decrease in cell death, rather than an increase. This suggests that IQGAP1, similar to NCKIPSD, acts via a different pathway to Arp2/3. Further work will be necessary to confirm this.

From the NPF combinations with the Arp2/3 complex, it appears that NCKIPSD may be activating Diaph1 promoting actin nucleation and confirms that Nap1 acts as an NPF for Arp2/3. On the contrary, the combination depletions suggest that IQGAP1 does not play a role in Arp2/3 activation and its rescue effect on Arp2/3 depletion warrants further study.

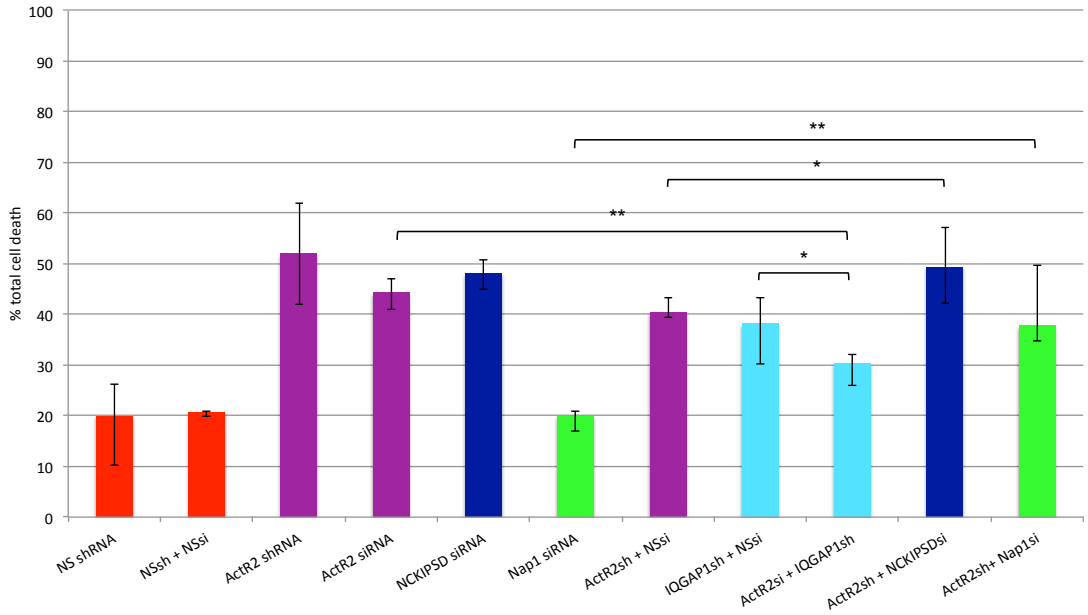

Figure 7-14 ACTR2 and NPF combined depletion affects progression through mitosis. When compared to cells transfected with siRNA, cells depleted in ACTR2 siRNA + IQGAP1 shRNA showed significantly reduced rates of total cell death (**p<0.01). When compared to cells transfected with IQGAP1 shRNA + NS siRNA, cells depleted in ACTR2 siRNA + IQGAP1 shRNA showed significantly reduced rates of total cell death (*p<0.05). When compared to cells transfected with ACTR2 shRNA + NS siRNA, cells depleted in ACTR2 shRNA + NCKIPSD siRNA showed increased reduced rates of total cell death (*p<0.05). When compared to cells transfected with NCKIPSD siRNA, cells depleted in ACTR2 shRNA + NCKIPSD siRNA showed no significant difference in total cell death (p=0.76). When compared to cells transfected with ACTR2 shRNA + NS siRNA, cells depleted in ACTR2 shRNA + Nap1 siRNA showed no significant difference in total cell death (p=0.33). When compared to cells transfected with Nap1 siRNA, cells depleted in ACTR2 shRNA + Nap1 siRNA showed significantly increased rates of total cell death (**p<0.01). Results were gathered from 3 independent experiments examining: non-silencing shRNA (n=399 cells), non-silencing shRNA + siRNA (n=256 cells), ACTR2 shRNA (n=383 cells), ACTR2 siRNA (n=595), NCKIPSD siRNA (n=515), Nap1 siRNA (n=542), ACTR2sh + NSsi (n=507 cells), IQGAP1sh + NSsi (n=385), ACTR2si + IQGAP1sh (n=498 cells), ACTR2sh + NCKIPSDsi (n=325 cells), ACTR2sh + Nap1si (n=831 cells).

7.5.2 Total cell death in double NPF knockdown in HeLa cells

In addition to co-depleting nucleator and NPF, I co-depleted two NPFs simultaneously. This could give some indication of the crosstalk that the NPFs may be involved in, especially with NCKIPSD and possibly with IQGAP1. Similar to the previous experiments, I used a stable shRNA line for silencing one NPF and silenced the other with the appropriate siRNA.

I began with studying IQGAP1 in combination with NCKIPSD and Nap1. Based on the previous results, I expected to see no change in cell death when co-depleting NCKIPSD and IQGAP1 because they appear to act as NPFs for Diaph1, and possibly an increase in death when co-depleting Nap1 and IQGAP1. IQGAP1 + NCKIPSD is comparable to IQGAP1 alone but less death compared to NCKIPSD alone. It is possible that there is some rescue in this case, but it the combined depletion is not significantly different to IQGAP1 alone (Figure 7-15). This could indicate that NCKIPSD: 1) is working through Arp2/3 as an activator, albeit not a crucial NPF, or 2) is working through Diaph1 as an inhibitor. If NCKIPSD is indeed acting as a Diaph1 inhibitor, when depleted Diaph1 returns to its active state and thus, no change is apparent from IQGAP1 depletion alone. Together, this certainly warrants further investigation of the role of NCKIPSD, and supports the strong possibility that NCKIPSD acts via both Arp2/3 and Diaph1 in a way not yet understood through these experiments.

Next, the combination of IQGAP1 + Nap1 is comparable to IQGAP1 depletion alone, but significantly more death compared to Nap1 alone. This suggests that the combined NPF depletion has potentiated the Arp2/3 pathway, leading to a greater proportion of cell death.

From the double NPF depletions, it appears that NCKIPSD may indeed be activating Arp2/3 promoting actin nucleation or even inhibiting Diaph1 as suggested in the literature. On the contrary, the NPF combinations further support WAVE as acting as an Arp2/3 complex activator.

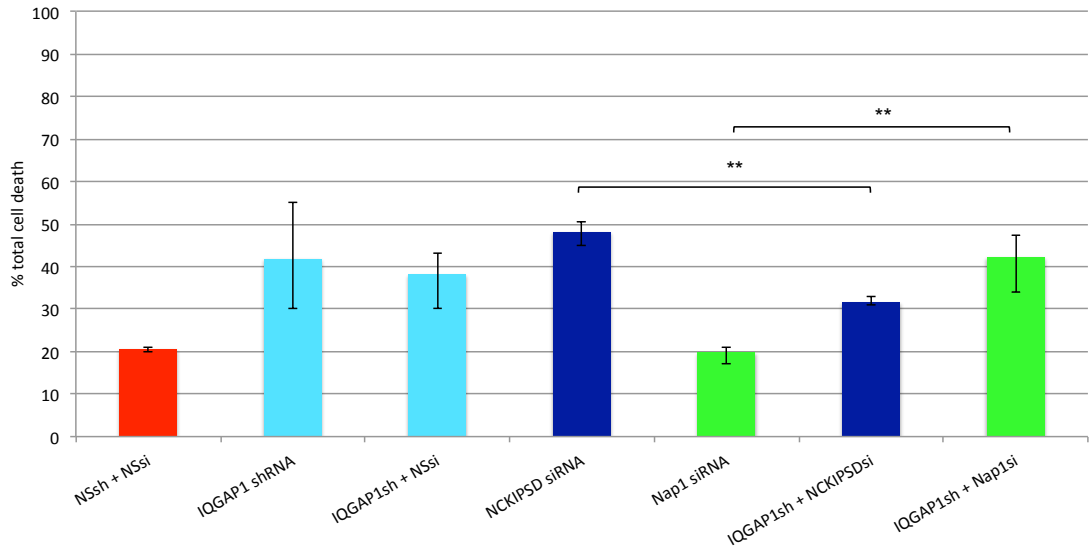

Figure 7-15 Double NPF depletion with IQGAP1 affects progression through mitosis. When compared to cells transfected with NCKIPSD siRNA, cells depleted in IQGAP1 shRNA + NCKIPSD siRNA showed significantly reduced rates of total cell death (**p<0.01). When compared to cells transfected with IQGAP1 shRNA + NS siRNA, cells depleted in IQGAP1 shRNA + NCKIPSD siRNA showed no significant difference in total cell death (p=0.05). When compared to cells transfected with Nap1 siRNA, cells depleted in IQGAP1 shRNA + Nap1 siRNA showed significantly increased rates of total cell death (**p<0.01). When compared to cells transfected with IQGAP1 shRNA + NS siRNA, cells depleted in IQGAP1 shRNA + Nap1 siRNA showed no significant difference in total cell death (p=0.23). Results were gathered from 3 independent experiments examining: non-silencing shRNA + siRNA (n=256 cells), IQGAP1 shRNA (n=528 cells), IQGAP1sh + NSsi (n=385 cells), NCKIPSD siRNA (n=515), Nap1 siRNA (n=542), IQGAP1sh + NCKIPSDsi (n=412 cells), IQGAP1sh + Nap1si (n=433 cells).

Next, I combined NCKIPSD depletion with IQGAP1 and Nap1 knockdown to attempt further exploration of potential NCKIPSD crosstalk (Figure 7-16). Of the NPFs studied in this project, NCKIPSD has yielded the least consistent results, at times suggesting that it interacts with Diaph1 (possibly as an inhibitory interactor) and other times suggesting that it activates Arp2/3.

In the previous graph, I discussed the combination of IQGAP1 and NCKIPSD depletion. NCKIPSD + Nap1 depletion results in an increase in cell death compared

to NCKIPSD alone and Nap1 alone. The combination of NCKIPSD + Nap1 led to a low significant increase (*p<0.05) in total cell death when compared to NCKIPSD knockdown alone, and this trend is worth looking at in more detail. From this NPF combination, it appears that NCKIPSD and Nap1 potentiate each other, and it is possible that the combination of both could completely shut down nucleation via Arp2/3. The total cell death with the depletion of both NCKIPSD + Nap1 is comparable to the death seen with ACTR2 alone; this could support NCKIPSD as an Arp2/3 activator. It is also important to consider that NCKIPSD may be working in a pathway different to that of Nap1, suggesting that in this instance, the increase in total cell death is a result of inhibition of the Diaph1 pathway. At this stage, the role of NCKIPSD is not understood.

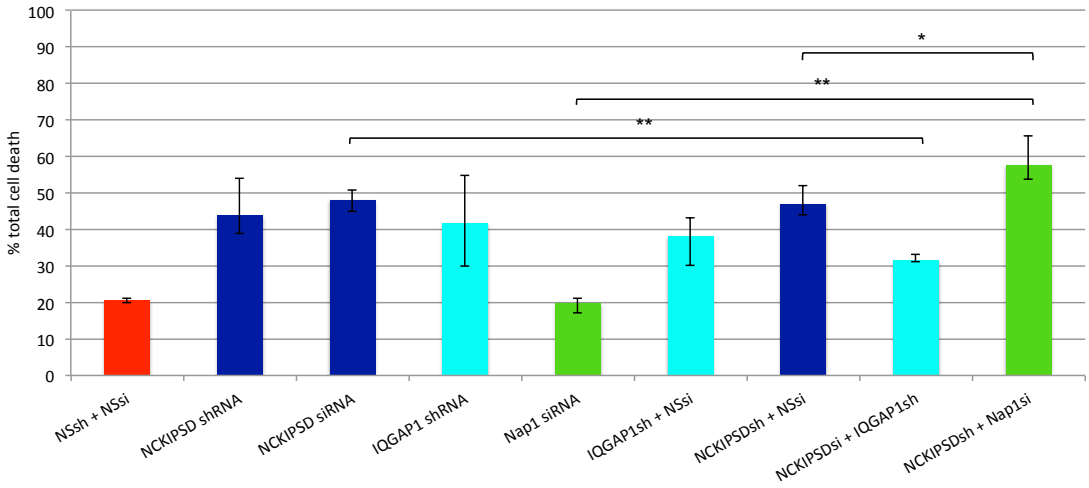

Figure 7-16 Double NPF depletion with NCKIPSD affects progression through mitosis. When compared to cells transfected with IQGAP1 shRNA + NS siRNA, cells depleted in NCKIPSD siRNA + IQGAP1 siRNA showed no significant difference in total cell death (p=0.05). When compared to cells transfected with NCKIPSD siRNA, cells depleted in NCKIPSD siRNA + IQGAP1 siRNA showed significantly reduced rates of total cell death (**p<0.01). When compared to cells transfected with Nap1 siRNA, cells depleted in NCKIPSD shRNA + Nap1 siRNA showed significantly increased rates of total cell death (**p<0.01). When compared to cells transfected with NCKIPSD shRNA + NS siRNA, cells depleted in NCKIPSD shRNA + Nap1 siRNA showed significantly increased rates of total cell death (*p<0.05). Results were gathered from 3 independent experiments examining: non-

silencing shRNA + siRNA (n=256 cells), NCKIPSD shRNA (n=462 cells), NCKIPSD siRNA (n=515), IQGAP1 shRNA (n=528), Nap1 siRNA (n=542), IQGAP1sh + NSsi (n=385), NCKIPSDsh + NSsi (n=402 cells), NCKIPSDsi + IQGAP1sh (n=412 cells), NCKIPSDsh + Nap1si (n=402 cells).

7.5.3 Cell cycle progression failure associated with IQGAP1 depletion is rescued by expression of the IQGAP1 Diaph1 binding domain

The rescue construct discussed in this section, IQGAP1-DBR, was cloned and provided to me for cell line production by Dr. Guillaume Charras.

To rescue cell deaths due to IQGAP1 depletion, I stably transfected shRNA resistant IQGAP1 constructs cloned from mouse IQGAP1 into my knockdown line. First, I attempted to make a rescue line using the full-length mouse IQGAP1 sequence. Unfortunately, I was unable to make a stable line with this construct. I then tried to make a rescue line with IQGAP1's Diaph1 binding region (DBR) domain fused to GFP because much of my data suggested an interaction between IQGAP1 and Diaph1. I successfully made stable lines with the DBR rescue and imaged the cells overnight to study their progression through the cell cycle. The DBR was able to rescue the cell death observed in IQGAP1 depleted lines, with no significant difference in the rescue line when compared to the non-silencing control (Figure 7-17). However, it must be noted that the appropriate control would be a cell line expressing IQGAP1shRNA and an empty rescue GFP-vector. For lack of time, this was not made. Nevertheless, the decrease in total cell death is evident, supporting the role of IQGAP1 as a Diaph1 activator in the actin cortex.

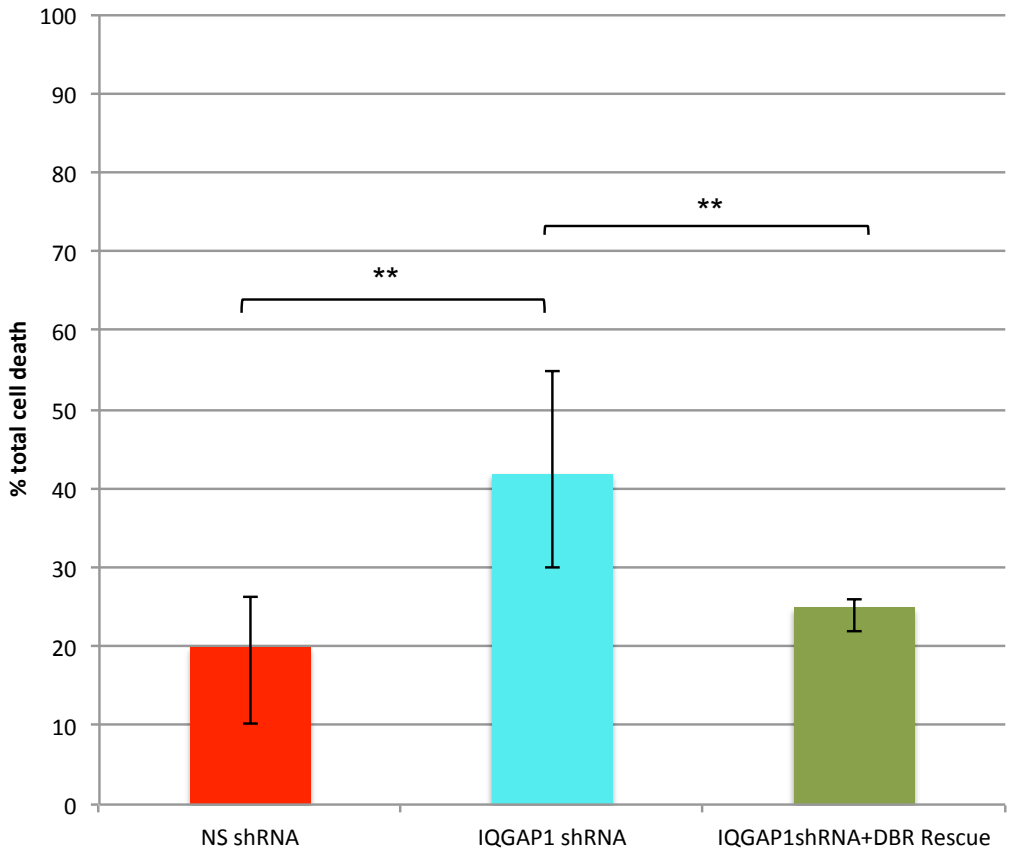

Figure 7-17 The Diaph1 binding region (DBR) domain rescues total cell death in IQGAP1 knockdown cells. When compared to IQGAP1 shRNA cells, cells rescued with the DBR showed a significant decrease in cell death (**p<0.01). There is no significant difference between non-silencing control cells and DBR rescue IQGAP1 cells (p=0.17), suggesting the DBR rescued the high death phenotype. Results were gathered from 3 independent experiments examining: non-silencing shRNA (n=399 cells), IQGAP1sh (n=528 cells), IQGAP1sh + DBR rescue (n=377 cells). Data was analysed with a chi-squared test.

7.6 Conclusion

It is known that Arp2/3 and Diaph1 form different types of filaments that are required in different processes during cell division. The Arp2/3 complex forms branched filaments, whilst formins such as Diaph1 makes filaments well suited for contractility, giving the two nucleators independent roles suited to their function. Given the importance of Arp2/3 and Diaph1 in regulating cell cycle progression, I investigated the role of each candidate NPF in modulating nucleator activity during

the cell cycle. I hypothesised that depletion of NPFs would present results similar to the depletion of the corresponding nucleator. This investigation also aimed to understand the crosstalk between Arp2/3 and Diaph1 that NCKIPSD may be involved in.

In my experiments, Flightless-I displayed no significant increase in death, consistent with its lack of effect on bleb size. Diaph1, IQGAP1 and NCKIPSD depletion increased the total percentage of cell deaths significantly. Sra1 and Nap1 depleted cells surprisingly did not phenocopy ACTR2 depletion with regards to total cell death in this experiment, however the cells exhibited other changes with regards to decreasing mitotic rounding time. It was also interesting to observe differences with regards to effect of depletion for different Arp2/3 subunits; ACTR2 depletion significantly increased total cell death, whilst depletion of ArpC2 did not have an effect on progression through the cell cycle. Importantly, the decrease in total cell death with the rescue of IQGAP1 with the Diaph1 binding region strongly supports IQGAP1 as a Diaph1 activator in the actin cortex.

The investigation into rounding timing in knockdown cells showed that IQGAP1, Diaph1 and WAVE depletions caused cells to round significantly quicker than controls. On the other hand, NCKIPSD and ACTR2 depleted cells took significantly longer for the completion of rounding. Rounding requires the rapid disassembly and reorganisation of the actin cytoskeleton network, highlighting the importance of actin nucleators such as Diaph1 and the Arp2/3 complex. A decrease of such nucleators could have an impact on actin filament turnover, directly impacting the process of cell rounding during the cell cycle. To further investigate how the change in physical properties of the cortical network impacts actin nucleation, Malti Vaghela, a PhD student in the lab, has been interrogating the contribution of actin nucleation kinetics and myosin recruitment as a result of nucleator/NPF depletion. The results for this are discussed in detail later in the discussion. Together, these results help to support the role of IQGAP1 as a Diaph1 activator, WAVE as an Arp2/3 activator, and leaves NCKIPSD as an NPF still not completely understood.

Chapter 8 NPF depletion impacts cortical architecture of interphase HeLa cells

I further probed the role of NPFs and nucleators in cortex architecture by investigating the impact of depletion or inhibition on cortex density and organisation in interphase HeLa cells. Identifying changes within the actin cortex organisation can potentially help determine how depletion of NPFs impacts processes such as cell division. The cortex is organised in a way that allows for cortical contractions, required densities, and thickness. The cortex organisation also dictates properties that affect the mechanics of the cortex, thus organisation has a great impact on its function. As the depletion of NPFs perturbs this tightly regulated process, I would expect to see a clear change in cortex organisation using electron microscopy.

For this investigation, I prepared stable HeLa cells lines (control, ACTR2, ArpC2 and IQGAP1) and drug treated cells (DMSO, CK666, SMIFH2, SMIFH2 + CK666, and LatrunculinB) for electron microscopy and imaged them. This allowed me to probe the molecular organisation of the cortex in these cells. The cortex of HeLa cells is heterogeneous, with long structures of well-aligned actin filaments, extending close to the periphery of spread interphase cells (Figure 8-1**A**, arrows). In between these long fibres are less organised and less dense filaments with no marked orientation (Figure 8-1**A**, asterisk). DMSO treated lines were imaged as a control and did not appear to have an impact on actin filament organisation. The long directional filaments are very clear (Figure 8-1**B**, arrows), and the lower density structures in between are still present (Figure 8-1**A**, asterisk). To observe the impact of actin depolymerisation, I treated the cells with latrunculin B, a drug that sequesters monomeric G-actin, stopping F-actin assembly. This drug disrupted the long aligned filament organisation of the actin cytoskeleton and caused aberrations to the usual spread interphase cell shape. Only single actin filaments were distinguishable (Figure 8-1**C**, arrowheads). From the electron micrographs, it is evident that latrunculin B is a powerful disruptor of microfilament organisation, impacting all normal characteristics of the organisation of HeLa cells.

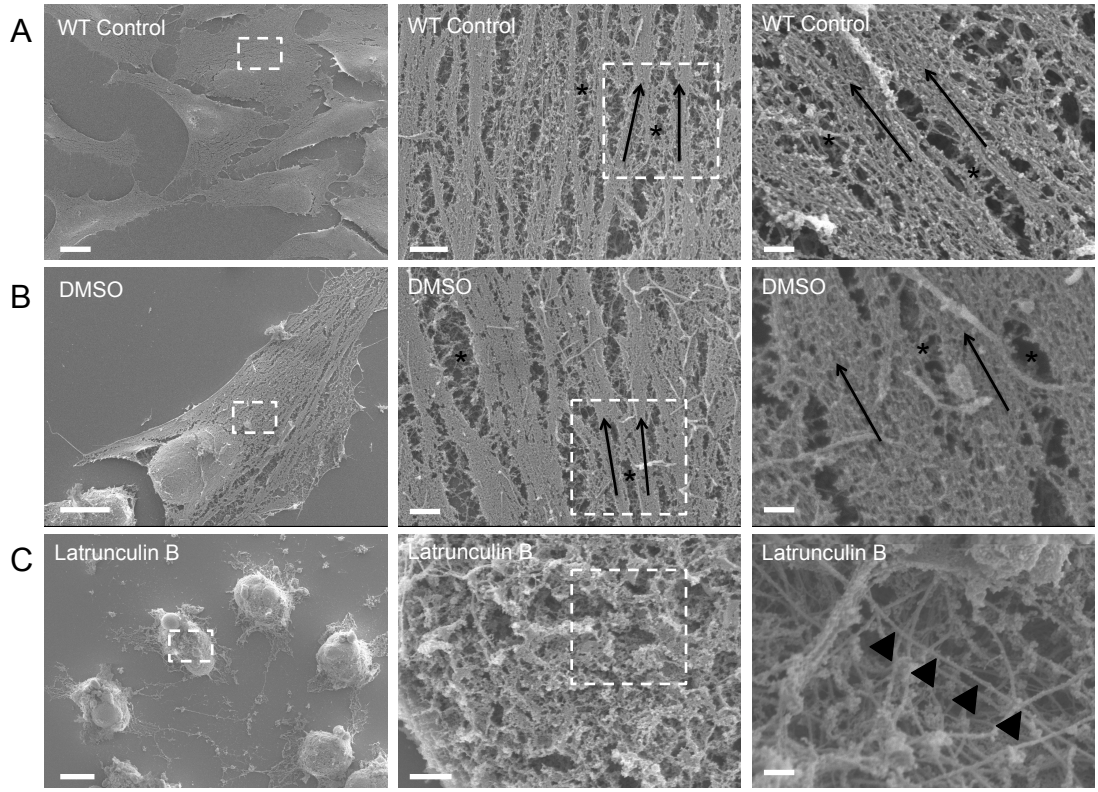

Figure 8-1 Scanning electron micrographs of the cortex of HeLa cells in interphase. A, The actin cortex of wild-type control cells features long bundles of directional actin filaments that can be followed along the spread cell (arrows), and in between connections of lower density (asterisk). **B,** The actin cortex of cells treated with 100uM DMSO appears to have no change compared to untreated wild-type cells**. C,** The actin cortex of cells treated with 750nM latrunculin B appears distorted, and all structures seen in the controls are lost**.** Single filaments are distinguishable (arrowheads). Scale bars: first column (10μm), second column (1μm), and third column (200nm).

I then wanted to investigate the impact of nucleator inhibition upon actin filament organisation. Cells treated with CK666 appeared to have less long directional actin filament bundles compared to controls, however these were still clearly visible (Figure 8-2**B**, arrows). On the hand, SMIFH2 treated cells appeared to have a more dense and homogenous cortex without as the long aligned structures seen in the controls. The aligned regions are very short (Figure 8-2**C**, arrows), however there are some small interconnecting filaments visible in between the more structured regions (Figure 8-2**C**, asterisk). Possibly, the inhibition of formins, a linear actin filament

nucleator, results in more nucleation via the branched actin nucleator, Arp2/3. It is also important to remember that there are other actin nucleators that may also play a role in actin nucleation. The apparent increase in density may result from increased branching of actin filaments due to increased activity of the Arp2/3 complex. SMIFH2 treated HeLa cells also appeared to have lost the spread interphase cell shape integrity visible in the low magnification micrograph.

Drug treatment with both CK666 and SMIFH2 resulted in a severe loss of the overall spread morphology, as seen in the low magnification image (Figure 8-2**D**). Cells appear shrunken with apparent changes in their shape. The organisation of the actin filaments appears to be patchy and single filaments can be identified within the loosely interconnected cortex. There are no long aligned regions as seen in the controls, and less so with single drug treatment. Single filaments can be identified (Figure 8-2**D**, arrowheads). Evidently, inhibition of CK666 and SMIFH2 had an impact upon the structure of the actin cortex, and thus explains the malfunctions in processes requiring proper cortex assembly such as cell division. Interestingly, previous work has shown that simultaneous inhibition of formins and Arp2/3 resulted in high cell death (Bovellan, 2014).

Based on the actin cortex aberrations observed in cells treated with CK666 and SMIFH2, I expected to see similar disorganisation in cells depleted of ACTR2, ArpC2 or IQGAP1. Depletion of ACTR2 (Figure 8-3**B**) or ArpC2 (Figure 8-3**C**) did not have a strong impact upon the organisation of the actin cortex. There were some changes in cell spreading in interphase as seen with CK666 treated cells. ArpC2 depleted cells still displayed the long regions of highly aligned and bundled filaments, however ACTR2 depletion appeared to have slightly disjointed filaments. This is consistent with the notion that this highly aligned F-actin is nucleated by formins. In contrast to Arp2/3 subunit depletion, IQGAP1 knockdown cells appeared to have lost the regions of high filament alignment, and actin filaments were less organised, similar to SMIFH2 treatment (Figure 8-3**D**). This further supports IQGAP1 as an important NPF controlling the activation of Diaph1 and thereby the organisation of the cortex.

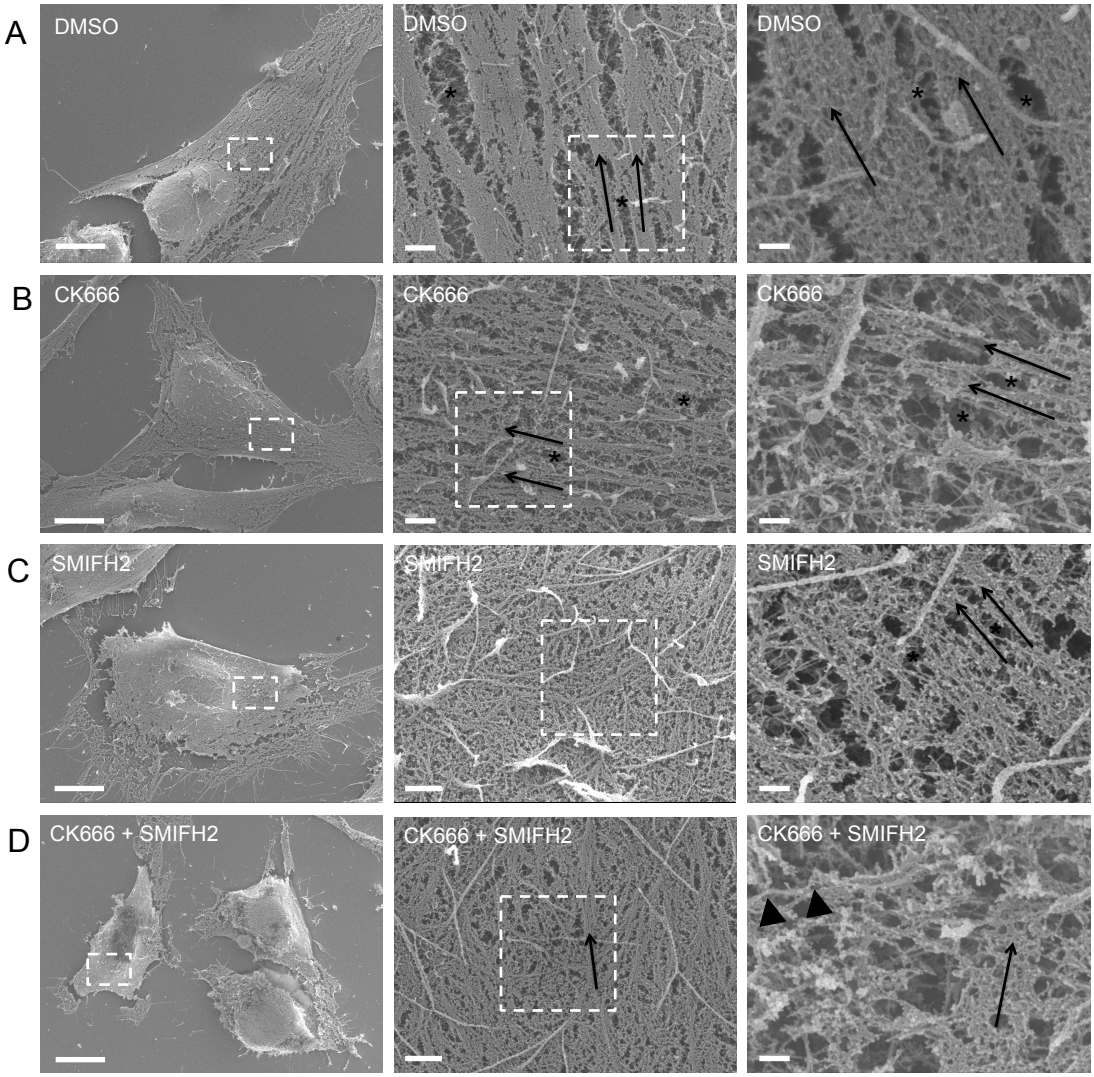

Figure 8-2 Scanning electron micrographs of membrane extracted HeLa cells in interphase. A, The actin cortex of 100µM DMSO treated cells, with well-aligned actin filaments bundles (arrows), and interconnecting regions with a lower density (asterisk)**. B,** The actin cortex of 100µM CK666 treated cells appears to have lost filament directionality, with some remaining areas of directionality (arrows) and more areas of lower density (asterisk). **C,** The actin cortex of 10µM SMIFH2 treated cells appears more homogenous and regions of strong alignment (arrows) and high density seem to have disappeared (asterisk). **D,** The actin cortex of SMIFH2 + CK666 treated cells appears very patchy and cells have rounded. Very rarely are areas evidencing alignment visible (arrows); single filaments can be identified (arrowheads). Scale; first column (10µm), second column (1µm), third column (200nm).

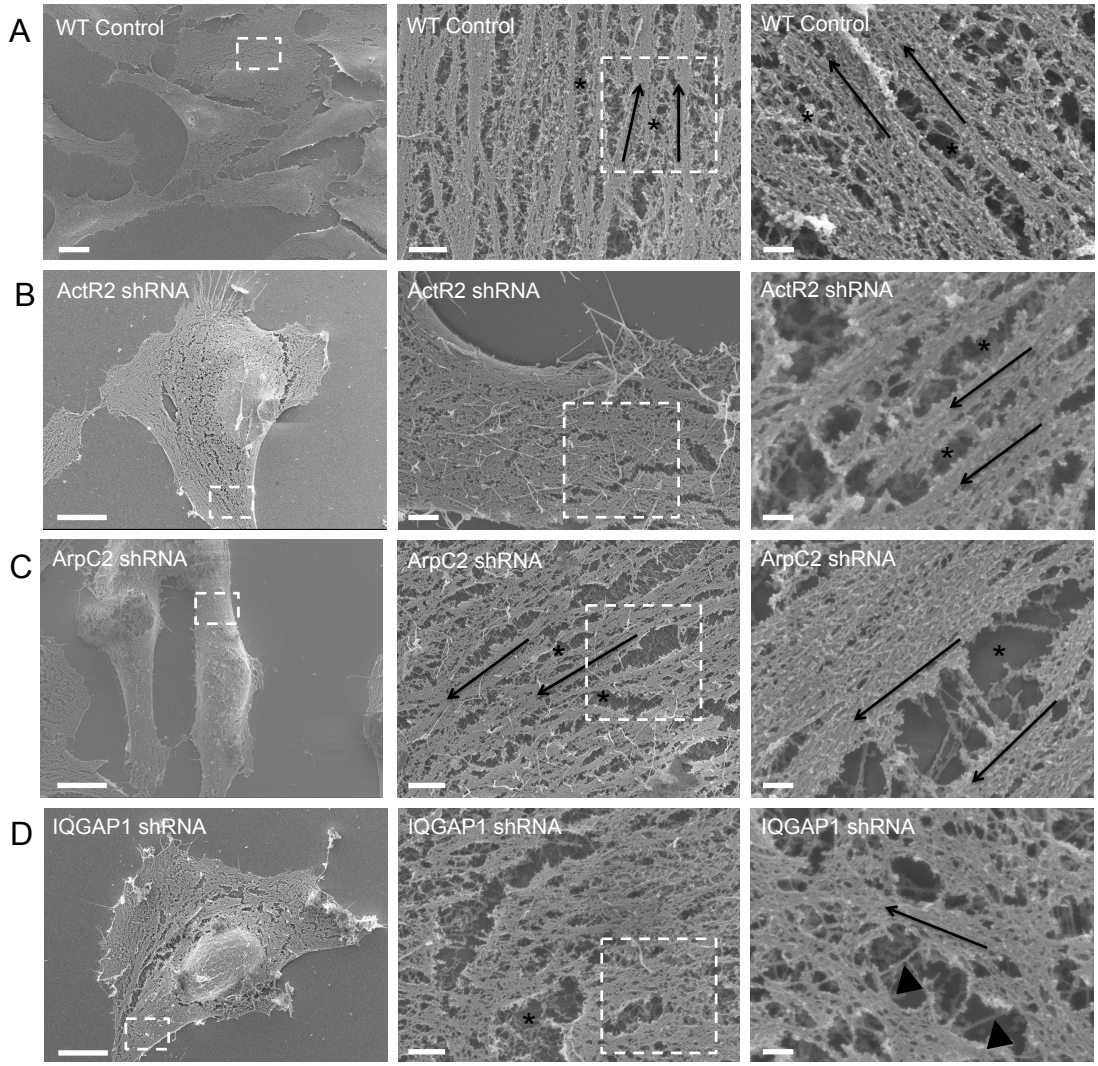

Figure 8-3 Scanning electron micrographs of membrane extracted HeLa cells in interphase. A, The actin cortex of wild-type control cells features long aligned actin filament bundles that can be followed along the spread cell (arrows). **B,** The actin cortex of ACTR2 shRNA cells appears to have no changes in the organisation of the aligned bundles of filaments. **C,** The actin cortex of ArpC2 shRNA cells appears similar to the control cells, with some change in the spread morphology, but little change in the organisation of the cortex**. D,** The actin cortex of IQGAP1 shRNA cells appears to have lost the long aligned actin filament bundles. Scale; first column (10μm), second column (1μm), and third column (200nm).

Chapter 9 Identifying Diaph1 interactors using biotin identification (BioID)

In July 2015, I was awarded a three-month Bogue Fellowship by the Department of Cell and Developmental Biology, funding a visit to the laboratory of Prof. Phillippe Roux at the IRIC of the University of Montréal. During my time in Montréal, biotin identification (BioID), a new and powerful proximity-dependent labelling approach was used to map novel interactions. Dr. Geneviève Lavoie carried out cloning of all BirA constructs. Antoine Meant generated all stable cell HeLa lines prior to the start of the project, and analysed the mass spectrometry data with SAINTexpress as detailed below.

9.1 Validation of the BirA*-fusion protein in HeLa cells

The wild type 35 kDa Escherichia coli (E. coli) bacterial protein, BirA, functions as a biotin protein ligase to regulate the biotinylation of an acetyl-CoA carboxylase subunit, as well as a DNA-binding transcriptional repressor for biotin biosynthesis (Roux et al. 2012). BirA recognises a stretch of 15 amino acids (GLNDIFEAQKIEWHE), known as the AviTag, with high specificity and catalyses the attachment of the cofactor, biotin, to the lysine residue (K) in this recognition site. However, a mutation of the arginine residue at position 118 to glycine (R118G) in BirA causes premature release of activated biotin (biotinoyl-AMP) that can readily react with primary amines from the mutated biotin ligase, BirA (R118G), resulting in the promiscuous biotinylation of proximal proteins (Choi-Rhee et al. 2004; Roux et al. 2012; Kwon & Beckett 2000). The BioID method uses this mutated BirA (R118G) and expresses it as a fusion to a bait protein of interest in live mammalian cells supplemented with biotin. Expression of this BirA (R118G)/bait fusion protein allows for the biotinylation of proteins that interact or come into close proximity with the bait in their natural environment. The practical labelling radius of promiscuous biotin ligases is an important experimental consideration since a large radius would predictably detect more proteins that may not be direct interactors of the bait; whereas conversely, a smaller radius would potentially limit detection of relevant protein interactors for a larger protein or a protein complex. Studies indicated the practical labelling radius of BioID is ~10 nm (D. I. Kim et al. 2014).

Cells can then be stringently lysed, and protein interactants can be denatured, captured via their biotin labels with high affinity on streptavidin-beads, and identified by MS or immunoblot analysis (Roux et al. 2012).

HeLa cells were selected to stably express the BioID fusion constructs. The following HeLa cell lines were used for the BioID experiments: FLAG φ (no BirA*) control, BirA* control, BirA*-GFP control, Diaph1-BirA*, Diaph1ΔDAD-BirA*, Arp3-BirA* and ArpC4-BirA*. The baits were chosen to provide a non-biased approach that would complement the candidate-based approach I used in previous chapters. In the mutated (ΔDAD) Diaph1 construct, Diaph1 activity is constitutively activated due to the removal of autoinhibition by the DAD domain. Comparison between this construct and full length Diaph1 allows to find interactions that depend on activation, as Diaph1 is only activated once the DID-DAD interaction is relieved. Arp3 and ArpC4 were chosen as important subunits of the Arp2/3 complex.

The goal of BioID was to identify proximity interactions in the normal context of a target protein, hence it was necessary to validate the biotinylation activity of the BirA*-fusion protein. Before carrying out large-scale BioID experiments, the BirA* stable cell lines were first characterised by western blotting (using streptavidin-HRP). I induced BirA expression using tetracycline for 0, 4, 8, 12, and 24 hours to determine the best duration for protein induction and to check the plasmid expression. I then added the substrate, biotin, for different durations to establish how is needed to obtain a sufficiently strong biotinylation signal, and to see the pattern of biotinylation. This is essential to the success of the method, so it was investigated first.

As expected, there was no biotinylation in the FLAG ϕ control line, as this construct was devoid of BirA* (Figure 9-1). The other two controls, BirA and BirA-GFP were induced as expected, and showed a pattern of biotinylation, most strongly in the BirA-GFP line. It is also important to note the expected shift in size of the BirA construct with the addition of GFP (27kDa), compared to BirA alone. It seems apparent that BirA-GFP interacts with more proteins than BirA. Previous studies have shown that the tethering of GFP has no effect on BirA activity; it is possible

that the difference here is due to non-specific protein binding to the large GFP protein and not related to the cell line.

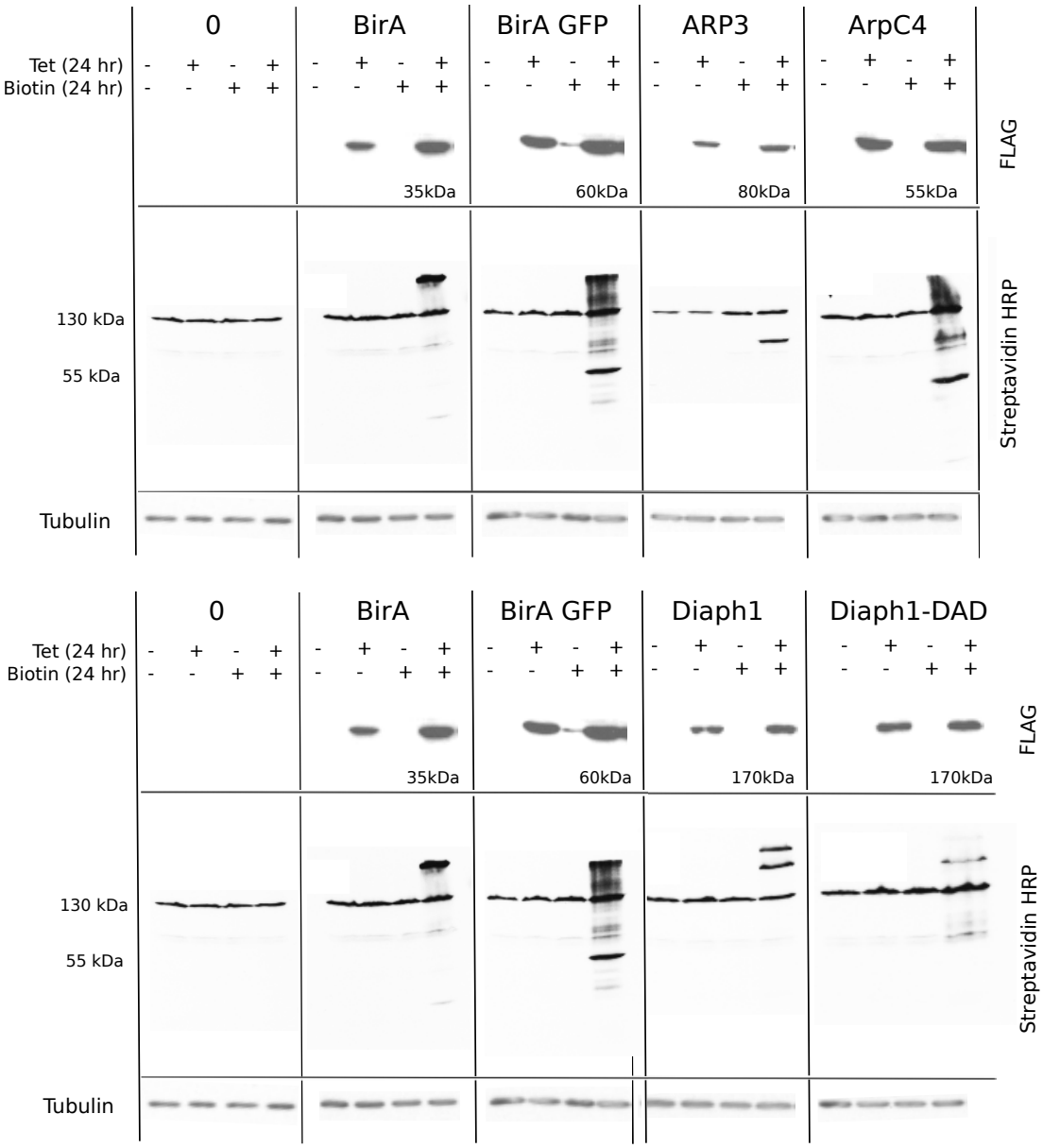

Figure 9-1 Detection of protein biotinylation by Western blot. HeLa BirA* fusion cell lines (FLAG φ, BirA, BirA-GFP, Arp3-BirA, ArpC4-BirA, Diaph1-BirA and Diaph1ΔDAD-BirA) were induced with 1μg/mL tetracycline for 24 hours and supplemented with 50μM biotin for 24 hours (+tet/+biotin). Induced proteins were probed with FLAG, and biotinylated proteins were detected with HRP-streptavidin. Tubulin was used as a loading control.

Of the baits examined, ArpC4 demonstrated the broadest range of biotinylated proteins whilst Arp3 demonstrated the narrowest. It has been shown that ArpC4 is critical for Arp2/3 complex activity as it mediates binding to F-actin (Goley et al. 2010). Mutation of residues within ArpC4 can compromise actin polymerisation activity, and reduce F-actin affinity. On the contrary, Arp3 is located within the centre of the Arp2/3 complex, and is not required for formation of the daughter filament nucleus (Liu et al. 2013). Having said that, both subunits are important for the function of the Arp2/3 complex and the results yielded in this initial BioID test may present a difference due to experimental issues as opposed to biochemical functions.

9.2 Identifying interacting proteins by mass spectrometry

Through this initial characterisation, the BirA*-fusion proteins were validated in HeLa cells and I was able to upscale the experiment from testing 1 million cells in 6-well plates to testing 20 million cells pooled from two 10 cm dishes. The BioID experiment was repeated three times, and proteins identity determined by SAINT to be high confidence interacting partners were analysed to create a list of top candidates.

In the case of ArpC4 and Arp3 (Figure 9-2, Figure 9-3), the entire Arp2/3 complex was identified, validating the approach. In addition, some new interactors were identified, however the majority of these were chaperones (all the TCP1/cpn60 chaperonin family proteins - CCT1-8). There were also folding proteins (NOB1), G-proteins (GNB4), and transcriptional activators (CHURC1) amongst those detected. I represented these results graphically using STRING analysis.

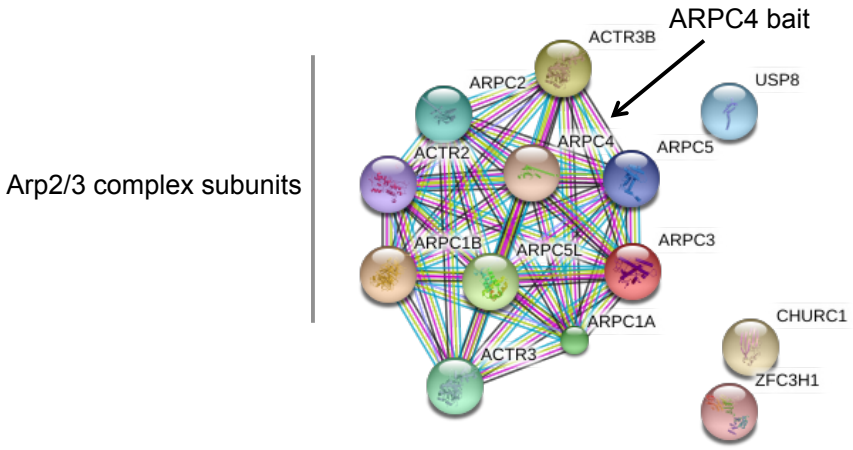

Figure 9-2 BioID string analysis of ARPC4 interactors. Mass spectrometry analysis of endogenous proteins that are in close proximity to ARPC4, determined by mass spectrometry isolated with streptavidin-coupled magnetic beads. The entire Arp2/3 complex was identified. Lines between proteins represent known interactions (determined via curated databases or experimentally) and predicted interactions (determined via gene fusions, gene neighbourhoods and gene co-occurrence). Small nodes represent proteins of unknown 3D structure and large nodes represent proteins with some known 3D structure. All candidates displayed have a SAINT score > 0.75 and STRING analysis was performed at the high confidence interval.

Table 9-1 ARPC4 interactors identified by BioID, Avg(P) score and function. Avg(P) represents the probability of a true interaction between the two proteins, prey and bait. Preys with an Avg(P) >0.85 are conserved and considered as good potential interactors. The other prey is discarded, as they are likely the result of non-specific interactions.

Protein	Avg(P) Score	Function
USP8	0.87	Removes conjugated ubiquitin from proteins, preventing degradation. Involved in endosomal dynamics, cargo sorting and membrane trafficking.
CHURC1	1	Transcriptional activator with role in regulation of cell movement.
ZFC3H1	0.84	Involved in RNA binding, protein coding gene.

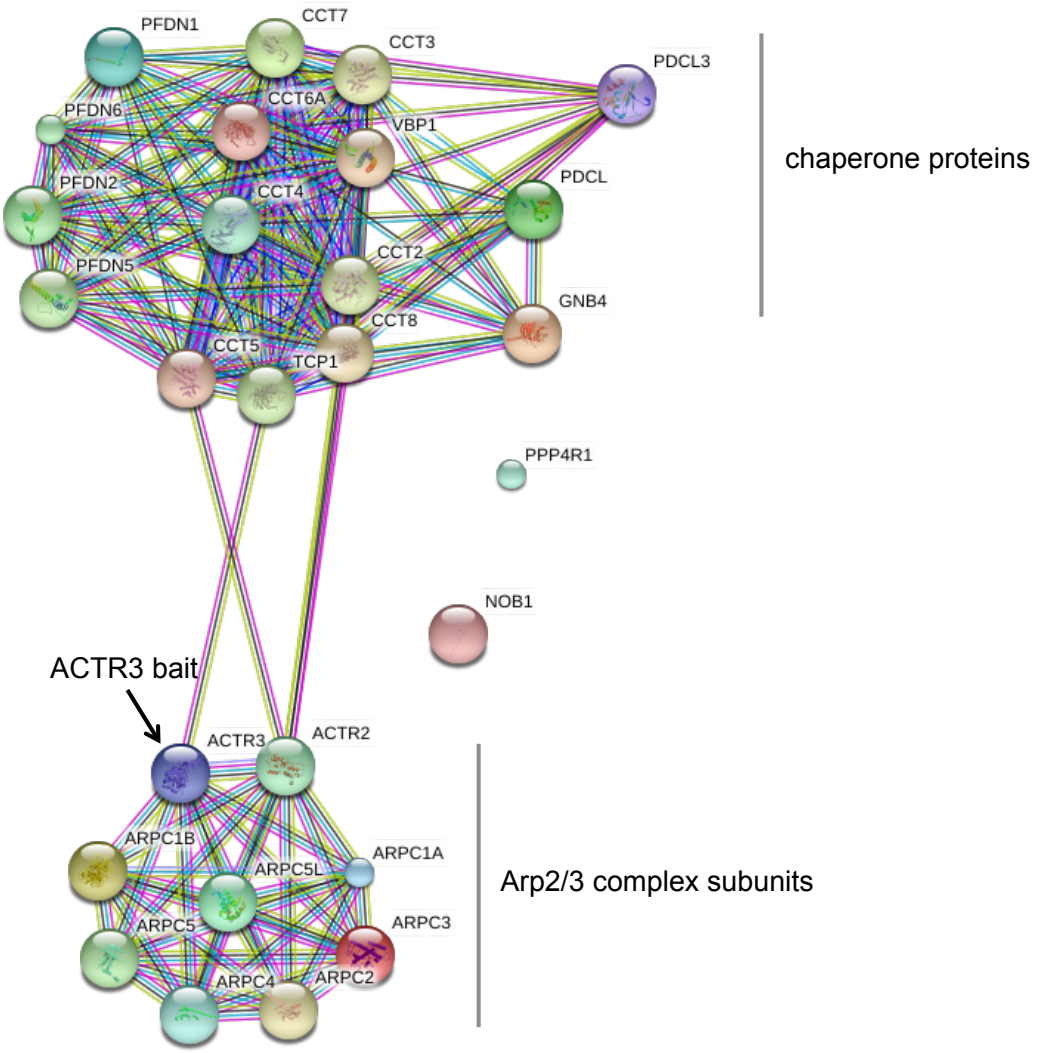

Figure 9-3 BioID string analysis of ACTR3 interactors. Mass spectrometry analysis of endogenous proteins that are in close proximity to ACTR3, determined by mass spectrometry isolated with streptavidin-coupled magnetic beads. The majority of hits were chaperone proteins, and the entire Arp2/3 complex. Lines between proteins represent known interactions (determined via curated databases or experimentally) and predicted interactions (determined via gene fusions, gene neighbourhoods and gene co-occurrence). Small nodes represent proteins of unknown 3D structure and large nodes represent proteins with some known 3D structure. All candidates displayed have a SAINT score > 0.75 and STRING analysis was performed at the high confidence interval.

Table 9-2 Arp3 interactors identified by BioID, Avg(P) score and function. Avg(P) represents the probability of a true interaction between the two proteins, prey and bait. Preys with an Avg(P) >0.85 are conserved and considered as good potential interactors. The other prey is discarded, as they are likely the result of non-specific interactions.

Protein	Avg(P) Score	Function
CCT1-8	1	Molecular chaperones, assists in folding of proteins upon ATP hydrolysis. Plays a role in the folding of actin and tubulin.
PDCL3	0.81	Modulator of G-proteins.
GNB4	0.87	Integrates signals between receptors and effector proteins.
PFDN1	1	Part of a molecular chaperone complex that binds and stabilises newly synthesised polypeptides, allowing them to fold correctly.
NOB1	0.97	Cofactor required for ribosome assembly, orchestrating modification and cleavage of the transcript.
PPP4R1	0.97	Regulator of PP4, a critical regulator of tumour-necrosis factor (TNF).

BioID with Diaph1 and Diaph1ΔDAD led to very different results between the two forms. There were only three interactors found for full length Diaph1 (Figure 9-4) compared to 71 interactors identified for the ΔDAD mutant (Figure 9-5). From the results, it seems that the Diaph1 protein interacts with fewer preys due to being in its auto-inhibited closed conformation. As expected, this doesn't appear to be the case for the mutant form, which lacks the ability to auto-inhibit.

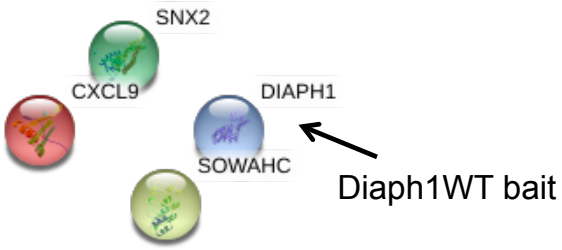

Figure 9-4 BioID string analysis of Diaph1WT interactors. Mass spectrometry analysis of endogenous proteins that are in close proximity to Diaph1WT, determined by mass spectrometry isolated with streptavidin-coupled magnetic beads. Proteins identified have no known interaction network with Diaph1WT. All candidates displayed have a SAINT score > 0.75 and STRING analysis was performed at the high confidence interval.

Table 9-3 Diaph1WT interactors identified by BioID, Avg(P) score and function. Avg(P) represents the probability of a true interaction between the two proteins, prey and bait. Preys with an Avg(P) >0.85 are conserved and considered as good potential interactors. The other prey is discarded, as they are likely the result of non-specific interactions.

Protein	Avg(P) Score	Function
SNX2	0.97	Component of a complex with a role in protein sorting in the endocytic pathway.
CXCL9	0.95	Antimicrobial gene involved in T cell trafficking.
SOWAHC	1	Protein coding gene.

The ΔDAD mutant, in particular, identified a number of proteins known to interact with the cell membrane (EFR3A, KIRREL) and involved in Cdc42-mediated reorganisation of the cortex (BAIAP2). BAIAP2, also known as IRSp53, has been shown to directly interact with Diaph1 and WAVE2 (Goh et al. 2012; Fujiwara et al. 2000), and further acts to regulate actin dynamics through signalling via the

protruding membrane and underlying actin cytoskeleton (Disanza et al. 2006). FERMT2, also known as mig-2, kindlin-2, pleckstrin domain protein-2, was another top ΔDAD mutant interactor. FERMT2 shares close amino acid homology with proteins shown to initiate Rac signalling and actin filament reorganisation. Previous research showed that loss of FERMT2 resulted in a defect in the cellular control of shape change and cytoskeletal organisation (Tu et al. 2003). Another interesting hit was PHACTR4, a well-studied group of proteins that bind actin and protein phosphatase 1 (Allen et al. 2004). PHACTR4 is known to regulate the phosphatase activity of PP1 under the control of actin (Huet et al. 2013) by eliciting mechanistically different responses to maintain cellular actin balance through cofilin activity. Overall, the proteins identified were interesting, and expanded the inventory of actin-binding proteins for further study.

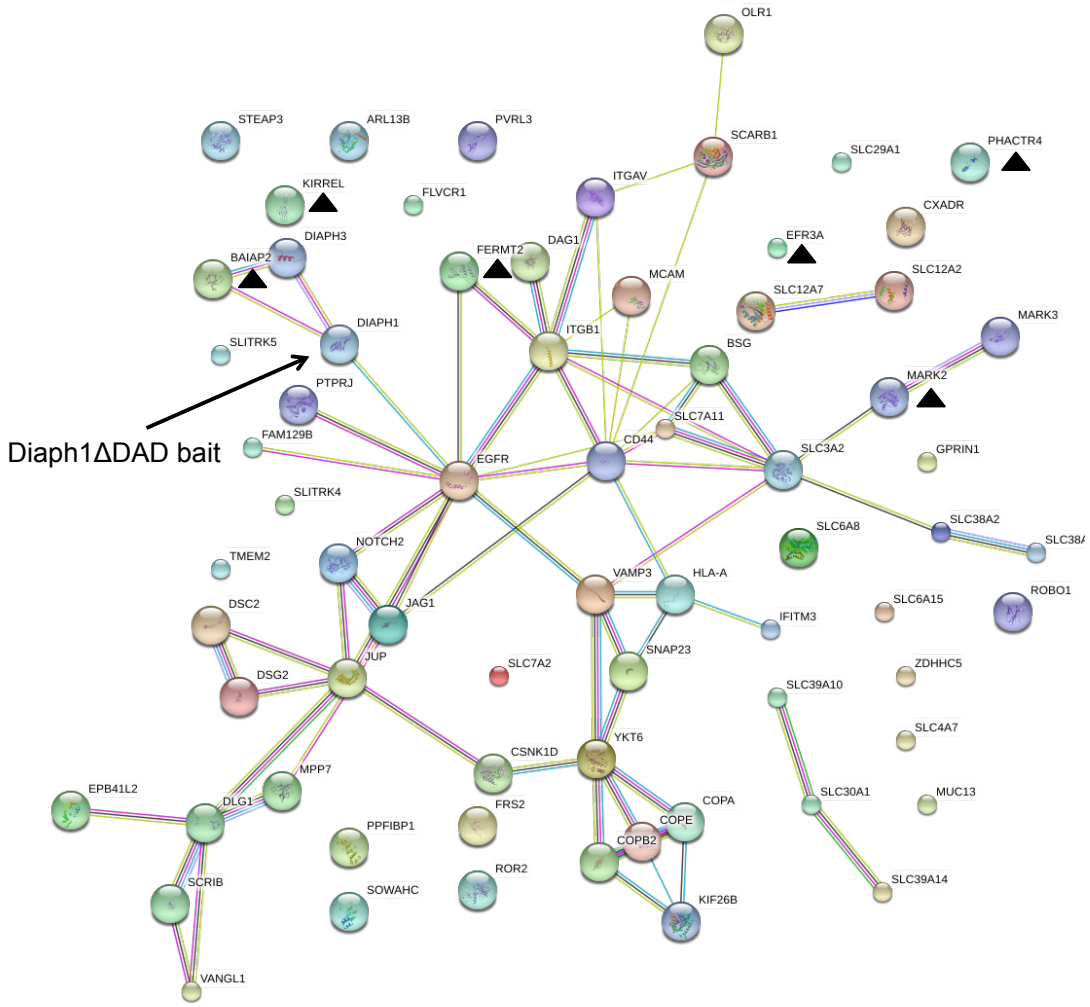

Figure 9-5 BioID string analysis of Diaph1ΔDAD interactors. Mass spectrometry analysis of endogenous proteins that are in close proximity to Diaph1ΔDAD, determined by mass spectrometry isolated with streptavidin-coupled magnetic beads. Lines between proteins represent known interactions (determined via curated databases or experimentally) and predicted interactions (determined via gene fusions, gene neighbourhoods and gene co-occurrence). Small nodes represent proteins of unknown 3D structure and large nodes represent proteins with some known 3D structure. Arrowheads point to proteins selected for further study as potential NPFs. All candidates displayed have a SAINT score > 0.75 and STRING analysis was performed at the high confidence interval.

Table 9-4 Diaph1ΔDAD interactors identified by BioID, Avg(P) score and function. Avg(P) represents the probability of a true interaction between the two proteins, prey and bait. Preys with an Avg(P) >0.85 are conserved and considered as good potential interactors. The other prey is discarded, as they are likely the result of non-specific interactions.

Protein	Avg(P) Score	Function
KIRREL	0.99	Significant role in the development and function of the glomerular permeability.
BAIAP2	0.97	Involved in signal transduction pathways that link deformation of the plasma membrane and remodelling of the actin cytoskeleton.
PVRL3	1	Involved in the formation of cell-cell junctions, including adherens junctions and synapses.
MARK2	0.94	Important regulator of cell polarity in neuronal cells, and also controls the stability of microtubules through phosphorylation.
IFITM3	0.84	Inhibits the entry of viruses to the host cell cytoplasm by preventing viral fusion with cholesterol-depleted endosomes.
PHACTR4	1	Required for neural tube and optic fissure closure, and enteric neural crest cell (ENCCs) migration during development.
ITGAV	1	Receptors for vitronectin, cytotactin, fibronectin, fibrinogen, laminin, osteomodulin, prothrombin, thrombospondin and vWF.
ROBO1	1	Member of the immunoglobulin gene superfamily and encodes an integral membrane protein that functions in axon guidance and neuronal precursor cell migration.
NOTCH2	1	Evolutionarily conserved intercellular signalling pathway, which regulates interactions between physically adjacent cells.
SOWAHC	1	Protein coding gene.
FERMT2	1	Scaffolding protein that enhances integrin activation.
JAG1	0.87	Involved in cell-fate decisions during hematopoiesis. Involved in early and late stages of mammalian cardiovascular development.

The main motivation for carrying out BioID with Diaph1 and Arp2/3 was to explore a new unbiased proximity-labelling method to find interactors of the Arp2/3 complex and Diaph1 and identify potential new NPFs. Through my research, two regulators IQGAP1 and NCKIPSD reported to interact with both Arp2/3 and Diaph1, have displayed phenotypes similar to Diaph1 depletion in a number of different experiments. Thus, I expected IQGAP1 and/or NCKIPSD to be detected in the BioID results. Surprisingly, neither IQGAP1 nor NCKIPSD were detected in the three BioID repeats. However, it is important to remember that there are many limitations to BioID. Generally, BioID is an applicable method to screen for both interacting and neighbouring proteins in their native cellular environment. However, the efficacy of BioID is contingent upon the ability to biotinylate neighbouring proteins, which is in turn dependent on the number and availability of primary amines in these proteins as well as the abundance of the proteins themselves. Consequently, the level of biotynalisation of a protein is not a direct indicator of the strength or frequency of an association. Similarly, the absence of biotinylation does not rule out interaction or proximity (Roux et al. 2012). Furthermore, it is possible that an interacting protein may be associated with the target in low concentrations, hence may be overlooked by mass spectrometry given the breadth of potential candidates (this is called a false negative). Most importantly, BioID-mediated biotinylation cannot be used to validate an actual protein interaction, but instead should be used as a screen to identify candidates that can be subsequently investigated systematically or in a hypothesis-based manner. Another methodical issue to consider is that the protein is probed over the whole cell for 24 hours. Thus, if the protein is only relevant in one part of the cell and one part of the cell cycle, it will likely be less biotynalated than a protein necessary throughout the cell cycle. Given the mechanism of BioID, biotinylated proteins can be placed into three categories; (i) direct interactions, either transient or stable, (ii) indirect interactions, or (iii) vicinal proteins that do not interact directly or indirectly.

A further goal is to explore the importance of the identified proteins in a given stage of mitosis. This could be done by synchronising cells with a drug that block cells at a given stage for several hours, before adding biotin for two hours, then collecting cells to identify interacting proteins during this specific cell cycle stage. It would be

interesting to see if known cell-cycle regulating proteins would be recognised, and to see if new proteins are revealed.

9.3 Depletion of BioID NPF candidates, BAIAP2 and MARK2, increase total cell death

To study the role of proteins identified in the Diaph1ΔDAD BioID, I assessed their impact of depletion on cell cycle progression in HeLa cells. In previous work, Diaph1 depletion led to a significant increase in cell death during the cell cycle (Bovellan et al. 2014). Due to time limitations, I was able to generate only two stable knockdown shRNA lines in HeLa cells: MARK2 and BAIAP2 (Figure 9-6). These proteins were chosen as they presented a high abundance in the BioID screen for interacting with Diaph1ΔDAD and there is evidence in the literature to suggest that they interact with actin nucleators.

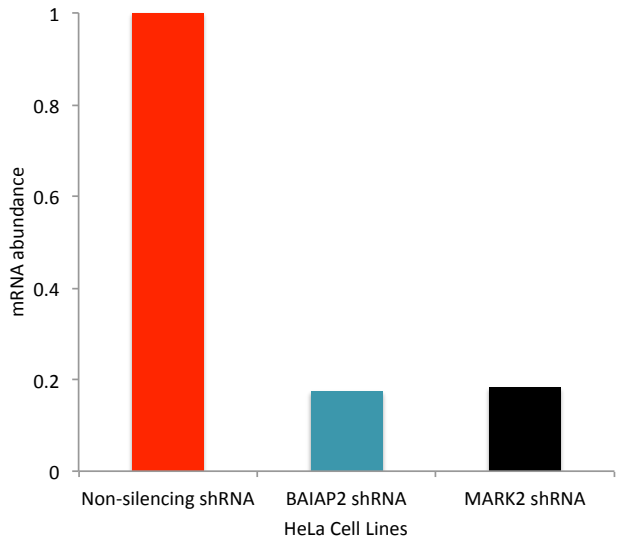

Figure 9-6 Validation of protein depletion in HeLa cells. mRNA transcript abundance of BAIAP2 and MARK2 shRNA using qPCR; this revealed high depletion in BAIAP2 (83% knockdown) and MARK2 (82% knockdown) in stable knockdown HeLa cell lines.

The SH3 domain of BAIAP2, also known as IRSp53, has been reported to directly bind to Diaph1 via its FH1 domain (Fujiwara et al. 2000). It has been suggested that BAIAP2 may be a downstream effector of Diaph1, mediating part of the RhoA-Diaph1 signalling pathway, implicated in stress fiber formation and cytokinesis

(Watanabe et al. 1999). Other studies show that BAIAP2 interacts with Eps8, an actin capper that is capable of regulating actin-based motility (Disanza et al. 2004), triggering a specific pathway required for the expression of cyclin D1, an important cell cycle driver during interphase (Liu et al. 2010). Moreover, BAIAP2 knockdown reduced cyclin D1 expression and resulted in the impediment of G_1-phase cell cycle progression. Previous studies have associated MARK2 with changes in aspects of cell polarity (Cohen & Müsch 2003), an important feature of eukaryotic cells in particular during the final stage of cell division (Hehnly & Doxsey 2012).

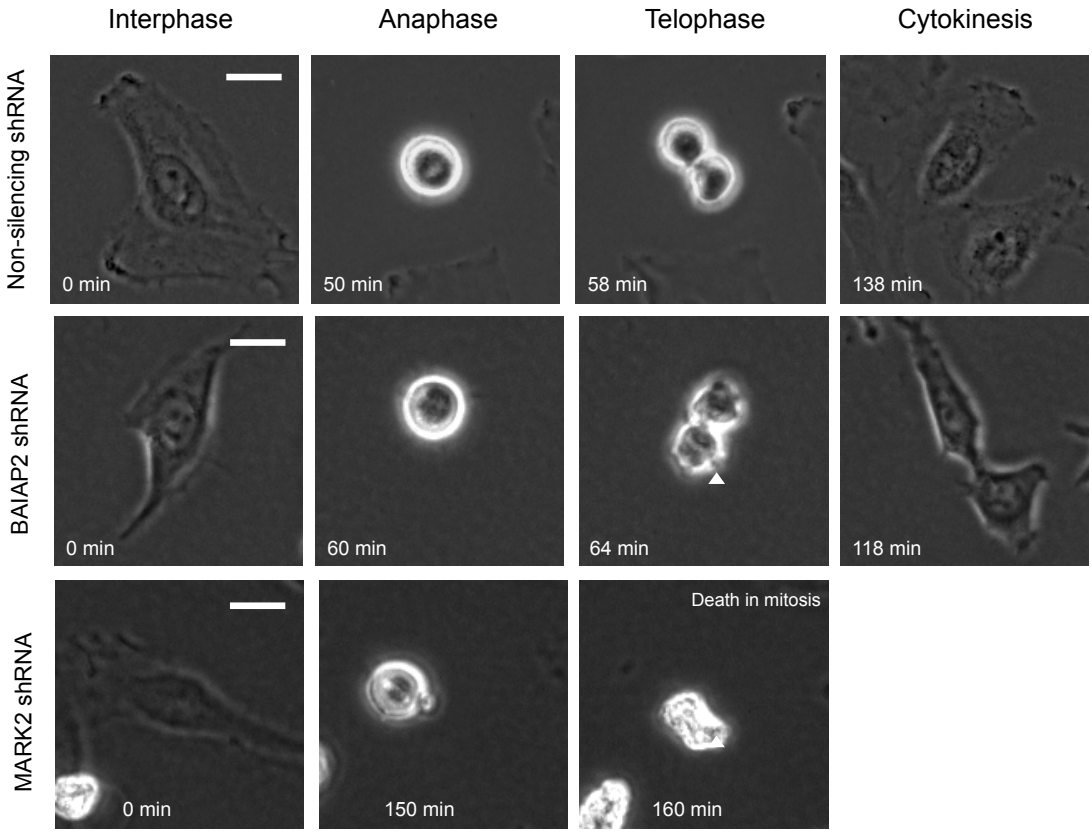

Figure 9-7 Live cell imaging of silenced HeLa cells using phase contrast microscopy. Control cells progress through the cell cycle as normal, abandoning the flat morphology of interphase, then advance through the stages of mitosis before cell cleavage and abscission where the daughter cells separate. BAIAP2 shRNA (see Vid11, USB) cells appear less spread in interphase with the presentation of large blebs during mitosis (arrowhead). MARK2 shRNA (see Vid12, USB) cells were very blebby during mitosis, with many cells dying at this stage.

Individual shRNA depletion of BAIAP2 and MARK2 had a significant effect on normal progression through cytokinesis (Figure 9-7, Figure 9-8, see Vid11/Vid12). Cells devoid of BAIAP2 demonstrated a similar proportion of total cell death (50%) in comparison to Diaph1 siRNA (58%). MARK2 depleted cells also failed to progress through the cell cycle as normal with 35% of cells failing to complete cytokinesis, a significant increase compared to NS shRNA but less significant than BAIAP2 depletion. These results suggest that BAIAP2 and MARK2 have an important role to play in the normal progression of the cell cycle in HeLa cells. Cells of both depletions displayed large blebs during telophase (Figure 9-7), with many failing before cytokinesis.

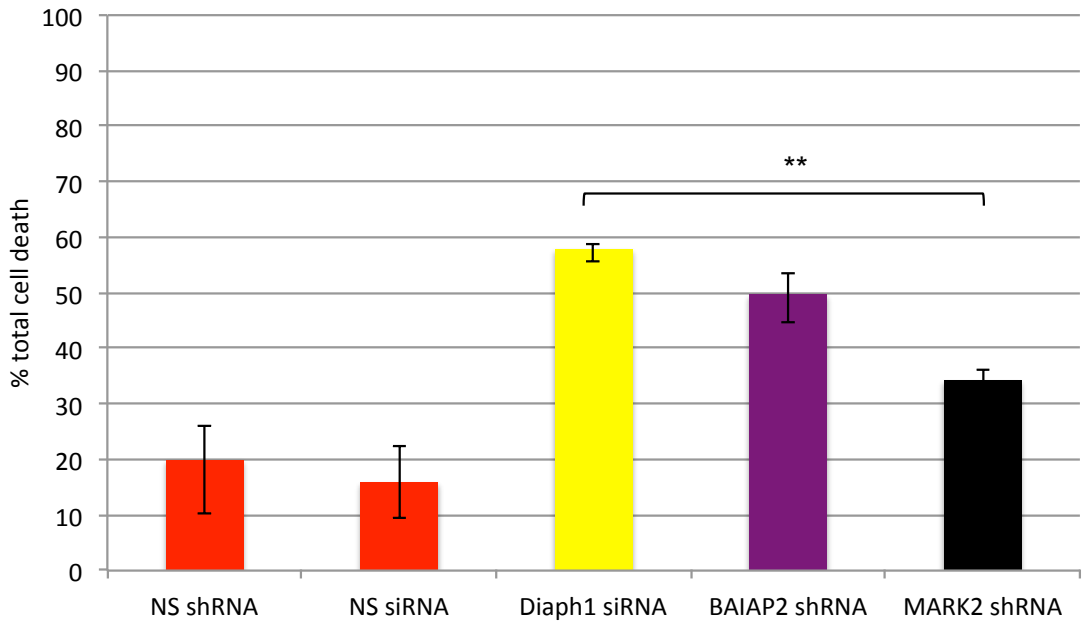

Figure 9-8 Actin-binding protein depletion affects progression through the cell cycle. When compared to cells transfected with non-silencing shRNA/siRNA, cells depleted in Diaph1, BAIAP2 or MARK2 showed significantly increased rates of cell death (**$p<0.01$). When compared to Diaph1 depletion, BAIAP2 depleted cells were not significantly different in proportion of total cell death ($p=0.07$), however, MARK2 depleted cells were significantly different in number of cells able to progress successfully through the cell cycle (**$p<0.01$). Results were gathered from 3 independent experiments examining: non-silencing shRNA (n=936 cells), non-silencing siRNA (n=178 cells), Diaph1 siRNA (n=200 cells), BAIAP2 shRNA

(n=348 cells), and MARK2 shRNA (n=300 cells). Data was analysed with a chi-squared test.

For further analysis, I classified my data according to the exact cell cycle stage that depleted cells were unable to progress beyond. In control conditions (NS shRNA/siRNA), the majority of cells that failed to progress through the cell cycle died during mitosis (Figure 9-9). Approximately 80% of cells that died were able to pass through interphase but not through mitosis. Interestingly, the majority of Diaph1 depleted cells 'snap' into death from their spread interphase state, whilst other cells bleb profusely before death.

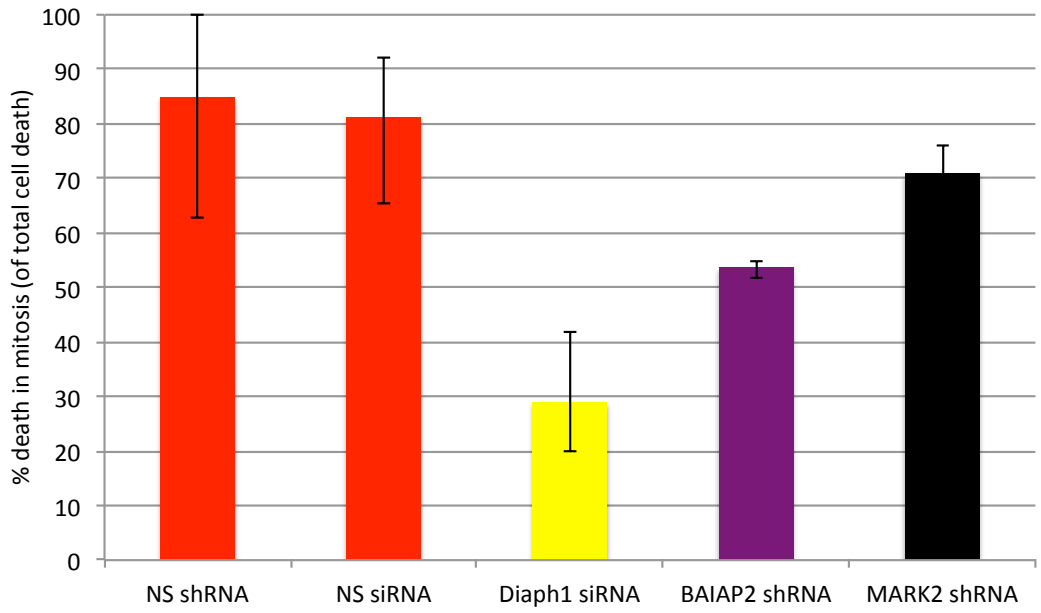

Figure 9-9 Actin-binding protein depletion affects progression through the cell cycle and interrupts it at different stages. Distribution of cell deaths as a function of cell cycle stage. Cells depleted of BAIAP2 show an almost equal death in mitosis as interphase, whilst cells depleted in MARK2 show a significant skew towards cells dying in mitosis compared to interphase. Results were gathered from 4 independent experiments examining: non-silencing shRNA (n=936 cells), non-silencing siRNA (n=178 cells), ACTR2 shRNA (n=611 cells), Diaph1 siRNA (n=200 cells), BAIAP2 shRNA (n=348 cells), MARK2 shRNA (n=300 cells).

BAIAP2 depleted cells presented an almost equal percentage of cells that died in mitosis as in interphase. Of those that died in mitosis, a high proportion (75%) of

cells failed at prophase, whilst the rest failed at metaphase (25%). On the other hand, the majority of MARK2 depleted cells died in mitosis (70%). Interestingly, there was a difference in the exact mitotic stage at which death occurred in MARK2 depleted cells: 65% failed at prophase, 25% failed at metaphase, 1% failed at metaphase, 5% failed at telophase and the rest died after cytokinesis but before spreading. In both knockdowns, most cells that died during mitosis failed to progress past prophase, suggesting there may be an important checkpoint that MARK2 and BAIAP2 participate in during normal cell cycle progression.

The reported interaction between BAIAP2 and Diaph1 could explain the similar pattern of cell death observed in the long-term depletion experiments. Overall, the literature suggests that BAIAP2 is an important protein required for actin-myosin dependent processes, including mitosis, cytokinesis and cytoskeletal reorganisation. Thus, the increased failure to progress through the cell cycle in HeLa cells is somewhat understandable. Unpublished data has also shown that BAIAP2 is upregulated 2-fold during the M-phase, further supporting its role in maintaining the cell cycle. Although not much is known about MARK2 and its direct role in actin nucleation or cytokinesis, it could be a component of the orderly establishment of cell polarity (Ducharme et al. 2006). This role may explain why my results show an increase in cell death with MARK2 protein depletion.

9.4 Conclusion

BioID is an alternative to more established protein-protein interaction assays such as affinity purification. Although extremely useful, such conventional techniques carry significant barriers that can result in erroneous and incomplete datasets (Roux et al. 2012). These limitations include the loss of protein due to protein insolubility or the lack of studying an interaction in its proper cellular environment. To help identify interacting proteins of Diaph1 and/or Arp2/3, I carried out BioID. BioID labels proteins within living cells, and has thus proved effective when applied to insoluble proteins (Mehus et al. 2016; Firat-Karalar & Stearnsx 2015; D. I. Kim et al. 2014).

Although in my BioID experiment, the expected IQGAP1-Diaph1 interaction was not observed as it narrowly missed significance, there have been recent

improvements to the BioID methods, centred on BioID2, a substantially smaller promiscuous biotin ligase. BioID2 enables more-selective targeting of fusion proteins, requires less biotin supplementation, and exhibits enhanced labelling of proximate proteins (Kim et al. 2016). BioID2 also improves localisation of its fusion protein, and even permits the modification of biotinylation range through a flexible linker. Possibly, with this new improved BioID2 system, the IQGAP1-Diaph1 interaction will be revealed.

A few new and promising candidate proteins NPFs that were highly abundant close to the Diaph1 mutant were identified: PHACTR4, MARK2, KIRREL3, BAIAP2 and FERMT2. Both MARK2 and BAIAP2 depletion interrupted the normal cell cycle progression. Interestingly, the crystal structure of BAIAP2 reveals a helical coiled-coil domain, shown to possess actin filament bundling ability (Millard et al. 2005). It is also thought to have a further role in binding to WAVE2 through its SH3 domain (Liu et al. 2010). Taken together, these findings suggest that the BAIAP2-Diaph1 system plays an important role in cytokinesis through mediating crosstalk between the formin cortical actin and the Arp2/3-nucleated cortical actin; however further study will be required to certify the interaction and localisation in the cortex. It will be necessary to repeat these experiments with siRNA depletion to validate the results, and to carry out some combination depletion experiments to see if the effect could be potentiated. Given more time, it would also be interesting to study the cortical architecture of M2 cells depleted of these BioID hits to determine if they lie upstream or downstream of Diaph1.

Chapter 10 Discussion

Malti B. Vaghela, a PhD student from my group, carried out all actin accumulation and myosin localisation experiments discussed in this chapter using cell lines that I generated and validated using Western blotting and qPCR.

10.1 Outline

Cells need to change their mechanical properties and cortical organisation to change shape during the cell cycle and for migration. Recent work has shown that as cells enter mitosis their cortical tension increases (Chugh et al. 2017). Concomitantly, their cortical thickness decreases. Computational simulations have indicated that this surprising result may stem from overall changes in cortical actin filament lengths between interphase and metaphase. These models further indicate that tension shows an optimum for a given filament length and that any variation from this leads to a decrease in tension. In support of this interpretation, proteins involved in actin filament nucleation and turnover either increased or decreased cortical thickness but all gave rise to a decrease in cortical tension (Chugh et al. 2017) This suggests that controlling cortical actin filament length may represent an efficient way for cells to change their cortical tension for mitosis or migration. One way in which cells could regulate the length of filaments within the cortex is through control of the activity of actin nucleators in the cortex. Recent work has identified two main nucleators within the cortex: the Arp2/3 complex and the formin Diaph1 (Bovellan et al. 2014). Furthermore, depletion of Diaph1 led to a thinner actin cortex and a lower cortical tension (Chuch et al., 2017). Previous work examining the regulation of the activity of Diaph1 and the Arp2/3 complex has shown that it is controlled by RhoGTPases either directly or indirectly (Watanabe et al. 1997; Jaffe & Hall 2005; Symons 1996; Aoki et al. 2016; Tominaga et al. 2000). Nucleation promotion factors (NPFs) are required for the proper spatial and temporal control of actin assembly in cells (Duleh & Welch 2010). It is thought that RhoGTPase-dependent activation is transient and other factors are involved in activating and stabilising the active conformation (Seth et al. 2006); and may play a crucial role in ensuring a long-lasting nucleation.

Proteomic analysis revealed the presence of several NPFs in the actin cortex of blebs: Flightless-I, NCKIPSD, IQGAP1 (Biro et al. 2013) and WAVE complex subunits (Nap1 and Sra1) (Bovellan et al. 2014). I conducted a literature search to investigate their known roles in modulating actin nucleation via either Arp2/3 or Diaph1 (Figure 10-1). Once activated by Rac1, the WAVE complex is known to nucleate actin filaments via the Arp2/3 complex (Campellone & Welch 2010). IQGAP1 has been reported to interact with N-WASp/WAVE (Le Clainche et al. 2007). IQGAP1 has also been shown to interact with the formin Diaph1 (Brandt et al. 2007) to prevent inactivation of its interactor, stabilising its nucleation activity. NCKIPSD has been reported to interact with both diaphanous-related formins as a negative regulator (Eisenmann et al. 2007) and the Arp2/3 complex as an activator (Wagner et al. 2013). Flightless-I is thought to interact with formins to prevent autoinhibition following activation by RhoA (Higashi et al. 2010). Thus, these NPFs all appeared to be promising candidates for controlling and coordinating the activity of cortical actin nucleators and may therefore play a role in controlling the length and organisation of actin filament networks as well as cortical tension.

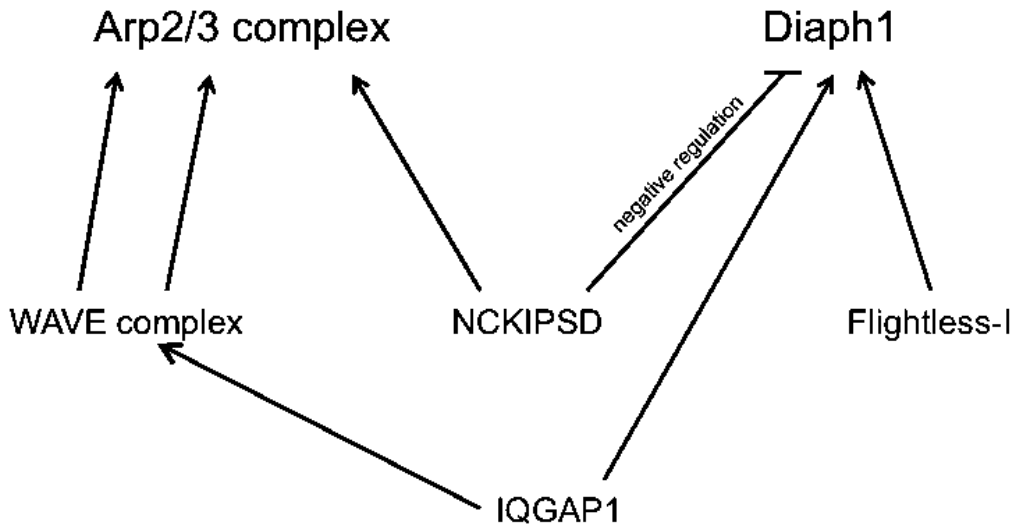

Figure 10-1 Schematic of potential interactions between NPFs and cortical nucleators. Based on the literature, the following interactions are grouped into those that activate nucleation via the Arp2/3 complex, and those that activate nucleation via Diaph1. There is evidence for NCKIPSD and IQGAP1 interacting with both

Arp2/3 and Diaph1, although the interaction between NCKIPSD and Diaph1 is thought to be inhibitory.

The goal of my thesis was to understand how NPFs function in modifying cortex organisation, dynamics and mechanical properties. Based on previous work, it was possible to interrogate the possible pathway that an NPF works through, by comparing its depletion to the depletion of Arp2/3 or Diaph1. In this thesis, both M2 and HeLa cells were used. M2 melanoma blebbing cells provide a snapshot into the cortex life cycle whilst cervical cancer HeLa cells present a well-defined cortex during mitosis and are an accepted model for cell division studies.

First, the localisation of the NPFs was determined in M2 and HeLa cells using immunostaining and live imaging of full-length GFP-tagged constructs. I confirmed that NPFs localised to the cell cortex. Then, to assess the involvement of each NPF in generation of cortical actin, the size distribution of blebs generated by stable M2 lines depleted of each NPF was determined. Previous work has shown that changes in bleb size reflect changes in the rate of cortical actin regrowth under the bleb membrane with increases in growth rate associated with small blebs and decreases associated with large blebs (Bovellan et al. 2014). Arp2/3 subunit depletions result in small blebs and fast regrowth, whereas Diaph1 depletion resulted in large blebs and slow regrowth. To link cellular scale observations to molecular level mechanisms, I then examined how NPFs controlled cortical organisation under the membrane of M2 cell blebs and in HeLa cell cortex using scanning electron microscopy. Previous work showed that depletion of Diaph1 led to large gaps within the cortex, while Arp2/3 depletion led to apparently longer filaments but no clear change in actin filament density (Bovellan et al. 2014).

To examine the role of NPFs in actin polymerisation activity, Malti Vaghela used a regrowth assay where blebs were artificially triggered by ablating the cortex or a HeLa cell arrested in metaphase. F-actin regrowth was imaged under the bleb membrane and the actin regrowth rate was determined (Figure 10-2).

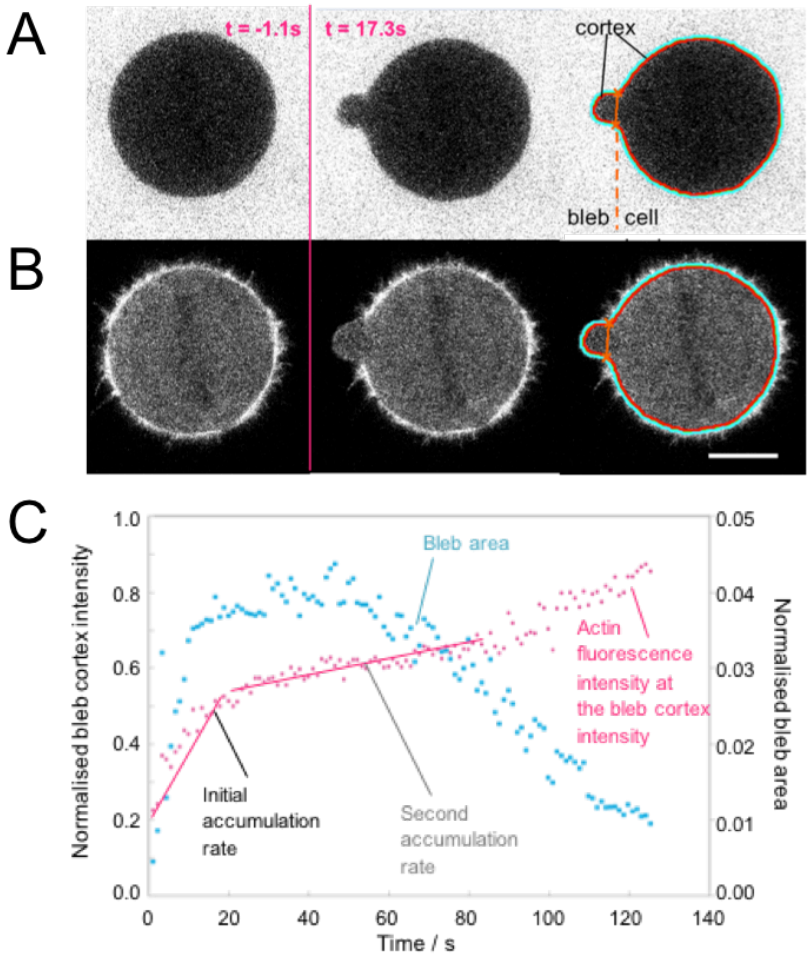

Figure 10-2 Laser ablation methods and analysis. A, Cortex regrowth in a bleb induced in a rounded HeLa cell. Scale bar: 10µm. Ablation at t = 0s. Addition of Alexa Fluor 568 allows for reliable cell body-bleb segmentation. **B,** HeLa cells stably express actin-GFP. Turquoise line: outer cortex boundary; red line: inner cortex-cytosol boundary; orange line: bleb neck. **C,** Temporal evolution of the mean fluorescence intensity of cortical actin (marked with actin-GFP) at the bleb cortex, normalised to the mean cortical fluorescence intensities in the cell body (pink), and temporal evolution of the bleb size, normalised to the cell body (blue).

After having confirmed the impact of NPF depletion on actin regrowth dynamics, I next assessed the impact of NPF depletion on cell cycle progression in HeLa cells. In previous work it was shown that Diaph1 depletion led to a significant increase in cell death during the cell cycle, whereas Arp2/3 depletion did not (Bovellan et al. 2014). Combination of Arp2/3 depletion and Diaph1 depletion led to an increase in cell death compared to Diaph1 alone. Lastly, Malti Vaghela also examined the

enrichment of cellular phosphomyosin (pMLC) in NPF or nucleator depleted cells. The aim of this experiment was to further understand if the changes in cortical mechanics induced by NPF depletion was a result of myosin delocalisation away from the cortex. It was hypothesises that this change in mechanics could come from changes in thickness of the cortex or changes in myosin recruitment, as formins make filaments that are better substrates for myosin contractility.

The approaches detailed above allowed us to examine how Flightless-I, IQGAP1, NCKIPSD and the WAVE complex regulate actin filament nucleation in the cortex via Diaph1 or Arp2/3, or both. Aside from the WAVE complex, the other NPFs are not well characterised in their interactions with Arp2/3 or Diaph1 to promote (or inhibit) actin nucleation in the cortex. Considering the importance of the actin cortex during processes involving shape change such as cytokinesis, cell locomotion and tissue morphogenesis, further study of the control of cortical nucleators is warranted.

10.2 How is the activity of Diaph1 regulated by NPFs?

In its autoinhibitory 'resting' state, Diaph1 does not possess actin-nucleating activity, requiring activation by Rho GTPases. However, it is thought that RhoGTPase-dependent activation is transient and other factors are involved in activating and stabilising the active conformation (Seth et al. 2006). Interactions with NPFs such as Flightless-I (Higashi et al. 2010), IQGAP1 (Brandt et al. 2007), and/or recruitment by the Abelson interactor 142 (Abl1, a component of the WAVE complex) have been suggested as possibly working together with Rho to activate Diaph1 and maintain it active by stabilising the relieved open conformation of Diaph1. RhoGTPases are far outnumbered by their substrates, thus NPFs may play a crucial role in ensuring a long-lasting nucleation activity. NCKIPSD has been shown to negatively regulate formins suggesting a novel role for the control of actin dynamics by NCKIPSD (Eisenmann et al. 2007).

Fli-I depletion did not appear to change bleb size in M2 cells or change progression through the cell cycle in HeLa cells, as hypothesised based on its proposed interaction with Diaph1 (Higashi et al. 2010). It is well known that actin nucleators such as the formin family have multiple binding partners that result in their

activation. Thus, it is possible that Fli-I has a biologically redundant role in the cortex, and its depletion is overcome by the interaction of other activating proteins to enable normal activity of Diaph1. Fli-I may also act at a specific stage of the cell cycle (e.g. in cell division) such that the appearance of blebs in interphase cells as a reporter is not a sufficient to indicate its function. Based on these experimental results, I decided not to pursue study of Fli-I further.

In blebbing assays, I found that IQGAP1 depletion and NCKIPSD depletion both had phenotypes associated with large blebs, suggesting that they primarily affect Diaph1 activity. Large blebs could either be due to slow regrowth or due to an increase in contractility. Arp2/3 depletion gives rise to a small bleb phenotype and an increase in contractility (unpublished research by Malti Vaghela), indicating that changes in bleb size correlate with slower cortical actin regrowth rate rather than a change in contractility. Malti Vaghela carried out a regrowth assay where bleb formation was induced in a controlled manner by laser ablation of the cortex in HeLa cells. The assay follows progression of bleb growth, arrest, and retraction and linescans are acquired around the bleb periphery from the first sign of cortex regrowth. In control conditions, the actin accumulation rate reports on the average of the accumulation rates of all participating nucleators. Thus, if a slower-than-average nucleator is depleted, accumulation rate will increase, and conversely, if a faster-than-average nucleator is depleted, assembly speed will decrease. IQGAP1 depletion led to a significant decrease in actin accumulation rate, consistent with its potential role in keeping Diaph1 active (Figure 10-3). NCKIPSD depletion also led to a significant decrease in actin regrowth rate, consistent with the large bleb phenotype and a potential role as an activator of Diaph1 rather than an inhibitor as suggested by a previous study (Eisenmann, 2007) (Figure 10-3).

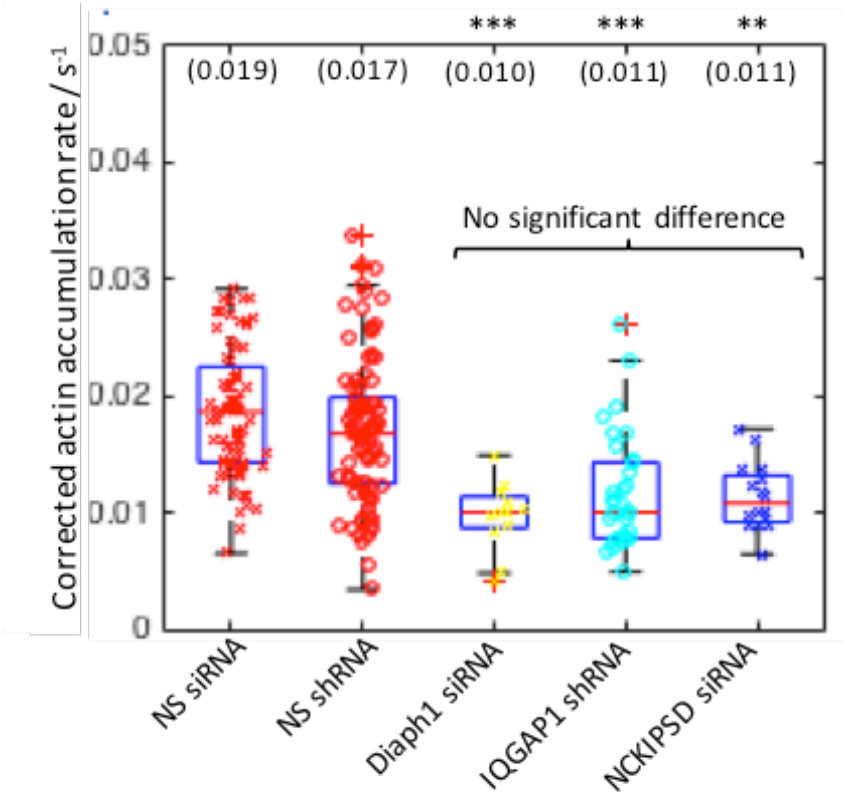

Figure 10-3 Actin accumulation rates of NPFs thought to interact with Diaph1. Regrowth rates follow bleb size data. Actin accumulation rates corrected for the relative cortical actin between cell lines for cells transfected with non-silencing siRNA, non-silencing shRNA, Diaph1 siRNA, IQGAP1 shRNA and NCKIPSD siRNA (n=76, 86, 11, 32, 16 p=4E-4, 4E-10 and 5E-4), (*p < 0.05, ** p< 0.01 and ***p<0.001).

Consistent with a role in maintaining Diaph1 active suggested by the blebbing phenotype, IQGAP1 depletion led to cortical actin networks with large gaps, although the effect was less pronounced than with Diaph1 depletion. It is possible that Diaph1 retains some nucleating activity without the requirement of further stabilising activity by IQGAP1, suggesting that IQGAP1 is not the only NPF regulating Diaph1 in the cortex. NCKIPSD depletion led to a clear increase in cortical density compared to control cortices. This was surprising because the large bleb phenotype observed in live imaging experiments is consistent with a reduction in Diaph1 activity and thus we would expect to observe cortices with gaps. The tight cortex mesh observed in NCKIPSD depleted cells was also different from what is observed in Arp2/3 knockdowns, suggesting a unique role for NCKIPSD in

modulating cortical actin nucleation. The increase in cortical actin density observed upon depletion suggests that NCKIPSD represses an actin nucleation pathway in addition to activating Diaph1. One potential candidate is the Wave pathway as NCKIPSD and Wave might compete for Arp2/3 complexes. The potential role of NCKIPSD will be discussed further in the following sections.

In previous work, Diaph1 depletion led to a thinning of the actin cortex (Chugh et al. 2017) and an increase in cell death as the cells progressed through the cell cycle (Bovellan et al. 2014). Thus, I examined how depletion of each NPF affected cell cycle progression and actin cortex morphology during cell division. Experiments examining the effects of NPF depletion on cortical thickness are ongoing in collaboration with Dr. Priyamvada Chugh in Prof. Ewa Paluch's lab. IQGAP1 depletion led to a large increase in cell death, similar to Diaph1. This high proportion of cell death was also recorded in cells following NCKIPSD depletion. In both cases, cell death was not as high as observed with Diaph1 depletion. This again supports the role of these NPFs as stabilising the Rho-activated open conformation of Diaph1. The high death rate observed in IQGAP1 depleted cells was able to be completely rescued by the Diaph1 binding region of IQGAP1, indicating that IQGAP1-mediated stabilisation of Diaph1 activity is key during the cell cycle. The combined depletion of Diaph1 and IQGAP1 caused a significant increase in cell death compared to Diaph1 depletion alone. This was similar to what was observed when Diaph1 and Arp2/3 complex were co-depleted, suggesting that IQGAP1 may also play a role in Arp2/3 activation or that Diaph1 activity is completely abrogated. I also found that combined depletion of NCKIPSD and IQGAP1 did not increase overall cell death in HeLa cells compared to IQGAP1 depletion alone, suggesting that they either act in concert or that IQGAP1 is the dominant NPF.

Further work is required to understand the exact role of IQGAP1 and NCKIPSD in modulating Diaph1 activity during cell cycle progression in HeLa cells. In particular, the exact mechanism and stage of the cell cycle in which Diaph1 depletion provokes cell death remains unclear. Depletion of IQGAP1 and NCKIPSD would perturb actin turnover in the cortex, which is necessary to enable cell shape change during rounding, resulting in a possibly unorganised rounded morphology. Alternatively, it

has been shown that formin-nucleated bundled F-actin networks tend to be more conducive to host myosin II contractility as opposed to Arp2/3-mediated branched F-actin (Ramanathan et al. 2015; Michelot & Drubin 2011). Depletion of IQGAP1 or Diaph1 might therefore perturb myosin contractility, resulting in failure of proper cortical contractions. To probe the effect of nucleator inhibition upon contractility, Malti Vaghela carried out immunostaining experiments on SMIFH2 and CK666 treated HeLa cells. Here, the aim was to observe a change of cortical localisation of myosin as a result of the change in nucleation of the actin cortex. In fact, loss of cortical myosin was observed as a result of SMIFH2 treatment, a broad spectrum formin inhibitor (Figure 10-4) and in addition, this led to a decrease in cell stiffness. This change was not observed in CK666 treated cells. This result is interesting as it could help understand the high proportion of cell death seen in Diaph1 or IQGAP1 depleted HeLa cells, as being due to a loss of cortical myosin and concomitant shape change problems. Thus, formin-mediated actin nucleation appears important for cortical myosin recruitment. Further experiments probing myosin localisation in NPF depleted lines with live imaging are ongoing and they may also aid in understanding reasons for the high cell death observed in IQGAP1 and NCKIPSD depleted lines.

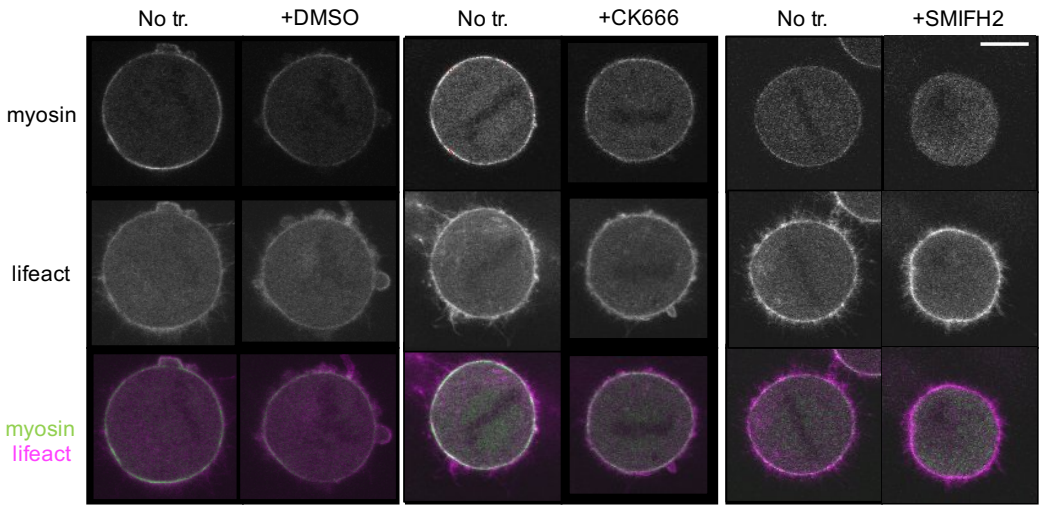

Figure 10-4 Formin inhibition leads to loss of cortical myosin. Live HeLa cells blocked in metaphase with MG132 expressing MRLC-GFP and LifeAct-Ruby imaged before and 1hr after being treated with DMSO (100µM), CK666 (100µM) or SMIFH2 (40µM). The MRCL-GFP (green) and LifeAct-Ruby (purple) for each cell are overlaid in the third row. Scale bar: 10µm.

The role of NCKIPSD remains puzzling. Although it was described as an inhibitor of formins in previous work, our experiments suggest it acts as an activator. Therefore, we have started collaborating with the group of Dr Guillaume Romet-Lemonne in Paris to explore how NCKIPSD affects Diaph1 mediate actin polymerisation at the single filament level. Preliminary data obtained by Dr Yan Cao-Lu suggests that NCKIPSD accelerates nucleation via Diaph1 (correspondence from Yan Cao-Lu). Experiments examining the interplay with Arp2/3 and Diaph1 are ongoing.

Overall, my data strongly supports IQGAP1 as an important class II Diaph1 activator, working to stabilise and maintain its active conformation. NCKIPSD appears to phenocopy Diaph1 in a number of assays, appears to inhibit Diaph1 in combination experiments, and possibly activate Arp2/3 in others, suggesting it may have a role in crosstalk between Diaph1 and Arp2/3, allowing the cell to fine tune its cortex.

10.3 How is the activity of Arp2/3 regulated by NPFs?

NPFs known to interact with the Arp2/3 complex, fall into two classes, depending on their activity. Class I NPFs activate nucleation, whilst class II NPFs maintain activation. The Wave regulatory complex (WRC) is a well-studied class I activator for the Arp2/3 complex (Goley & Welch 2006). I expected the depletion of Wave complex subunits to phenocopy Arp2/3 subunit depletion in blebbing assays and in long term imaging experiments. In my experiments, I focused on the subunits Sra1 and Nap1, as they were detected in the proteomics. Depletion of both subunits gave rise to small blebs, and a cortex with longer filaments, consistent with the phenotypes observed for Arp2/3 depletion. Furthermore, Nap1 depletion significantly increased actin regrowth rate, similar to depletion of ACTR2 (Figure 10-5). Cortical stiffness measurements also carried out by Malti Vaghela with AFM also mirrors bleb size results. Arp2/3 subunit depletion, Nap1 depletion and treatment with CK666 led to an increase in stiffness. Through all of my assays and those used by Malti Vaghela, WAVE complex depletion always phenocopied Arp2/3 depletion indicating that WRC plays a central role in the regulation of Arp2/3 in the cortex.

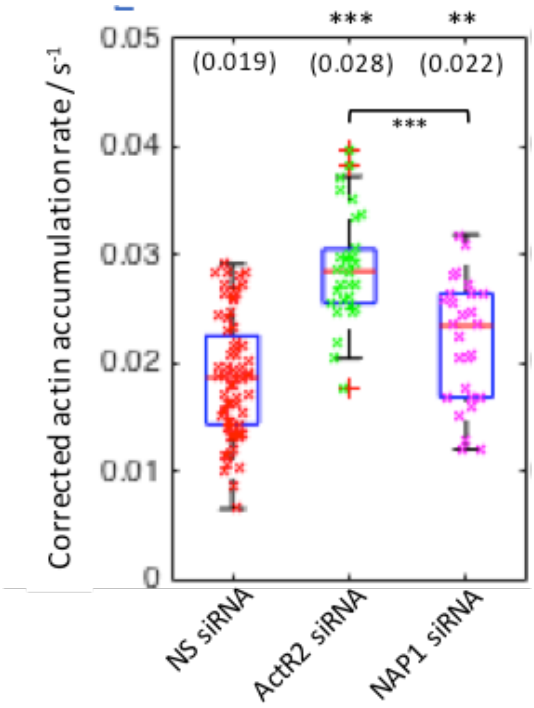

Figure 10-5 Actin accumulation rates of NPFs thought to interact with Diaph1. Regrowth rates follow bleb size data. Actin accumulation rates corrected for the relative cortical actin between cell lines for cells transfected with (e) non-silencing siRNA, ACTR2 siRNA and Nap1 siRNA (n=76, 30, 29, p=2E-13 and 0.008) (* $p < 0.05$, ** $p < 0.01$ and *** $p<0.001$).

Interestingly, my experiments also showed that depletion of ACTR2 and ArpC2 did not affect cell cycle progression to the same extent. Cells depleted of ArpC2 did not have any significant change in cell death, similar to depletion of Nap1/Sra1, whereas cells depleted of ACTR2 had a high incidence of cells failing to progress through the cell cycle. This observation is interesting, as it raises the question of whether different Arp2/3 subunits play different roles in the activity of the complex. Structurally, it has been documented that the ArpC2 and ArpC4 subunits are located at the interface between the Arp2/3 complex and mother filaments during branching (Gournier et al. 2001; Goley et al. 2004). It was previously thought that Arp2/3 actin nucleation required the presence of the mother filament, however recent work has shown that nucleation can occur without the requirement for a mother filament (Wagner et al. 2013). In this case, interfacing with the mother filament may be dispensable, and this may explain why the depletion of the ArpC2 subunit did not reflect any abnormalities in the progression through cell division.

In contrast to ARPC2, ACTR2 is central to the function of the Arp2/3 complex. It is one of the two subunits that template the new filament. ACTR2 must be phosphorylated (by Nck-interacting kinase) for the Arp2/3 complex to be activated by NPFs (Choi et al. 2013). It has been further suggested that the Arp2/3 complex acts as a coincidence detector, requiring both the binding to NPFs and the phosphorylation of ACTR2 for increased activity (LeClaire et al. 2015). Therefore, the depletion of ACTR2 would clearly diminish nucleating activity of the Arp2/3 complex, and thus, this may be one explanation for the observed difference between the impact of ACTR2 and ARPC2 depletion. To test this prediction, a construct mutated for the ACTR2 phosphorylation sites could be generated and expressed into HeLa cells to examine effects of this mutation in cell division. This differential role for different Arp2/3 subunits has recently been reported more in literature (Abella et al. 2015), and is an important aspect of the Arp2/3 complex to consider when studying its activity.

Unlike other Arp2/3 complex activators, it has been reported that NCKIPSD does not bind actin monomers or filaments, and interacts with the complex using a non-WASP-like binding mode (Wagner et al. 2013). In addition, it has been suggested that NCKIPSD-activated Arp2/3 complex creates linear instead of branched actin filament networks. In my experiments and in those of Malti Vaghela, NCKIPSD sometimes phenocopied Arp2/3 depletion, sometimes Diaph1 depletion, and sometimes neither, hinting at a complex role. In particular, in blebbing cells, it led to large blebs, something observed with Diaph1 depletion, but also led to a dense cortex. In the framework I proposed for NCKIPSD's role in coordinating Diaph1 and Arp2/3 nucleation, its depletion would lead to reduction of Diaph1 activity and would lead to less nucleation of unbranched F-actin via Arp2/3, leaving on nucleation of branched actin via WRC mediated Arp2/3 activation. Thus the high density of F-actin present in NCKIPSD depleted cortices might reflect enhanced WRC Arp2/3 nucleation and enhanced branching leading to the tighter actin meshed observed. Finally, as previously mentioned, it appears that IQGAP1 may have a lesser role in regulating nucleation via the Arp2/3 complex, although in our (my own and Malti Vaghela's) experiments, this only appeared when we co-depleted Diaph1 and IQGAP1 in long term imaging assays.

It is possible that WAVE and NCKIPSD may compete for the Arp2/3 complex. It is possible that NCKIPSD generates an actin seed via Arp2/3 nucleation, and then brings a Diaph1 dimer into contact with the newly created barbed end. Here, NCKIPSD regulates nucleation through both Diaph1 and the Arp2/3 complex, rather than predominantly through one nucleator. This may explain the discrepancy in results observed in the different assays.

The role of NCKIPSD remains unclear; further work is required to understand the role of NCKIPSD in controlling actin nucleation in the actin cortex. Confirmation of this data in single filament assays would be worthwhile for continuing this investigation.

Chapter 11 Appendix

11.1 BioID bait cloning sequences

Dr. Geneviève Lavoie carried out cloning of all BirA constructs (sequences below).

>Arp3

NNNNNNNNNNNNNNNNNNNNNNNNNCNANNNNGGGNNNNNGGCCCCGGCGGCGGCGCGCCTGT
ACNNNNNTNTGCGGCCGCAATGGCGGGACGGCTGCCGGCCTGTGTGGTGGACTGTGGCACGGGGTA
TACAAAACTAGGATATGCTGGAAATACAGAACCACAGTTTATCATCCCTTCCTGTATTGCTATTAAG
GAGTCAGCAAAAGTGGGTGATCAAGCTCAAAGGAGGGTGATGAAAGGTGTTGATGACCTAGACTTC
TTCATTGGTGATGAAGCAATAGAAAAACCTACATATGCAACAAAGTGGCCAATCCGCCATGGTATA
GTTGAAGATTGGGACTTAATGGAAAGGTTTATGGAGCAAGTGATCTTTAAATATTTAAGGGCAGAA
CCTGAAGACCATTATTTTCTTTTGACTGAACCTCCATTGAATACTCCAGAAAACAGGGAATATACTG
CTGAAATAATGTTTGAGTCCTTCAATGTTCCAGGCTTGTACATTGCTGTGCAGGCTGTTCTTGCCTTA
GCTGCATCTTGGACCTCAAGACAAGTAGGAGAACGGACGTTGACCGGTACGGTAATAGACNNNGG
AGATGGTGTCACTCATGTCATTCCTGTGGCTGAAGGGTATGTGATTGGCAGCTGTATTAAACACATT
CCAATCGCAGGACGAGATATAACATATTTTATTCAGCAACTGCTGANAGACCGAGAAGTAGGAATC
CCTCCAGAACAATCCTTGGAAACTGCTAAGGCAGTAAAGGANCGCTATAGTTATGTCTGNCCAGAN
TTAGTAAAAGAANTTAACANTATGATACAGATGGGTCAAAATGGATTAAACAGTATACTGGAATCA
ATGCTATCTCNAAGAAAGAGTTTTCTATCNNTGTTNGNNNTGAGAGANTTTTGGGACCTGAANTCTT
TTTCATCCNGNNNTTTGCTAATCCAGANNTTACNCANCNATCTCNNANTTGTANATGAAGNAATTN
NNANTTGTCCNNNGATGTNNNNANGTCNTNNNNNACNANANTNTGNCCTNTCNGGANGNTCANCC
NTGNNCNGGNNTTTNGNANNTC

>Arpc4

NNNNNNNNNNNNNNNGCGGNNCGCGNNNGGGGGGNNCTGGCCCCGGCGGCGGCGCGCCTGTAC
AGATATCTGCGGCCGCAATGACTGCCACTCTCCGCCCCTACCTGAGTGCCGTGCGGGCCACATTGCA
GGCTGCCCTCTGCCTGGAGAACTTCTCCTCCCAGGTTGTGGAACGACACAACAAGCCGGAAGTGGA
AGTCAGGAGTAGCAAAGAGCTCCTGTTACAACCTGTGACCATCAGCAGGAATGAGAAGGAAAAGG
TTCTGATTGAGGGCTCCATCAACTCTGTCCGGGTCAGCATTGCTGTGAAACAGGCTGATGAGATCGA
GAAGATTTTGTGCCACAAGTTCATGCGCTTCATGATGATGCGAGCAGAGAACTTCTTTATCCTTCGA
AGGAAGCCTGTGGAGGGGTATGATATCAGCTTTCTGATCACCAACTTCCACACAGAGCAGATGTAC
AAACACAAGTTGGTGGACTTTGTGATCCACTTCATGGAGGAGATTGACAAGGAGATCAGTGAGATG
AAGCTGTCAGTCAATGCCCGTGCCCGCATTGTGGCTGAAGAGTTCCTTAAGAATTTTTAACTCGAGT
CTAGAGGGCCCGTTTAAACCCGCTGATCAGCCTCGACTGTGCCTTCTAGTTGCCAGCCATCTGTTGT
TTGCCCCTCCCCCGTGCCTTCCTTGACCCTGGAAGGTGCCACTCCCACTGTCCTTTCCTAATAAAATG
AGGAAATTGCATCGCATTGTCTGAGTAGGTGNNNTTCTATTCTGGGGGGGTGNNNNNNNNN

>Diaph1deltaDAD

NNNNNNNNNNNNNNNNNNNNNNNCGCCGNNNNGGGGGNNCTGGCCCCGGCGGCGGCGCGCCTG
TACAGATATCTGCNGNCGCNATGGAGCCGCCCGGCGGGAGCCTGGGGCCCGGCCGCGGGACCCGG
GACAAGAAGAAGGGCCGGAGCCCAGATGAGCTGCCCTCGGCGGGCGGCGACGGCGGCAAATCTAA
GAAATTTCTGGAGAGATTTACCAGCATGAGAATTAAGAAGGAGAAGGAAAAGCCCAATTCTGCTCA
TAGAAATTCTTCTGCATCATATGGGGATGATCCCACAGCACAGTCATTGCAAGATGTTTCAGATGAA
CAAGTGCTGGTTCTCTTTGAACAGATGCTGCTGGATATGAACCTGAATGAGGAGAAACAGCAACCT
TTGAGGGAGAAGGACATCATCATCAAGAGGGAGATGGTGTCCCAATACTTGTACACCTCCAAGGCT
GGCATGAGCCAGAAGGAGAGCTCTAAGTCTGCCATGATGTATATTCAGGAGTTGAGGTCAGGCTTG
CGGGATATGCCTCTGCTCAGCTGCCTGGAGTCCCTTCGTGTGTCTCTCAACAACAACCCTGTCAGTT
GGGTGCAAACATTTGGTGCTGAAGGCTTGGCCTCCTTATTGGACATTCTTAAACGACTTCNTGATGA
GAAAGAAGAGACTGCTGGGAGTTACGATAGCCGGAACAAGCATGAGATCATTCGCTGCTTGAAAG
CTTTTATGAACAACAAGTTTGGAATCNAGACCATGTTGGAGACAGAAGAAAGAATCCTACTGCTGG
TCANAGCCATGGATCCTGCTGTTCCCAACATGATGANTGATGCAGCTAANCTGCTTTCTGCTCTTTG
TATTCTACCGCANCCAGAGGACATGAATGAAAGGGTTTTGGANGNNATGACNGAAANAGCTGANA
NGGATGANTGGANNNTTTCCNGCCGCTGCTGGANNGATTAAAAGNGANCNCTATTGNNNNGNNGN
TGGATGCCTANNGCTGATCAATGCTCTCATCNCNCCNGCGGAGNNCNTGNNNTNCNANNNCNNNNN
NANNNACTGATNCNTTNGGGNTANNNN

>Diaph1WT

GNNNNNNNNNNNNNNNCNNNNNNCNNNNNGNGGGNNCTGGCCCCGGCGGCGGCGCGCCTGTAC
AGATATCTGCGGCCGCAATGGAGCCGCCCGGCGGGAGCCTGGGGCCCGGCCGCGGGACCCGGGAC
AAGAAGAAGGGCCGGAGCCCAGATGAGCTGCCCTCGGCGGGCGGCGACGGCGGCAAATCTAAGAA
ATTTCTGGAGAGATTTACCAGCATGAGAATTAAGAAGGAGAAGGAAAAGCCCAATTCTGCTCATAG
AAATTCTTCTGCATCATATGGGGATGATCCCACAGCACAGTCATTGCAAGATGTTTCAGATGAACAA
GTGCTGGTTCTCTTTGAACAGATGCTGCTGGATATGAACCTGAATGAGGAGAAACAGCAACCTTTG
AGGGAGAAGGACATCATCATCAAGAGGGAGATGGTGTCCCAATACTTGTACACCTCCAAGGCTGGC
ATGAGCCAGAAGGAGAGCTCTAAGTCTGCCATGATGTATATTCAGGAGTTGAGGTCAGGCTTGCGG
GATATGCCTCTGCTCAGCTGCCTGGAGTCCCTTCGTGTGTCTCTCAACAACAACCCTGTCAGTTGGG
TGCAAACATTTGGTGCTGAAGGCTTGGCCTCCTTATTGGACATTCTTAAACGACTTCATGATGAGAA
AGAAGAGACTGCTGGGAGTTACGATAGCCGGAACAAGCATGAGATCATTCGCTGCTTGAAAGCTTT
TATGAACAACAAGTTTGGAATCAAGACCATGTTGGAGACAGAAGAAGGAATCCTACTGCTGGTCAG
AGCCATGGATCCTGCTGTTCCCAACATGATGATTGATGCAGCTAAGCTGCTTTCTGCTCTTTGNATTC
TACCGCAGCCAGAGGACATGAATGAAAGGGTTTTNGNAGGCAATGACAGAAAGAGCTGAGATGGA
TGAAGTGGNACGTTTCCAGCCGCTGCTGGNTGGATTAAAANTGGNNCNNCNNNNGCNCTGNNNNN
NNTGNCTANNNCTGATCNATGCTCNCATCNN

References

Abella, J.V.G. et al., 2015. Isoform diversity in the Arp2/3 complex determines actin filament dynamics. *Nature cell biology*, 18(1), pp.76–86.

Abmayr, S.M. & Pavlath, G.K., 2012. Myoblast fusion: lessons from flies and mice. *Development*, 139(4), pp.641–656.

Adachi, M. et al., 2014. Involvement of IQGAP family proteins in the regulation of mammalian cell cytokinesis. *Genes to Cells*, 19, pp.803–820.

Allen, P.B. et al., 2004. Phactrs 1-4: A family of protein phosphatase 1 and actin regulatory proteins. *Proceedings of the National Academy of Sciences of the United States of America*, 101(18), pp.7187–92.

Ammer, A.G. & Weed, S.A., 2008. Cortactin branches out: Roles in regulating protrusive actin dynamics. *Cell Motility and the Cytoskeleton*, 65(9), pp.687–707.

Aoki, K. et al., 2016. A RhoA and Rnd3 cycle regulates actin reassembly during membrane blebbing. *Proceedings of the National Academy of Sciences of the United States of America*, 113(13), pp.E1863-71.

Baggett, A. et al., 2012. Structural characterization and computer-aided optimization of a small-molecule inhibitor of the arp2/3 complex, a key regulator of the actin cytoskeleton. *Chem Med Chem*, 7, pp.1286–1294.

Bamburg, J.R., 1999. Proteins of the ADF/cofilin family: essential regulators of actin dynamics. *Annual Review of Cell and Developmental Biology*, 15, pp.185–230.

Bañón-Rodríguez, I. et al., 2014. EGFR controls IQGAP basolateral membrane localization and mitotic spindle orientation during epithelial morphogenesis. *EMBO Journal*, 33(2), pp.129–145.

Barr, F.A. & Gruneberg, U., 2007. Cytokinesis: Placing and Making the Final Cut. *Cell*, 131(5), pp.847–860.

Bartolini, F. et al., 2008. The formin mDia2 stabilizes microtubules independently of its

actin nucleation activity. *Journal of Cell Biology*, 181(3), pp.523–536.

Bergert, M. et al., 2012. Cell mechanics control rapid transitions between blebs and lamellipodia during migration. *Proceedings of the National Academy of Sciences of the United States of America*, 109(36), pp.14434–9.

Bertoli, C., Skotheim, J.M. & de Bruin, R.A.M., 2013. Control of cell cycle transcription during G1 and S phases. *Nature reviews. Molecular cell biology*, 14(8), pp.518–28.

Biro, M. et al., 2013. Cell cortex composition and homeostasis resolved by integrating proteomics and quantitative imaging. *Cytoskeleton*, 70(11), pp.741–754.

Blanchoin, L. & Pollard, T.D., 2002. Hydrolysis of ATP by polymerized actin depends on the bound divalent cation but not profilin. *Biochemistry*, 41(2), pp.597–602.

Bohnert, K.A. et al., 2013. Formin-based control of the actin cytoskeleton during cytokinesis. *Biochemical Society transactions*, 41(6), pp.1750–4.

Bosk, S. et al., 2011. Activation of F-actin binding capacity of ezrin: Synergism of PIP2 interaction and phosphorylation. *Biophysical Journal*, 100(7), pp.1708–1717.

Bovellan, M. et al., 2014. Cellular control of cortical actin nucleation. *Current Biology*, 24, pp.1628–1635.

Brandt, D.T. et al., 2007. Dia1 and IQGAP1 interact in cell migration and phagocytic cup formation. *Journal of Cell Biology*, 178(2), pp.193–200.

Bray, D. & White, J.G., 1988. Cortical flow in animal cells. *Science (New York, N.Y.)*, 239(4842), pp.883–8.

Bugyi, B. & Carlier, M.-F., 2010. Control of Actin Filament Treadmilling in Cell Motility. *Annual Review of Biophysics*, 39(1), pp.449–470.

Burlacu, S., Janmey, P. a & Borejdo, J., 1992. Distribution of actin filament lengths measured by fluorescence microscopy. *The American journal of physiology*, 262(3 Pt 1), pp.C569-77.

Cadart, C. et al., 2014. Exploring the function of cell shape and size during mitosis. *Developmental Cell*, 29(2), pp.159–169.

Campbell, H.D. et al., 1993. The Drosophila melanogaster flightless-I gene involved in gastrulation and muscle degeneration encodes gelsolin-like and leucine-rich repeat domains and is conserved in Caenorhabditis elegans and humans. *Proceedings of the National Academy of Sciences of the United States of America*, 90(23), pp.11386–11390.

Campellone, K.G. & Welch, M.D., 2010. A nucleator arms race: cellular control of actin assembly. *Nature reviews. Molecular cell biology*, 11(4), pp.237–51.

Carlier, M.-F., 1991. Actin: protein structure and filament dynamics. *J Biol Chem*, 1(266), pp.1–4.

Carreno, S. et al., 2008. Moesin and its activating kinase Slik are required for cortical stability and microtubule organization in mitotic cells. *Journal of Cell Biology*, 180(4), pp.739–746.

Casella, J.F., Flanagan, M.D. & Lin, S., 1981. Cytochalasin D inhibits actin polymerization and induces depolymerization of actin filaments formed during platelet shape change. *Nature*, 293(5830), pp.302–305.

Casteel, D.E. et al., 2012. Rho Isoform-specific Interaction with IQGAP1 promotes breast cancer cell proliferation and migration. *Journal of Biological Chemistry*, 287(45), pp.38367–38378.

Castrillon, D.H. & Wasserman, S. a, 1994. Diaphanous is required for cytokinesis in Drosophila and shares domains of similarity with the products of the limb deformity gene. *Development*, 120(12), pp.3367–3377.

Chalut, K.J. & Paluch, E.K., 2016. The Actin Cortex: A Bridge between Cell Shape and Function. *Developmental Cell*, 38(6), pp.571–573.

Charras, G. & Paluch, E., 2008. Blebs lead the way: how to migrate without lamellipodia. *Nature reviews. Molecular cell biology*, 9(9), pp.730–736.

Charras, G.T., 2008. A short history of blebbing. In *Journal of Microscopy*. pp. 466–478.

Charras, G.T. et al., 2005. Non-equilibration of hydrostatic pressure in blebbing cells. *Nature*, 435(7040), pp.365–369.

Charras, G.T. et al., 2006. Reassembly of contractile actin cortex in cell blebs. *Journal of Cell Biology*, 175, pp.477–490.

Chen, Z. et al., 2010. Structure and control of the actin regulatory WAVE complex. *Nature*, 468(7323), pp.533–538.

Chesarone, M.A., DuPage, A.G. & Goode, B.L., 2010. Unleashing formins to remodel the actin and microtubule cytoskeletons. *Nature reviews. Molecular cell biology*, 11, pp.62–74.

Chhabra, E.S. & Higgs, H.N., 2007. The many faces of actin: matching assembly factors with cellular structures. *Nature cell biology*, 9(10), pp.1110–1121.

Choi-Rhee, E., Schulman, H. & Cronan, J.E., 2004. Promiscuous protein biotinylation by Escherichia coli biotin protein ligase. *Protein science : a publication of the Protein Society*, 13(11), pp.3043–50.

Choi, C.H. et al., 2013. Phosphorylation of actin-related protein 2 (Arp2) is required for normal development and cAMP chemotaxis in dictyostelium. *Journal of Biological Chemistry*, 288(4), pp.2464–2474.

Choi, H. et al., 2011. SAINT: probabilistic scoring of affinity purification-mass spectrometry data. *Nature methods*, 8(1), pp.70–3.

Chugh, P. et al., 2017. Actin cortex architecture regulates cell surface tension. *Nature Cell Biology*, 19(6), pp.689–697.

Le Clainche, C. et al., 2007. IQGAP1 stimulates actin assembly through the N-wasp-Arp2/3 pathway. *Journal of Biological Chemistry*, 282(1), pp.426–435.

Claudianos, C. & Campbell, H.D., 1995. The novel flightless-I gene brings together two gene families, actin-binding proteins related to gelsolin and leucine-rich-repeat proteins

involved in Ras signal transduction. *Molecular biology and evolution*, 12(3), pp.405–414.

Cohen, D. & Müsch, A., 2003. Apical surface formation in MDCK cells: Regulation by the serine/threonine kinase EMK1. *Methods*, 30(3), pp.269–276.

Cooper, J.A. et al., 1983. Kinetic evidence for a monomer activation step in actin polymerization. *Biochemistry*, 22(9), pp.2193–202.

Coué, M. et al., 1987. Inhibition of actin polymerization by latrunculin A. *FEBS Letters*, 213(2), pp.316–318.

Courson, D.S. & Rock, R.S., 2010. Actin cross-link assembly and disassembly mechanics for ??-actinin and fascin. *Journal of Biological Chemistry*, 285(34), pp.26350–26357.

Cramer, L.P. & Mitchison, T.J., 1997. Investigation of the mechanism of retraction of the cell margin and rearward flow of nodules during mitotic cell rounding. *Molecular biology of the cell*, 8(1), pp.109–119.

Cunningham, C.C. et al., 1992. Actin-binding protein requirement for cortical stability and efficient locomotion. *Science (New York, N.Y.)*, 255, pp.325–327.

D'Angelo, R. et al., 2007. Interaction of ezrin with the novel guanine nucleotide exchange factor PLEKHG6 promotes RhoG-dependent apical cytoskeleton rearrangements in epithelial cells. *Molecular biology of the cell*, 18(12), pp.4780–93.

Dae, J.K. et al., 2006. Interaction of SPIN90 with the Arp2/3 complex mediates lamellipodia and actin comet tail formation. *Journal of Biological Chemistry*, 281(1), pp.617–625.

Dao, V.T. et al., 2009. Dynamic changes in Rap1 activity are required for cell retraction and spreading during mitosis. *Journal of cell science*, 122(Pt 16), pp.2996–3004.

Dayel, M.J., Holleran, E.A. & Mullins, R.D., 2001. Arp2/3 complex requires hydrolyzable ATP for nucleation of new actin filaments. *Proc Natl Acad Sci U S A*, 98(26), pp.14871–14876.

Dephoure, N. et al., 2008. A quantitative atlas of mitotic phosphorylation. *Proceedings of the*

National Academy of Sciences, 105(31), pp.10762–10767.

Derivery, E. et al., 2008. Free Brick1 is a trimeric precursor in the assembly of a functional wave complex. *PLoS ONE*, 3(6).

DeWard, A.D. et al., 2010. The role of formins in human disease. *Biochimica et Biophysica Acta - Molecular Cell Research*, 1803(2), pp.226–233.

Disanza, A. et al., 2004. Eps8 controls actin-based motility by capping the barbed ends of actin filaments. *Nature cell biology*, 6(12), pp.1180–1188.

Disanza, A. et al., 2006. Regulation of cell shape by Cdc42 is mediated by the synergic actin-bundling activity of the Eps8-IRSp53 complex. *Nature cell biology*, 8(12), pp.1337–1347.

Djinović-Carugo, K. et al., 1999. Structure of the α-actinin rod: Molecular basis for cross-linking of actin filaments. *Cell*, 98(4), pp.537–546.

Dominguez, R. & Holmes, K.C., 2011. Actin structure and function. *Annual review of biophysics*, 40(April), pp.169–86.

Ducharme, N.A. et al., 2006. MARK2/EMK1/Par-1Balpha phosphorylation of Rab11-family interacting protein 2 is necessary for the timely establishment of polarity in Madin-Darby canine kidney cells. *Molecular biology of the cell*, 17(8), pp.3625–37.

Duleh, S.N. & Welch, M.D., 2010. WASH and the Arp2/3 complex regulate endosome shape and trafficking. *Cytoskeleton*, 67(3), pp.193–206.

Durkin, C.H. et al., 2017. RhoD Inhibits RhoC-ROCK-Dependent Cell Contraction via PAK6. *Developmental Cell*, 41(3), p.315–329.e7.

Edwards, M. et al., 2014. Capping protein regulators fine-tune actin assembly dynamics. *Nature Reviews Molecular Cell Biology*, 15(10), pp.677–689.

Egile, C. et al., 2005. Mechanism of filament nucleation and branch stability revealed by the structure of the Arp2/3 complex at actin branch junctions. *PLoS ONE*, 3(11).

Eisenmann, K.M. et al., 2007. Dia-Interacting Protein Modulates Formin-Mediated Actin Assembly at the Cell Cortex. *Current Biology*, 17, pp.579–591.

Elie, A. et al., 2015. Tau Co-Organizes Dynamic Microtubule and Actin Networks. *Scientific Reports*, 5, p.9964.

Etienne-Manneville, S. & Hall, A., 2002. Rho GTPases in cell biology. *Nature*, 420(6916), pp.629–635.

Evangelista, M. et al., 2002. Formins direct Arp2/3-independent actin filament assembly to polarize cell growth in yeast. *Nature cell biology*, 4(3), pp.260–269.

Faix, J. & Rottner, K., 2006. The making of filopodia. *Current Opinion in Cell Biology*, 18(1), pp.18–25.

Fan, L. & Mellor, H., 2012. The small Rho GTPase Rif and actin cytoskeletal remodelling. *Biochemical Society transactions*, 40(1), pp.268–72.

Fededa, J.P. & Gerlich, D.W., 2012. Molecular control of animal cell cytokinesis. *Nature Cell Biology*, 14(5), pp.440–7.

Fehon, R.G., McClatchey, A.I. & Bretscher, A., 2010. Organizing the cell cortex: the role of ERM proteins. *Nature Reviews Molecular Cell Biology*, 11(9), pp.674–674.

Firat-Karalar, E.N. & Stearnsx, T., 2015. Probing mammalian centrosome structure using BioID proximity dependent biotinylation. In *Methods in Cell Biology*. pp. 153–170.

Foroutannejad, S. et al., 2014. Biochemical and Biophysical Research Communications A novel role for IQGAP1 protein in cell motility through cell retraction. *Biochemical and Biophysical Research Communications*, 448(1), pp.39–44.

Friedl, P. & Bröcker, E.B., 2000. The biology of cell locomotion within three-dimensional extracellular matrix. *Cellular and Molecular Life Sciences*, 57(1), pp.41–64.

Fritzsche, M. et al., 2016. Actin kinetics shapes cortical network structure and mechanics. *Cell Biology*, 2(4), pp.1–12.

Fujiwara, T. et al., 2000. Rho small G-protein-dependent binding of mDia to an Src homology 3 domain-containing IRSp53/BAIAP2. *Biochemical and biophysical research communications*, 271(3), pp.626–9.

Fukuoka, M. et al., 2001. A novel neural Wiskott-Aldrich syndrome protein (N-WASP) binding protein, WISH, induces Arp2/3 complex activation independent of CDc42. *Journal of Cell Biology*, 153(3), pp.471–482.

Ganem, N., Storchova, Z. & Pellman, D., 2007. Tetraploidy, aneuploidy and cancer. *Curr Opin Genet Dev.*, 17(2), pp.157–62.

Goh, W.I. et al., 2012. mDia1 and WAVE2 proteins interact directly with IRSp53 in filopodia and are involved in filopodium formation. *Journal of Biological Chemistry*, 287(7), pp.4702–4714.

Goley, E.D. et al., 2010. An actin-filament-binding interface on the Arp2/3 complex is critical for nucleation and branch stability. *Proceedings of the National Academy of Sciences of the United States of America*, 107(18), pp.8159–64.

Goley, E.D. et al., 2004. Critical conformational changes in the Arp2/3 complex are induced by nucleotide and nucleation promoting factor. *Molecular Cell*, 16(2), pp.269–279.

Goley, E.D. & Welch, M.D., 2006. The ARP2/3 complex: an actin nucleator comes of age. *Nature reviews. Molecular cell biology*, 7(10), pp.713–726.

Gorman, J.A. et al., 2012. The Cytoskeletal Adaptor Protein IQGAP1 Regulates TCR-Mediated Signaling and Filamentous Actin Dynamics. *The Journal of Immunology*, 188(12), pp.6135–6144.

Gournier, H. et al., 2001. Reconstitution of human Arp2/3 complex reveals critical roles of individual subunits in complex structure and activity. *Molecular cell*, 8(5), pp.1041–1052.

Graceffa, P. & Dominguez, R., 2003. Crystal structure of monomeric actin in the ATP state: Structural basis of nucleotide-dependent actin dynamics. *Journal of Biological Chemistry*, 278(36), pp.34172–34180.

Graham, F.L. et al., 1977. Characteristics of a human cell line transformed by DNA from human adenovirus type 5. *The Journal of general virology*, 36(1), pp.59–74.

Grohmanova, K. et al., 2004. Phosphorylation of IQGAP1 modulates its binding to Cdc42, revealing a new type of Rho-GTPase regulator. *Journal of Biological Chemistry*, 279(47), pp.48495–48504.

Haase, K. & Pelling, A.E., 2013a. Resiliency of the plasma membrane and actin cortex to large-scale deformation. *Cytoskeleton*, 70(9), pp.494–514.

Haase, K. & Pelling, A.E., 2013b. The role of the actin cortex in maintaining cell shape. *Communicative and Integrative Biology*, 6(6).

Hahne, P. et al., 2001. Scar/WAVE is localised at the tips of protruding lamellipodia in living cells. *FEBS Letters*, 492(3), pp.215–220.

Hall, A., 1998. Rho GTPases and the actin cytoskeleton. *Science*, 279(5350), pp.509–514.

Hehnly, H. & Doxsey, S., 2012. Polarity sets the stage for cytokinesis. *Molecular biology of the cell*, 23(1), pp.7–11.

Heng, Y.-W. & Koh, C.-G., 2010. Actin cytoskeleton dynamics and the cell division cycle. *The International Journal of Biochemistry & Cell Biology*, 42(10), pp.1622–1633.

Henson, J.H. et al., 2015. Arp2/3 complex inhibition radically alters lamellipodial actin architecture, suspended cell shape, and the cell spreading process. *MBoC*, 26, pp.887–900.

Hetheridge, C. et al., 2012. The formin FMNL3 is a cytoskeletal regulator of angiogenesis. *J Cell Sci*, 125(Pt 6), pp.1420–1428.

Higashi, T. et al., 2010. Flightless-I (Fli-I) regulates the actin assembly activity of diaphanous-related formins (DRFs) Daam1 and mDia1 in cooperation with active Rho GTPase. *Journal of Biological Chemistry*, 285, pp.16231–16238.

Higashida, C. et al., 2013. F- and G-actin homeostasis regulates mechanosensitive actin nucleation by formins. *Nature cell biology*, 15(4), pp.395–405.

Holmes, K.C. et al., 1990. Atomic model of the actin filament. *Nature*, 347(6288), pp.44–49.

Huet, G. et al., 2013. Actin-regulated feedback loop based on Phactr4, PP1 and cofilin maintains the actin monomer pool. *Journal of cell science*, 126(2), pp.497–507.

Ibarra, N., Pollitt, A. & Insall, R.H., 2005. Regulation of actin assembly by SCAR/WAVE proteins. *Biochem Soc Trans*, 33(Pt 6), pp.1243–1246.

Ikenouchi, J. & Aoki, K., 2016. Membrane bleb: A seesaw game of two small GTPases. *Small GTPases*, pp.1–5.

Iwasa, J.H. & Mullins, R.D., 2007. Spatial and Temporal Relationships between Actin-Filament Nucleation, Capping, and Disassembly. *Current Biology*, 17(5), pp.395–406.

Jacquemet, G. & Humphries, M.J., 2013. IQGAP1 is a key node within the small GTPase network. *Small GTPases*, 4(4), pp.199–207.

Jaffe, A.B. & Hall, A., 2005. Rho GTPases: biochemistry and biology. *Annual review of cell and developmental biology*, 21, pp.247–269.

Jodoin, J.N. et al., 2015. Stable Force Balance between Epithelial Cells Arises from F-Actin Turnover. *Developmental Cell*, 35(6), pp.685–697.

Kabsch, W. et al., 1990. Atomic structure of the actin: DNase I complex. *Nature*, 347(6288), pp.37–44.

Kato, T. et al., 2001. Localization of a mammalian homolog of diaphanous, mDia1, to the mitotic spindle in HeLa cells. *Journal of cell science*, 114(Pt 4), pp.775–784.

Kelleher, J.F., Atkinson, S.J. & Pollard, T.D., 1995. Sequences, structural models, and cellular localization of the actin-related proteins Arp2 and Arp3 from Acanthamoeba. *Journal of Cell Biology*, 131(2), pp.385–397.

Kelly, A.E. et al., 2006. Actin binding to the central domain of WASP/Scar proteins plays a critical role in the activation of the Arp2/3 complex. *Journal of Biological Chemistry*, 281(15), pp.10589–10597.

Kim, D.I. et al., 2016. An improved smaller biotin ligase for BioID proximity labeling. *Molecular biology of the cell*, 27(8), pp.1188–1196.

Kim, D.I. et al., 2014. Probing nuclear pore complex architecture with proximity-dependent biotinylation. *Proc Natl Acad Sci U S A*, 111(24), pp.E2453-61.

Kim, T., Gardel, M.L. & Munro, E.D., 2014. Determinants of fluidlike behavior and effective viscosity in cross-linked actin networks. *Biophysical Journal*, 106(3), pp.526–534.

Kimura, K. et al., 1996. Regulation of Myosin Phosphatase by Rho and Rho-Associated Kinase (Rho-Kinase). *Science*, 273(5272), pp.245–248.

King, J.S. et al., 2010. SCAR/WAVE is activated at mitosis and drives myosin-independent cytokinesis. *Journal of cell science*, 123(Pt 13), pp.2246–2255.

Kohno, H. et al., 1996. Bni1p implicated in cytoskeletal control is a putative target of Rho1p small GTP binding protein in Saccharomyces cerevisiae. *EMBO Journal*, 15(22), pp.6060–8.

Korn, E.D., 2000. Coevolution of head, neck, and tail domains of myosin heavy chains. *Proceedings of the National Academy of Sciences of the United States of America*, 97(23), pp.12559–64.

Kovar, D.R. et al., 2006. Control of the assembly of ATP- and ADP-actin by formins and profilin. *Cell*, 124(2), pp.423–435.

Kunda, P. et al., 2008. Moesin Controls Cortical Rigidity, Cell Rounding, and Spindle Morphogenesis during Mitosis. *Current Biology*, 18(2), pp.91–101.

Kunda, P. et al., 2012. PP1-mediated moesin dephosphorylation couples polar relaxation to mitotic exit. *Current Biology*, 22(3), pp.231–236.

Kureishy, N. et al., 2002. Fascins, and their roles in cell structure and function. *BioEssays*, 24(4), pp.350–361.

Kusumi, A. et al., 2011. Hierarchical mesoscale domain organization of the plasma

membrane. *Trends in Biochemical Sciences*, 36(11), pp.604–615.

Kwon, K. & Beckett, D., 2000. Function of a conserved sequence motif in biotin holoenzyme synthetases. *Protein science : a publication of the Protein Society*, 9(8), pp.1530–1539.

Lämmermann, T. et al., 2008. Rapid leukocyte migration by integrin-independent flowing and squeezing. *Nature*, 453(7191), pp.51–5.

Lammers, M. et al., 2008. Specificity of interactions between mDia isoforms and Rho proteins. *Journal of Biological Chemistry*, 283(50), pp.35236–35246.

Lancaster, O.M. & Baum, B., 2014. Shaping up to divide: Coordinating actin and microtubule cytoskeletal remodelling during mitosis. *Seminars in Cell and Developmental Biology*.

Lebensohn, A.M. & Kirschner, M.W., 2009. Activation of the WAVE Complex by Coincident Signals Controls Actin Assembly. *Molecular Cell*, 36, pp.512–524.

LeClaire et al., 2015. The Nck-interacting kinase NIK increases Arp2/3 complex activity by phosphorylating the Arp2 subunit. *Journal of Cell Biology*, 208(2), pp.161–170.

Lecuit, T. & Wieschaus, E., 2000. Polarized insertion of new membrane from a cytoplasmic reservoir during cleavage of the Drosophila embryo. *Journal of Cell Biology*, 150(4), pp.849–860.

Lee, J.H. et al., 2004. Roles of p-ERM and Rho-ROCK signalling in lymphocyte polarity and uropod formation. *Journal of Cell Biology*, 167(2), pp.327–337.

Lee, K. & Song, K., 2007. Actin dysfunction activates ERK1/2 and delays entry into mitosis in mammalian cells. *Cell Cycle*, 6(12), pp.1487–95.

Li, F. & Higgs, H.N., 2005. Dissecting requirements for auto-inhibition of actin nucleation by the formin, mDia1. *Journal of Biological Chemistry*, 280(8), pp.6986–6992.

Li, F. & Higgs, H.N., 2003. The mouse formin mDia1 is a potent actin nucleation factor regulated by autoinhibition. *Current Biology*, 13(15), pp.1335–1340.

Lim, J. & Danuser, G., 2009. Live Cell Imaging of F-actin Dynamics via Fluorescent Speckle Microscopy (FSM). *Journal of Visualized Experiments*, (30).

Lin, R. et al., 2001. Dopamine D2 and D3 receptors are linked to the actin cytoskeleton via interaction with filamin A. *Proc Natl Acad Sci U S A*, 98(9), pp.5258–5263.

Linder, S. et al., 1999. Wiskott-Aldrich syndrome protein regulates podosomes in primary human macrophages. *Proc Natl Acad Sci U S A*, 96(17), pp.9648–9653.

Liu, J., Guidry, J.J. & Worthylake, D.K., 2014. Conserved sequence repeats of IQGAP1 mediate binding to ezrin. *Journal of Proteome Research*, 13(2), pp.1156–1166.

Liu, P.-S. et al., 2010. The interplay between Eps8 and IRSp53 contributes to Src-mediated transformation. *Oncogene*, 29(27), pp.3977–89.

Liu, S.L. et al., 2013. Insertions within the actin core of actin-related protein 3 (Arp3) modulate branching nucleation by Arp2/3 complex. *Journal of Biological Chemistry*, 288(1), pp.487–497.

Luan, Q. & Nolen, B.J., 2013. Structural basis for regulation of Arp2/3 complex by GMF. *Nature Reviews Molecular Cell Biology*, 20(9), pp.1062–1069.

Luxenburg, C. et al., 2011. Developmental roles for Srf, cortical cytoskeleton and cell shape in epidermal spindle orientation. *Nature Cell Biology*, 13(3), pp.203–214.

Maas, R.L. et al., 1990. Disruption of formin-encoding transcripts in two mutant limb deformity alleles. *Nature*, 346(6287), pp.853–855.

Machesky, L. et al., 1999. Scar, a WASp-related protein, activates nucleation of actin filaments by the Arp2/3 complex. *Proc Natl Acad Sci U S A*, 96(7), pp.3739–44.

Machesky, L.M. et al., 1994. Purification of a Cortical Complex Containing 2 Unconventional Actins from Acanthamoeba by Affinity-Chromatography on Profilin-Agarose. *Journal of Cell Biology*, 127(1), pp.107–115.

Maciver, S.K. & Hussey, P.J., 2002. The ADF/cofilin family: actin-remodeling proteins. *Genome biology*, 3(5), p.reviews3007.

Maddox, A.S. & Burridge, K., 2003. RhoA is required for cortical retraction and rigidity during mitotic cell rounding. *Journal of Cell Biology*, 160(2), pp.255–265.

Maekawa, M., 1999. Signaling from Rho to the Actin Cytoskeleton Through Protein Kinases ROCK and LIM-kinase. *Science*, 285(5429), pp.895–898.

Maiti, S. et al., 2012. Structure and activity of full-length formin mDia1. *Cytoskeleton*, 69(6), pp.393–405.

Matsui, T. et al., 1998. Rho-kinase phosphorylates COOH-terminal threonines of ezrin/radixin/moesin (ERM) proteins and regulates their head-to-tail association. *Journal of Cell Biology*, 140(3), pp.647–657.

Mehta, A.D. et al., 1999. Myosin-V is a processive actin-based motor. *Nature*, 400(6744), pp.590–3.

Mehus, A.A., Anderson, R.H. & Roux, K.J., 2016. BioID Identification of Lamin-Associated Proteins. *Methods in Enzymology*, 569, pp.3–22.

Meyer, R.K. & Aebi, U., 1990. Bundling of actin filaments by α-actinin depends on its molecular length. *Journal of Cell Biology*, 110(6), pp.2013–2024.

Michelot, A. & Drubin, D.G., 2011. Building distinct actin filament networks in a common cytoplasm. *Current Biology*, 21(14).

Miki, H., Suetsugu, S. & Takenawa, T., 1998. WAVE, a novel WASP-family protein involved in actin reorganization induced by Rac. *The EMBO journal*, 17(23), pp.6932–6941.

Millard, T.H. et al., 2005. Structural basis of filopodia formation induced by the IRSp53/MIM homology domain of human IRSp53. *The EMBO journal*, 24(2), pp.240–250.

Moulding, D. a et al., 2007. Unregulated actin polymerization by WASp causes defects of mitosis and cytokinesis in X-linked neutropenia. *The Journal of experimental medicine*, 204(9), pp.2213–2224.

Mullins, R.D., Stafford, W.F. & Pollard, T.D., 1997. Structure, subunit topology, and actin-binding activity of the Arp2/3 complex from Acanthamoeba. *Journal of Cell Biology*, 136(2), pp.331–343.

Nammalwar, R., Heil, A. & Gerke, V., 2014. Ezrin interacts with the scaffold protein IQGAP1 and affects its cortical localisation. *Biochemica et Biophysica Acta*, In Press.

Narayanan, A. et al., 2011. Phosphorylation of the Arp2 Subunit Relieves Auto-inhibitory Interactions for Arp2/3 Complex Activation. *PLoS ONE*, 7(11).

Nezami, A.G., Poy, F. & Eck, M.J., 2006. Structure of the autoinhibitory switch in formin mDia1. *Structure*, 14(2), pp.257–263.

Nishida, E. & Sakai, H., 1983. Kinetic analysis of actin polymerization. *Journal of biochemistry*, 93(4), pp.1011–1020.

Nolen, B.J. et al., 2009. Characterization of two classes of small molecule inhibitors of Arp2/3 complex. *Nature*, 460(7258), pp.1031–1034.

Nolen, B.J., Littlefield, R. & Pollard, T., 2004. Crystal structures of actin-related protein 2/3 complex with bound ATP or ADP. *Proc Natl Acad Sci U S A*, 101(44), pp.15627–32.

Ohta, Y. et al., 1999. The small GTPase RalA targets filamin to induce filopodia. *Proceedings of the National Academy of Sciences of the United States of America*, 96(5), pp.2122–2128.

Olson, E.N. & Nordheim, A., 2010. Linking actin dynamics and gene transcription to drive cellular motile functions. *Nature Reviews Molecular Cell Biology*, 11(5), pp.353–365.

Ou, G. et al., 2010. Polarized myosin produces unequal-size daughters during asymmetric cell division. *Science (New York, N.Y.)*, 330(6004), pp.677–680.

Page, R., Lindberg, U. & Schutt, C.E., 1998. Domain motions in actin. *Journal of molecular biology*, 280(3), pp.463–474.

Paluch, E. et al., 2005. Cortical actomyosin breakage triggers shape oscillations in cells and cell fragments. *Biophysical journal*, 89(1), pp.724–733.

Paul, A. & Pollard, T., 2008. The Role of the FH1 Domain and Profilin in Formin-Mediated Actin-Filament Elongation and Nucleation. *Current Biology*, 18(1), pp.9–19.

Pelikan-Conchaudron, A. et al., 2011. The IQGAP1 protein is a calmodulin-regulated barbed end capper of actin filaments: Possible implications in its function in cell migration. *Journal of Biological Chemistry*, 286(40), pp.35119–35128.

Perelroizen, I. et al., 1996. Role of nucleotide exchange and hydrolysis in the function of profilin in actin assembly. *Journal of Biological Chemistry*, 271(21), pp.12302–12309.

Perrin, B.J. & Ervasti, J.M., 2010. The actin gene family: Function follows isoform. *Cytoskeleton*, 67(10), pp.630–634.

Petrecca, K., Miller, D.M. & Shrier, A., 2000. Localization and enhanced current density of the Kv4.2 potassium channel by interaction with the actin-binding protein filamin. *J Neurosci*, 20(23), pp.8736–8744.

Pinner, S. & Sahai, E., 2008. PDK1 regulates cancer cell motility by antagonising inhibition of ROCK1 by RhoE. *Nature cell biology*, 10(2), pp.127–137.

Pinyol, R. et al., 2007. Regulation of N-WASP and the Arp2/3 complex by Abp1 controls neuronal morphology. *PLoS ONE*, 2(5).

Pollard, T.D. & Borisy, G.G., 2003. Cellular motility driven by assembly and disassembly of actin filaments. *Cell*, 112(4), pp.453–465.

Pollard, T.D. & Cooper, J.A., 1986. Actin and actin-binding proteins. A critical evaluation of mechanisms and functions. *Annual review of biochemistry*, 55, pp.987–1035.

Pollard, T.D. & Cooper, J.A., 1986. Actin and actin-binding proteins. A critical evaluation of mechanisms and functions. *Annual review of biochemistry*, 55, pp.987–1035.

Pollard, T.D. & Mooseker, M.S., 1981. Direct measurement of actin polymerization rate constants by electron microscopy of actin filaments nucleated by isolated microvillus cores. *Journal of Cell Biology*, 88(3), pp.654–659.

Ponuwei, G.A., 2016. A glimpse of the ERM proteins. *Journal of Biomedical Science*, 23(1),

p.35.

Pruyne, D. et al., 2002. Role of formins in actin assembly: nucleation and barbed-end association. *Science (New York, N.Y.)*, 297(5581), pp.612–615.

Ramalingam, N. et al., 2015. A resilient formin-derived cortical actin meshwork in the rear drives actomyosin-based motility in 2D confinement. *Nature communications*, 6, p.8496.

Ramanathan, S.P. et al., 2015. Cdk1-dependent mitotic enrichment of cortical myosin II promotes cell rounding against confinement. *Nature cell biology*, 17(2), pp.148–59.

Ramkumar, N. & Baum, B., 2016. Coupling changes in cell shape to chromosome segregation. *Nature reviews. Molecular cell biology*, 17(8), pp.511–21.

Raynal, P. & Pollard, H., 1994. Annexins: the problem of assessing the biological role for a gene family of multifunctional calcium- and phospholipid-binding proteins. *Biochem Biophys Acta.*, 1, pp.63–93.

dos Remedios, C.G. et al., 2003. Actin binding proteins: regulation of cytoskeletal microfilaments. *Physiological reviews*, 83(2), pp.433–473.

Rescher, U., 2004. Annexins - unique membrane binding proteins with diverse functions. *Journal of Cell Science*, 117(13), pp.2631–2639.

Reymann, A.-C. et al., 2012. Actin Network Architecture Can Determine Myosin Motor Activity. *Science*, 336(6086), pp.1310–1314.

Ridley, A.J., 2011. Life at the leading edge. *Cell*, 145(7), pp.1012–1022.

Ridley, A.J., 2001. Rho family proteins: Coordinating cell responses. *Trends in Cell Biology*, 11(12), pp.471–477.

Riedl, J. et al., 2008. Lifeact: a versatile marker to visualize F-actin. *Nature methods*, 5, pp.605–607.

Robinson, R.C. et al., 2001. Crystal structure of Arp2/3 complex. *Science (New York, N.Y.)*,

294(5547), pp.1679–1684.

Rodnick-Smith, M. et al., 2016. Role and structural mechanism of WASP-triggered conformational changes in branched actin filament nucleation by Arp2/3 complex. *PNAS*, 113(27), pp.1834–43.

Romero, S. et al., 2004. Formin is a processive motor that requires profilin to accelerate actin assembly and associated ATP hydrolysis. *Cell*, 119(3), pp.419–429.

Rosa, A. et al., 2015. Ect2/Pbl Acts via Rho and Polarity Proteins to Direct the Assembly of an Isotropic Actomyosin Cortex upon Mitotic Entry. *Developmental Cell*, 32(5), pp.604–616.

Rosenblatt, J. et al., 2004. Myosin II-dependent cortical movement is required for centrosome separation and positioning during mitotic spindle assembly. *Cell*, 117(3), pp.361–372.

Rossman, K.L., Der, C.J. & Sondek, J., 2005. GEF means go: turning on RHO GTPases with guanine nucleotide-exchange factors. *Nature Reviews Molecular Cell Biology*, 6(2), pp.167–180.

Rouiller, I. et al., 2008. The structural basis of actin filament branching by the Arp2/3 complex. *Journal of Cell Biology*, 180(5), pp.887–895.

Roux, K.J. et al., 2012. A promiscuous biotin ligase fusion protein identifies proximal and interacting proteins in mammalian cells. *Journal of Cell Biology*, 196, pp.801–810.

Roy, M., Li, Z. & Sacks, D.B., 2005. IQGAP1 is a scaffold for mitogen-activated protein kinase signaling. *Mol Cell Biol*, 25(18), pp.7940–7952.

Ruprecht, V. et al., 2015. Cortical contractility triggers a stochastic switch to fast amoeboid cell motility. *Cell*, 160(4), pp.673–685.

Ryu, J.R. et al., 2009. Regulation of cell-cell adhesion by Abi/Diaphanous complexes. *Molecular and cellular biology*, 29(7), pp.1735–1748.

Sakata, D. et al., 2007. Impaired T lymphocyte trafficking in mice deficient in an actin-

nucleating protein, mDia1. *The Journal of experimental medicine*, 204(9), pp.2031–2038.

Sakuma, T., Barry, M.A. & Ikeda, Y., 2012. Lentiviral vectors: basic to translational. *Biochem J*, 443(3), pp.603–618.

Salbreux, G., Charras, G. & Paluch, E., 2012. Actin cortex mechanics and cellular morphogenesis. *Trends in Cell Biology*, 22, pp.536–545.

Sampson, L.J., Leyland, M.L. & Dart, C., 2003. Direct interaction between the actin-binding protein filamin-A and the inwardly rectifying potassium channel, Kir2.1. *J Biol Chem*, 278(43), pp.41988–41997.

Sarmiento, C. et al., 2008. WASP family members and formin proteins coordinate regulation of cell protrusions in carcinoma cells. *Journal of Cell Biology*, 180(6), pp.1245–1260.

Schafer, D.A., Jennings, P.B. & Cooper, J.A., 1996. Dynamics of capping protein and actin assembly in vitro: Uncapping barbed ends by polyphosphoinositides. *Journal of Cell Biology*, 135(1), pp.169–179.

Schmidt, A. et al., 2007. Rho GTPases regulate PRK2/PKN2 to control entry into mitosis and exit from cytokinesis. *EMBO Journal*, (26), pp.1624–36.

Schönichen, A. & Geyer, M., 2010. Fifteen formins for an actin filament: A molecular view on the regulation of human formins. *Biochimica et Biophysica Acta - Molecular Cell Research*, 1803(2), pp.152–163.

Schutt, C.E. et al., 1993. The structure of crystalline profilin-beta-actin. *Nature*, 365(6449), pp.810–816.

Semba, S. et al., 2006. Coexpression of actin-related protein 2 and Wiskott-Aldrich syndrome family verproline-homologous protein 2 in adenocarcinoma of the lung. *Clinical Cancer Research*, 12, pp.2449–2454.

Seth, A., Otomo, C. & Rosen, M.K., 2006. Autoinhibition regulates cellular localization and actin assembly activity of the diaphanous-related formins FRL?? and mDia1. *Journal of Cell Biology*, 174(5), pp.701–713.

Shannon, K.B. & Li, R., 1999. The multiple roles of Cyk1p in the assembly and function of the actomyosin ring in budding yeast. *Molecular biology of the cell*, 10(2), pp.283–296.

Sharma, C.P., Ezzell, R.M. & Arnaout, M. a, 1995. Direct interaction of filamin (ABP-280) with the beta 2-integrin subunit CD18. *Journal of immunology (Baltimore, Md. : 1950)*, 154(8), pp.3461–3470.

Shekhar, S. et al., 2015. Formin and capping protein together embrace the actin filament in a ménage à trois. *Nature communications*, 6, p.8730.

Sivakumar, S., Daum, J.R. & Gorbsky, G.J., 2014. Live-cell fluorescence imaging for phenotypic analysis of mitosis. *Methods in Molecular Biology*, 1170, pp.549–562.

Sjöblom, B., Salmazo, A. & Djinović-Carugo, K., 2008. Alpha-actinin structure and regulation. *Cellular and molecular life sciences : CMLS*, 65(17), pp.2688–701.

Skau, C.T., Neidt, E.M. & Kovar, D.R., 2009. Role of tropomyosin in formin-mediated contractile ring assembly in fission yeast. *Molecular biology of the cell*, 20(8), pp.2160–2173.

Small, J.V., 2010. Dicing with dogma: De-branching the lamellipodium. *Trends in Cell Biology*, 20(11), pp.628–633.

Small, J.V., 1988. The actin cytoskeleton. *Electron Microscopy Reviews*, 1(1), pp.155–174.

Sossey-Alaoui, K., Li, X. & Cowell, J.K., 2007. c-Abl-mediated phosphorylation of WAVE3 is required for lamellipodia formation and cell migration. *Journal of Biological Chemistry*, 282(36), pp.26257–26265.

Steffen, A. et al., 2004. Sra-1 and Nap1 link Rac to actin assembly driving lamellipodia formation. *The EMBO Journal*, 23(4), pp.749–759.

Steigemann, P. et al., 2009. Aurora B-Mediated Abscission Checkpoint Protects against Tetraploidization. *Cell*, 136(3), pp.473–484.

Stepanenko, A.A. & Dmitrenko, V. V., 2015. HEK293 in cell biology and cancer research: Phenotype, karyotype, tumorigenicity, and stress-induced genome-phenotype

evolution. *Gene*, 569(2), pp.182–190.

Stewart, M.P. et al., 2011. Hydrostatic pressure and the actomyosin cortex drive mitotic cell rounding. *Nature*, 469(7329), pp.226–230.

Straub, F., 1942. Actin. *Studies Med Inst Szeged*, 2, pp.3–15.

Sun, H.Q. et al., 1999. Gelsolin, a multifunctional actin regulatory protein. *Journal of Biological Chemistry*, 274(47), pp.33179–33182.

Sun, S.X., Walcott, S. & Wolgemuth, C.W., 2010. Cytoskeletal cross-linking and bundling in motor-independent contraction. *Current Biology*, 20(15).

Suraneni, P. et al., 2012. The Arp2/3 complex is required for lamellipodia extension and directional fibroblast cell migration. *Journal of Cell Biology*, 197(2), pp.239–251.

Svitkina, T.M. & Borisy, G.G., 1999. Arp2/3 complex and actin depolymerizing factor/cofilin in dendritic organization and treadmilling of actin filament array in lamellipodia. *Journal of Cell Biology*, 145(5), pp.1009–1026.

Symons, M., 1996. Rho family GTPases: the cytoskeleton and beyond. *Trends in biochemical sciences*, 21(5), pp.178–81.

SYVERTON, J.T. & SCHERER, W.F., 1952. Studies on the propagation in vitro of poliomyelitis viruses. I. Viral multiplications in tissue cultures employing monkey and human testicular cells. *The Journal of experimental medicine*, 96, pp.355–367.

Tang, D.D. & Gerlach, B.D., 2017. The roles and regulation of the actin cytoskeleton, intermediate filaments and microtubules in smooth muscle cell migration. *Respiratory Research*, 18(1), p.54.

Théry, M. et al., 2007. Experimental and theoretical study of mitotic spindle orientation. *Nature*, 447(7143), pp.493–6.

Théry, M. & Bornens, M., 2008. Get round and stiff for mitosis. *HFSP journal*, 2(2), pp.65–71.

Tominaga, T. et al., 2000. Diaphanous-Related Formins Bridge Rho GTPase and Src Tyrosine Kinase Signaling. *Molecular Cell*, 5(1), pp.13–25.

Tseng, Y. et al., 2002. Functional synergy of actin filament cross-linking proteins. *Journal of Biological Chemistry*, 277(28), pp.25609–25616.

Tu, Y. et al., 2003. Migfilin and Mig-2 link focal adhesions to filamin and the actin cytoskeleton and function in cell shape modulation. *Cell*, 113(1), pp.37–47.

Uzbekov, R., Kireyev, I. & Prigent, C., 2002. Centrosome separation: Respective role of microtubules and actin filaments. *Biology of the Cell*, 94(4–5), pp.275–288.

Vignjevic, D. et al., 2006. Role of fascin in filopodial protrusion. *Journal of Cell Biology*, 174(6), pp.863–875.

Di Vizio, D. et al., 2009. Oncosome formation in prostate cancer: association with a region of frequent chromosomal deletion in metastatic disease. *Cancer Res*, 69(13), pp.5601–9.

Wagner, A.R. et al., 2013. Dip1 defines a class of Arp2/3 complex activators that function without preformed actin filaments. *Current Biology*, 23, pp.1990–1998.

Wang, W. et al., 2005. Tumor cells caught in the act of invading: Their strategy for enhanced cell motility. *Trends in Cell Biology*, 15(3), pp.138–145.

Watanabe, N. et al., 1999. Cooperation between mDia1 and ROCK in Rho-induced actin reorganization. *Nature cell biology*, 1(3), pp.136–143.

Watanabe, N. et al., 1997. p140mDia, a mammalian homolog of Drosophila diaphanous, is a target protein for Rho small GTPase and is a ligand for profilin. *EMBO Journal*, 16(11), pp.3044–3056.

Weaver, A.M. et al., 2001. Cortactin promotes and stabilizes Arp2/3-induced actin filament network formation. *Current Biology*, 11(5), pp.370–374.

Weiss, E.L., 2012. Mitotic exit and separation of mother and daughter cells. *Genetics*, 192(4), pp.1165–1202.

Weissbach, L. et al., 1994. Identification of a human RasGAP-related protein containing calmodulin-binding motifs. *Journal of Biological Chemistry*, 269(32), pp.20517–20521.

Welch, M.D. et al., 1998. Interaction of human Arp2/3 complex and the Listeria monocytogenes ActA protein in actin filament nucleation. *Science*, 281, pp.105–108.

Wen, Y. et al., 2004. EB1 and APC bind to mDia to stabilize microtubules downstream of Rho and promote cell migration. *Nature cell biology*, 6(9), pp.820–830.

Wilson, C.A. et al., 2010. Myosin II contributes to cell-scale actin network treadmilling through network disassembly. *Nature*, 465(7296), pp.373–377.

Winter, D. et al., 1997. The complex containing actin-related proteins Arp2 and Arp3 is required for the motility and integrity of yeast actin patches. *Current biology : CB*, 7(7), pp.519–29.

Woolner, S. et al., 2008. Myosin-10 and actin filaments are essential for mitotic spindle function. *Journal of Cell Biology*, 182(1), pp.77–88.

Woychick, R. et al., 1990. "Formins": proteins deduced from the alternative transcripts of the limb deformity gene. *Nature*, 346, pp.850–853.

Xiao, M. et al., 2003. An actin-dependent conformational change in myosin. *Nature structural biology*, 10(5), pp.402–408.

Yamashiro-Matsumura, S. & Matsumura, F., 1985. Purification and characterization of an F-actin-bundling 55-kilodalton protein from HeLa cells. *Journal of Biological Chemistry*, 260(8), pp.5087–5097.

Yamazaki, D. et al., 2005. A novel function of WAVE in lamellipodia: WAVE1 is required for stabilization of lamellipodial protrusions during cell spreading. *Genes to Cells*, 10(5), pp.381–392.

Yao-Cheng et al., 2014. Genome dynamics of the human embryonic kidney 293 lineage in response to cell biology manipulations. *Nature*, 5, pp.1–12.

Zaoui, K. et al., 2008. Memo-RhoA-mDia1 signaling controls microtubules, the actin network, and adhesion site formation in migrating cells. *J Cell Bio*, 183(3), pp.401–8.

Zhang, W. & Robinson, D.N., 2005. Balance of actively generated contractile and resistive forces controls cytokinesis dynamics. *Proceedings of the National Academy of Sciences of the United States of America*, 102(20), pp.7186–7191.

Zigmond, S.H., 2004. Formin-induced nucleation of actin filaments. *Current Opinion in Cell Biology*, 16(1), pp.99–105.

Zigmond, S.H. et al., 2003. Formin Leaky Cap Allows Elongation in the Presence of Tight Capping Proteins. *Current Biology*, 13(20), pp.1820–1823.